JOURNAL OF THE Electrochemical Society

106, No. 6 June 1959

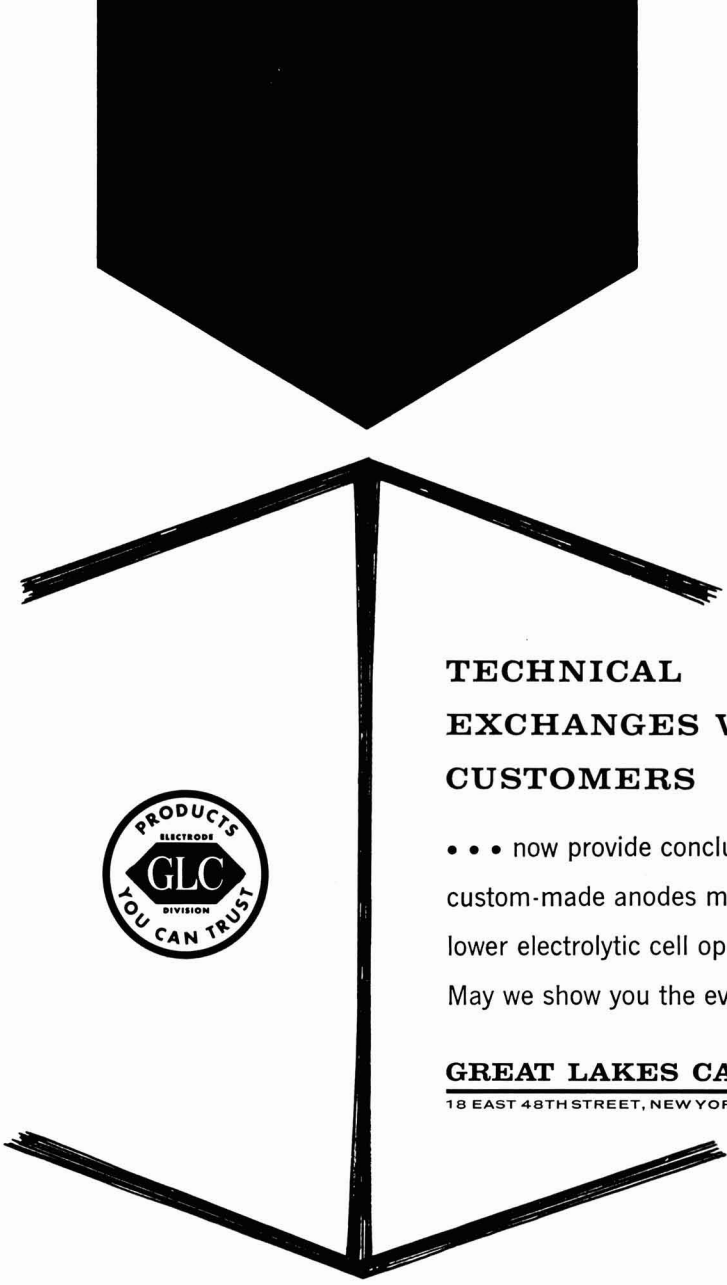

TECHNICAL EXCHANGES WITH CUSTOMERS

• • • now provide conclusive proof that custom-made anodes materially lower electrolytic cell operating costs. May we show you the evidence?

GREAT LAKES CARBON CORPORATION

18 EAST 48TH STREET, NEW YORK 17, N.Y. OFFICES IN PRINCIPAL CITIES

Journal of the Electrochemical Society

JUNE 1959 **VOL. 106 • NO. 6**

CONTENTS

Published monthly by The Electrochemical Society, Inc., from Manchester, N. H., **Executive Offices, Editorial Office** and **Circulation Dept.,** and **Advertising Office** at 1860 Broadway, New York 23, N. Y., combining the JOURNAL and TRANSACTIONS OF THE ELECTROCHEMICAL SOCIETY. Statements and opinions given in articles and papers in the JOURNAL OF THE ELECTROCHEMICAL SOCIETY are those of the contributors, and The Electrochemical Society assumes no responsibility for them. Nondeductible subscription to members $5.00; subscription to nonmembers $18.00. Single copies $1.25 to members, $1.75 to nonmembers.

Entered as second-class matter at the Post Office at Manchester, N. H., under the act of August 24, 1912.

KEITHLEY MODEL 502 MILLIOHMMETER

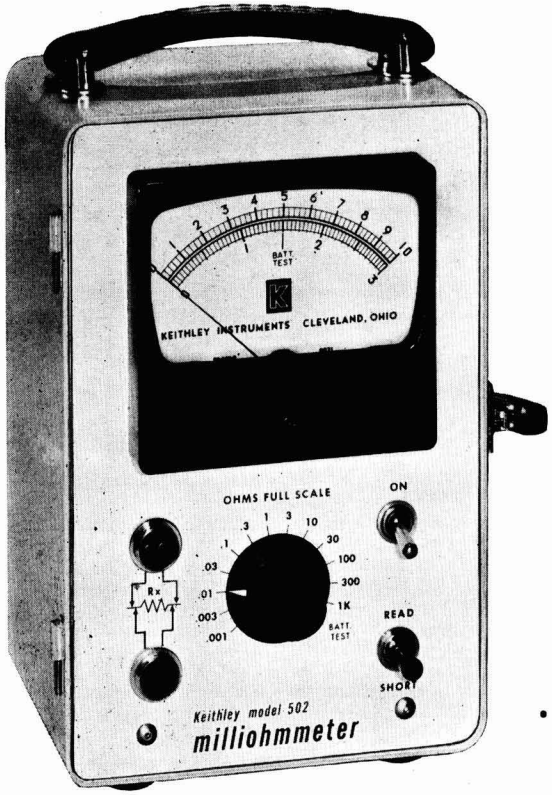

measures resistances down to 30 *micro-ohms with only two micro-watts through sample*

THE KEITHLEY MODEL 502 provides fast, accurate, easy measurement of low resistances. Its linear scales assure high resolution on 13 overlapping ranges from 0.001 ohm to 1000 ohms full scale, minimum detectable resistance is about 30 micro-ohms, and maximum dissipation through a sample is two micro-watts. Full scale accuracy is within 3%, except on the one-milliohm range where it is within 5%.

FEATURES include instantaneous indication of resistance without zero drift, calibration adjustments, or errors due to thermal EMF's; battery operation; ruggedized construction, light weight and a protective cover.

USES of the Model 502 include measurements of conductivity in semi-conductors and liquids, corrosion tests, and checking resistivity of relay contacts, printed circuits, fuses and grounding systems. Emphasis on safety makes it ideal for field tests of squibs, carbon bridges and similar explosive devices.

SEND TODAY for your copy of Keithley Engineering Notes, Vol. 6, No. 3, containing detailed data about the Model 502.

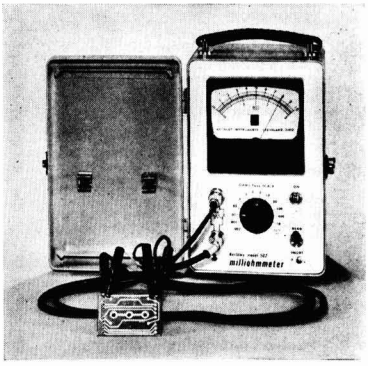

MODEL 502 measuring 0.008 ohm printed circuit path. Four terminal measuring system eliminates errors due to clip and lead resistance.

BRIEF SPECIFICATIONS

RANGES: linear scales with 13 overlapping ranges from 0.001 ohm to 1000 ohms full scale.

ACCURACY: within 3% of full scale on all ranges except the 0.001 range, where it is 5%.

MAXIMUM POWER DISSIPATION through a sample is normally two micro-watts; with a component failure, four micro-watts.

PRICE: $375.00

KEITHLEY INSTRUMENTS, INC.
12415 EUCLID AVENUE CLEVELAND 6, OHIO

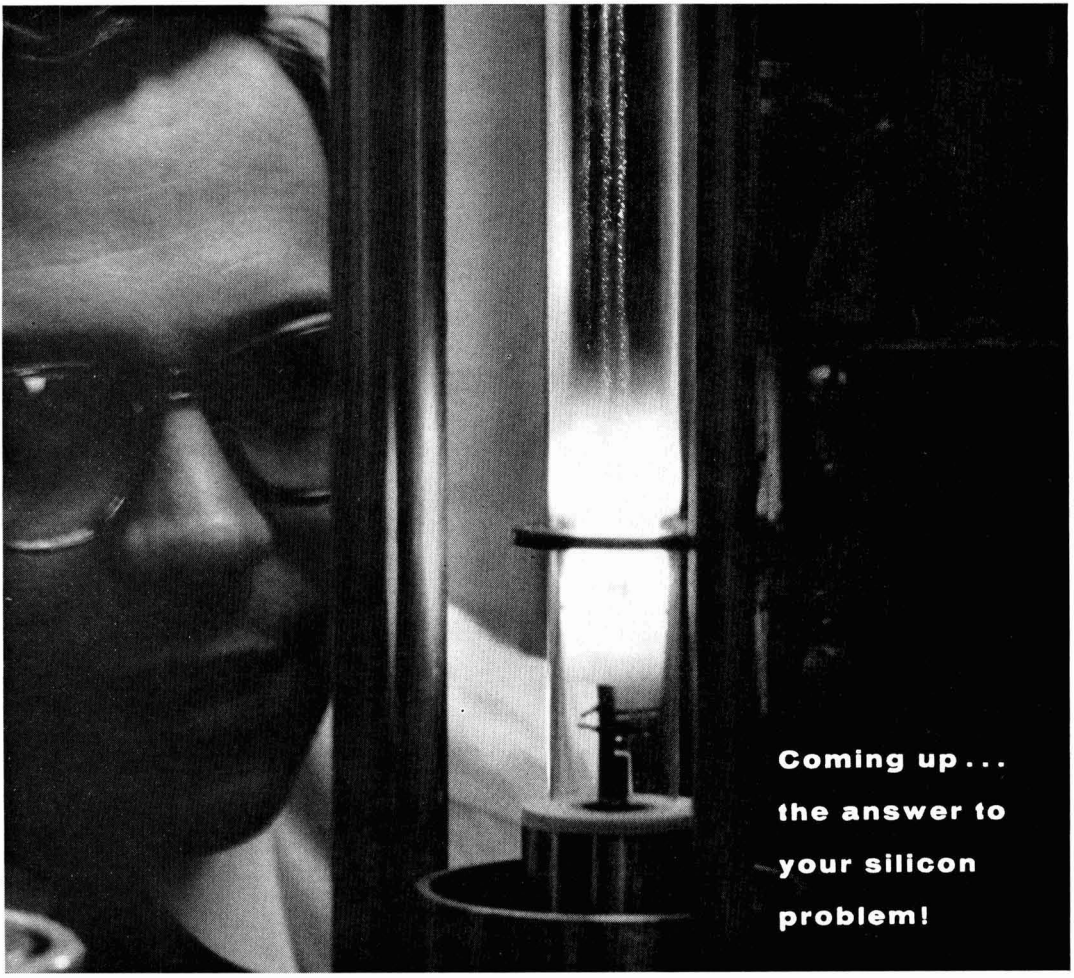

Du Pont . . . manufacturer of Hyperpure Silicon offers the services of technical specialists

When you specify Du Pont HYPERPURE Silicon, you get a product of highest dependability as well as expert technical assistance, when needed. Experienced Du Pont Technical Specialists will gladly discuss techniques of crystal growing and materials processing with you. What's more, you can take advantage of Du Pont's new $3,000,000 Technical-Service Laboratory designed for researching customer problems.

Floating zone single crystals of Du Pont HYPERPURE Silicon are available in a wide range of resistivities. Du Pont HYPERPURE Silicon is also supplied in densified cut rods . . . and rods suitable for float zone refining. They're offered in several grades with carefully controlled purity levels.

Here's more news: Du Pont's new Brevard, N. C., plant has a capacity of 70,000 lbs. of HYPERPURE Silicon per year. That means you're assured of a prompt supply of high-purity silicon in the form you need. For more information, write Du Pont . . . pioneer producer of semiconductor-grade silicon.

Free booklet is available upon request. It describes the manufacture, properties and uses of HYPERPURE Silicon. E. I. du Pont de Nemours & Co. (Inc.), Pigments Dept., Silicon Development Group, Wilmington 98, Delaware.

HYPERPURE SILICON

DU PONT
REG. U.S. PAT. OFF.

BETTER THINGS FOR BETTER LIVING
. . . THROUGH CHEMISTRY

Editorial

Pugwash Conferences

SOME three years ago, Mr. Cyrus S. Eaton visited Russia and came home with the opinion that something concrete should, and could, be done to promote better understanding and more cordial relations between the U.S.S.R. and the Western World, and to alleviate the tensions of the cold war. Being a man of action and of considerable wealth, and well aware of the role played by science in modern civilization, he promptly arranged an international conference of well-known scientists, which was held at Pugwash, Nova Scotia (Mr. Eaton's birthplace). Two additional "Pugwash Conferences" have been held since that time, the latest at Kitzbühel and Vienna in Austria, in September 1958.

The last Conference set up the Pugwash Continuing Committee, to publicize the proceedings and to explore the possibility of further useful conferences and other activities. It also adopted the "Vienna Declaration," which reviews the dangers to the entire human race of another World War, and emphasizes the responsibility of scientists to contribute in establishing trust and cooperation between nations. Scientists throughout the world are solicited to declare their approval of the "Vienna Declaration" and to make suggestions for further action.

When one receives such an invitation, endorsed with the personal rubber stamp signature of Bertrand Russell as Chairman of the Committee, the first inclination is to throw it into the wastebasket immediately. We do not question the sincerity of Mr. Eaton, or the objectives of the Pugwash Committee. We believe that any scientist can heartily endorse the Declaration, but that in doing so he should completely reserve all commitment to approval of future Committee actions. The Pugwash movement is not one brought about by the spontaneous efforts of leading scientists. It is somewhat reminiscent of Henry Ford's "Peace Ship" of World War I, and also of many organizations which during the last thirty years have displayed prominent names on their letterheads

Scientists normally work in the direction of international understanding and peaceful cooperation in a quite different manner, namely by getting acquainted and exchanging all the scientific information which they are permitted to. They learn each other's languages; they exchange books, journals, reprints; they hire translators. They invite each other to visit, to attend scientific meetings, to lecture, to write articles concerning experiment and theory. They do not publicly discuss politics at their meetings, but in the long run they have a great deal of influence in political matters. Governments are supporting scientific research as never before, and are giving increasing support to the international exchange of scientists for short or long visits: though sometimes this seems to be done with great reluctance, suspicion, and even hostility.

Scientific advisors at all levels of government are no longer a rarity. Perhaps some day these advisors can say: No, war is not the answer. Let us call a meeting of the leading scientists in this field, we can work out another solution. If the Pugwash Committee can act as host for this Conference, it will have fulfilled a mission.

—CVK

NEROFIL

A Family of Specially-Processed Carbon-Based Filteraids

BASIC CAUSTIC PRODUCERS USE NEROFIL FOR:

1. Filtering caustic production particularly where high purity is required, such as for the rayon industry, etc.

2. Nerofil filtration of brine over and above ordinary clarification methods more than justifies itself through increased efficiency of the DeNora and other type mercury cell operations. Nerofil's low vanadium content makes it the preferred filteraid for this new approach to brine preparation.

PARTICULAR PROPERTIES OF NEROFIL PRODUCTS

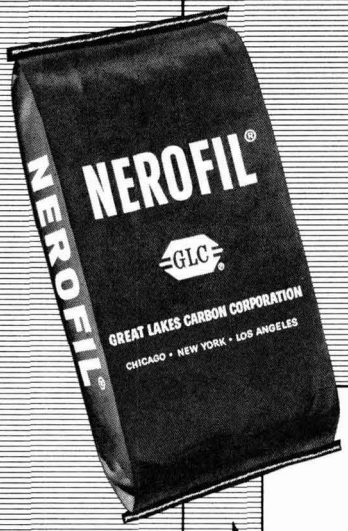

Fast Flowrates, Excellent Clarity—On these points, Nerofil filteraids are comparable to many grades of diatomite filteraids.

Lower Cake Density—Because of its lower cake density and high porosity, Nerofil affords filteraid savings of up to 20%.

Full Range of Grades—Six grades of Nerofil filteraids are now available to cover a wide range of process liquors.

Physical and Chemical Stability—Tests show no silicon solubility in 30 minutes in 50% sodium hydroxide at 125°F.

Compatibility with Process Liquors—Being practically pure carbon, Nerofil is unaffected by either acids or alkalies, and is readily wettable to either aqueous or non-aqueous solutions.

Combustible Filtercake—A Nerofil filtercake has a fuel value of 13,000 BTU per pound. Disposal thus presents no problem and metal values recovery in metallurgical filtration is made easy.

Uniform Quality—Exacting quality control maintains particle size range and distribution constant in every grade.

NERO-PRODUCTS DEPT., Great Lakes Carbon Corp.
333 No. Michigan Ave. Chicago 1, Ill.

Please send me further information on Nerofil

NAME_____

POSITION_____

COMPANY_____

ADDRESS_____

CITY_____ ZONE____ STATE_____

FUTURE MEETINGS OF
The Electrochemical Society

Columbus, Ohio, October 18, 19, 20, 21, and 22, 1959

Headquarters at the Deshler-Hilton Hotel

Sessions probably will be scheduled on

Batteries, Corrosion (including a joint Corrosion—Electronics-Semiconductors session), Electrodeposition (including symposia on "Electrodeposition from Organic Solvents" and "Electro- and Chemical-Polishing"), Electronics (Semiconductors), Electro-Organics, and Electrothermics and Metallurgy

★ ★ ★

Chicago, Ill., May 1, 2, 3, 4, and 5, 1960

Headquarters at the Lasalle Hotel

Sessions probably will be scheduled on

Electric Insulation, Electronics (including Luminescence and Semiconductors), Electrothermics and Metallurgy, Industrial Electrolytics, and Theoretical Electrochemistry

★ ★ ★

Houston, Texas, October 9, 10, 11, 12, and 13, 1960

Headquarters at the Shamrock Hotel

★ ★ ★

Indianapolis, Ind., April 30, May 1, 2, 3, and 4, 1961

Headquarters at the Claypool Hotel

★ ★ ★

Detroit, Mich., October 1, 2, 3, 4, and 5, 1961

Headquarters at the Statler Hotel

Papers are now being solicited for the meeting to be held in Chicago, Ill., May 1-5, 1960. Triplicate copies of each abstract (*not exceeding 75 words in length*) are due at Society Headquarters, 1860 Broadway, New York 23, N. Y., *not later than January 1, 1960* in order to be included in the program. *Please indicate on abstract for which Division's symposium the paper is to be scheduled, and underline the name of the author who will present the paper.* Complete manuscripts should be sent in triplicate to the Managing Editor of the JOURNAL at 1860 Broadway, New York 23, N.Y.

ANODE UNIFORMITY

...that really pays-off!

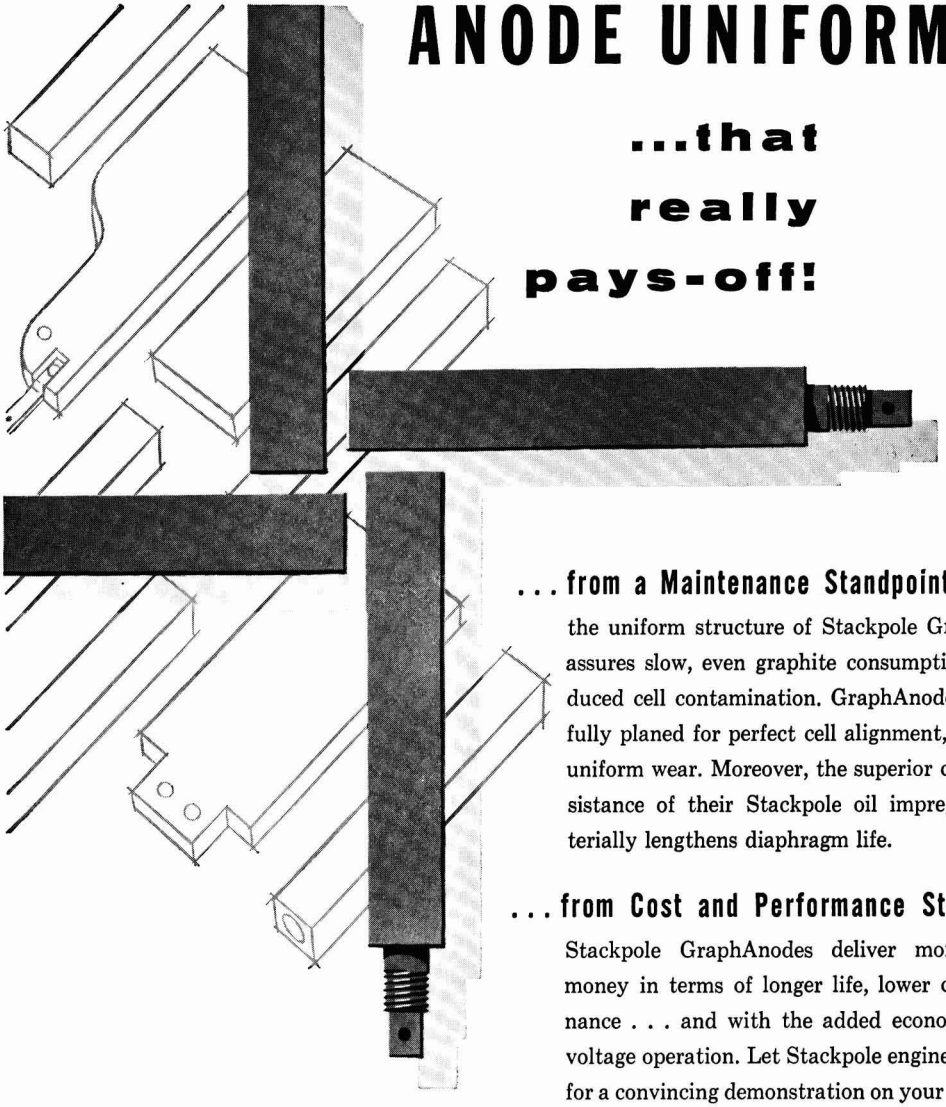

. . . from a Maintenance Standpoint

the uniform structure of Stackpole GraphAnodes assures slow, even graphite consumption with reduced cell contamination. GraphAnodes are carefully planed for perfect cell alignment, longer life, uniform wear. Moreover, the superior chemical resistance of their Stackpole oil impregnants materially lengthens diaphragm life.

. . . from Cost and Performance Standpoints

Stackpole GraphAnodes deliver more for the money in terms of longer life, lower cell maintenance . . . and with the added economy of low-voltage operation. Let Stackpole engineers arrange for a convincing demonstration on your equipment. *Stackpole Carbon Company, St. Marys, Penna.*

STACKPOLE

GRAPHANODES

graphite anodes in grades, sizes and shapes for all electrolytic cells

TUBE ANODES • CATHODIC PROTECTION ANODES • FLUXING & DE-GASSING TUBES • BRUSHES for all rotating electrical equipment • ELECTRICAL CONTACTS • VOLTAGE REGULATOR DISCS • "CERAMAGNET"® CERAMIC MAGNETS • ROCKET NOZZLES • BEARINGS • SALT BATH RECTIFICATION RODS • SEAL RINGS • FRICTION RINGS • ELECTRODES & HEATING ELEMENTS • MOLDS & DIES • WELDING CARBONS • POROUS CARBON • and many other carbon, graphite, and electronic components.

GRACE SILICON

(ultra-high-purity)

Minute instruments in the nose cones of American space explorers record vital phenomena beyond the pull of earth's gravity. The phenomena: the unknowns of outer space including bands of radiation, cosmic rays, temperatures, etc. The data recorders: complex electronic devices packed with transistors, diodes, rectifiers and other subminiature signal transmitters.

It wasn't possible ten years ago. It wouldn't be possible today if it weren't for ultra-high-purity silicon. Purity such as is produced by the Pechiney process used in the manufacture of Grace Silicon.

May we suggest that wherever silicon of top quality is required—for semiconductor devices in research, military, industrial and entertainment uses—call or write GRACE ELECTRONIC CHEMICALS, INC., PL 2-7699, 101 N. Charles Street in Baltimore.

GRACE ELECTRONIC CHEMICALS, INC.

101 N. Charles St., Baltimore, Maryland

Subsidiary of W. R. Grace & Co.

A New Separator for the Aluminum Dry Cell

N. C. Cahoon[1] and M. P. Korver

Research Laboratories, National Carbon Company, Division of Union Carbide Corporation, Cleveland, Ohio

ABSTRACT

A new and improved separator medium for the aluminum dry cell is described. It provides an adhesive contact with the anode and a satisfactory electrolytic contact with the cathode. The method by which this separator is prepared involves a new technique which is described. The separator layer significantly improves the keeping quality and delayed service performance of the aluminum-manganese dioxide cell.

Aluminum as an anode for primary batteries has received periodic attention during the past 30 years. Recent studies with renewed interest by Stokes and Ruben have shown greater progress (1, 2). As an anode for a battery system, aluminum looks particularly attractive for several reasons. Electrochemically, the aluminum anode theoretically consumes only 0.336 g of metal per ampere hour of electrical output, or about 27% of that consumed by the zinc anode. In addition, drawn aluminum cans offer attractive economic features.

Since any new system imposes many problems, a considerable amount of study was required with this particular system because of the very acidic nature of the altogether new electrolyte employed. Stokes has reported considerable progress on studies of the anode, the cathode, and the electrolyte. These studies have yielded the "Alclad"-type anode and the chloride-chromate type electrolyte (1, 3).[2] Our studies have been concerned primarily with the selection of an improved separator for this system. An effective separator medium is essential if a battery is to operate satisfactorily and to possess acceptable keeping quality.

Experimental

This study has followed a pattern somewhat similar to that previously described for separator studies in the Leclanché cell (4, 5). As in the Leclanché cell, it was deemed advisable to select a separator which would possess the following properties: (*a*) A medium which would contact the cathode satisfactorily and form a positive adhesive contact with the anode; (*b*) A medium which would be compatible with the battery components and nonreactive for a reasonable period of time, i.e. at least one to three years; (*c*) A separator which would possess adequate wet strength to allow ease of cell assembly.

It has been shown (4) that the usual cereal paste does not meet these requirements satisfactorily, since both starch and flour hydrolyze and break down in an acid electrolyte. The choice of possible separators, therefore, must be made from the field of other natural or synthetic colloids.

First, one must select one or more colloids which satisfy items (*a*) and (*b*) above. Since the depolarizer is the same in both systems, with the background knowledge of the stability of various colloids with manganese dioxide, one may choose colloids which might satisfy item (*a*) when used with an aluminum anode. This group included water soluble methyl cellulose, two types of hydroxypropyl methyl cellulose, Lytron X-887,[3] polyacrylamide 50, locust bean gum, and gum Karaya. Self-supporting films of all colloids of this group except Lytron X-887, locust bean gum, and gum Karaya were prepared. These three materials were difficult or impossible to prepare as self-supporting layers. Therefore, a new technique was used to incorporate the gums into an acceptable separator layer. It involves the suspension of the powdered colloid in a resin solution and is thereby designated the resin-bonded separator. The resin, e.g., polyvinyl acetate, is dissolved in a volatile solvent, e.g., acetone. The colloidal material chosen is then dispersed in this solution. The suspension may be coated onto a paper possessing high wet strength, an anode metal, film, or other support, and dried. In this application high wet strength paper was used.

These prepared films were exposed to the chloride-chromate electrolyte solution, the composition of which is presented in Table I. Periodically they were examined to determine their behavior in the electrolyte. Those materials which absorbed electrolyte to become gel-like and tacky to the touch were locust bean gum, gum Karaya, and polyacrylamide 50. At the end of one week these same materials appeared to have the same bibulous characteristics. The other materials appeared only slightly damp and did not appear to be bibulous enough to act as satisfactory separator media.

[1] Present address: Edgewater Development Laboratories, National Carbon Company, Division of Union Carbide Corporation, Cleveland, Ohio.

[2] The Aluminum Company of America Research Laboratory has been very helpful to us in our work by recommending electrolyte formulations, furnishing cans and helpful technical information.

[3] Lytron X-887, an organic copolymer of maleic anhydride, is an experimental Krilium compound made by the Monsanto Chemical Company.

Table I. Chloride-chromate electrolyte formulation used for experimental studies

Component	Composition, %
$AlCl_3 \cdot 6H_2O$	36
$CrCl_3 \cdot 6H_2O$	12
$(NH_4)_2CrO_4$	12
H_2O	40

Table II. Composition of experimental D-size Al-MnO_2 cells

Electrolyte formulation	African Ore		Acetylene black	Electrolyte composition, g/cell				
	G/cell	Theor. output amp-hr	g/cell	$AlCl_3 \cdot 6H_2O$	$CrCl_3 \cdot 6H_2O$	$(NH_4)_2 \cdot CrO_4$	$MnCl_2$	H_2O
Cl-CrO_4	28.6	7.15	5.70	7.64	2.55	2.55	—	16.55
$MnCl_2$	32.71	8.18	6.54	—	—	—	10.90	14.86

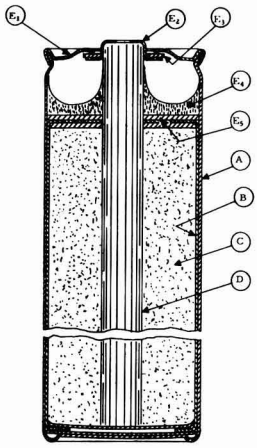

Fig. 1. Cross-section view of a film-lined experimental D-size cell. A, aluminum can; B, film separator; C, cathode; D, carbon electrode; E, cell closure—E_1, cover, E_2, brass cap, E_3, insulating washer, E_4, seal, E_5, washers.

Experimental cells were made evaluating these three separators and also, as a direct comparison, a filter-paper separator.[4] A 5:1::manganese dioxide: acetylene black mix ratio was used with the electrolyte formulation given in Table I. Natural manganese dioxide ore from the African Gold Coast was the depolarizer used. D-size experimental units were assembled which possessed equal weights of the same mix so that the only variable introduced was the different separators. A cross-sectional view of the construction used appears in Fig. 1. In addition, one group of cells was made with manganous chloride electrolyte (2) and assembled with the locust bean gum separator. Comparison of these formulations appears in Table II.

Discussion of Results

Comparative service data on these experimental batteries are presented in Table III. It may readily be seen from these data, especially on delayed and longer term tests, such as intermittent, that the improved separators show a significant advantage. These data show that, although the cells made with manganous chloride give somewhat better initial service than those with the chloride-chromate electrolyte, they do not maintain this service level. The

[4] Filter paper was the separator employed by Aluminum Company of America Research Laboratory in their studies.

Table III. Service summary of experimental D-size Al-MnO_2 dry cells

Separator	Electrolyte	4 Ohm continuous min to 0.75 v			4 Ohm HIF min to 0.9 v	
		Initial	6 Months	12 Months	Initial	6 Months
Filter paper	Cl-CrO_4	469	30	Cells failed	402	440
Locust bean gum resin bonded	Cl-CrO_4	479	469	615	368	418
Gum Karaya resin bonded	Cl-CrO_4	429	382	471	322	No cells available
Polyacrylamide 50	Cl-CrO_4	250	343	No cells available	125	286
Locust bean gum resin bonded	$MnCl_2$	694	523	No cells available	400	102

		4 Ohm LIF min to 0.9 v		
		Initial	6 Months	12 Months
Filter paper	Cl-CrO_4	452	68	Cells failed
Locust bean gum resin bonded	Cl-CrO_4	271	457	401
Gum Karaya resin bonded	Cl-CrO_4	444	420	351
Polyacrylamide 50	Cl-CrO_4	437	315	No cells available
Locust bean gum resin bonded	$MnCl_2$	250	231	No cells available

		2.25 Ohm LIF min to 0.65 v			2.25 Ohm intermittent min to 0.65 v	
		Initial	6 Months	12 Months	Initial	6 Months
Filter paper	Cl-CrO_4	301	Cells failed	Cells failed	21	35
Locust bean gum resin bonded	Cl-CrO_4	355	289	361	427	355
Gum Karaya resin bonded	Cl-CrO_4	333	357	274	206	332
Polyacrylamide 50	Cl-CrO_4	No test run	216	No cells available	No test run	No test run
Locust bean gum resin bonded	$MnCl_2$	500	279	No cells available	285	162

chloride-chromate electrolyte, because of the chromate present, would be expected to possess better keeping quality. With the improved separator medium present to maintain adequate anode contact coupled with satisfactory stability of the separator, it is evident that the aluminum dry cells will operate satisfactorily even after 12 months shelf storage at 21°C.

The mechanism by which the resin-bonded separator operates is twofold. As the separator absorbs electrolyte the polyvinyl acetate bond hydrolyzes to form polyvinyl alcohol which absorbs electrolyte of the composition, given in Table I, to a very limited extent. This action releases the colloid present, e.g., locust bean gum, which then absorbs electrolyte. This combination provides a stable adhesive mass which readily contacts the aluminum anode, allowing the battery to have both good keeping quality and delayed service characteristics. The paper serves a dual purpose. It serves as a carrier for the resin-bonded film and as a barrier layer to maintain the colloid layer at the anode.

Although only a limited number of batteries was available with the polyacrylamide film, which was not of the resin-bonded type, the data show that it is a satisfactory film separator for this system. These data show that it is not completely the equivalent of the resin-bonded gum separator but could be employed if less stringent service requirements are demanded.

Conclusions

It is believed that these studies have contributed materially to the improvement and advancement of the aluminum dry cell. The establishment of a satisfactory separator medium removes one additional limitation of this system. The discovery of a separator which will provide adequate stability and improved keeping quality should permit further progress and study of the other phases of the aluminum-manganese dioxide system.

Manuscript received Dec. 5, 1958. This paper was prepared for delivery before the Ottawa Meeting, Sept. 28-Oct. 2, 1959.

Any discussion of this paper will appear in a Discussion Section to be published in the December 1959 JOURNAL.

REFERENCES

1. J. J. Stokes, "The Aluminum Dry Cell," paper presented at the Pittsburgh Meeting of The Electrochemical Society, Oct. 10, 1955.
2. S. Ruben, U. S. Pat. 2,638,489, May 12, 1953.
3. J. J. Stokes, U. S. Pat. 2,796,456, June 18, 1957; U. S. Pat. 2,838,591, June 10, 1958.
4. N. C. Cahoon, U. S. Pat. 2,534,336, Dec. 19, 1950.
5. N. C. Cahoon and M. P. Korver, *This Journal*, **105**, 292 (1958).

On the Internal Resistance of Dry Cells

A New Pulse Method

Ralph J. Brodd

National Bureau of Standards, Washington, D. C.

ABSTRACT

The internal resistance of Leclanché cells of various sizes and manufacture was measured by imposing a current pulse on the cell and observing the instantaneous *IR* drop in the cell. The internal resistance of Leclanché cells was determined also as cells were discharged on various standard tests and on continuous or momentary current drains. The increase in internal resistance of the cells on discharge depended on the type of discharge, cell size, and manufacture. The use of the internal resistance of a Leclanché cell to estimate the life expectancy of the cell is suggested.

The internal resistance of Leclanché cells and its measurement have been controversial subjects for many years. In one of the oldest and probably the most universal method (1) the internal resistance of a cell is determined by employing the equation:

$$\text{Internal resistance} = \frac{V - V'}{I} \qquad [1]$$

where V is the open-circuit voltage of the cell and V' is the voltage when current I flows in through the cell. The resistance measured in this fashion is a sum of the resistances of all parts of the cell plus the resultant of any emf including polarizations generated in the cell. Also the resistance depends on the current, age of the cell, temperature, and degree of exhaustion of the cell. In a similar method in wide use today (2) the short-circuit current (SCC) is measured with a critically damped ammeter having a total resistance including the leads of 0.01 ohm. In this instance the ratio V'/I in Eq. [1] is replaced by 0.01. The Wheatstone bridge and the method of charging capacitor are other d-c methods that have been used to measure the resistance of a cell.

Recently, a new d-c method for measuring the internal resistance of dry cells has been reported (3). The *IR* drop of a cell occurring in 10^{-3}-$^{-4}$ sec was measured on an oscilloscope when current pulses were drawn from the cell. The internal resistance of the cell could be calculated by applying Ohm's law, knowing the current in the pulse. In recent years a-c bridge techniques (4-6) for measuring resistance have been employed in an effort to eliminate errors caused by polarization of the electrodes of a cell.

A method for measuring the internal resistance of

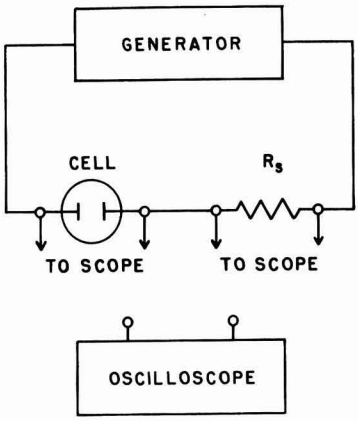

Fig. 1. Schematic diagram of circuit

dry cells is described below wherein the errors caused by polarization of electrodes are reduced to a minimum. The usefulness of this method will be illustrated by measuring the internal resistance of Leclanché cells as they are discharged on momentary drains, on various standard tests, and through constant resistance.

Experimental

A schematic diagram of the circuit used to determine the internal resistance of Leclanché cells is shown in Fig. 1. The pulse generator was a Hewlett-Packard Model 212. The oscilloscope was a Tektronix Model 532. The resistance standard was a deposited carbon resistor of known value. To measure the internal resistance of a Leclanché cell, the oscilloscope leads were connected across the dry cell in Fig. 1 and the instantaneous *IR* drop measured at the trailing edge of the pulse. The instantaneous drop of the oscilloscope pattern occurred in 10^{-7} sec or less. The oscilloscope was connected across the resistance standard, the instantaneous *IR* drop of the resistor was noted, and the current in the pulse was calculated by applying Ohm's law. From this value of the current in the pulse, the resistance of the dry cell was calculated by applying Ohm's law to the *IR* drop in the cell in the first measurement. Typical oscilloscope traces for these measurements are shown in Fig. 2.

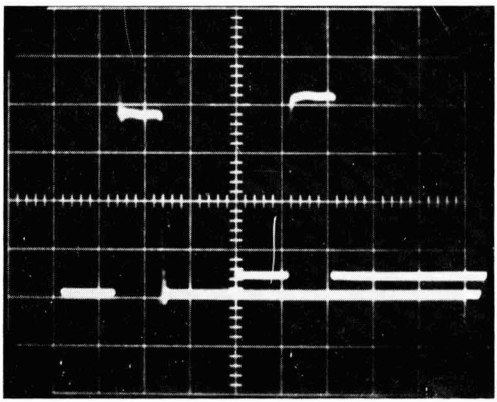

Fig. 2. Typical oscilloscope traces: trace of current pulse through cell on left (0.05 v/cm), trace of current pulse through standard resistor (10 ohms) on right (5.0 v/cm), pulse length 3 μsec.

The effects of both momentary and continuous current drain (in addition to the constant drain by the generator of about 10^{-4} amp) on the internal resistance of Leclanché cells were also investigated. In these cases a loading resistor was connected across the cell. The current drain was calculated by measuring the voltage drop in the resistor with a potentiometer and applying Ohm's law. The internal resistance of the cells was determined in the fashion described above. However, in this case the loading resistor and cell were in parallel. In investigating the effect of momentary drain, measurements of the internal resistance and current drain were made as rapidly as possible so the capacity of the cell would remain essentially unchanged. Measurement of the highest drain was made first; the lowest drain was made last. This procedure was then reversed. The internal resistance with no load was measured after each current drain.

The internal resistance of Leclanché cells was determined also as the cells were discharged on the general purpose 4-ohm intermittent test (4-ohm test), the general purpose 2.25-ohm test (2.25-ohm test), and the light industrial flashlight test (LIF test) (7).

Results and Discussion

When the resistance of a circuit, in this case a Leclanché cell, is determined it is necessary to ascertain whether the measured resistance includes other impedance components than the purely resistive component. In order to establish that the resistance of Leclanché cells measured by the pulse technique had the characteristics of a purely resistive element, the effects of varying various experimental parameters on the value of the measured internal resistance of the cells was investigated first. The current in the pulse was varied from 0.008 to 3.96 amp with no change in the internal resistance of the cell. Likewise there was no change in the internal resistance of the cell when the direction of the pulse was reversed or when the repetition rate of the pulse was altered from 100 to 5000 pulses per second. The measured internal resistance of the cell did not change when the pulse length was varied from 1 to 10 μsec. Thus, the measurement of the internal resistance of Leclanché cells by this method appears to fulfill the conditions for the measurement of the resistive portion of the cell; that is, the current pulse and the voltage pulse have the same shape and the ratio E/I is independent of variations in magnitude and sign of the current, repetition rate, and length of the pulse.

The internal resistance of fresh undischarged AA-, C-, and D-size cells (R_i) is found in Table I. The group number has no significance from one cell size to the other. Also reported in Table I are the open-circuit voltage (OCV), the short-circuit current

Table I. Characteristics of various Leclanché cells, standard specification tests

Group	R_i, ohm	OCV, v	SCC, amp	LIF P.T., min	LIF R_f, ohm	2.25-ohm P.T., min	2.25-ohm R_f, ohm	4-ohm P.T., ohm	4-ohm R_f, ohm
D-size cells									
1	0.146	1.58	8.6	696	0.2	581	0.7	805	0.5
2	0.147	1.60	8.7	709	0.5	486	1.0	807	—
3	0.152	1.58	7.0	616	1.1	420	1.6	618	—
4	0.153	1.61	7.7	789	0.4	518	—	873	—
5	0.178	1.59	6.9	870	0.3	631	1.5	1014	1.0
6	0.180	1.57	6.7	471	0.6	323	0.8	575	—
7	0.186	1.64	6.8	657	0.4	473	0.7	808	0.9
8	0.196	1.61	6.1	828	0.3	647	—	931	1.2
C-size cells									
1	0.196	1.59	6.3					407	1.2
2	0.271	1.61	5.0					468	0.9
3	0.353	1.62	3.7					405	1.0
AA-size cells									
1	0.167	1.64	4.1					146	0.5
2	0.192	1.56	5.2					127	0.6
3	0.232	1.57	4.7					117	0.8
4	0.379	1.58	3.2					136	0.6
No. 6 size cells									
1	0.0465	1.64	27.4						
2	0.031_8	1.65	30.3						
3	0.038_9	1.59	32.9						

(SCC), the performance on test (P.T.), and the internal resistance at the cutoff voltage (R_f) of the cells when discharged on the LIF, 2.25-ohm, and 4-ohm tests. All values in Table I are the arithmetic mean of three or more cells. The values of the R_f should be considered only as an indication of the internal resistance of the cell at the cutoff voltage as some of the cells were discharged past the cutoff voltage before their internal resistance could be measured. An examination of Table I fails to reveal a general relation between R_i and R_f of a cell and its performance on test. In general, the SCC increases as the internal resistance decreases. It is also noted that the internal resistance of all the cells increased on discharge. The internal resistance computed from the SCC and OCV is always larger than the internal resistance measured by the pulse method.

The effect of current drain of momentary duration on the internal resistance of an undischarged cell is shown in Table II. After each drain, the internal resistance of the cell with no load was measured. The internal resistance with no load remained constant. The internal resistance of the cells in Table II remained essentially constant at all current drains with a slight tendency to increase at the highest current drain. These results do not confirm the work of other investigators (3, 8) who reported that the internal resistance of Leclanché cells decreased as the momentary current drain increased.

Table II. Effect of momentary current drain on the internal resistance of Leclanché cells

D-size cells		C-size cells		AA-size cells	
Drain, ma	Internal resistance, ohm	Drain, ma	Internal resistance, ohm	Drain, ma	Internal resistance, ohm
0	0.180	0	0.220	0	0.274
1.54	0.180	1.52	0.220	0.42	0.273
15.4	0.180	15.1	0.220	14.1	0.273
32.4	0.178	32.0	0.220	29.6	0.272
149.	0.180	146.	0.221	133.	0.276
508.	0.180	480.	0.225	426.	0.282
1156.	0.186	1141.	0.230		

These investigators interpreted their results by postulating an adsorbed film of hydrogen on the zinc electrode. It is possible that the oscillations observed at the leading edge of the pulse in Fig. 2 are caused by the destruction of an adsorbed film of hydrogen on the zinc electrode. If this is the case, there is no conflict in results.

The discharge behavior of AA, C, and D cells from one manufacturer was determined. The typical behavior of AA- and C-size cells as they were discharged on the 4-ohm test is shown in Fig. 3 and 4, respectively. The typical behavior of D-size cells as

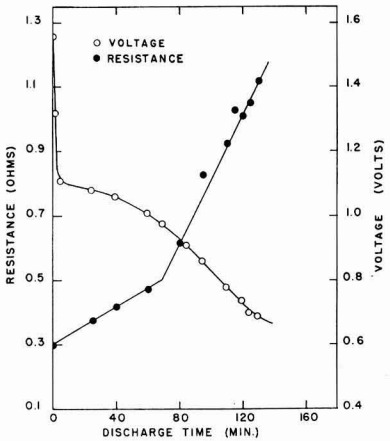

Fig. 3. Behavior of AA-size cell on the 4-ohm test.

Table III. Discharge characteristics of Leclanché cells from one manufacturer

	AA-size cells, 4-ohm test		C-size cells, 4-ohm test		D-size cells, LIF test	
	A.M.	σ_s	A.M.	σ_s	A.M.	σ_s
P.T. (min)	117.	7.6	373.	71.	648.	21.
R_i (ohms)	0.269	0.042	0.215	0.027	0.188	0.012
R_f (ohms)	0.85	0.12	0.915	0.093	0.415	0.042
ΔR (ohms)	0.589	0.076	0.70	0.11	0.227	0.39
$S \times 10^{-4}$ (ohms/min)	28.3	3.4	9.3	3.4	3.46	0.61
T_b (min)	71.0	5.9	243.	56.		
R_b (ohms)	0.470	0.042	0.44	0.10		
E_b (volts)	0.981	0.17	1.05	0.05		

they were discharged on the LIF test is shown in Fig. 5. A summary of the results of discharges of 6 cells of each size is given in Table III, where the arithmetic mean, A.M., and the standard deviations, σ_s, are given for P.T., R_i, R_f, the change in resistance during discharge, ΔR, the slope of the plot of discharge time vs. internal resistance, S. In the case of AA- and C-size cells the discharge time, T_b, internal resistance, R_b, and voltage, V_b, are given at the point of departure from initial linear behavior of the internal resistance-discharge time plot. D-size cells were discharged past 0.6 v on the LIF test with no change in the slope, S. P.T. for control samples of each size cell was within 3% of the values in Table III.

In Fig. 6 the behavior of the internal resistance of AA-size cells is shown as they were discharged continuously through the fixed resistances noted in the figures. The arrows indicate the point at which the cell voltage was 0.8 v. If the discharges were stopped at any point, the internal resistance of the cell remained constant even though the cell voltage recovered to its normal value. C-size cells exhibit behavior similar to that for AA-size cells shown in Fig. 6.

A common feature of the discharges through fixed resistances or on the standard tests was the increase in the internal resistance of the cells as the discharge continued. In general, it was found that the lower values of R_i corresponded to the lower values of R_f. One of the most interesting possibilities that the data in Table III suggest is the use of the internal resistance of a cell to estimate life expectancy for a particular test or use. Unfortunately, the variation of the internal resistance of Leclanché cells with group found in Table I makes impossible any general statements. It appears possible, however, to make a calibration for each group of cells, as Table III and Fig. 3, 4, and 5 illustrate, and then to use the calibration for predictions of life expectancy. For instance, if the internal resistance of D-size cells of the same group as those in Table III increased 0.113 ohms from R_i (refer to Table III and Fig. 5) it would have a life expectancy of 324 min on the LIF test. Similar predictions can be made for the C-and AA-size cells allowing for the change in slope of the plot of time on discharge vs. internal resistance. Of

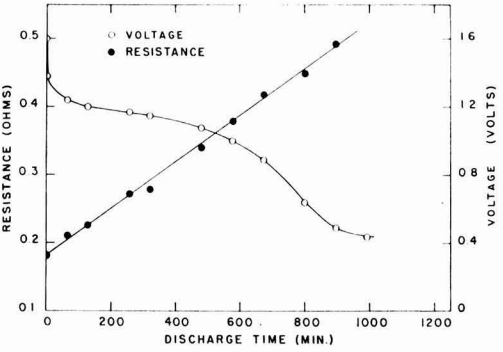

Fig. 5. Behavior of D-size cell on the LIF test.

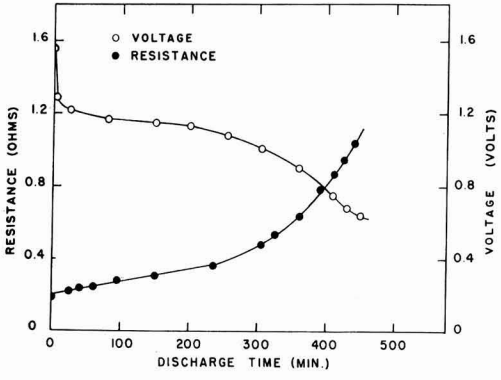

Fig. 4. Behavior of C-size cell on the 4-ohm test.

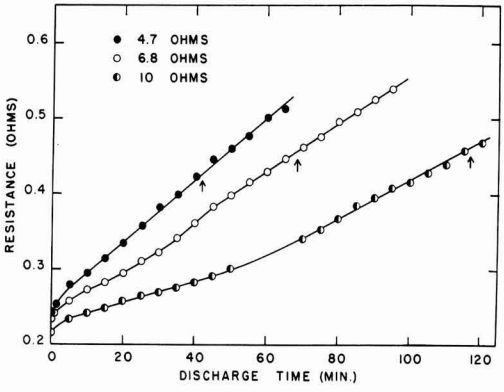

Fig. 6. Behavior of AA-size cells discharged continuously through 4.7, 6.8, and 10 ohms.

course, the predictions are subject to the same statistical errors as the calibration. Investigations are under way to determine if the decrease in life expectancy with age can be predicted from measurements of the internal resistance of the cell. Recently (9) a method for predicting the capacity of a battery has been reported. It is based on repeated short discharges measuring the current and voltage of the battery during discharge.

Acknowledgment

The author wishes to thank H. J. DeWane for his advice and help in conducting the standard specification tests.

Manuscript received Sept. 2, 1958. This paper was prepared for delivery before the Buffalo Meeting, Oct. 6-10, 1957.

Any discussion of this paper will appear in a Discussion Section to be published in the December 1959 JOURNAL.

REFERENCES

1. D. L. Ordway, *Trans. Electrochem. Soc.*, **17**, 341 (1910).
2. G. W. Vinal, "Primary Batteries," p. 133, John Wiley & Sons, Inc., New York (1950).
3. R. Glicksman and C. K. Morehouse, *This Journal*, **102**, 273 (1955).
4. N. C. Cahoon, *Trans. Electrochem. Soc.*, **92**, 159 (1947).
5. W. Heubner, *Elektrotech. Z.*, **61**, 149 (1940).
6. J. Euler and K. Dehmelt, *Z. Elektrochem.*, **61**, 1200 (1957).
7. National Bureau of Standards "Specifications for Dry Cells and Batteries," Circular 559 (1955).
8. W. K. Chaney, *Trans. Electrochem. Soc.*, **29**, 183 (1916).
9. G. B. Ellis, U. S. Pat. 2,853,676, Sept. 23, 1958.

Iodine-Activated Solid Electrolyte Cell for Use at High Temperature

Joseph L. Weininger

Research Laboratory, General Electric Company, Schenectady, New York

ABSTRACT

Iodine-activated miniature cells, Ta(I_2)/AgI/Ag, with solid silver iodide as the electrolyte, have been studied at 150°-550°C. In this range of temperatures the cells have the following characteristics: complete conversion of the consumable silver anode into its electrical equivalent, open-circuit voltage of 0.67 v, short-circuit currents up to 18 ma, capacity of 10 ma-hr, energy output up to 5 mw-hr/cell, a definite activation temperature obtained by selecting a suitable source of iodine vapor, and indefinitely long shelf life below that temperature. The size of the smallest cells is 0.15 cm in diameter and 0.5 cm in length.

Recently halogen-activated solid-electrolyte cells were discussed from a general viewpoint with regard to their history, mechanism, and applications (1). They have the advantage of simpler construction over cells with liquid electrolytes. By reducing the size and weight of individual cells, batteries can be miniaturized. However, solid electrolyte cells have high internal impedance which limits the short-circuit currents to a few microamperes at room temperature. The high-temperature modification α-AgI, which is stable in the range of 146°-552°C is one of the few ionic compounds with large ionic conductivity. Therefore, a study was made of primary cells with an α-AgI electrolyte in that temperature range.

Tantalum-Tube Cells

Figure 1 is a schematic drawing of the cell. The cathode is a tantalum tube containing a "cathode mix," which is a source of the cathode reactant, iodine vapor. The cathode mix may be itself iodine or a suitable chemical system which will produce iodine at a definite elevated temperature. In the course of assembly, the tube is sealed with silver iodide in a stream of dry nitrogen. A silver anode is imbedded then in the iodide, the source of iodine is added, and the other end of the tube is sealed by cold-welding under vacuum. A photograph of one of the first models, which was about 9 mm long, indicates the possibility for miniaturization (Fig. 2). The silver anode can be seen as it protrudes out of

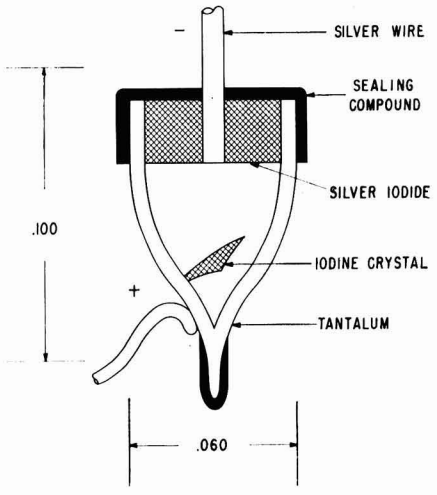

Fig. 1. Schematic of Ta-tube cell

Fig. 2. Photograph of Ta-tube cell

the electrolyte located in the tube. Most of the cell volume is taken up by the iodine reservoir which can be reduced considerably.

The electrode and cell reactions are:

At the anode	$Ag = Ag^+ + e^-$	[1]
At the cathode	$\frac{1}{2}I_2 + e^- = I^-$	[2]
Cell reaction	$Ag + \frac{1}{2}I_2 = AgI$	[3]

Thus, the silver anode is consumed with formation of additional electrolyte, AgI, as the product of the cell reaction.

Preliminary Experiments with Iodine Depolarizer

In preliminary experiments, cells with elemental iodine as the cathode mix as well as cathode reactant were investigated. The following is a typical performance of such a cell, which was 0.477 cm (3/16 in.) long and had an outside diameter of 0.159 cm (1/16 in.): Current-voltage curves at room temperature and at 170°C resulted in the data of Fig. 3. The internal resistance at 170°C was only 40 ohms; hence short-circuit currents were larger than 5 ma. Theoretical open-circuit voltage (0.67 v) also was achieved. With a load of 10 kΩ, 0.11 ma-hr were obtained. This and other cells failed as high temperature was approached because boiling iodine (bp 188°C) burst the cathode tube. For complete cell reaction each cubic centimeter of silver would require the equivalent amount of 1.9 liters of iodine vapor at 1 atm and 200°C. Thus, in the preliminary experiments the cell volume was too small to contain all the iodine vapor. Generally, if maximum capacity, high-temperature operation, and miniaturization are desired, then iodine must be introduced and remain in the cell, as far as possible, in a condensed state.

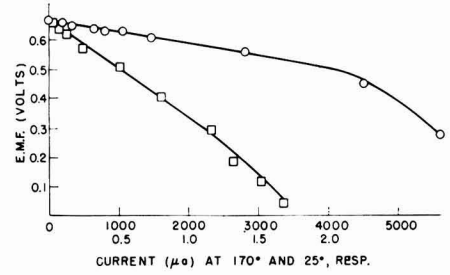

Fig. 3. Current-voltage curves for a cell with iodine as the cathode reactant at 25° (lower curve) and 170°C (upper curve).

Methods of Activating Cells

Two methods were employed to achieve high-temperature stability and gradual evolution of iodine, so that iodine could be used in the cell without building up undue vapor pressure. First, a polyiodide was used which was in thermodynamic equilibrium with iodine over a fairly wide temperature range. In the case of cesium polyiodides, a very thorough study was made by Briggs and co-workers for cesium iodide + iodine + water (3), and for iodine + cesium iodide (4). Second, certain oxidation-reduction reaction mixtures, e.g., $Cu_2I_2 + KMnO_4$, evolved iodine slowly at high temperatures. These systems were investigated by thermogravimetric analyses.

Activation by Decomposition of Iodine Compounds

The following compounds were suitable sources of iodine above the boiling point of iodine: CsI_4, CsI_3, BiI_3, I_2O_5, and CHI_3. In the present work, emphasis was placed on cesium polyiodides as sources of iodine because they decompose at temperatures consistent with their use in tantalum-tube cells.

Preparation of CsI_3 *and* CsI_4

Precipitation from aqueous solutions and crystallization from the melt (in the case of CsI_4) were used to prepare the compounds. As starting material CsI C. P. was added to an aqueous solution of iodine from which precipitation of CsI_3 or CsI_4 took place. Another method involved mixing in stoichiometric ratio 2 mole CsI and 3 mole I_2. This mixture was sealed in a quartz tube under vacuum and raised to 235°C. It was cooled slowly to 135°C and equilibrated at that temperature for 16 hr. Samples were checked for iodine content by wet analysis on a routine basis, and the existence of the tri-iodide and tetraiodide was established in this manner. Samples were also analyzed by x-ray diffraction. The Debye-Scherrer pattern of CsI_4 was not known. In fact, crystals of CsI_4 were identified as I_2O_5. A literature check showed that the pattern given by Hanawalt, *et al.* (5) for I_2O_5, which is accepted as the ASTM standard, also matched the pattern of our sample of CsI_4. To prove our sample as CsI_4, the cesium content was also determined by wet analysis (Table I).

Table I. Analysis of CsI_4 prepared by crystallization from the melt

	Theor. wt (%)	Found
Iodide content	79.3	78.2
Cesium content	20.7	22.7

Table II. Thermolysis data for decomposition of iodine compounds

Sample	Atmosphere	Primary temp. range, °C	Other temp. ranges, °C	Mechanism	Weight loss	
					Theoretical, %	Experimental (thermobalance), %
I_2O_5	Dry N_2	350-430	—	$I_2O_5 \rightarrow I_2\uparrow + 2\frac{1}{2}\,O_2\uparrow$	100	98.8
MgI_2	Dry N_2	145-250	300-400	$MgI_2 \rightarrow Mg + I_2\uparrow$	91.1	89.5
BiI_3	Dry N_2	300-359	359-520 80-120	$BiI_3 \rightarrow BiI + I_2\uparrow$	43.0	42.9
BiI_3	Dry O_2	285-320	400-480 85-95	$BiI_3 \rightarrow BiI + I_2\uparrow$ or $2BiI_3 + 1\frac{1}{2}\,O_2 \rightarrow Bi_2O_3 + 3\,I_2\uparrow$	43.0 39.0	42.2
CsI_4	Dry N_2	155-230	90-155	$CsI_4 \rightarrow CsI + 1\frac{1}{2}\,I_2\uparrow$	58.1	57.7
CsI_4	Dry O_2	142-225	95-140	$CsI_4 \rightarrow CsI + 1\frac{1}{2}\,I_2\uparrow$	58.1	56.8*

* This weight loss determined on analytical balance.

Application of Phase Diagram CsI-I_2 to Solid Electrolyte Cells

By means of the phase diagram, one can choose a suitable cesium polyiodide as the source of iodine. A composition is required which in the desired temperature range will have a vapor pressure of iodine smaller than 1 atm.

Traces of iodine would be sufficient to produce an appreciable open-cell voltage of the cell Ta(I_2)/AgI/Ag, but they could not sustain any current output. Hence, the phase diagram of CsI-I_2 may be used to estimate the temperature ranges in which sufficient iodine will be produced to maintain appreciable current density. Thus, iodine first should appear on heating at about 138°C in the case of CsI_4, and at 210° in the case of CsI_3. If it is desired to avoid melts rich in iodine, one can shift the composition of the CsI-I_2 mixture toward more CsI, e.g., an over-all composition of 60 mole % CsI and 40 mole % I_2. Such a source of iodine would form less iodine vapor below 306°C than others described previously which also contain CsI_4. The phase diagram of reference (4) refers, however, to the open system CsI-I_2 at a pressure of 745 mm, whereas in the cells the polyiodide is in a closed system. In the latter system the iodine pressure increases from vacuum to 1 atm below 306°C as the decomposition reaction proceeds. This difference in the atmospheric environment of the polyiodide will lead to slightly different values for transition temperatures and vapor pressures of the cell as compared to the phase diagram.

Thermolyses of Iodine Compounds

The results of thermobalance measurements of iodine compounds are shown in Table II. Samples were tested in dry oxygen or dry nitrogen to detect any oxidation reactions. In the case of BiI_3 and CsI_4 the oxide was not formed, but decomposition took place in steps. This is indicated in Table II by primary and other temperature ranges. The primary range refers to the temperature interval in which the major part of the decomposition occurred. The other temperature ranges of the next column are those in which smaller weight changes took place. Weight losses to 560°C were considered as final and are compared with calculated values based on the reactions indicated in the table. In each case agreement was very good so that with these compounds the existence of the required iodine-producing reaction is proved.

Activation by Oxidation of Iodides

Mechanism

The second mechanism of activation of tantalum-tube cells is based on the oxidation of an iodide to iodine vapor, e.g.

$$Cu_2I_2 + O_2 \rightarrow 2CuO + I_2\uparrow \qquad [4]$$

This reaction takes place at 240°C, which is the temperature of activation for a cell with Cu_2I_2 as the iodine-source, if oxygen or air is present. If it is desired to achieve a higher activation temperature, one may introduce oxygen chemically bound in compounds such as $KMnO_4$ or KIO_3. These decompose at a higher temperature, and the oxygen formed in the initial decomposition step will react then with Cu_2I_2 above 240°C to produce the necessary iodine vapor, e.g.

$$KIO_3 \rightarrow KI + 3/2\ O_2\uparrow \qquad (\leqq 330°C) \qquad [5]$$

followed by reaction [4] at a temperature above 240°C. Thus, the temperature of activation of tantalum-tube cells may be increased by finding a compound which will give off oxygen at the desired temperature.

Cuprous iodide was used as the source of iodine. When oxygen was added in the form of $KMnO_4$ or KIO_3, the tube was sealed under vacuum. When molecular oxygen was the oxidizing agent, the tube likewise was closed off, but without evacuation. This caused leaks to develop in the cell on heating because of the expanding air. The leaks were necessary to provide a fresh supply of oxygen as the original amount was used up.

Thermolyses of Reaction Mixtures

The thermogravimetric data of iodine-reaction mixtures are listed in Table III. Figure 4 shows the thermobalance curves for cuprous iodide in the presence and absence of oxygen. In dry nitrogen there was 0.6% weight loss at 550°C, which is negligible. The curve of Cu_2I_2 + dry O_2 confirms the temperature of 240°C as the temperature at which reaction [4] takes place (6). In the experiment, 92.2% of the theoretical weight loss corresponding to this reaction had occurred.

Table III. Thermolysis data for iodine-reaction mixtures

Sample	Atmosphere	Primary temp. range, °C	Other temp. range, °C	Mechanism	Weight loss: Theoretical, %	Weight loss: Experimental (thermobalance), %
Cu_2I_2	Dry N_2	No reaction				
Cu_2I_2	Dry O_2	249-330	—	$Cu_2I_2 + O_2 \rightarrow 2CuO + I_2 \uparrow$	58.2	54.0
2.5 Cu_2I_2 + KIO_3	Dry N_2	262-330	332-550	$KIO_3 \rightarrow KI + 3/2\ O_2 \uparrow$ $3/2\ O_2 + 3/2\ Cu_2I_2 \rightarrow 3CuO + 3/2\ I_2 \uparrow$	67.4	66.5
KIO_3	Dry N_2	480-540	540 up	$KIO_3 \rightarrow KI + 3/2\ O_2 \uparrow$	77.6	Reaction not complete at high-temperature limit (620°C)

Figure 5 is the thermobalance curve of a mixture of 2.5 Cu_2I_2 + KIO_3 in dry nitrogen. It shows two separate reaction steps at 260° and 330°C. The weight loss is the result of the oxidation of Cu_2I_2 by oxygen (cf. Fig. 4), but the two steps indicate the successive loss of oxygen from KIO_3, first a partial decomposition to KIO_2, then an accelerated decomposition to KI. This is in agreement with the thermolysis of pure KIO_3, which also takes place in two steps, but at temperatures about 200° higher than in the presence of Cu_2I_2. This lowering of the reaction temperature by a catalyst has been observed in a similar system, that of $KClO_3$ catalyzed by CuO (7). A limitation to a thermogravimetric study of this type is that the oxygen formed would not react entirely with the Cu_2I_2. However, the comparison of the two curves of Fig. 5 and the evidence of the thermolysis of Cu_2I_2 + dry nitrogen, in which Cu_2I_2 did not decompose below 500°C, confirm that KIO_3 decomposes first and then reacts with Cu_2I_2 in the cathode-mix of the solid electrolyte cell.

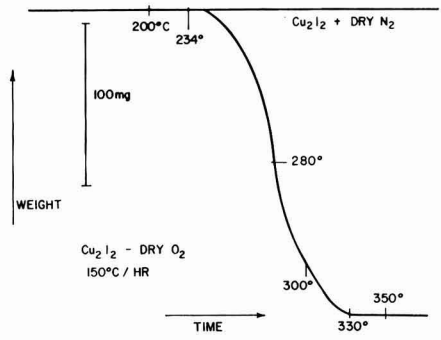

Fig. 4. Thermobalance curves of Cu_2I_2, heated in dry O_2 and N_2, respectively, at 150°/hr (initial wt: 0.3531 g and 0.3205 g, respectively).

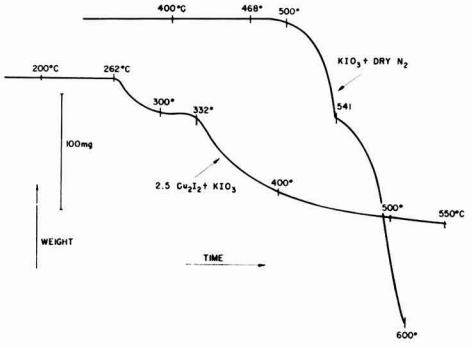

Fig. 5. Thermobalance curve of a mixture 2.5 Cu_2I_2 + KIO_3, (initial wt = 0.3921 g) and KIO_3 + pure N_2 (initial wt = 0.8822 g), heated at 150°/hr.

Another interesting aspect of the thermobalance curve of the mixture Cu_2I_2 + KIO_3 is the weight loss of the mixture, which proceeds quite slowly. This indicates, in comparison with the thermolyses of the individual components, that the production of oxygen is likewise slow. This makes it possible to reach the high-temperature limit of the cell if oxygen is not evolved too rapidly. The reaction mixture of 2.5 mole of Cu_2I_2 per mole of KIO_3 contains an excess of 40% iodide. Assuming that all of the oxygen originally present in KIO_3 is used up in the formation of I_2 from Cu_2I_2, the thermobalance curve shows that at 550°C the reaction was 98.8% complete. This supports the proposed mechanism of decomposition and oxidation.

Results

Performance data.—Cells with the first type of iodine source behaved similarly once the characteristic decomposition of the iodine donor was reached. Besides the iodides listed in Table II, the following compounds were tested successfully as sources of iodine at elevated temperatures: CsI_3, CsI_3 + CsI, Cu_2I_2, CHI_3, and CI_4. Cu_2I_2 reacted with oxygen or oxidizing agents. The organic compounds, CHI_3 and CI_4, were intended primarily as radiation-sensitive iodine compounds which would decompose and trigger off a solid electrolyte cell. For this application CHI_3 and also CBr_4, with the corresponding AgBr electrolyte, are promising, but CI_4 is too unstable at room temperature to act as a radiation detector. Instead, it has a good response to thermal activation in the range 145°-169°C.

In the second type of iodine source, i.e., oxidation couples of iodides, Cu_2I_2 was tested with O_2, $KMnO_4$, and KIO_3, respectively. Results obtained with both types are discussed below.

Temperature response can be obtained from 145° to 500°C. Thus, CsI_4 or CI_4 depolarize satisfactorily at the lower temperature limit; BiI_3, CsI_3, and mixtures of CsI_3 and CsI can be used up to about 320°, and finally, by means of the oxidation couples, e.g., Cu_2I_2 + $KMnO_4$, one can reach the high-temperature limit. Shelf life is unlimited below the activation temperature, because free iodine is absent before

thermal activation of the depolarizer. Capacity and energy-output of cells, whether in series or separately, were as high as 14.4 ma-hr for a single cell of $Cu_2I_2 + KIO_3$ depolarizer or 7.12 ma-hr and 3.62 mw-hr for a battery (four CsI_4 cells in series). Conversion of active cell materials by the cell reaction into their electrical equivalent was nearly complete. The capacity of the cells was limited either by the amount of iodine or silver available to the cell, but generally it is the quantity of silver present as the consumable anode which is limiting. Only in the case of one cell (cathode-mix $Cu_2I_2 + KIO_3$) was the capacity limited by the amount of available iodine. There, 78% of the iodine was converted into its electrochemical equivalent (chemically, into AgI). The open-circuit voltage (OCV) of 0.67 v, equal to the calculated emf of the AgI system based on thermal values at 25°C, was obtained with most cells, although the cells were operated at high temperature. This can be explained qualitatively by the decrease in the free energy of formation of AgI with increasing temperature which is counterbalanced by an increase as a result of higher iodine pressure. This was not the case with oxidation couples. The OCV usually dropped to a lower value after prolonged loading of the cells, but occasionally it recovered to its original value. Complete recovery of OCV was again a question of proper cell design. Likewise, the short-circuit current and internal impedance of cells depended on their structure. Best values of 18 ma and 11 ohms were obtained with a cell of flat tube design (CI_4 depolarizer), but in that case the capacity was only 3.6 ma-hr. It is difficult to estimate a current density for this cell because the dimensions of the silver anode change with time, but at least in its initial operation the surface of the wire anode is known. If 0.159 cm (1/16 in.) is immersed in the solid electrolyte, then the short-circuit current of 18 ma corresponds to about 290 ma/cm^2. The response to activation also depends on the design of the cell. On heating the cell above 145°C from room temperature, the attainment of open-cell voltage required about 1 min or less, whereas proper current response required several minutes of activation.

Tables IV and V show performance data characteristic of the two different sources of iodine. There was considerable variation from cell to cell with regard to internal resistance and capacity, but this is to be expected from the dimensions of the cells, in which the silver anode was a wire 0.127 cm long, imbedded in a solid electrolyte within a tube with inside diameter of about 0.23 cm. The electrochemical equivalent of 0.159 cm (1/16 in.) length of such a silver wire is 5.32 ma-hr. The conversion of silver into the equivalent number of coulombs is described, for brevity, below and in the figures as "percent yield of Ag." Complete utilization of silver can also be demonstrated by microscopic examination of the original locus of the silver anode which has been converted completely into silver iodide. The difference in texture between the original AgI electrolyte and that formed in the course of the experiment gives a clear picture of the cell reaction. A lower but steady output is obtained when one uses smaller diameter tubing. Thus, Fig. 6 shows the discharge

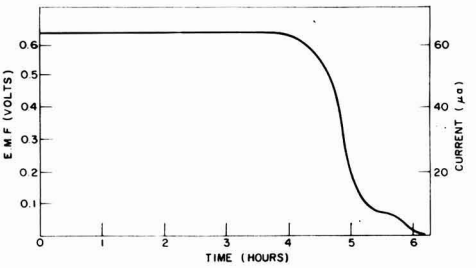

Fig. 6. Ta-tube cell on 10 kΩ load at 300°C; source of iodine: CsI_4; capacity 0.370 ma-hr, theoretical 0.435 ma-hr.

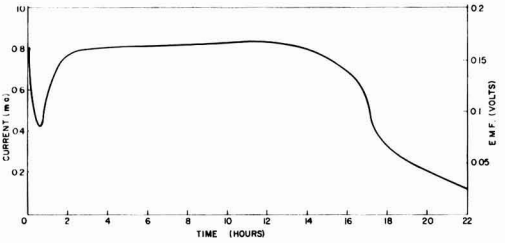

Fig. 7. Ta-tube on 200 Ω load at 258°C; cathode mix: $Cu_2I_2 + KIO_3$; output 14.43 ma hr, 2.32 mw-hr.

Table IV. Performance of AgI cells with thermally activated iodine compounds as iodine sources

No. of cells	OD of Ta-tube, cm	Depolarizer	Temp. of operation, °C	Open-cell voltage, v	Short-circuit current, ma	Internal resistance, ohms	Capacity, ma-hr	Notes
1	0.159	CsI_4	300	0.65	4.0	140	—	
1	0.318	CsI_4	250	0.675	1.5	440	5.23	Discharge at 1 kΩ.
1	0.159	CsI_4	300	0.63	0.5	1510	0.37	3 ma at 0.25 v, per cent yield: 85% Ag, see Fig. 6.
4	0.318	CsI_4	225	2.55	5.8	250	7.19	Energy output 3.62 mw-hr.
1	0.318	CsI_4	265	0.60	11.0	55	3.76	Operated also at 520°C.
5	0.318	CsI_3	250	3.25	6.0	540	0.85	Failure caused by bad contact.
4	0.318	I_2O_5	250	2.75	7.0	130	6.45	
1	0.318	BiI_3	308	0.59	3.0	200	3.22	Temperature may have been slightly too low for BiI_3 the source of iodine.
1	0.318	CHI_3	287	0.63	2.2	320	0.31	
1	0.318	CI_4	170	0.68	6.0	120	10.1	Energy output 1.03 mw-hr.
1	0.318	CI_4	180	0.655	2.4	270	11.2	Energy output 1.43 mw-hr.

Table V. Performance of AgI cells with Cu_2I_2 plus oxidizing agent as iodine sources

Oxidizing agent	Temp. of operation, °C	Open-cell voltage, v	Short-circuit current, ma	Internal resistance, ohms	Capacity, ma-hr	Notes
Air	450	0.95	~34	28	8.58	Two cells in series.
Air	422	0.45	~12	35	5.23	
$KMnO_4$	450	0.60	3.0	120	2.6	
$KMnO_4$	330	0.56	1.2	625	5.5	
$KMnO_4$	450	0.45	—	—	0.53	
KIO_3*	258	0.55	~2.5	200	14.43	Energy output, 2.32 mw-hr.
KIO_3	287 and 360	0.66	>10	11	5.22	1.56 mw-hr. At 360°C obtained capacity of 4.80 ma-hr compared to 0.42 ma-hr at 287°C.
KIO_3	275	0.655	1.2	1320	7.78	Consumed 78% of total iodine present in Cu_2I_2.

* See Fig. 7.

of a cell with small outside diameter across 10-kΩ load. Figure 7 gives the performance of a larger cell. The minimum near the beginning of this discharge curve can be attributed to the relatively low temperature of operation (258°C) for the $KIO_3 + Cu_2I_2$ cathode mix of this cell. The minimum is not a characteristic of the cathode mix or the cell. In other cases, the current terminated abruptly, which indicated that all of the silver anode had been used up.

Comparison of cell performance with thermobalance experiments.—The cells could be operated in definite temperature ranges which were somewhat lower than the temperature of decomposition of the iodine donor obtained from thermobalance curves. This can be explained by the temperature lag between the recording thermocouple and the sample, which would give slightly higher temperature readings in the thermolyses. Also, in the decomposition mechanism an equilibrium or steady-state reaction occurs at constant temperature at which the iodine donor decomposes. The equilibrium may be displaced toward lower temperatures if iodine is removed constantly by the cell reaction.

Thermoactivation current and emf.—By employing a technique similar to that of the thermobalance one can use the solid electrolyte cell as a halogen detector. The cell output is recorded while the temperature is increased in the same manner as the weight is recorded with the thermobalance. This is shown for a cell with CsI_4 in Fig. 8. It is seen that the current rose rapidly starting at about 246°C from 0.3 to 2.9 ma, the steady-state value for this cell at 200 Ω load. Similar curves were obtained for cells with other iodine donors.

Comparison of cell performance with phase diagram of the system CsI-I_2.—On the basis of the phase diagram, it was predicted that a cell with CsI_4 as iodine source should be operable at 190°-245°C, with full activation at the higher temperature. This observation has been confirmed by the thermoactivation current illustrated in Fig. 8. The fact that full current output was not obtained until 257°C was reached can again be explained, as above, by the temperature lag between the recording thermocouple and the cell. It is the temperature at which the increase of current begins that is characteristic of full activation. Below 190°C a current of 0.3 ma is also appreciable for a Ta-tube cell, but the increase in current demonstrated the decomposition of the iodine source. Thus, there is qualitative agreement of cell performance and its prediction from the phase diagram of the open system. The correlation must not, however, be pushed too far, because in the cell we deal with a closed system.

To evaluate different iodine donors, a series of cells was chosen for initial room temperature similarity in structure (0.318 cm OD Ta-tube cells) and internal room temperature impedance (280-500 kΩ). The cells were filled with different iodine sources, namely, iodine, CsI_4, CsI_3, and the mixture of 4 mole CsI_3 + 1 mole CsI, which was discussed previously. The polarization of the cells then was measured at increasing temperatures. Specific values obtained

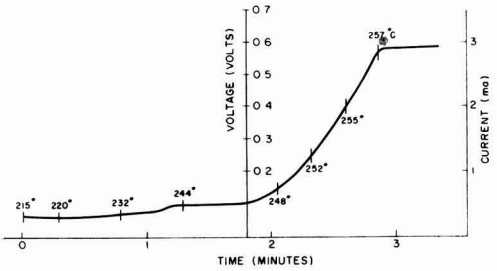

Fig. 8. Thermal activation of a Ta-tube cell, iodine source: CsI_4. Cell on 200 Ω load.

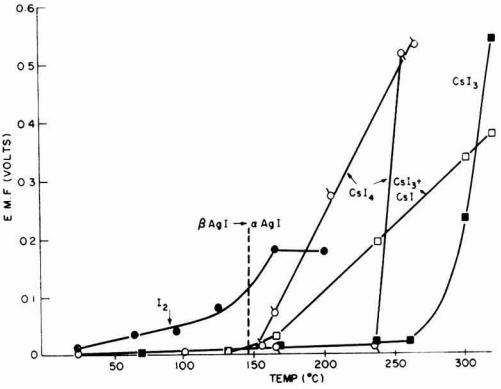

Fig. 9. Thermal activation of cells with AgI electrolyte (emf at 25 kΩ load).

with an external load of 25 kΩ are shown in Fig. 9. Where iodine crystals were the source of iodine vapor the cell responded even below the transformation temperature and broke down at 200°C. This is to be expected because iodine has a boiling point of 188°C. The cell with CsI_3 was not activated fully until 320°C was reached. Two cells with CsI_4 behaved differently; one was activated slowly over the temperature range 155° to 245°C, and the other one attained full output abruptly between 235° and 255°C. Finally, the mixture of $4CsI_3 + CsI$ also was activated slowly from 150°C up and had not reached full activation at 320°C. Despite the discrepancy in the two CsI_4 runs, these curves qualitatively agree with the interpretation of the phase diagram.

Acknowledgments

The author is indebted to D. L. Douglas, W. T. Grubb, A. E. Newkirk, and E. L. Simons for very helpful discussions. Miss I. Aliferis performed the thermolyses, and P. R. Schmidt assisted in the preparation of cells. The x-ray analysis of CsI_4 was performed by the metallography group of the Research Laboratory.

Manuscript received June 25, 1958. This paper was prepared for delivery before the Ottawa Meeting, Sept. 28-Oct. 2, 1958.

Any discussion of this paper will appear in a Discussion Section to be published in the December 1959 JOURNAL.

REFERENCES

1. J. L. Weininger, *This Journal*, **105**, 439 (1958).
2. C. Tubandt and F. Lorenz, *Z. physik. Chem.*, **87**, 513 (1914); K. H. Lieser, *Z. physik. Chem.*, (*n.F.*), **9**, 302 (1956).
3. T. R. Briggs, J. A. Greenawald, and J. W. Leonard, *J. Phys. Chem.*, **34**, 1951 (1930).
4. T. R. Briggs, *ibid.*, **34**, 2260 (1930).
5. J. D. Hanawalt, H. W. Rim, and L. K. Frevel, *Ind. Eng. Chem., Anal. Ed.*, **10**, 457 (1938).
6. J. R. Partington, "Textbook of Inorganic Chemistry," 5th ed., p. 364, Macmillan and Co., New York (1939).
7. G. B. Kolhatkar and V. A. Sant, *J. Univ. Bombay*, **11**, Pt. 3, 96 (1942); *C.A.*, 37:3325[5].

Studies of the Structure of Anodic Oxide Films on Aluminum, I

D. J. Stirland and R. W. Bicknell

Caswell Research Laboratories, Towcester, Northants, England

ABSTRACT

The influence of the formation voltage on the structure of nonporous anodic aluminum oxide films has been studied by electron microscope and electron diffraction methods. It has been shown that low formation voltages (<100 v) produce an amorphous oxide layer, whereas high formation voltages produce amorphous oxide together with some crystalline γ'-alumina. The location of this crystalline oxide within the anodic layer is discussed.

In general the so-called direct methods for examination of thin films (such as optical and electron microscopy, x-ray and electron diffraction) can provide information regarding the "structure of the films," but it is necessary to define carefully what is meant by this phrase. Conventional microscopical methods can show details of the topography of both surfaces of the film and, providing the film is sufficiently transparent either to light or to electrons, may also reveal bulk physical features within the film. Diffraction methods can be used to determine the crystallographic structure either of a thin surface layer of the film or of the bulk material. These methods thus give two structural parameters, the physical and the crystallographic.

A number of workers (1-5) have investigated these parameters in the case of films formed on aluminum by electrolytic oxidation and have shown that anodic aluminum oxide films can be divided into two classes, determined by the solvent action of the forming electrolyte on the oxide. Electrolytes which dissolve the oxide produce porous coatings whose thickness depends primarily on both formation current and time, whereas electrolytes which do not attack the oxide appreciably produce thin nonporous coatings, whose thickness depends mainly on formation voltage. Although the electrical properties of nonporous films have led to a wide application in the industrial field of electrolytic capacitors, most fundamental investigations of the structure of anodic coatings have dealt with the porous types of oxide only.

This paper presents and discusses the results of electron microscope and electron diffraction studies on both the physical and crystallographic structures of nonporous anodic oxide coatings.

Methods of Examination of Anodic Films

A systematic x-ray investigation of the crystallographic structure of anodic coatings has been made by Taylor, *et al.* (6). Oxide films were formed on 99.8% pure aluminum foil in a variety of electrolytes (giving both porous and nonporous coatings) under differing conditions of temperature and formation voltage. X-ray examination of the oxide films showed that some crystalline alumina was obtained in all cases where the formation voltage exceeded 100 v, and that the amount of crystalline oxide increased with increase in formation voltage. This was determined by comparing the relative intensities of the x-ray diffraction lines given by each specimen.

Taylor, *et al.* do not discuss the significance of the x-ray pattern in detail and, as Burwell (7) has

pointed out, the excessive line broadening of the pattern does not permit conclusive identification of the crystallographic structure of the oxide. We have found that in general only two lines are clear enough for measurement, and these are very broad. A typical x-ray diffraction pattern obtained from an anodic film formed at 525 v on 99.99% pure aluminum (see next section for preparative details) shows two such broad reflections which have d-spacings of 1.97 and 1.39Å. If the observed line broadening is due to the small crystallite size of the alumina, then it might be expected that the smaller equivalent wave length of an electron beam (as compared with an x-ray beam) would give a sharper diffraction pattern suitable for a complete identification of the structure, but it is found that the specimen is then too thick to give any transmission electron diffraction pattern at all. In fact, using a diffraction camera operating at a beam voltage of 50 kv, the practical upper limit to the specimen thickness will be ~400Å, and since for nonporous anodic films the thickness formation voltage ratio is almost constant at ~14Å/v (8), this limits the maximum permissible anodic formation voltage to ~30 v.

However, it is possible to examine higher voltage films in the electron diffraction camera if their thickness can be reduced by some suitable method. It was found that a phosphoric-chromic acid mixture, previously used (9) to dissolve anodic films from aluminum, would also serve to thin down the thick coatings to an appropriate thickness for transmission diffraction. Thus films formed over a wide range of voltages could be examined. Furthermore, these thinned specimens were also suitable for electron microscope examination, providing a direct method of observing the stripping action of the acid mixture on the anodic coatings.

Experimental Details

Aluminum foil of 99.99% purity was used for all the experiments, and in each case the specimens were cleaned prior to anodization by a 3-min immersion in a 3% NaOH solution. They then were washed thoroughly in distilled water and dried in a warm air stream. The anodizing electrolyte consisted of a 3% boric acid-0.05% borax aqueous solution used at 20°C. All specimens were anodized at constant voltage for a set period of 5 min. The acid mixture used to thin down the anodic coatings consisted of 35 cc of 85% phosphoric acid and 20 g of chromic acid per liter of solution used at 80°C.

The investigation was carried out in two parts. (*a*) *Action of the acid mixture.*—Specimens were anodized at 500 v, 20°C, and then immersed for 1, 3, 10, and 20 min, respectively, in the acid mixture. Then they were washed thoroughly and re-anodized at 10 v. One reason for this second anodization was to provide a thin (~150Å) supporting film to hold in position fragments of the original anodic coating which had survived the acid treatment. This 10-v film only formed on the aluminum surfaces exposed by the dissolution of the original coating. Examination of specimens in the electron microscope showed that the second anodization was unnecessary for the lightly attacked films, but the same procedure was adopted for all specimens in order to standardize conditions. The composite film was stripped in small squares from the aluminum by the usual mercuric chloride method (10), washed, and picked up on electron microscope specimen grids for subsequent examination.

(*b*) *Effect of differing formation voltages on the structure of the oxide.*—Specimens were anodized over a range of voltages between 12 v and 500 v at 20°C. They then were immersed in the acid mixture for various times, sufficient in each case to reduce the oxide thickness to less than ~400Å. For example, specimens anodized at 12 and 25 v did not need to be treated at all, the 200-v specimen was immersed for 2 min, and the 500-v specimen for 5 min. The treated specimens were then re-anodized at 10 v and oxide squares prepared for examination as before.

Besides providing a coherent supporting membrane for the remaining parts of the original anodic film, the 10-v oxide film also acted as a normal oxide replica (10) of the exposed parts of the underlying aluminum surface. Thus it was possible to examine, on the same specimen, both the partially dissolved original anodic coating together with an oxide replica of the metal surface from which the coating had been dissolved completely. Since this aluminum had been exposed to the acid mixture, however, it was necessary to investigate whether any reaction had occurred.

A cleaned sheet of aluminum foil was placed in the acid bath for 20 min, and then oxide replicas of its surface were prepared and examined. These showed that the only observable effect of the acid mixture was to produce a small number of easily identifiable etch pits (dimensions ~0.05μ) in the aluminum surface. Since the size of these pits was considerably smaller than that of the surface detail which was being studied, and since the 20-min acid attack was the maximum period employed during the dissolution of the anodic films, it was considered that the effects of the reaction between the acids and the aluminum could be ignored.

Finally, it was found that all the low voltage anodic films (<100 v) dissolved quickly and completely in the acid mixture. For example, squares of oxide removed from foil anodized at 25 v dissolved completely in ~1 min.

Interpretation of Results

Figures 1-7 show typical areas of the anodic layers after different times of immersion in the acid mixture. Figures 1 and 2 demonstrate at once the nonuniformity of the acid attack, which has dissolved the oxide preferentially in cylindrical pores. With a longer attack the pores increase in size and number, and the less soluble parts eventually become thin enough to enable some fine structure to be visible in them (Fig. 3-5, with finely structured areas arrowed on Fig. 4). Figures 6 and 7 show areas in which the high voltage oxide has been dissolved almost completely, and therefore consist mainly of 10-v oxide replicas of the surface beneath the original anodic layer. Micrographs of oxide replicas do not differentiate between identically shaped raised or depressed features, but by metal-shadowing (11) it

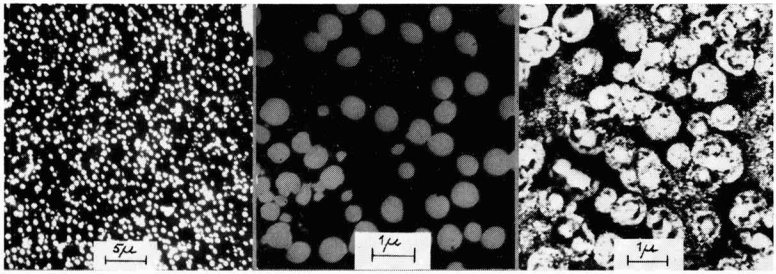

Fig. 1 (left) Fig. 2 (center). Transmission electron micrographs of 500 v anodic oxide film after 3 min in acid mixture. Fig. 3 (right). Transmission electron micrograph of 400 v anodic oxide film after 5 min in acid mixture.

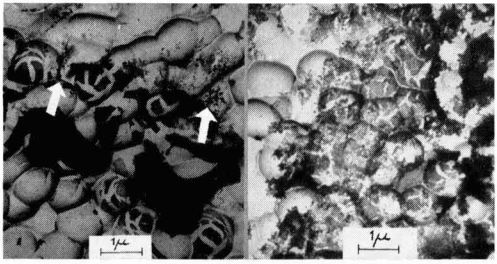

Fig. 4 (left) and Fig. 5 (right). Transmission electron micrographs of 500 v film after 10 min in acid mixture, together with replica of exposed aluminum surface.

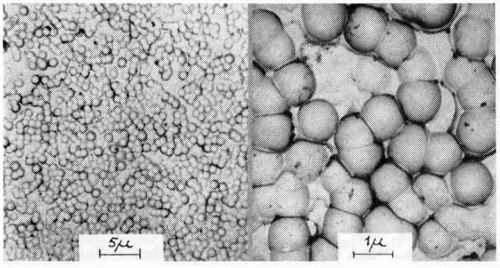

Fig. 6 (left). Cell-base structure beneath a 500 v anodic oxide film, exposed after 20 min in acid mixture. Fig. 7 (right). Transmission electron micrographs of 10 v oxide replica.

has been shown that the features on Fig. 6 and 7 represent shallow craters in the aluminum surfaces.

Electron diffraction examination of specimens containing the areas shown in Fig. 3-5 gave the sharp ring pattern of Fig. 8. Table I gives the indexed reflections, together with their estimated relative intensities, for this pattern. It agrees very closely with x-ray diffraction results obtained by Verwey (12) from anodic aluminum oxides. He identified the material as a face-centered cubic structure of cell-size $a_o = 3.96$Å, and called the oxide γ'-alumina. This is not to be confused with the aluminum oxide which can be prepared by the thermal decomposition of alumina hydrates and has a deficient spinel structure ($a_o = 7.89$Å). In the English nomenclature this oxide is called γ-alumina (13); in American literature it is known as η-alumina (14). Both γ'-alumina and γ (or η)-alumina have in their diffraction spectra two strong lines with d-spacings of 1.97 and 1.39Å; in the case of γ'-alumina these are from (200) and (220) reflections, and in the case of γ (or η)-alumina they are from (400) and (440) reflections. These two may be the only lines capable of measurement on an x-ray pattern, and thus the identification of the oxide structure is not certain. However, the sharp electron diffraction pattern conclusively identified the crystalline oxide as γ'-alumina.

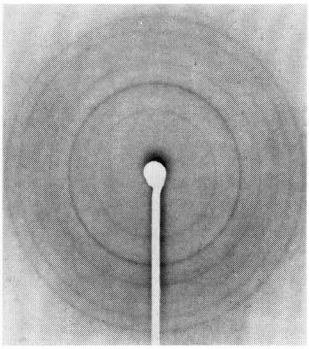

Fig. 8. Electron diffraction pattern from finely structured material present in high voltage anodic oxide films.

Exactly the same diffraction pattern was obtained from all the anodic films formed at voltages greater than 100 v, thus confirming the results of Taylor, *et al.* (6). Films formed below 100 v gave patterns consisting of two broad diffuse rings, typical of those obtained from amorphous materials. Amorphous in this sense is defined as a structure whose crystallite size is less than ~10Å. Electron micrographs of these films appeared to be normal oxide replicas, showing surface detail which could be correlated with that observed by optical examination of the unformed aluminum specimens.

Location of the Crystalline Oxide within the Anodic Layer

It was possible to deduce theoretically and confirm experimentally that the finely structured areas shown in Fig. 3-5 could be identified with the crystalline γ'-alumina. On each micrograph three types of area can be seen; black areas, light gray areas, and the finely structured areas. The black areas cannot give a diffraction pattern since they represent partially dissolved oxide which is still too thick to be penetrated by the electron beam. The light gray areas cannot give a ring pattern because they con-

Table I. Comparison of diffraction spectra of γ'- and γ-alumina

Measured spacings and estimated intensities from Fig. 8		Indexed spacings and intensities of γ'-alumina, according to Verwey (12)			Indexed spacings and intensities of γ-alumina, according to Rooksby (13)		
d_{hkl} (Å)	Intensity	(hkl)	d_{hkl} (Å)	Intensity	d_{hkl} (Å)	Intensity	(hkl)
					4.55	MF	(111)
					2.79	F	(220)
					2.381	MS	(311)
2.287	VVF	(111)	2.281	F	2.271	M	(222)
1.980	S	(200)	1.975	VS	1.973	VS	(400)
					1.517	F	(511)
1.399	VS	(220)	1.397	VS	1.392	VS	(440)
1.193	VF	(311)	Not observed				
1.143	M	(222)	1.140	M	1.138	F	(444)
					1.025	VF	(731)
0.990	F	(400)	0.988	MS	0.987	VF	(800)
Not observed		(331)	Not observed				
0.885	M	(420)	0.883	MS	0.882	VF	(840)
0.805	S	(422)	0.806	S	0.804	F	(844)

sist of the 10-v amorphous film. Hence the remaining areas must be responsible for the γ'-alumina diffraction pattern.

Experimentally this was confirmed by the "selected area diffraction technique." A variable aperture in the electron microscope was adjusted so that only a restricted area of the specimen was visible, and the diffraction pattern from this area was then obtained. On scanning the specimen it was found that the thin film replica areas gave two broad diffuse rings, and the black areas gave no transmission pattern at all. Only the finely structured gray areas produced the γ'-alumina pattern, and hence they indicate the disposition of the γ'-alumina within the anodic layer. These areas are most probably agglomerates of crystallized alumina.

Discussion

The first conclusion which can be drawn from a study of the micrographs is that a short attack by the phosphoric-chromic acid mixture does not dissolve the high voltage anodic coatings uniformly. Instead, a selective dissolution of thin cylindrical columns of material takes place. It was found by examination of the lightly attacked oxide specimens before they had been anodized to give the 10-v replica support film that, in fact, no material was present within the columns after a 3-min immersion in the acid mixture. This means that there is a variation in solubility of the anodic coatings, which in turn implies a variation in their composition. It has been mentioned previously that all the low voltage (that is, amorphous) films dissolved quickly and completely in the acid mixture, and so it is reasonable to propose that the very soluble part of the film consists of amorphous oxide.

Altenpohl (15) used a weighing method to study the action of the phosphoric-chromic acid mixture on nonporous anodic films formed in hot aqueous boric acid electrolytes. From the experimental results he suggested that these anodic films consisted of at least two different types of oxide; an outer layer readily soluble in the acid mixture, and an insoluble layer beneath this. He also found that the relative proportion of insoluble oxide increased with increase of formation voltage. Since the results described in the present paper are not strictly comparable with those obtained by Altenpohl because of the difference in electrolyte temperatures, some preliminary experiments using the boric acid-borax forming electrolyte at 100°C may be mentioned. These showed that 500-v anodic coatings could not be thinned down sufficiently to give any transmission diffraction pattern, even after 30 min in the acid mixture, although in every case of formation at 20°C it was possible to dissolve the oxide completely.

The results obtained with electrolyte at 100°C agree with Altenpohl's observations, but with electrolyte at 20°C it has been shown that all the oxide is removed from the metal. It is not certain whether this is because the cold formation oxide eventually is dissolved completely, or whether dissolution of part of the anodic layer (i.e., the amorphous oxide columns) weakens the adherence of the remainder. Figure 4 suggests that the latter explanation may hold in some cases, since the black fragments on this micrograph have been unattacked during the dissolution of the rest of the film, and yet a further treatment in the acid mixture would result in a film free surface (e.g., Fig. 6 and 7). It is difficult to imagine that these unattacked fragments dissolve completely during the second treatment, if they have already resisted the initial attack, and it seems more likely that they eventually become detached by a weakening of their adherence to the aluminum. The micrographs do demonstrate, however, that the distribution of readily soluble oxide and insoluble (or slowly soluble) oxide is very much more complex than the simple double layer arrangement proposed by Altenpohl.

The electron micrographs also provide information regarding the physical structure of the anodic films. At any instant during its formation the anodic layer is in intimate contact with the aluminum surface beneath it, and so the aluminum must reproduce every topographical detail of the oxide surface. Hence, replicas of the aluminum surface are also replicas of the oxide surface at the metal-oxide interface. This provided Keller, *et al.* (9) with a method of examining the oxide surface of porous anodic coatings, and by using low formation voltages they were also able to examine the stripped films in transmission. From these observations they derived a structure for the porous anodic films. The

Table II. Comparison of cell-sizes for porous and nonporous oxide films formed at 500 v

Forming electrolyte	Forming temp, °C	Cell size at 500 v in μ	Type of oxide
15% Sulfuric acid*	10	0.83	Porous
2% Oxalic acid*	24	0.98	Porous
4% Phosphoric acid*	24	1.03	Porous
3% Chromic acid*	38	1.04	Porous
3% Boric acid, 0.05% borax	20	0.96 ± 0.12	Nonporous

* Data obtained from ref. 9.

basis of this derivation was that the oxide contained a uniformly spaced array of tiny pores surrounded by close-packed hexagonal columns of oxide. These oxide cells had bases with the shape of a spherical section somewhat less than a hemisphere. Measurements of the pore spacings showed that they corresponded with the cell sizes (spacing between cell-base centers) measured from replicas of the aluminum surfaces beneath the coatings. Since the essential feature giving rise to this structure was assumed to be the existence of pores through the anodic films, it is surprising to find that micrographs of the metal-oxide interface of nonporous anodic films (Fig. 6 and 7) are almost identical in appearance with those shown by Keller, *et al.* for the same interface of porous anodic films (Fig. 8 of ref. 9, p. 415). Furthermore, it was possible to show that the similarity between the two structures is also quantitative.

Keller, *et al.* used four different electrolytes, all producing porous films. They found that over a voltage range of 20-120 v a linear relationship existed between cell size and formation voltage. By assuming that this linear relationship continued for higher voltages and by making a large extrapolation, the cell sizes which might be expected for a 500-v formation in each of the four electrolytes could be calculated. These values, compared with the cell size measured directly from micrographs of the 500-v nonporous formation, are shown in Table II.

This remarkably close agreement between the cell-base sizes for both porous and nonporous oxides is indicative of a similarity in physical structure. Franklin (16) has described some aspects of anodic oxidation and suggested that, since nonporous oxide films have a pronounced cell-type of structure, similar growth processes may occur for both types of oxide.

Conclusions

It has been shown that anodic oxide films formed in a boric acid-borax electrolyte contain some crystalline γ'-alumina provided that they are formed at voltages in excess of 100 v; otherwise they consist entirely of an amorphous oxide. The amorphous oxide dissolves more readily in a phosphoric-chromic acid mixture than does the crystalline oxide, and it appears to be present in cylindrical columns penetrating right through the anodic coating. Finally, the nonporous oxide structure is found to be similar in some ways to a structure previously proposed for porous anodic films.

Acknowledgments

It is a pleasure to acknowledge the helpful advice and assistance given to the authors by Mr. R. W. Franklin. They also wish to thank the Plessey Co. Ltd. for permission to publish this work.

Manuscript received Feb. 3, 1958. This paper was prepared for delivery before the Ottawa Meeting, Sept. 28-Oct. 2, 1958.

Any discussion of this paper will appear in a Discussion Section to be published in the December 1959 JOURNAL.

REFERENCES

1. W. G. Burgers, A. Claasen, and J. Zernicke, *Z. Physik.*, **74**, 593 (1932).
2. F. Keller, *Am. Soc. Testing Materials,* **40**, 948 (1940).
3. R. A. Harrington and H. R. Nelson, *Trans. Amer. Inst. Mining Met. Engrs.*, **137**, 62 (1940).
4. E. Brandenberger and R. J. Hafeli, *Helv. Chim. Acta.*, **31**, 1168 (1948).
5. C. J. L. Booker, J. L. Wood, and A. Walsh, *Brit. J. App. Phys.*, **8**, 347 (1957).
6. C. S. Taylor, C. M. Tucker, and J. D. Edwards, *Trans. Electrochem. Soc.*, **88**, 225 (1943).
7. R. L. Burwell, *ibid.*, **88**, 332 (1943).
8. P. D. Lomer, *Proc. Phys. Soc.*, **638**, 818 (1950).
9. F. Keller, M. S. Hunter, and D. L. Robinson, *This Journal*, **100**, 411 (1953).
10. H. Mahl, *Metallwirtschaft*, **19**, 1082 (1940).
11. R. C. Williams and R. W. C. Wyckoff, *J. Appl. Phys.*, **15**, 712 (1944).
12. E. J. W. Verwey, *Z. Krist*, **91**, 317 (1935).
13. H. P. Rooksby, "The X-ray Identification and Structure of Clay Minerals," p. 250, Mineralogical Society, London (1957).
14. H. C. Stumpf, A. S. Russell, J. W. Newsome, and C. M. Tucker, *Ind. Eng. Chem.*, **42**, 1398 (1950).
15. D. Altenpohl, Convention record of I.R.E. Part III, 35 (1954).
16. R. W. Franklin, *Nature*, **180**, 1470 (1957).

Aqueous Uranium Corrosion at 100°C

J. B. Schroeder,[1] D. A. Vaughan, and C. M. Schwartz

Battelle Memorial Institute, Columbus, Ohio

ABSTRACT

The mechanism of aqueous uranium corrosion has been studied using weight loss and hydrogen evolution measurements. Microscopic x-ray diffraction and chemical analyses were made of the corrosion product. The results indicate that uranium corrodes by forming an oxide of the type UO_{2+x}. The lack of chemical balance reported by earlier workers is explained by the existence of metallic uranium in the oxide layer.

Many of the atomic reactors in existence today use a metallic, natural uranium fuel which is cooled with either heavy or light water. The design of some fuel elements is discussed by Gurinsky and Dienes (1) in their review of the first Geneva conference on atomic energy. All of these designs overcome the high corrosion rate of uranium by providing some protective container to prevent the coolant from coming in direct contact with the uranium fuel. The fabrication of reactor fuel elements would be greatly simplified and the potential hazard of contamination resulting from a cladding failure reduced if a corrosion-resistant uranium alloy were available. This study was undertaken to provide information about the mechanism of the aqueous corrosion of alpha uranium to aid in the development of corrosion-resistant alloys.

Previous work on the corrosion of uranium has been summarized in the Reactor Handbook (2) and by Gurinsky and Dienes (1). The early work showed that the uranium corrosion rate below 100°C was lower for oxygen-saturated water than for hydrogen-saturated water. In aerated water, uranium corroded slowly at first and then assumed the higher linear rate for hydrogen-saturated water. The mechanism proposed to account for these observations was that the oxide formed in water containing oxygen was self-healing and, therefore, protective. When the dissolved oxygen was depleted from the water, uranium hydride was believed to form beneath the oxide and break the oxide film. Hydride was identified on samples corroded in steam and water in the temperature range between 150° and 180°C. The formation of UH_3 also was considered necessary in order to account for the small quantity of hydrogen liberated during corrosion.

In the work reported here no evidence was found of either form of UH_3. The observations are explained on the basis of metallic uranium being present in the corrosion produced oxide.

Experimental

The samples were rectangular coupons (½ x ½ x ⅛ in.) of selected, center-cut ingot.[2] Before fabricating into samples the uranium was reduced 50% by rolling in the high alpha region.

[1] Present address: Ohio Semiconductors, Inc., Columbus, Ohio.
[2] Supplied by Mallinckrodt Chemical Works.

Preliminary tests showed that the corrosion rate of uranium in water at 100°C was linear and varied between 2.70 and 3.50 mg/cm²/hr, with an average value of 3.28. Three methods of surface preparation were investigated: electropolishing,[3] abrading through 600 grit paper, and abrading followed by a HNO_3 pickle. Corrosion rates were independent of the method of surface preparation. After this preliminary work all of the samples were electropolished, rinsed in distilled water and alcohol, and tested in boiled, deionized water.

Rate measurements.—Weight loss measurements were made by weighing the sample prior to testing and again after the corrosion-produced oxide had been removed by pickling in concentrated HNO_3. The final weight was corrected for the amount of uranium lost in the pickling step by repeating the pickling step, which was usually of 45-sec duration, and reweighing. The weight lost during the second pickling was added to the final weight in order to calculate the corrosion rate. The average corrosion rate was found to be 3.28 mg/cm²/hr by this method.

Hydrogen evolution during corrosion was measured by bubbling tank argon through the corrodant and drying the gas stream in a $Mg(ClO_4)_2$ train, converting the H_2 to water by passing it through hot CuO, and measuring the weight gain in a $Mg(ClO_4)_2$ absorption tube. The system was flushed until a constant weight was obtained for the absorption tube both before and after the test. The average amount of hydrogen evolved during four 24-hr and four 8-hr tests was 91.5 ± 1.2% of the amount calculated from the weight loss using Eq. [1].

$$U + 2H_2O \rightarrow UO_2 + 2H_2 \qquad [1]$$

Analysis of the Corrosion Product

Microscopic examination.—The oxide produced during corrosion was not adherent after the first few minutes at temperature. Figure 1 is a photomicrograph of the oxide layer after a 24-hr test. Metallographic examination of the metal-oxide interface did reveal some hydride; however, no more hydride was present at the interface after corrosion than was observed in the interior of the sample both

[3] The electropolishing bath was 40% H_2SO_4, 40% H_2O, 10% H_3PO_4, and 10% C_2H_5OH. The open-circuit voltage was 10 v. A more uniform polish was obtained when the bath temperature was maintained below 15°C.

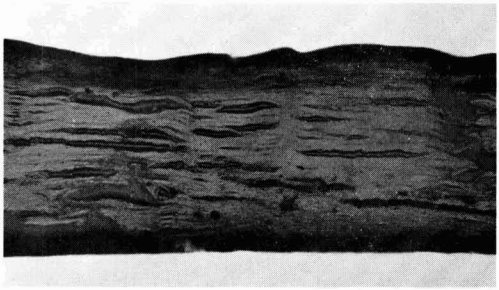

Fig. 1. Oxide layer formed on uranium metal during a 24-hr corrosion test at 100°C.

before and after testing. Vacuum-fusion analysis also failed to detect any increase in the hydrogen content of the metal as corrosion progressed.

X-ray diffraction.—Using copper radiation, diffractometer traces were obtained of the wet sample surfaces after various times during the corrosion tests. These showed alpha uranium and UO_2. After the oxide had grown to such a thickness that it was no longer possible to obtain the diffraction pattern of the metal, the oxide was removed by directing a stream of alcohol or water against the surface. Using this treatment it was possible to remove enough of the oxide to make the metal the most intense phase in the pattern. A hydride phase was not detected.

In both the diffractometer traces and Debye-Scherrer patterns the corrosion produced oxide gave very broad lines, due to extremely small particle size. For this reason it was not possible to obtain accurate lattice parameters of the oxide.

When the corrosion product was reacted with dilute HNO_3 (5%) the UO_2 was attacked preferentially leaving feather shaped particles. These particles were identified by x-ray diffraction as being metallic uranium.

After metallic uranium was detected in the corrosion product, tests were performed which showed that both the metal and the beta hydride could withstand the dilute HNO_3 cleaning and would probably be detected, if present in the corrosion product. Samples which showed no oxide were oxidized to such an extent that only oxide could be seen in the diffraction pattern. This "oxide" was then treated with dilute HNO_3 and the residue examined by x-ray diffraction. The patterns showed a mixture of UO_2 and either the metal or UH_3, depending on the starting material.

Oxygen-to-uranium ratio.—Uranium dioxide, prepared by the hydrogen reduction of higher oxides, is frequently unstable, resorbing oxygen (3-5). This was found to be the case with the corrosion product when it was vacuum dried. The apparent oxygen-to-uranium ratio of the air-dried corrosion product was found by ignition to be 2.40.

The oxygen-to-uranium ratio of oxide samples generally is determined by measuring the weight gain when the sample is ignited to U_3O_8 by heating it in air to 750°C and holding it at that temperature for 15 min. This type of analysis cannot distinguish between oxygen, hydroxyl, or water. Therefore, the valence of the uranium is not necessarily twice the oxygen-to-uranium ratio.

Because of the instability of the dry corrosion product, wet samples were loaded into a controlled atmosphere, differential thermal balance. They were dried overnight in vacuum (5×10^{-5} mm Hg), weighed, heated to constant weight at 750°C, and then ignited to U_3O_8. Three samples lost 3.2, 1.6, and 4.2% of their weight during the drying operation and were found to have oxygen-to-uranium ratios of 2.19, 2.24, and 2.19, respectively. A sample of commercial oxide was placed in a simulated corrosion test and then run through the differential thermal analysis. It was found to lose 0.3% of its weight during the drying cycle and have an oxygen-to-uranium ratio of 2.04, which is in excellent agreement with other measurements.

Mean valence.—The mean valence of the uranium in the corrosion product was determined by a modification of an analytical method developed by Melton (6). It consists of dissolving the sample in a solution of $AgNO_3$ and NH_4F, 1*N* with respect to each. The silver ion acts as an oxidizing agent and produces hexavalent uranium and a precipitate of free silver. The silver is filtered off, dissolved, and measured gravimetrically as silver chloride, and the uranium content determined by a weight-volumetric method employing ceric sulfate.

The mean valence of uranium in the corrosion product was found to be 3.70, which is in good agreement with the hydrogen-evolution experiments. However, when the loose corrosion product was allowed to drop into a cool zone (approximately 25°C), rather than remain in the proximity of the metal, the mean valence was found to be 3.16. A sample of the corrosion product which remained in the boiling solution 24 hr after the metallic sample had been removed gave a mean valence of 3.87.

In order to obtain independent data on uranium valence the x-ray absorption spectrum of the bulk corrosion product was compared with that of UO_2 and UO_3. Spectrometer data were obtained over the range of x-ray wave lengths extending above and below the L_{III} absorption edge of uranium. The powders were briquetted in absorption cells of about the same x-ray density. The corrosion samples were coated with water soluble resin before drying in an attempt to minimize air oxidation. The curve of intensity vs. wave length in the region of the absorption edge was analyzed for maximum, minimum, and point of inflection. The results for the three materials are given in Table I. By each criterion char-

Table I. Characteristic points on the L_{III} x-ray absorption edge of uranium for uranium dioxide, uranium trioxide, and uranium corrosion product

Sample	Maximum absorption, Å	Inflection point, Å	Minimum absorption, Å
UO_2	0.7267_9	0.7226_1	0.7184_1
Corrosion product	0.7263_1	0.7223_2	0.7183_1
UO_3	0.7263_1	0.7222_7	0.7182_4

Note: The absorption-edge wave length was calculated on the basis of a LiF analyzing crystal with an assumed 2d spacing of 4.0275Å.

acteristic values for the corrosion product are intermediate between those of UO_2 and UO_3. These results tend to verify the oxygen-to-uranium ratio measurements and to indicate that the oxide phase should not be considered as stoichiometric UO_2, as written in Eq. [1], but that the valence state of the uranium is somewhat greater than 4.

Solubles.—Samples of the corrodant were filtered and analyzed for solubles. The uranium content of the solid obtained by evaporating the filtered corrodant to dryness was 16%. Spectrographic analysis showed that the major constituents were calcium, magnesium, and chromium. All of these elements were present in the original metal.

The uranium content of the corroding water was measured as a function of time during tests carried out at 60°C. After 50 days the uranium concentration attained a value of 5×10^{-5} mole/l. This is an order of magnitude higher than the solubility data reported (7) for $U(OH)_4$ and is probably due to the formation of complexes. This was considered to be unimportant in the over-all mechanism because samples tested in water containing the dissolved uranium exhibited the same corrosion rates as those run in fresh water.

Effect of Surface Treatments

Oxide films.—Metal samples were heated in low oxygen pressures to form coherent oxide films prior to corrosion testing for study of the protective properties of uranium oxide. Table II presents the results of short term corrosion tests and the heat treatment employed. These data show that the protection of these films increases as the temperature of film formation is increased to 650°C. When the oxide film was removed by electropolishing, the corrosion rate was the same as that for unannealed samples. This demonstrates that the increased corrosion resistance was due to a surface effect and not a bulk effect. When the films were formed at temperatures above the alpha-beta transformation (663°C), deep cracks appeared in the metal, producing discontinuities in the oxide film. All of the samples heated above the alpha-beta transformation corroded at the same rate as untreated samples. Figure 2 shows the results of longer tests on oxide-coated samples. All of the samples used in this test were held for 2 hr at 650°C in an oxygen atmosphere at a pressure of 5×10^{-4} mm Hg. Oxide films were put on only two samples at a time in order to keep them well separated in the furnace. The samples that were coated together are enclosed by one circle in Fig. 2. The spread observed is probably due to minor uncontrolled variations in the conditions used in forming the films. The oxide films failed after approximately 20 hr by developing a few small pits and undercutting. No inclusions were detected at the site of the original failure. X-ray diffraction patterns of the material formed in these pits showed that no hydride was present. Line broadening of the x-ray diffraction pattern showed that the coherent oxide films may have been highly stressed. The failure possibly occurred where the local stress level was sufficient to rupture the film.

Table II. Corrosion results on uranium

Sample No.	Condition of oxide film formation: Temp., °C	Condition of oxide film formation: Pressure, mm Hg	Time in corrosion test, hr	Rate, mg/cm²/hr
90	100	5×10^{-5}	4	2.93
91	100	5×10^{-5}	4	3.04
92	200	5×10^{-5}	4	3.26
93	200	5×10^{-5}	4	3.34
94	300	5×10^{-5}	4	2.78
95	300	5×10^{-5}	4	3.01
96	400	5×10^{-5}	4	3.00
97	400	5×10^{-5}	4	2.71
98	500	5×10^{-5}	4	1.56
99	500	5×10^{-5}	4	2.16
100	600	5×10^{-5}	4	0.68
101	600	5×10^{-5}	4	1.20
102	600	5×10^{-5}	4	1.24
103	600	5×10^{-5}*	4	3.10
104	600	5×10^{-5}	4	1.77
105	600	5×10^{-5}*	4	3.12
108	600	5×10^{-4}	4	Not detectable
109	600	5×10^{-4}	4	Not detectable
110	600	5×10^{-4}	4	Not detectable
111	600	5×10^{-4}	4	Not detectable
112	650	5×10^{-4}	21	0.06
113	650	5×10^{-4}	21	0.10
114	650	5×10^{-4}	21	0.09
122	600	1×10^{-3}	21	0.16
123	600	1×10^{-3}	21	0.28
124	600	1×10^{-3}	21	0.21

* Electropolished after film formation.

It seems likely that the stresses in the oxide film resulted from the difference between the thermal expansion coefficients of the oxide and the metal. In an attempt to reduce the stress and thereby increase the life of the film, samples were run at lower temperatures and, when necessary to obtain a reaction, at higher pressures (10^{-3} to 10^{-2} mm Hg). Above 400°C no change was observed in the line broadening. Below 400°C a mixture of UO_2 and a higher oxide was formed which did not provide protection against aqueous corrosion.

Cathodic charging.—In order to test the effect of surface hydride on corrosion behavior, a hydride layer was produced by cathodic charging in weakly acid (0.5%) solution. By varying the temperature, the structure of the coating could be changed. At

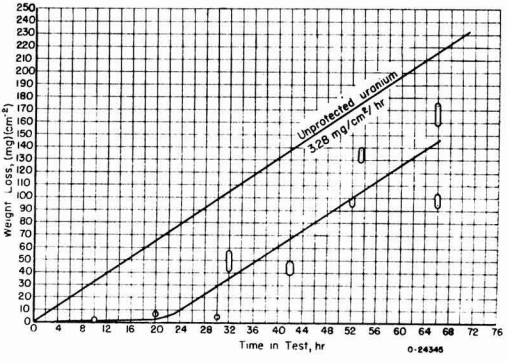

Fig. 2. Effect of oxide film on corrosion of uranium. Samples were held 2 hr at 650°C in oxygen atmosphere at 5×10^{-4} mm Hg. Two samples were coated together and are enclosed by one circle.

temperatures above 80°C only the beta form of UH_3 was produced, while at lower temperature a mixture of alpha and beta UH_3 was formed. No pure alpha coatings were produced.

Corrosion tests were run on samples coated with the beta UH_3 and with the mixture of alpha and beta. When corrected for the amount of uranium in the hydride layer no difference in corrosion rate could be detected between the charged and the uncharged samples.

Discussion of Results

The corrosion product formed when uranium reacts with 100°C water at atmospheric pressure does not offer protection to the underlying metal. In contrast, UO_2 films produced on the metal at temperatures above 400°C in oxygen, temporarily protect the base metal against corrosion in 100°C water. Ignition analyses of the water corrosion product indicate that its composition may be as high as $UO_{2.2}$, and increases to $UO_{2.4}$ after exposure to air at room temperature. Some confirming evidence that the valence state of uranium in the bulk corrosion product is greater than 4 was obtained from x-ray absorption spectroscopy.

This high oxygen-to-uranium ratio is in apparent contradiction to that from hydrogen-evolution measurement which indicates a composition of $UO_{1.9}$. The latter value is in good agreement with valence determination by chemical analysis. However, it is obvious that the oxygen-uranium ratio and the mean-valence and hydrogen-balance measurements are in error, being low by the amount of unattacked metal particles present in the samples. The metal content, although significant in explaining the low values of mean valence, must be considered an extraneous constituent of the corrosion product.

Thus the oxidized product is a phase or phases giving a UO_2-type x-ray pattern. It cannot be concluded from the oxygen-uranium ratio that the material is indeed UO_{2+x}, since, under conditions of reaction in the presence of water, hydrous oxide or the phase $U(OH)_4$ is a likely alternative indistinguishable from UO_{2+x}, by ignition analysis, in the presence of free metal. The solubility of $U(OH)_4$ is known (5), and its powder pattern has been reported to be very similar to that of UO_2 (9). It is possible that the decrease in the oxygen-to-uranium ratio of air-dried corrosion product from 2.40 to 2.21, during vacuum drying, may represent the partial decomposition of $U(OH)_4$. The product cannot be $U(OH)_4$ alone, since this phase would lose weight on ignition, requiring excessive amounts of free metal to compensate. Furthermore, its valence state is not consistent with the x-ray absorption-edge data. Thus, it is suggested that the corrosion product is a mixture of UO_{2+x} and $U(OH)_4$.

Although no hydride was detected in the present investigation, its stability under the conditions of the present tests was verified, and, therefore, it is likely that previous observations (1) of a hydride phase in the corrosion layer were due to hydrogen overpressure in the reaction vessel. It would be of interest to determine the hydrogen pressure required to form hydride in the presence of water and the effect of pressure on the corrosion rate of uranium.

Manuscript received June 21, 1957.

Any discussion of this paper will appear in a Discussion Section to be published in the December 1959 JOURNAL.

REFERENCES

1. D. H. Gurinsky and G. J. Dienes, "Nuclear Fuels," D. Van Nostrand Company, Inc., Princeton, N. J. (1956).
2. "The Reactor Handbook," Vol. 3, Section 1, AECD-3647, U. S. Atomic Energy Commission (1955).
3. D. A. Vaughan, J. R. Bridge, and C. M. Schwartz, To be published.
4. J. S. Anderson, *Bull. soc. chim. France*, **1953**, 781.
5. P. Perio, *ibid.*, **1953**, 256.
6. C. W. Melton, Private communication.
7. K. H. Gayer and H. Leider, *Can. J. Chem.*, **35**, 5 (1957).
8. J. T. Waber, Private communication.

Measuring Equipment for Polarization Studies in Distilled Water

J. E. Draley, W. E. Ruther, F. E. DeBoer, and C. A. Youngdahl

Argonne National Laboratory, Lemont, Illinois

ABSTRACT

A technique of measuring polarization in distilled water is described. The Luggin capillary and the a-c–d-c bridge methods are discussed and judged inapplicable. The decay of polarization voltage (of aluminum) is shown to be relatively slow in this environment. A recording voltmeter and current interrupter suitable for making polarization measurements in low conductivity solutions are described. The important design features of the electrolytic cell are discussed, and polarization data for aluminum in boiling water are given as an experimental example.

A number of articles (1) have discussed the theoretical analysis of metal potential vs. applied current curves for corroding metals. In those cases in which a specific experiment is described, the corroding medium has been of relatively low electrical resistance. Extending these potential-current analyses to a high-resistance medium such as distilled water modifies several of the usual measurement problems and introduces certain new ones.

The most serious problem in high-resistance solutions is that of the solution *IR* drop. Three methods are known for overcoming the solution resistance problem (Fig. 1): (*a*) by use of the Luggin capillary, (*b*) by balancing out this potential with an appropriate bridge circuit, and (*c*) by measuring the metal potential when no current is flowing (the interrupter technique). The Luggin capillary cannot be used in pure water because it shields the metal and because the small leak of the conducting salt at the metal surface would change the results entirely. Furthermore, the Luggin capillary would not eliminate the *IR* drop in so high a resistance medium.

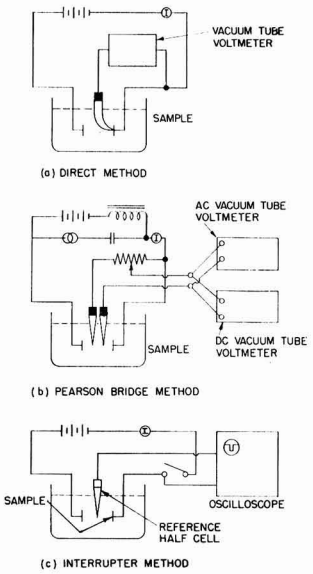

Fig. 1. Methods of overcoming solution IR drop in polarization measurements.

Initially the bridge technique appeared more promising since the circuitry was comparatively simple and the instruments (a-c and d-c vacuum tube voltmeters, etc.) were available from commercial sources. After preliminary experimentation several serious sources of trouble due to the high-resistance solution became apparent. As a result, attention was directed to the third or interrupter technique. A brief description of the experimental difficulties encountered with the bridge circuit is presented before the detailed discussion of the interrupter equipment to illustrate some of the unusual aspects of the problem.

Bridge Circuit

Various modifications of the Pearson (2) circuit were tried. It is assumed that the large specimen-solution pseudocapacitance effectively bypasses the electrode resistance for alternating currents, leaving only the solution resistance. Various impedance bridge circuits may then be devised, using a.c., to balance the solution *IR* drop with an equivalent external *IR* drop. Thus, when the current is changed to d.c., only the polarized potential of the specimen is measured in the previously balanced arm of the bridge. In distilled water at least two serious complications were encountered. First, the capacitative portions of the impedances between bridge members in the polarization cell were the same order of magnitude as the resistive component of the impedance in the solution. Balancing the a-c bridge under these conditions required a Wagner ground connection and multiple adjustments. Since a relatively large total d-c voltage (5-20 v) was required to drive the desired small polarizing currents, the a-c bridge had to be set with extreme precision to reduce the d-c error voltage (due to unbalanced *IR* drop) to within a few millivolts. Another difficulty was experienced with the reference electrodes. Since

most reference electrodes contaminated the pure water (a possible, but cumbersome, exception was the platinum-hydrogen electrode in hydrogen saturated water), the area of contact between the solution of the reference electrode and the pure water was deliberately made quite small. This small area resulted in a high-resistance contact shunted by a capacitative reactance. As a result, a-c and d-c impedances through the reference cell were not equal, whereas the analysis of the bridge circuits used demanded that they be equal. Because of these difficulties the work on bridge circuits was suspended.

Interrupter Technique

High solution resistance also complicates the interrupter type of measurement (Fig. 1c). The electronic detector must be sensitive to millivolts with the polarizing current off and yet not be overloaded by solution *IR* drops of up to 20 v with the current flowing. The high impedance of the measuring path between the reference electrode and the specimen makes it susceptible to stray a-c pickup (usually 60 cycles). Also, the input capacitance of the measuring circuit must be minimized to prevent relatively long RC decay times from introducing spurious polarization voltages.

Many circuits have been described for making quantitative measurements during the current interruption period (3). The recent, more complicated circuits have been required for precise measurements in the microsecond range. However, in the case of corroding specimens in distilled water, examination of current interruptions with a Model 531 Tektronix oscilloscope indicated several favorable features. For example, pure aluminum in 100°C distilled water and the simple circuit of Fig. 1c gave the trace shown in Fig. 2. A low resistance reference cell (platinized Pt, H_2 gas) and a special input circuit to the oscilloscope were used to permit viewing in the short time range. Even so, the period up to 60 μsec was obscured by the decay of the *IR* voltage. A very rapid polarization decay reaction, essentially complete in this time, may have occurred, but in view of the subsequent slow decay this seems unlikely. Since the direct method is not feasible we know of no way to eliminate this possibility.

It was also noted that the polarization decay in this preliminary experiment (with hydrogen gas) was about three times more rapid than that obtained in boiling distilled water without deliberate gaseous additions. In the latter more common case with the above polarizing conditions, the polarization voltage (about 300 mv at 0.2 msec) decayed about 6% in 1 sec, 63% in 33 sec, and 86% in 108 sec. It was obvious that this was not a simple RC decay.

The decay time for polarization voltages in distilled water thus appeared longer than that measured in the usual solutions. It was not similar to the usual rapid decay of the overpotential of a reversible system (3b). Since a smooth platinum sample behaved in approximately the same fashion in hydrogen-free water, the slow decay was not associated with the aluminum oxide film. The slow decay was not caused by the particular form of the reference electrode as is evidenced by the fact that the results with aluminum samples were not changed by interchanging reference electrodes (Pt-H_2 and calomel). It is not intended in this paper to discuss the theoretical implications of the observed values; it is hoped that a future publication will cover this aspect of the subject.

While the oscilloscope is an excellent method of obtaining a single piece of polarization data it is not well suited to the recording of complete curves in which both the *I* and *E* vary with time. A special piece of equipment was designed for this purpose.

Electronic Equipment

A thyratron tube with constant plate voltage fires nearly instantly whenever the grid-cathode voltage is more positive than a constant critical firing voltage. Hickling (4) devised a potentiometer circuit for determining the polarization voltage during a brief current interruption using this principle (Fig. 3a). The potentiometer is connected so that the voltage due to the solution resistance drives the grid negative with respect to the cathode (Fig. 3c). Manual adjustment of P_2 to the threshold of oscillation was required for each reading. However, the thresh-

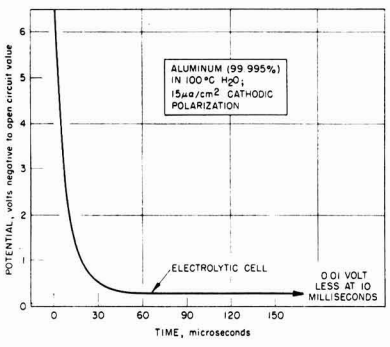

Fig. 2. Oscilloscope trace of current interruption

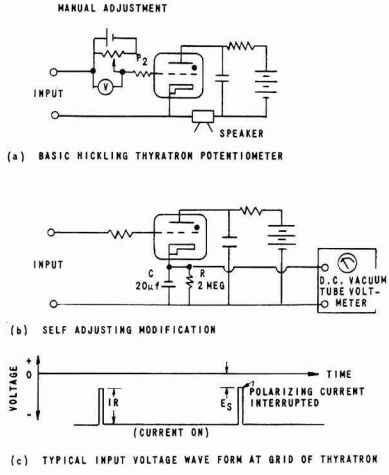

Fig. 3. Basic circuit of self-adjusting polarization voltmeter.

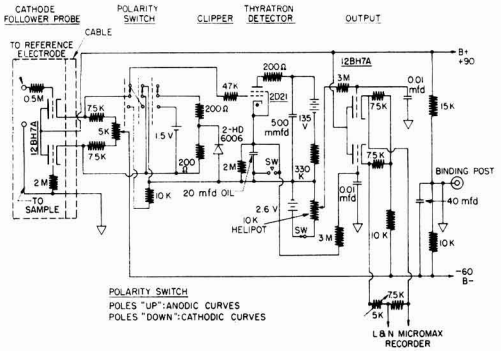

Fig. 4. Circuit diagram of polarization voltmeter

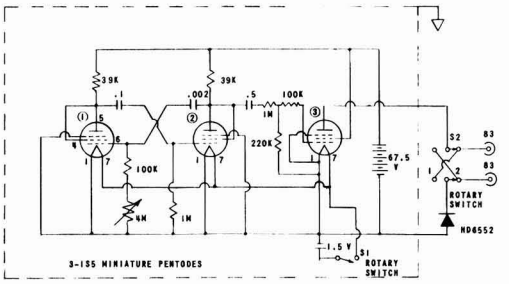

Fig. 5. Battery operated current interrupter

old adjustment can be performed automatically by the RC circuit of Fig. 3b. As the circuit operates as a saw-tooth oscillator, the current through the thyratron charges the condenser C until the grid-cathode potential is just equal to the critical firing potential for the thyratron. If the input voltage to be measured (E_s) changes, the condenser C is charged automatically by renewed oscillation or discharged by leakage through R until the total grid-cathode voltage again equals the critical firing potential. The change in potential across RC (measured with a d-c vacuum tube voltmeter) is therefore the change in the input voltage. This type of detector measures the most positive excursion of the grid potential during the interruption period.

In Fig. 4 the circuit diagram of the complete detector is shown. The cathode follower (12BH7A) provides high input resistance and isolates the sample from voltage pulses generated by the firing of the thyratron detector (2D21). The output circuit (12BH7A) prevents the loading of the RC self-balancing circuit by the L&N recorder. The range of polarization voltage of the specimen that can be handled by the peak detector itself is about 0.6-0.7 v. An adjustable bucking potential arrangement permits extension of this basic range, when it is necessary.

Certain precautions in construction will improve the performance of the instrument materially. The 12BH7A tube used in the cathode follower probe is selected for low grid current. The test is performed by applying +15 v (with respect to ground) to the "reference electrode" connection of the instrument with a galvanometer in series. A maximum of 10^{-9} amp should be drawn by the grid under these conditions.

Permitting the tubes to age for 5-10 days with their filaments operating tends to stabilize their performance, especially the 2D21 thyratron. The 135-v battery in the plate circuit of the 2D21 should be isolated from the instrument chassis to avoid stray leakage currents and large capacitance to ground. The usual care should be taken to isolate signal leads from those carrying 60 cps currents.

The polarizing current is supplied in the normal manner from a multiturn potentiometer and dry cells. The potentiometer may be motor driven, and a large resistance may be in the circuit to provide a linear rate of change of polarization current when desired. An adjustable, battery operated multivibrator provides the interruption pulses (Fig. 5). The frequency of interruption is about 10 cps. Period of current interruption is adjustable from 1 to 20 msec. A silicon diode in the output lead is used to prevent capacitatively coupled spurious pulses. Reversing switches provide a maximum of flexibility in operation.

Cell Design

The commonly used stop off materials (Bakelite, Lucite, and various waxes) contaminate pure water. As shown in Fig. 6, the sample is clamped tightly against the side of the chamber in a manner similar to that described by Sheff, *et al.* (5) and covers a 1-cm² hole. Only the edge of the thin polyethylene washer is exposed to the solution. The specimen-polyethylene-glass assembly is heat sealed (3 min, 150°C oven) to define the corroding area sharply. Experiments with and without the polyethylene gasket produced identical results within the experimental error.

Contamination of the pure water was also a consideration in choosing materials for construction of the cell. Tygon and Neoprene parts in the water feed line were found to be unsatisfactory where the temperature was high. Teflon parts were difficult to clean properly. Stainless steel appeared to contami-

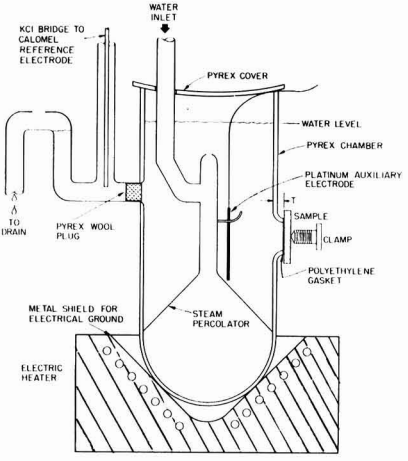

FIGURE 6
TEST CELL USED WITH BOILING DISTILLED WATER

Fig. 6. Test cell used with boiling distilled water

nate the hot water to some extent as judged by its influence on polarization curves. In the present design platinum and Pyrex glass are used throughout, except for the polyethylene gasket.

The 1-cm² hole permits the use of small samples. Any metal which can be ground or otherwise worked to expose one flat surface can be used. These considerations are important when an investigation of a wide range of metals is desired.

A relatively large ratio of water volume (250 cc)/sample area (1 cm²) reduces contamination of the solution by a corroding sample, as does a substantial rate of solution refreshment (10 cc/min).

In order to avoid a stray electrical ground the solution is allowed to form discrete drops at the end of the exit tube and drip into the drain. Also, the cell to ground capacitance is minimized to permit rapid decay of the *IR* voltage pulses.

The calomel cell is used because of its convenience. The slowly leaking salt bridge is constructed by fusing a strand of "Refrasil" insulation in Pyrex. The sweep of distilled water through the cell and the glass wool plug prevent chloride contamination of the sample chamber. On several occasions a portion of the flow was syphoned slowly from the chamber and collected for analysis. No chloride was found (sensitivity better than 0.1 ppm Cl^-).

Dimension T (Fig. 6) should be controlled. If it is made too small, the current distribution is nonlinear to a significant extent. If it is too large, the solution *IR* voltage can exceed +20 v. Under these conditions the grid of the input tube draws current and spurious polarization in the reference path occurs.

To evaluate the problem of nonuniform current distribution a Pt test probe was made by mounting a piece of 2.8 mm OD rod through a piece of Teflon and grinding the exposed face flush with the surface. This probe was mounted on the test cell in place of the usual specimen, and the resistance between the Pt working electrode in the cell and the small probe face was measured with an a-c impedance bridge as the probe was moved from edge to center of the 1 cm² opening. A maximum variation of 4% was found for 100°C distilled water with $T = 1.5$ mm. If greater uniformity were desired, T could be varied so that the maximum *IR* drop did not exceed 20 v or alternatively the input stage to the polarization voltmeter could be operated with higher plate voltage. Experiments have shown that up to 100 v *IR* can be tolerated using this latter technique.

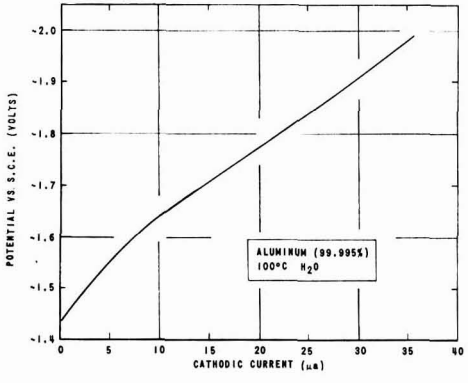

Fig. 7. Aluminum cathodic polarization curve

Annoying fluctuations in the current and voltage measurements were traced to steam bubbles moving across the face of the specimen. The present percolator design provides good temperature distribution, aids in degassing the replenishing water, sweeps the corrosion product away from the sample, and eliminates the steam bubble problem.

Experimental Example

The distilled water (resistivity —1.1 to 1.5 x 10^6 ohm-cm at 28°C) is usually slightly electrolyzed between Pt plates prior to its entry into the polarization chamber. When high-purity Al is used as the sample, this pre-electrolysis causes a slight decrease in the initial slope of the E vs. I cathodic curve and also prevents a sharp bend in the E-I curve at about 30 μa of cathodic polarization current. It is usually thought (6) that this pre-electrolysis takes some impurities out of the solution, but it is not clear that this mechanism applies here. The design of the pre-electrolysis cell and the amount of current do not seem to be critical.

Figure 7 is a trace of the recording of one experiment of potential (vs. saturated calomel electrode at room temperature) against applied cathodic current for high-purity Al in boiling water. The current was increased linearly with time ($\Delta I/\Delta t = 0.08$ μa/sec). This rate had little effect on these curves within the range investigated (0.04 to 0.11 μa/sec) and was controlled easily within this range. A 5-msec interruption period was used. The curve of Fig. 7 is one of thirteen similar curves. For this group of curves the average deviation at $I = 0$ is 0.006 v, that at 35 μa is 0.027 v; the maximum deviation at $I = 0$ is 0.011 v, that at 35 μa is 0.054 v. The slope of the straight line part (15 μa to 30 μa) is 14.4 x 10^3 v/amp with an average deviation of 1.1 x 10^3 v/amp. Samples were prepared by wet grinding pieces of a single stock of rolled and annealed sheet. They were exposed to the boiling water for about 20 hr (to an approximately constant value of open-circuit potential) before these measurements. Great care must be exercised to exclude impurities, since a small amount of contaminant corresponds to a large percentile change in the impurity level of the solution.

Reproducible E-I curves are being obtained for a variety of metals in distilled water at 100°C. Certain other variables of sample preparation are yet to be evaluated before a theoretical interpretation of the data is made.

Manuscript received Oct. 10, 1958. This work was done under the auspices of the U. S. Atomic Energy Commission.

Any discussion of this paper will appear in a Discussion Section to be published in the December 1959 JOURNAL.

REFERENCES

1. For example see: (a) U. R. Evans, "Metallic Corrosion, Passivity, and Protection," pp 47ff, 348ff, Longmans, Green & Co., New York (1948); (b) C. Wagner and W. Traud, *Z. Elektrochem.*, **44**, 391 (1938); (c) M. Stern and A. L. Geary, *This Journal*, **104**, 56, 559, 600, 645 (1957).

2. J. M. Pearson, *Trans. Electrochem. Soc.*, **81**, 485 (1942).
3. For example see: (a) S. Schuldiner and R. E. White, *This Journal*, **97**, 433 (1950); (b) D. Staicopoulos, E. Yeager, and F. Havorka, *ibid.*, **98**, 69 (1951).
4. A. Hickling, *Trans. Faraday Soc.*, **33**, 1540 (1937).
5. S. Sheff, H. C. Gatos, and S. Zwerdling, *Rev. Sci. Instr.*, **29**, 531, (1958).
6. A. M. Azzam, J. O'M. Bockris, B. E. Conway, and H. Rosenberg, *Trans. Faraday Soc.*, **46**, 918 (1950).

Electroplating of Nickel from the Pyrophosphate Bath

S. K. Panikkar and T. L. Rama Char

Electrochemistry Laboratory, Department of Inorganic and Physical Chemistry, Indian Institute of Science, Bangalore, India

ABSTRACT

The pyrophosphate bath has been found to be satisfactory for the plating of nickel. It gives good quality deposits over a wide range of operating conditions and has some advantages over the Watts bath.

Nickel is commonly plated from the sulfate-chloride or choride baths, and the fluoborate and sulfamate types have been established recently for industrial work. These solutions are all right in most respects, but they have a poor throwing power and are not suitable for direct plating on zinc. A complex salt bath suggests itself as an alternative. Brockman and Nowlen (1) have plated nickel on zinc from the triethanolamine bath. Langbein (2) cites an alkaline nickel pyrophosphate solution, and there is a patent (3, 4) on the zialite bath, containing nickel in the form of ammoniacal pyrophosphate and citrate complexes, for plating the metal on zinc. In view of the meager information available in literature, the plating of nickel from the pyrophosphate bath was studied in detail. The initial work has been reported briefly from this laboratory (5, 6), and a general review of plating metals and alloys from the pyrophosphate bath was made recently (7, 8).

Experimental

Plating solutions were prepared in the early work (5) by the addition of alkali pyrophosphate to a wet precipitate of nickel pyrophosphate obtained from nickel sulfate and pyrophosphate. Alkali chloride was then added to facilitate anode corrosion. It was necessary to add at least 6 g/l potassium chloride to the solution; otherwise the anode efficiency was zero. The bath preparation was therefore altered, potassium pyrophosphate being added to nickel chloride. The potassium salt was chosen in place of the sodium in view of the beneficial effects of the former as in other plating solutions. The pyrophosphate content of the bath was always in excess of that required for complex formation. Physicochemical measurements have shown (9) that the molar ratio of pyrophosphate to nickel in the complex is 2 as well as 1, the instability constant as determined from spectrophotometric data being of the order of 10^{-4}. There was no immersion deposition of nickel on zinc.

In solutions containing more than 0.3M nickel there was a tendency for precipitation after electrolysis. Ammonium citrate was added as a bath constituent since it was beneficial from the viewpoint of stability and buffering of the solution, quality of the deposits, cathode efficiency, and limiting c.d. (current density). Solutions with 0.3M nickel were titrated electrometrically with alkali using the glass electrode. Figure 1 shows that the precipitation pH is raised slightly by citrate, the best buffering action being imparted by 20 g/l of the salt. It was not advisable to increase the citrate content of the solution, thereby making it a mixed bath. The concentration of citrate was proportional to the nickel content of the solution, the ratio being 66.6 g/l ammonium citrate for 1M (58.7 g/l) nickel. Figure 2 shows that the resistivity of the solution is slightly decreased by citrate.

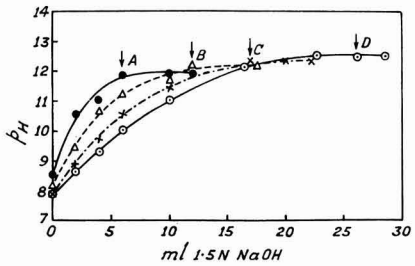

Fig. 1. Electrometric titrations. Ni 0.3M, ratio (i.e., ratio of pyrophosphate to metal by weight) 8. (A) am.citrate nil, (B) am.citrate 10 g/l, (C) am.citrate 20 g/l, (D) am.citrate 30 g/l. Each arrow shows the precipitation point for a curve, and the letter above it refers to the curve.

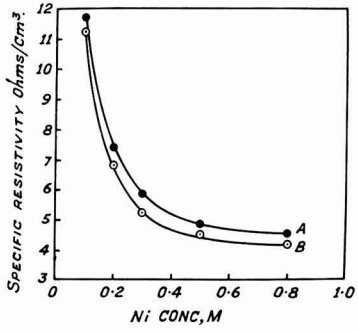

Fig. 2. Specific resistivity. Temp. 60°C, ratio 8. (A) am.citrate nil, (B) am.citrate 66.6 g/l for 1M Ni.

Fresh solutions, 200 ml, were taken for each experiment. Nickel anodes[1] (3 x 1 x ⅛ in.) and copper sheet cathodes (3 x 1 x 1/32 in.) were used, the inter-electrode distance being 1 in. and the immersed area of each electrode 2 in.^{2}; plating time for an experiment was 10-45 min. The experimental details concerning cleaning of electrodes, plating equipment, current efficiencies, temperature, agitation, pH, resistivity, and electrode potentials were the same as described before (10). The pH was varied by the addition of potassium hydroxide or hydrochloric acid. Conditions were carefully controlled to obtain electrode potential values (hydrogen scale) to the accuracy of ± 0.005 v.

The throwing power of the plating solution was measured under optimum conditions with a modification of the Haring-Blum throwing power box (11). The object was to obtain a relative idea of the throwing power of different plating solutions. A cylindrical glass cell 15 cm long and 4.5 cm in diameter was used, with 2 copper cathodes and a perforated nickel anode in between. The distance between the cathodes was 12 cm. The cathodes were weighed after electrolysis and cathode potentials and resistivity of the solution determined. The throwing power was calculated from the Field formula (12) and also from the equation of Gardam (13) for a linear relationship between cathode potential and log c.d., there being no variation of the cathode efficiency with c.d.

Photomicrographs of a thick coating (0.001 in.) of the surface of nickel deposit were taken with a Leitz projection microscope. X-ray powder patterns of the deposit were obtained from a Rich Seifert 13 unit with 57.3-mm diameter camera. Hardness measurements were made on the surface of the deposit with Leitz 1151 Durimet Midget hardness tester.

[1] Supplied by Canning and Co.

Experimental Results

Electrodeposition was carried out under the following conditions: nickel concentration 0.05, 0.1, 0.2, 0.3, 0.4, 0.5, and 0.8M; ratio of pyrophosphate (P_2O_7) to metal (weight) 6, 7, 8, and 10 (3.375 molar ratio); pH 7.8, 8.5, 9, 9.5, and 10.5; temperature 30°, 50°, 60°, and 70°C. Results are presented in Fig. 3-14 and in Tables I-III. All the results have not been covered to avoid overlapping. For the same reason, points corresponding to static potentials have not been marked. The data recorded correspond to good quality deposits. The decomposition potential for the plating solution was 1.8-1.9 v, and the bath voltage 0.9-3.0 v.

Nature of deposit.—The bath gave smooth, white, bright, fine-grained, and adherent deposits of nickel on copper (brass or zinc) cathodes over a wide range of plating conditions. Table I shows the effect of beneficial addition agents on cathode efficiency, potential (where there was a significant change), and quality of the deposit. Among other substances tried, diphenylamine had no effect, and selenium dioxide resulted in a deterioration. Plates 1 to 5 (Fig. 3) show the photomicrographs of the surface of nickel plates obtained under different conditions. Addition of ammonium citrate made the deposit finer grained and brighter, and there was no indication of escape of gas from the surface (plates 1 and 2). Increase of c.d. or temperature (not shown) or addition of cobalt chloride gave a brighter deposit; in the last case there was gas evolution and stress (plates 3-5). X-ray studies showed that the deposit has a f.c.c. structure, with $a = 3.516$Å.

Current efficiencies.—The cathode efficiency was increased by the addition of ammonium citrate, increase of nickel content, or pH of the solution. There was a slight increase with increase of temperature, and decrease with agitation. Most of the addition agents increased the efficiency at higher

Table I. Effect of addition agents on cathode efficiency, potential, and quality of the deposit

Bath composition: Ni 0.5M, ratio 8, ammonium citrate 33.3 g/l; pH 9.5; temperature 60°C, still plating. The first figure under c.d. gives the cathode efficiency % and the second (in parentheses) gives the cathode potential (-ve sign) in volts in H scale. Quality of deposit: A—marked improvement, B—slight improvement.

Addition agent	Conc. g/l	c.d., amp/dm^2 0	4	6	8	10	Brightness of deposit
Nil	—		92	86	65		—
		(0.41)	(1.08)	(1.18)	(1.24)		
Cobalt chloride	4.8		93	93	87	72	A
Cadmium chloride	0.8		89	88	86	83	B
Lead acetate	1.0		88	83	79	75	A
		(0.40)	(1.08)	(1.12)	(1.14)	(1.18)	
Zinc pyrophosphate	1.5		82	82	81	80	B
Sodium sulfite	0.5		90	89	82	82	A
Sodium bisulfite	0.2		90	89	89	87	A
Thiourea	0.5		78	71	55	32	B
		(0.52)	(0.94)	(1.07)	(1.14)	(1.24)	
Gelatin	0.5		78	69	59	56	B
		(0.46)	(1.21)	(1.29)	(1.36)	(1.48)	
β-naphthol	0.05		81	81	77	62	B
		(0.43)	(1.02)	(1.10)	(1.11)	(1.36)	
Coumarin	0.5		86	80	78	72	A
α-nitroso β-naphthol	0.1		79	79	79	76	A
Azoxybenzene sulfanilamide	0.1		96	93	86	82	A
Sodium β-naphthalene sulfonate	0.1		91	88	85	76	B
Triethanolamine	0.1 ml/l		90	85	85	82	B

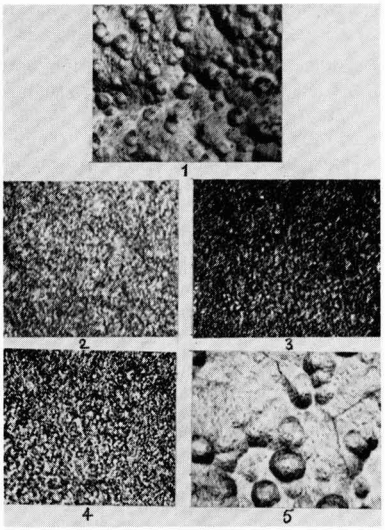

Fig. 3. Photomicrographs of deposits. Temp. 60°C, Cu cathode, magnification 1 x 700. Plate 1—Ni 0.3M, ratio 8, 1 amp/dm²; Plate 2—Ni 0.3M, ratio 8, am.citrate 20 g/l, 1 amp/dm²; Plate 3— Ni 0.5M, ratio 8, am.citrate 33.3 g/l, 2 amp/dm²; Plate 4—Ni 0.5M, ratio 8, am.citrate 33.3 g/l, 4 amp/dm²; Plate 5—Ni 0.5M, ratio 8, am.citrate 33.3 g/l, cobalt chloride 4.8 g/l, 2 amp/dm².

c.d. In the majority of cases the values were from 80 to 94% (Table I and Fig. 4-8). The deposits were satisfactory even though the efficiency was less than 100%. It was possible to work the bath up to 10 amp/dm² with addition agents. The anode efficiency was about 100% throughout, and the values have therefore not been recorded under different conditions (Fig. 8). There was some sludge formation at the anode. The corrosion was, however, quite normal even beyond the limiting cathode c.d.

Potentials.—The cathode potential decreased[2] with increase of nickel or citrate content of the solution, temperature or agitation, and decrease in the ratio or pH (not shown). However, the potential changes were not very marked. The values were decreased by the addition of lead acetate, thiourea, beta-naphthol, and selenium dioxide (0.15 v decrease), and increased by gelatin (Table I and Fig. 9-11). The effect of the variables on the anode potential was in general similar to that on the cathode side (not recorded). Figure 12 shows that the chloride ion promotes anode corrosion.

[2] "Decreased" means that the potential has become more noble, i.e., has shifted toward the potential of a gold electrode.

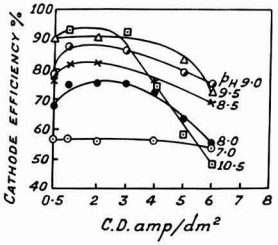

Fig. 4. Effect of pH on cathode efficiency. Temp. 60°C, Ni 0.3M, ratio 8, am.citrate 20 g/l.

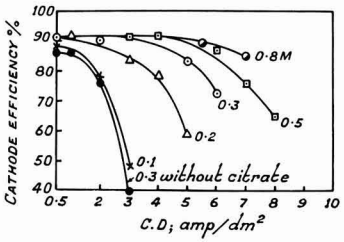

Fig. 5. Effect of nickel concentration on cathode efficiency. Temp. 60°C, ratio 8, pH 9.5, am.citrate 66.6 g/l for 1M Ni.

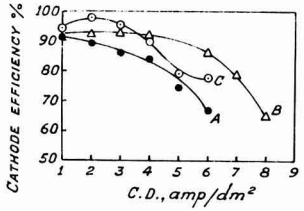

Fig. 6. Effect of ratio and am.citrate on cathode efficiency. Temp. 60°C, Ni 0.5M, pH 9.5. (A) ratio 8, am.citrate 20 g/l, (B) ratio 8, am.citrate 33.3 g/l, (C) ratio 6, am.citrate 33.3 g/l.

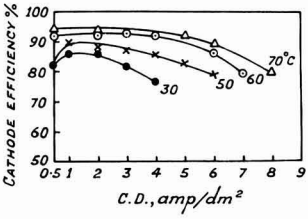

Fig. 7. Effect of temperature on cathode efficiency. Ni 0.5M, ratio 8, pH 9.5, am.citrate 33.3 g/l.

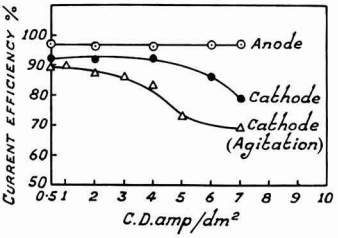

Fig. 8. Effect of agitation on cathode efficiency and anode efficiency. Temp. 60°C, Ni 0.5M, ratio 8, pH 9.5, am.citrate 33.3 g/l.

Throwing power.—Table II gives the results on throwing power measurements for the pyrophosphate, Watts (4), and chloride (14) baths under optimum conditions. The throwing power decreased with increase of c.d., and increased to some extent with increase in the linear ratio. There was reasonable agreement between the values calculated from the Field and Gardam equations. The reciprocal of the slope of the plot of the metal ratio against linear ratio, called the throwing index (15), gives a direct measure of the throwing power. Figure 14 gives this plot for the three baths; the index values are given in Table II.

Table II. Throwing power

ρ sp. resistivity ohm/cm³; b slope of cathode potential- log c.d. curve; N throwing number $= b/2\rho$; L, M, and R linear, metal, and current ratios, respectively (13)

	ρ	b	N
Pyrophosphate	4.51	0.545	0.0604
Watts	11.60	0.090	0.0039
Chloride	5.48	0.125	0.0114

Bath	c.d., amp/dm²	L	M	R	Throwing field	Power % Gardam	Throwing index
Pyrophosphate	0.5	5	2.11	1.57	57	—	10.0
	1.0	5	2.32	2.00	50	—	
	2.0	5	3.12	2.54	39	41	
	4.0	5	—	3.28	—	27	
	6.0	5	—	3.66	—	20	
	1.0	11	2.53	2.42	74	—	
	1.0	3	1.75	1.66	46	—	
Watts	0.5	5	3.38	3.97	25	—	2.8
	1.0	5	3.80	4.35	17	—	
	2.0	5	4.05	4.64	14	5	
	4.0	5	—	4.81	—	3	
	6.0	5	—	4.87	—	2	
	1.0	11	5.34	8.19	40	—	
	1.0	3	2.59	2.77	11	—	
Chloride	0.5	5	2.98	2.87	40	—	4.7
	1.0	5	3.00	3.55	33	—	
	2.0	5	3.27	4.11	37	14	
	4.0	5	—	4.50	—	7	
	6.0	5	—	4.65	—	5	
	1.0	11	4.27	5.21	43	—	
	1.0	3	2.51	2.45	33	—	

Control and maintenance of bath.—The bath was quite stable under the conditions of operation. In a typical case with a solution containing 0.5M nickel, ratio 8, and ammonium citrate 33.3 g/l, the cathode and anode efficiencies were 92 and 96%, respectively. The changes before and after electrolysis for 1 hr at 4 amp/dm² and 60°C were: nickel 29.8, 29.9; total pyrophosphate (P_2O_7) 234.6, 234.5 g/l; *p*H 9.50, 9.52; specific resistivity 4.51, 4.50 ohm/cm³; orthophosphate nil. A freshly prepared solution could be used for several runs with consistent and satisfactory results. Ageing of the electrolyte up to six months had no effect on the performance.

Testing of deposits.—Satisfactory coatings of any desired thickness from 0.0003 in. onward, calculated from area and weight, could be obtained. Bending and breaking tests indicated excellent adherence of the electroplate to the copper base. Deposits were free from porosity as shown by the electrographic method. A filter paper moistened with a 5% solution of sodium nitrite is applied to a coating of nickel on brass, and a sheet of platinum is placed on top. The test specimen is made the anode and the metal plate the cathode while a current of 2 ma/in.² is passed for 3 min. The paper is then developed for 1 min in a solution of 50 g/l potassium ferrocyanide and 30 g/l glacial acetic acid. Porosity is shown by brown spots on the paper. The hardness of deposits, 0.001 in. thick, increased with increase of c.d. from 1 to 6 amp/dm²: 380 to 450 Vickers, and decreased with increase of temperature from 50° to 80°C: 470 to 240.

Comparison of pyrophosphate and acid baths.—Table III gives the plating characteristics under optimum conditions for the pyrophosphate, Watts, and chloride baths for nickel plating. Data for the last two have been obtained experimentally for typical commercial compositions (4, 14).

The pyrophosphate bath is comparable to the acid baths in all important characteristics. The advantages of this bath over the others are: low metal content, high throwing power, and ability to plate directly on zinc.

Discussion

Experimental results show that the pyrophosphate bath is satisfactory for the plating of nickel. The solution mentioned by Langbein (2) contains nickel pyrophosphate 19.5 and sodium pyrophosphate 79.4 g/l; it is operated at 0.5 amp/dm², the bath voltage being 3.5 v. The zialite bath (3) consists of nickel in the form of pyrophosphate and citrate complexes, sodium and ammonium sulfates, chlorides, and free ammonia. It has been used for plating on zinc at 21°-35°C, *p*H 7.5-9.0, and current densities up to 2.5 amp/dm². The current efficiency

Table III. Comparison between pyrophosphate and acid baths

	Pyrophosphate		Watts		Chloride	
Composition g/l	Nickel chloride ($NiCl_2$, $6H_2O$)	118.9	Nickel sulfate ($NiSO_4$, $7H_2O$)	300	Nickel chloride	300
	Pyrophosphate (P_2O_7)	234.8	Nickel chloride	60	Boric acid	30
	Ammonium citrate	33.3	Boric acid	38		
	Nickel (0.5M)	29.4	Nickel	77.5	Nickel	74.1
*p*H	9.5		5.5		3.8	
Temp, °C	60		50		54	
Sp. resistivity, ohm/cm³	4.51		11.60		5.48	
Bath voltage, v	1.3-2.6		0.8-2.5		0.6-1.9	
Cathode c.d. (max.), amp/dm²	6		6		8	
Anode c.d. (max.), amp/dm²	8		8		8	
Cathode efficiency %	86-93		87-100		85-100	
Anode efficiency %	96-97		100-104		94-102	
Cathode polarization, v 0.5-6.0 amp/dm²	0.43-0.78		0.33-0.40		0.18-0.32	
Throwing power %, Gardam, 2 amp/dm²	41		5		14	
Hardness of deposit Vickers, 2 amp/dm²	390		200		350	

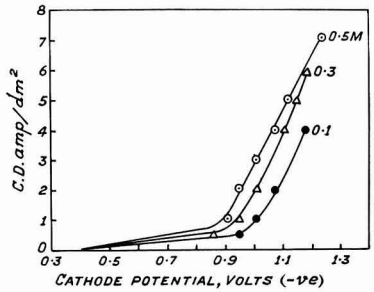

Fig. 9. Effect of nickel concentration on cathode potential. Temp. 60°C, ratio 8, pH 9.5, am.citrate 66.6 g/l for 1M Ni.

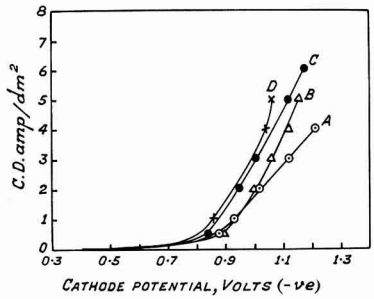

Fig. 10. Effect of ratio, am.citrate concentration and agitation on cathode potential. Temp. 60°C, Ni 0.5M, pH 9.5. (A) ratio 8, am.citrate 20 g/l; (B) ratio 10, am.citrate 33.3 g/l; (C) ratio 8, am.citrate 33.3 g/l, (D) ratio 8, am.citrate 33.3 g/l, agitation.

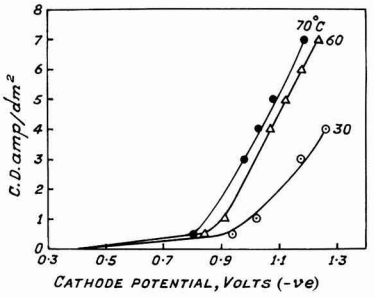

Fig. 11. Effect of temperature on cathode potential. Ni 0.5M, ratio 8, pH 9.5, am.citrate 33.3 g/l.

is 92% at 1.5 amp/dm², the values decreasing with increasing c.d. Solutions used in the present investigation are simple in composition, and even at 30°C the limiting c.d. is 4 amp/dm².

Most of the addition agents given in Table I act as brighteners in the Watts bath. Sodium sulfite and bisulfite have also been used in the zialite bath (3) and the pyrophosphate (16) and cyanide (4) baths for copper. The beneficial effects of ammonium citrate are similar to those obtained in the deposition of copper (16) and zinc (17) from the pyrophosphate bath. Brighteners in other baths include: gelatin and beta-naphthol in zinc (17) and tin (10) pyrophosphate, and lead acetate, sodium beta-naphthalene sulfonate and triethanolamine in copper (16) pyrophosphate baths. Cobalt, lead, and zinc codeposit with nickel from this bath. All these

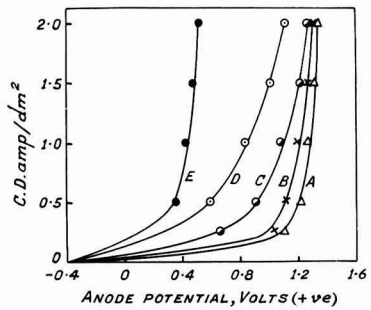

Fig. 12. Effect of chloride on anode potential. Bath prepared from: (A) to (D) nickel pyrophosphate, (E) nickel chloride and potassium pyrophosphate. Temp. 60°C, Ni 0.5M, ratio 8, pH 9.5 am.citrate 33.3 g/l, (A) KCl nil, (B) KCl 3 g/l, (C) KCl 6 g/l, (D) KCl 10 g/l.

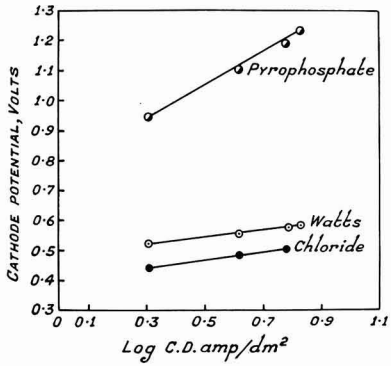

Fig. 13. Cathode potential—Log c.d. lines. Pyrophosphate bath—nickel chloride 118.9, pyrophosphate 234.8, am.citrate 33.3 g/l; pH 9.5, 60°C. Watts bath—nickel sulfate 300, nickel chloride 60, boric acid 38 g/l; pH 5.5, 50°C. Chloride bath—nickel chloride 300, boric acid 30 g/l; pH 3.8, 54°C.

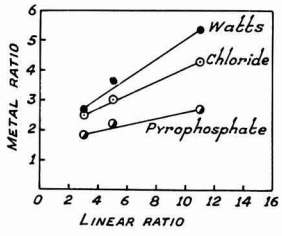

Fig. 14. Throwing index. L and M values at 1 amp/dm² from Table II.

substances belong to three broad types from the viewpoint of the current theories of addition agent action (18): complex formation, codeposition, and the formation of compounds which may exist as adsorbable colloids in the cathode film or function as brighteners on the analogy of their acid pickling inhibiting tendency.

The nickel electrode did not give reproducible potentials; this has been observed by other workers. It appears to be due to a passive film on the metal surface, giving a more noble potential. The passage of nitrogen or a freshly deposited nickel surface

changed the static potential in a negative direction, and a combination of these two gave the most satisfactory value. In a 0.5M nickel solution the potential values were: −0.1 under normal conditions, −0.4 for deposited surface, and −0.5 v for deposited surface under nitrogen. Taking the last value the instability constant for the complex (molar ratio of pyrophosphate to metal 2) was of the order of 10^{-9}, indicating a fairly stable complex. The static potential values including those given in Table I correspond to the deposited condition.

Cathode polarization was high, as in the deposition of other metals from this bath (7). Polarization is considerable during the deposition of nickel from the sulfate and sulfamate (19) baths; in the former case it is about 0.2 to 0.3 v. In the pyrophosphate bath the polarization was in the range 0.4 to 0.9 v. The relationship between cathode potential and log c.d. is linear under optimum conditions for the pyrophosphate, Watts, chloride (Fig. 13), and sulfamate (19) baths, and fine-grained deposits are obtained. This is in accordance with the views of Gardam (20) that the logarithmic relationship is an indication of frequent formation of new nuclei. Similar results have been obtained in the plating of tin (10), zinc (17), and copper (7) from the pyrophosphate bath. The slope of the potential-log c.d. straight line was 0.55, much greater than the values for the Watts and chloride baths (Fig. 13 and Table II). For the pyrophosphate bath the slope of the plot of polarization under agitation, against log c.d., was 0.34 (from Fig. 10, curve D). Calculations from the Tafel equation gave a value of the order of 10^{-4} amp/cm^2 for the exchange current density, and 0.1 for alpha under these conditions. The corresponding values reported in literature (21) for nickel from sulfate bath are 10^{-9} amp/cm^2 and 0.5, respectively.

The bath possesses good throwing power. In view of the greater slope of the potential-log c.d. lines and the lower resistivity the throwing power of this bath is much better than that of the acid baths. The throwing index is also greater.

The anode potentials of nickel in pyrophosphate solutions indicate the phenomenon of passivity (Fig. 12). The passive anode shows a potential of 1.2 v., close to the oxygen evolution value. Increasing additions of potassium chloride change the potentials to more negative values, and finally at the chloride concentrations used for plating the potential is 0.4 v, the active value. Unlike the partial passivity in acid solutions, the nickel anode is totally passive in the pyrophosphate bath. Addition of chloride raises the efficiency from 0 to 100%. Anode polarization was rather high, 0.8-0.9 v, but the values cannot be regarded as accurate in view of the sludge formation.

The electrodeposition of alloys of nickel with tin, copper, zinc, cobalt, iron, manganese, tungsten, and molybdenum from this bath has been reported elsewhere (8, 22-24).

Acknowledgment

Our thanks are due to Professor K. R. Krishnaswami, Head of the Department, for his keen interest in the work. One of the authors (S. K. Panikkar) is grateful to the Government of India for the award of a Senior Research Scholarship during the period of the investigation.

Manuscript received May 20, 1958. This paper was prepared for delivery before the Ottawa Meeting, Sept. 28-Oct. 2, 1958.

Any discussion of this paper will appear in a Discussion Section to be published in the December 1959 JOURNAL.

REFERENCES

1. C. J. Brockman and J. P. Nowlen, *Trans. Electrochem. Soc.*, **69**, 541 (1936).
2. G. Langbein, "Electrodeposition of Metals," p. 318, Hodder and Stoughton, London (1920).
3. R. L. Tuttle, U. S. Pat. 2,069,566 (1937).
4. A. G. Gray, Editor, "Modern Electroplating," John Wiley & Sons, Inc, New York (1953).
5. S. K. Panikkar and T. L. Rama Char, *J. Sci. Ind. Research, India*, **14B**, 603 (1955).
6. S. K. Panikkar and T. L. Rama Char, Symposium on Electrodeposition and Metal Finishing, 1957, India Section, Electrochemical Soc., under publication.
7. T. L. Rama Char, *Electroplating and Metal Finishing*, **10**, 347 (1957).
8. T. L. Rama Char, *ibid.*, **10**, 391 (1957).
9. J. Vaid and T. L. Rama Char, *Bull. India Sect., Electrochem. Soc.*, **7**, 5 (1958).
10. J. Vaid and T. L. Rama Char, *This Journal*, **104**, 282 (1957).
11. H. E. Haring and W. Blum, *Trans. Electrochem. Soc.*, **44**, 313 (1923).
12. S. Field, *J. Electrodepositors' Tech. Soc.*, **9**, 144 (1934).
13. G. E. Gardam, *Trans. Faraday Soc.*, **34**, 698 (1938).
14. W. A. Wesley and J. W. Carey, *Trans. Electrochem. Soc.*, **75**, 209 (1939).
15. R. V. Jelinek and H. F. David, *This Journal*, **104**, 279 (1957).
16. S. K. Panikkar, R. P. Singh, and T. L. Rama Char, *Bull. India Sect., Electrochem. Soc.*, **6**, 69 (1957).
17. J. Vaid and T. L. Rama Char, *J. Sci. Ind. Research, India*, **15B**, 509 (1956).
18. J. A. Henricks, *Trans. Electrochem. Soc.*, **82**, 113 (1942).
19. S. Sathyanarayana and T. L. Rama Char, *J. Sci. Ind. Research, India*, **16A**, 78 (1957).
20. G. E. Gardam, *Discussions Faraday Soc.*, **1**, 182 (1947).
21. J. O'M. Bockris, "Modern Aspects of Electrochemistry," p. 217, Butterworths Scientific Publications, London (1954).
22. S. K. Panikkar and T. L. Rama Char, *J. Electrochem. Soc., Japan*, **25**, E121, 573 (1957).
23. S. K. Panikkar and T. L. Rama Char, *J. Sci. Ind. Research, India*, **17A**, 95 (1958).
24. Vasanta Sree and T. L. Rama Char, *Bull. India Sect., Electrochem. Soc.*, **7**, 72 (1958).

Phase Equilibria and Fluorescence in the System $Zn(PO_3)_2$-$Mg(PO_3)_2$

J. F. Sarver and F. A. Hummel

Department of Ceramic Technology, College of Mineral Industries, The Pennsylvania State University, University Park, Pennsylvania

ABSTRACT

The equilibrium diagram for the system $Zn(PO_3)_2$-$Mg(PO_3)_2$ was established as a solid solution type by quenching and solid-state methods. About 10 mole % $Mg(PO_3)_2$ was found soluble in β-$Zn(PO_3)_2$ at 850°C, but less than 2 mole % was soluble in α-$Zn(PO_3)_2$ at 650°C. Solid solution of $Zn(PO_3)_2$ in $Mg(PO_3)_2$ was extensive, ranging from approximately 35 to 100 mole % $Mg(PO_3)_2$.

The cathodoluminescence of compositions in the three solid-solution series was examined for peak emission and brightness when activated with manganese. A shift in the position of the emission peak from 6000 to 6200Å in the magnesium metaphosphate solid-solution series has been interpreted in terms of the difference in influence between magnesium and zinc ions on the polarizability of oxygen ions in the neighborhood of the manganese activator.

Equilibrium relationships in the system $Zn(PO_3)_2$-$Mg(PO_3)_2$ were established as an aid to the identification and understanding of the host lattices which are responsible for the luminescence of preparations in the system ZnO-MgO-P_2O_5. It is well known that the ortho-, pyro-, and metaphosphate compounds of zinc and magnesium are bases for several phosphors which emit in the red portion of the visible spectrum and a few others which emit in the orange or green portion.

Two previous papers have dealt with the phase relationships in the system ZnO-P_2O_5 (1) and the emission characteristics of the manganese-activated zinc phosphate compounds under cathode ray excitation (2).

Berak (3) has established the melting points and eutectic compositions and temperatures in the system MgO-P_2O_5. The fluorescence of the magnesium phosphate compounds has not been explored as extensively as that of their zinc phosphate counterparts, probably due to the generally low brightness obtained with manganese activation. No equilibrium data have been published for the ternary system ZnO-MgO-P_2O_5.

Experimental Procedure

Compositions Used for Determination of Equilibrium Relationships

Ten-gram batches of the compositions shown in Table I (weighed to 0.0001 g) were made from C.P. ZnO, C.P. basic magnesium carbonate, and C.P. $(NH_4)_2HPO_4$ and were melted to glasses in platinum crucibles for use in quench determinations.

To minimize P_2O_5 volatilization during melting, the batch materials were reacted in the solid state at about 800°C for 24 hr. The batches were melted then in platinum crucibles for 10 min between 900° and 1200°C. The glasses were air quenched, crushed in a steel mortar, and passed through 100 and 120 mesh sieves. The fraction retained on the 120 mesh screen was reserved for index of refraction measurements, and the minus 120 mesh material was used for quench experiments after magnetic removal of traces of metallic iron introduced by the crushing process.

Heat Treatment and Physical Measurements

The melting, quenching, solid-state reactions, phase identification, differential thermal analyses, and measurement of emission spectra were carried out as described in previous papers (1, 2). Calibration of thermocouples used in the quench work was done using Li_2SiO_3 (1201°C), Au (1063°C), and Ag (961°C); the accuracy of temperature measurement was generally ±2°C.

CuKα radiation was used for x-ray identification

Table I. Composition and refractive indexes of metaphosphate glasses

Comp. No.	Mole % $Zn(PO_3)_2$	Mole % $Mg(PO_3)_2$	Refractive index, $n_D \pm 0.001$ Sodium light, $\lambda = 5890$Å
1	100.0	0.0	1.517
2	95.0	5.0	1.517
3	90.0	10.0	—
4	85.0	15.0	1.515
5	80.0	20.0	—
6	75.0	25.0	1.513
7	70.0	30.0	—
8	65.0	35.0	1.511
9	55.0	45.0	1.508
10	45.0	55.0	1.505
11	35.0	65.0	1.503
12	25.0	75.0	1.500
13	15.0	85.0	1.496
14	5.0	95.0	1.492
15	0.0	100.0	1.491

Table II. X-ray diffraction data for the metaphosphate compounds

α-$Zn(PO_3)_2$			β-$Zn(PO_3)_2$			$Mg(PO_3)_2$		
2θ	d	I/I_o	2θ	d	I/I_o	2θ	d	I/I_o
13.5	6.56	5	16.5	5.37	5	14.5	6.11	10
13.7	6.46	15	17.3	5.13	5	19.5	4.55	45
13.8	6.42	55	17.6	5.04	5	21.0	4.23	25
14.4	6.15	5	19.6	4.53	10	25.4	3.51	15
19.3	4.60	5	20.1	4.42	10	26.5	3.36	25
20.0	4.44	55	21.8	4.08	40	27.8	3.21	45
20.8	4.27	50	23.1	3.85	10	28.2	3.16	35
25.2	3.53	5	23.4	3.80	30	29.9	2.99	100
25.8	3.45	55	24.0	3.71	15	31.3	2.86	20
26.4	3.38	5	25.5	3.49	45	32.9	2.37	5
27.1	3.29	—	25.8	3.45	100	35.0	2.56	20
27.6	3.23	5	26.2	3.40	25	37.9	2.37	15
28.1	3.18	5	27.2	3.28	10	39.7	2.27	5
29.3	3.05	15	27.8	3.21	15	40.2	2.24	5
30.1	2.97	95	29.8	3.00	—	41.5	2.18	10
30.7	2.91	100	31.8	2.81	10	43.3	2.09	20
31.2	2.87	5	32.5	2.75	10	46.7	1.940	5
31.7	2.82	20	33.6	2.67	10	47.2	1.925	5
34.8	2.58	5	35.4	2.54	—	48.4	1.887	5
35.5	2.53	5	36.3	2.47	5	51.0	1.791	5
37.3	2.41	45	37.4	2.40	10	53.1	1.728	5
37.7	2.39	10	37.7	2.39	10	54.3	1.689	5
38.2	2.36	25	39.6	2.28	10	55.8	1.650	5
42.4	2.13	10	40.0	2.25	5	56.6	1.626	10
42.9	2.11	10	40.8	2.21	5	57.2	1.610	10
43.8	2.07	25	41.2	2.19	10	60.3	1.535	10
45.1	2.01	10	41.5	2.18	5	61.2	1.514	10
45.4	2.00	10	44.1	2.05	5	62.0	1.497	5
46.8	1.94	5	44.3	2.04	15	67.9	1.380	10
47.9	1.90	20	47.8	1.90	5	Other reflections		
50.1	1.82	—	48.2	1.89	5			
50.6	1.80	—	48.7	1.87	5			
51.0	1.79	10	49.6	1.84	5			
52.0	1.76	—	51.4	1.78	5			
52.4	1.75	5	53.9	1.70	10			
53.5	1.71	5	Other reflections					
56.6	1.63	10						
56.9	1.62	10						
57.5	1.60	10						
59.6	1.55	10						
60.1	1.54	50						
60.7	1.53	5						
Other reflections								

of crystalline materials. Petrographic microscope determinations of refractive indexes of glasses and crystals were accurate to ±0.001 using index oils which had been calibrated with an Abbé refractometer. Cathodoluminescent emission spectra were determined on a demountable tube using an electron beam with a current density of 2.0 μamp/cm² and an accelerating potential of 16 kv.

Results and Discussions

Magnesium Metaphosphate

Although it was already known that ortho-, pyro-, and metaphosphate compounds of magnesium exist, the system was briefly re-examined by solid-state reactions and the three compounds were confirmed. Then further work was carried out on the thermal behavior of $Mg(PO_3)_2$ to check for possible inversions and the nature of melting. The congruent melting point was determined by quenching experiments to be 1165° ±5°C which agrees well with that reported by Berak (3).

No inversions were detected after extensive solid-state, quenching, D.T.A., and dilatometric experiments. Crystals prepared by devitrification of $Mg(PO_3)_2$ glass were found to be biaxial negative with $n_\beta = 1.585$ and 2 v equal to about 30°C. The x-ray diffraction data for $Mg(PO_3)_2$ and the two forms of $Zn(PO_3)_2$ are given in Table II.

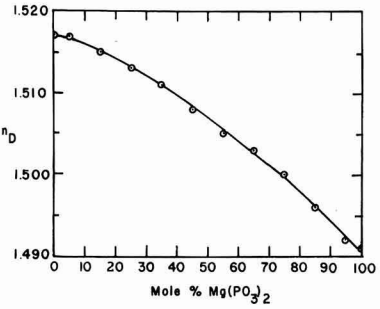

Fig. 1. Indexes of refraction of metaphosphate glasses

Phase Equilibrium Relationships in the System $Zn(PO_3)_2$-$Mg(PO_3)_2$

The refractive index curve for the metaphosphate glasses is shown in Fig. 1. These data were used extensively during the petrographic examination of the many quenches made in the system. The important quench data are summarized in Table III and the equilibrium diagram based on these data is shown in Fig. 2. The starting material for the quench work was a glass, and all phase identifications were made with the petrographic microscope, except for composition No. 16. In this case the starting material was batch which had been reacted below 650°C and the phase identifications were made by x-ray diffraction.

The system is characterized by two small regions of solid solution near the $Zn(PO_3)_2$ compound, a large region of $Mg(PO_3)_2$ solid solutions, and a mis-

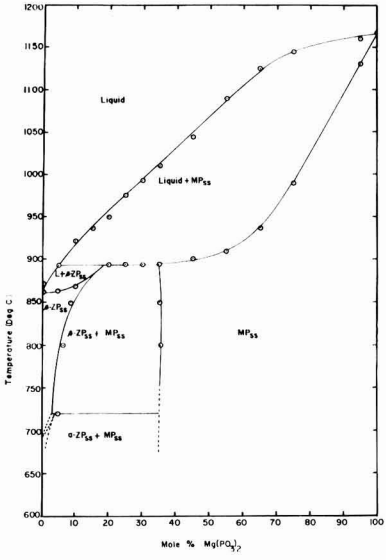

Fig. 2. Equilibrium relationships in the system $Zn(PO_3)_2$-$Mg(PO_3)_2$.

Table III. Quench data for the system $Zn(PO_3)_2$-$Mg(PO_3)_2$

Comp. No.	Mole % ZP	Mole % MP	Quench temp, °C	Time, min	Phases*	Remarks
1	100	0	860	30	β-ZP	
	100	0	865	15	G+β-ZP	
	100	0	871	15	G+β-ZP	Trace crystals
2	95	5	838	30	β-ZP_{ss}	
	95	5	859	30	β-ZP_{ss}	
	95	5	864	30	G+β-ZP_{ss}	Trace glass
	95	5	878	20	G+β-ZP_{ss}	
	95	5	890	20	G+β-ZP_{ss}	Trace crystals
	95	5	895	15	G	
3	90	10	861	30	β-ZP_{ss}	
	90	10	865	30	G+β-ZP_{ss}	
	90	10	872	30	G+β-ZP_{ss}	
	90	10	920	20	G+MP_{ss}	Trace crystals
	90	10	925	15	G	
4	85	15	870	30	β-ZP_{ss}	
	85	15	875	30	G+β-ZP_{ss}	Trace glass
	85	15	881	30	G+β-ZP_{ss}	
	85	15	888	30	G+MP_{ss}	
	85	15	935	20	G+MP_{ss}	
	85	15	940	20	G	
5	80	20	892	30	β-ZP_{ss}+MP_{ss}	
	80	20	896	30	G+MP_{ss}	
	80	20	902	30	G+MP_{ss}	
	80	20	918	30	G+MP_{ss}	
	80	20	937	30	G+MP_{ss}	
	80	20	944	20	G+MP_{ss}	
	80	20	949	20	G+MP_{ss}	Trace crystals
6	75	25	893	30	β-ZP_{ss}+MP_{ss}	
	75	25	897	30	G+MP_{ss}	Trace glass
	75	25	912	30	G+MP_{ss}	
	75	25	965	15	G+MP_{ss}	
	75	25	973	15	G+MP_{ss}	Trace crystals
	75	25	976	15	G	
7	70	30	892	30	β-ZP_{ss}+MP_{ss}	
	70	30	897	30	G+MP_{ss}	Trace glass
	70	30	910	30	G+MP_{ss}	
	70	30	916	30	G+MP_{ss}	
	70	30	922	30	G+MP_{ss}	
	70	30	982	15	G+MP_{ss}	
	70	30	992	15	G+MP_{ss}	Trace crystals
8	65	35	890	30	MP_{ss}	
	65	35	898	30	G+MP_{ss}	
	65	35	911	20	G+MP_{ss}	
	65	35	963	20	G+MP_{ss}	
	65	35	981	20	G+MP_{ss}	
	65	35	1003	15	G+MP_{ss}	Trace crystals
	65	35	1008	20	G	
9	55	45	898	30	MP_{ss}	
	55	45	910	30	G+MP_{ss}	
	55	45	914	30	G+MP_{ss}	
	55	45	930	30	G+MP_{ss}	
	55	45	1033	15	G+MP_{ss}	
	55	45	1038	15	G+MP_{ss}	
	55	45	1041	15	G+MP_{ss}	Trace crystals
	55	45	1068	15	G	

Table III (Continued)

Comp. No.	Mole % ZP	Mole % MP	Quench temp, °C	Time, min	Phases*	Remarks
10	45	55	908	20	MP_{ss}	
	45	55	912	20	G+MP_{ss}	
	45	55	917	20	G+MP_{ss}	
	45	55	1080	10	G+MP_{ss}	
	45	55	1087	10	G+MP_{ss}	
	45	55	1092	12	G	
11	35	65	932	30	MP_{ss}	
	35	65	940	15	G+MP_{ss}	Trace glass
	35	65	1122	15	G+MP_{ss}	
	35	65	1126	15	G	
12	25	75	977	30	MP_{ss}	
	25	75	987	30	MP_{ss}	
	25	75	1004	30	G+MP_{ss}	
	25	75	1012	30	G+MP_{ss}	
	25	75	1140	15	G+MP_{ss}	
	25	75	1144	15	G+MP_{ss}	
	25	75	1149	15	G	
14	5	95	1115	30	MP_{ss}	
	5	95	1130	30	MP_{ss}	Trace glass
	5	95	1157	15	G+MP_{ss}	
	5	95	1163	15	G	
15	0	100	1161	15	G+MP	Trace glass
	0	100	1168	15	G	
16	95	5	687	20 hr.	α-ZP_{ss}+MP_{ss}	
	95	5	701	20 hr.	α-ZP_{ss}+MP_{ss}	
	95	5	716	24 hr.	α-ZP_{ss}+MP_{ss}	
	95	5	725	24 hr.	β-ZP_{ss}+MP_{ss}	

* G, glass; ZP, $Zn(PO_3)_2$; MP, $Mg(PO_3)_2$; ss, solid solution.

cibility gap involving β-$Zn(PO_3)_2$ and $Mg(PO_3)_2$ solid solutions. At 850°C, the two-phase region extends from about 10-35 mole % $Mg(PO_3)_2$.

Further confirmation of the nature and extent of solid solution was obtained on a series of well-crystallized compositions which had been prepared by devitrification of glasses at 800°C for 24 hr. Diffraction patterns shown in Fig. 3 were obtained with a rotating specimen holder and a goniometer speed of 1°/min. An examination of the patterns of compositions containing 100-35 mole % $Mg(PO_3)_2$ showed that there was practically no change in peak positions, but only a change in intensity for certain 2θ reflections, notably those at 14.5°, 19.5°, 21°, and 27.8°.

A more detailed examination of the $Mg(PO_3)_2$ solid-solution series was made by obtaining diffraction patterns at a goniometer speed of ¼° (2θ)/min. When the patterns of the end members of the solid-solution series (Fig. 3a) were compared [$Mg(PO_3)_2$ vs. ($Mg_{0.35}Zn_{0.65}$) $(PO_3)_2$], the maximum shift in position of any particular high angle reflection was 0.05°, indicating a very low order of magnitude of change in lattice dimensions. With increasing amounts of zinc in solid solution, the small shift was toward lower angles, indicating only the slightest increase in lattice dimensions.

When attention is focused on the patterns of compositions containing 30-10 mole % $Mg(PO_3)_2$ (Fig. 3b), it is evident that two solid solutions are present in this range. The strong lines of $Mg(PO_3)_2$ at 29.9°

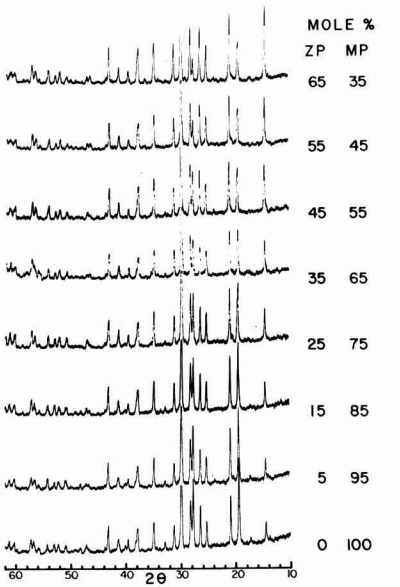

Fig. 3a. X-ray diffraction patterns of $Mg(PO_3)_2$ solid solutions.

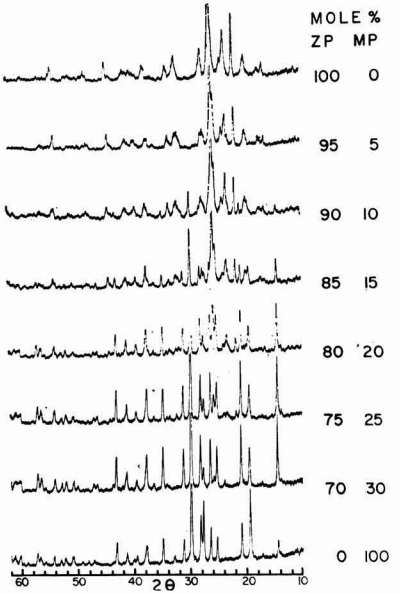

Fig. 3b. X-ray diffraction patterns of β-$Zn(PO_3)_2$ solid solutions and mixtures of β-$Zn(PO_3)_2$ solid solution and $Mg(PO_3)_2$ solid solution.

and 21.0° persist in this region as do the characteristic 25.8° and 21.8° lines of β-$Zn(PO_3)_2$. The relative intensities of the reflections of each of the two solid solutions do not change in this range, indicating constancy of composition.

Finally, it should be noted (Fig. 3b) that only the relative intensities in the 5 mole % $Mg(PO_3)_2$ pattern change when compared to the pattern for pure $Zn(PO_3)_2$, indicating that it is a solid solution having the structure of the beta form of zinc metaphosphate.

Table IV. Peak emission and brightness of metaphosphate phosphors

Comp., mole % ZP	Comp., mole % MP	°C/hr	Phases	Peak emission, Å	Brightness (f-L)
100	0	850/24	β-ZP	5700	33.9
95	5	850/24	β-ZP_{ss}	5700	17.0
85	15	850/24	β-ZP_{ss}+MP_{ss}	5900	18.2
100	0	650/48	α-ZP	6300	1.0
97.5	2.5	650/48	α-ZP_{ss}	6300	0.8
95	5	650/48	α-ZP_{ss}+MP_{ss}	6300	1.6
55	45	850/24	MP_{ss}	6000	25.2
45	55	850/24	MP_{ss}	6100	23.3
35	65	850/24	MP_{ss}	6100	23.0
25	75	850/24	MP_{ss}	6100	21.1
15	85	850/24	MP_{ss}	6100	18.9
5	95	850/24	MP_{ss}	6200	12.1
0	100	850/24	MP_{ss}	6200	9.8
NBS standard β-$Zn_3(PO_4)_2$				6380	36.0

Note: In the MP_{ss} series, one would expect the peak emission to vary systematically and continuously rather than in steps as shown (6200, 6100, 6000). However, the spectroradiometer curves could not be read with greater accuracy than that listed in the table.

It is conceivable that the brightness values listed above may have been affected by the method of preparation (settling in an aqueous medium) since metaphosphates are known to have relatively poor chemical durability.

It had been shown previously that pure α-$Zn(PO_3)_2$ could never be obtained by devitrifying a glass (1). A mixture of α and β forms always resulted from the crystallization. Likewise, from the glass containing 5 mole % $Mg(PO_3)_2$, a mixture of the α and β forms of $Zn(PO_3)_2$ and a $Mg(PO_3)_2$ solid solution always resulted from devitrification below 700°C. Quench work with this crystalline mixture showed that this assemblage could be converted to β-$Zn(PO_3)_2$ plus a $Mg(PO_3)_2$ solid solution between 716° and 725°C. Due to the uncertainties about the increase in the α and β inversion temperature with increase in Mg $(PO_3)_2$ in solid solution, the phase boundaries in this region of the diagram are showed in dashed lines.

Luminescence Studies

On the basis of the phase relationships determined above, the compositions shown in Table IV were selected for the preparation of manganese-activated phosphors. To each composition 0.01 mole MnO/mole (ZnO + MgO) was added, and heat treatments were carried out at subsolidus temperatures as listed in Table IV. The constitution of the phosphors was checked by x-ray diffraction patterns as shown in the fourth column of Table IV.

β-$Zn(PO_3)_2$ solid solutions.—The β-$Zn(PO_3)_2$ phosphors did not show any shift in their peak emission positions (5700Å). However, there was a noticeable decrease in brightness with increasing magnesium content. In the composition 85 $Zn(PO_3)_2$, a second phase was present, a $Mg(PO_3)_2$ solid solution. Its emission dominated that of the β-$Zn(PO_3)_2$ phosphor, raising the apparent brightness, and causing the peak emission to lie at 5900Å.

An interesting observation was made regarding the brightness of the β-$Zn(PO_3)_2$ phosphor. Katnack (2) prepared this phosphor by additions of 1 wt % MnO to preformed $Zn(PO_3)_2$ and obtained a brightness of 4.8 ft-L as compared with 33.9 obtained in this work. His preparation was fired 50°C lower than

the β-$Zn(PO_3)_2$ listed in Table IV, but the greatest part of the difference probably was due to starting materials.

α-$Zn(PO_3)_2$ *solid solutions.*—These phosphors do not exhibit a shift in the position of peak emission (6300Å) with increasing magnesium content. Magnesium seems to lower the brightness (Table IV), and with as little as 5 mole %, $Mg(PO_3)_2$ solid solution appears as a second phase.

The α-$Zn(PO_3)_2$ phosphors had a second emission band with a peak around 4000Å, but of much lower intensity than that at 6300Å.

$Mg(PO_3)_2$ *solid solutions.*—This is the most interesting series, since the $Mg(PO_3)_2$ lattice accommodates 65 mole % $Zn(PO_3)_2$ in solid solution without appreciable change in dimensions. However, there is a significant shift in peak emission from 6200Å for pure $Mg(PO_3)_2$ to 6000Å for the $(Zn_{0.55}Mg_{0.45})(PO_3)_2$ solid solution (Table IV).

Fonda (4) recently reviewed the influence of activator environment on the spectral emission of isomorphous compounds and solid solutions and indicated that lattice dimensions and polarizability of the ions are major factors which determine the position of the peak emission.

Since changes in cation to anion distances in this series of solid solutions are apparently extremely small, an explanation of the shift in peak emission might be based on the polarization of oxygen ions in the structures.

Unfortunately, the crystal structure of $Mg(PO_3)_2$ is not known. However, it is reasonable to assume that some kind of P-O unit forms the basic network and that zinc isomorphously replaces magnesium in MO_6 groups in the $Mg(PO_3)_2$ structure. If there were no difference in polarizing power between Zn^{2+} and Mg^{2+} and the ions acted as rigid spheres, some increase in lattice dimensions would be expected with increasing substitution of zinc (0.83Å) for magnesium (0.78Å). However, due to its 18 electron shell, the zinc ion distorts the oxygen ion, resulting in a Zn-O distance which gives essentially the same effective size for ZnO_6 and MgO_6 groups. Addition of manganese results in MnO_6 groups which are adjacent to MgO_6 groups in $Mg(PO_3)_2$ and to an increasing number of ZnO_6 groups as one proceeds to the $(Zn_{0.55}Mg_{0.45})(PO_3)_2$ solid solution. The electron density distribution in the oxygen around the manganese ion is controlled by the relative amount of zinc and magnesium in the solid solution. Substitution of zinc for magnesium apparently lowers the electron density around the Mn^{2+}, causing a change in the energy of electronic transitions and a resultant shift toward shorter wave lengths.

The change in energy required for the electronic transitions due to substitution of Zn^{2+} ions for Mg^{2+} ions is attended by an increase in brightness of these phosphors from 9.8 ft-L for $Mg(PO_3)_2$:Mn to 25.2 ft-L for $(Zn_{0.55}Mg_{0.45})(PO_3)_2$:Mn.

Summary

1. The solid solubility of $Mg(PO_3)_2$ in β-$Zn(PO_3)_2$ increases from about 3 mole % at 725° to about 10 mole % at 850°C. Increasing solubility of $Mg(PO_3)_2$ decreases the cathodoluminescent brightness of manganese-activated solid solutions which have a peak emission at 5700Å.

2. The solid solubility of $Mg(PO_3)_2$ in α-$Zn(PO_3)_2$ is very low, probably less than 2 mole % at 700°C. Manganese activated α-$Zn(PO_3)_2$ solid solutions have a very low cathodoluminescence brightness with a maximum at 6300Å.

3. Solid solubility of $Zn(PO_3)_2$ in $Mg(PO_3)_2$ is very extensive, ranging from 100-35 mole % Mg $(PO_3)_2$. The peak emission of manganese-activated cathodoluminescence varies from 6200Å for pure $Mg(PO_3)_2$ to 6000Å for a $(Zn_{0.55}Mg_{0.45})(PO_3)_2$ solid solution. Brightness increases with increase in Zn $(PO_3)_2$ in solid solution.

Acknowledgment

Emission curves were obtained through cooperation of Marjorie Brines of the Chemical Products Plant, General Electric Co. The investigation was made possible by the support of the Chemical Products Plant, General Electric Co., Cleveland, Ohio.

Manuscript received Dec. 3, 1958. This paper was prepared for delivery before the Philadelphia Meeting, May 3-7, 1959. Contribution No. 58-42 from the Department of Ceramic Technology, College of Mineral Industries, The Pennsylvania State University, University Park, Pennsylvania.

Any discussion of this paper will appear in a Discussion Section to be published in the December 1959 JOURNAL.

REFERENCES

1. F. L. Katnack and F. A. Hummel, *This Journal,* **105**, 125 (1958).
2. F. A. Hummel and F. L. Katnack, *ibid.*, 528.
3. Józek Berak, *Roczniki Chem.*, **32**, 17 (1958); *Chemical Abstracts* (June 25, 1958).
4. G. R. Fonda, *J. Optical Soc. America,* **47**, 877 (1957).

Chemical Etching of Silicon

I. The System HF, HNO_3, and H_2O

Harry Robbins and Bertram Schwartz

Hughes Semiconductors, Newport Beach, California

ABSTRACT

The kinetics of the etching of silicon in the system HF, HNO_3, and H_2O was studied as a function of the composition of the etchant at 25°C. A triaxial plot of the etch rate vs. composition of the etchant shows two extreme modes of behavior. In the region of high nitric acid compositions, etch rates are functions only of the hydrofluoric acid concentration. In the region of high hydrofluoric acid compositions, nitric acid concentration determines the etch rates. The kinetic behavior in the latter region is complicated by autocatalysis in which the reduction products of nitric acid are involved.

The reaction proceeds by an oxidation step followed by the dissolution of the oxide. In the high hydrofluoric acid region the oxidation step is rate limiting. In the high nitric acid region the dissolution step is rate limiting. In both regions the flow of reagent to the surface by diffusion determines the etch rates. A plot of the etch rates as a function of the concentration of the rate-limiting reagent indicates an exponential relationship between the etch rates and the concentration. This relationship has been explained qualitatively on the basis of a second, nonchemical autocatalytic factor, the heat of reaction.

This study was undertaken for the purpose of elucidating the physical and chemical processes that determine the behavior of an acid etching solution. The system HF, HNO_3, H_2O was chosen for study because it is the simplest, from the point of view of composition, of all the acid etching systems used on silicon. It was felt that an understanding of the simple system was a prerequisite for the understanding of the more complicated systems containing additives such as acetic acid, bromine, or heavy metal salts.

Experimental Procedure

The kinetics of the etching system was studied as a function of the composition of the etchant at constant initial temperature (25°C), and data were taken over the composition range where the decrement in die thickness exceeded 0.1 mil/min. Silicon specimens were ⅛ x ⅛ x 0.025 in. n-type dice of approximately 3 ohm-cm resistivity. The two large surfaces of the die were 111 oriented with an accuracy of about 90 min, while the remaining four surfaces were not oriented with respect to any crystal plane. All surfaces had been lapped with an abrasive grit and were work damaged to a depth of about ¼ mil.

The dice were etched, one at a time, in 10 cc of solution in a small Teflon beaker. Agitation was provided by an electric stirring motor equipped with a polyethylene paddle. The reaction was quenched at the proper time with a large volume of water. The dice were then rinsed in distilled water, dried, and measured with a micrometer.

All dice were etched three times, and each etch was performed in a fresh portion of the same solution. Since each etching period had been selected to remove from 4 to 6 mils from the specimen, it may be assumed that the work damage had been removed after the first etch. The third etch was performed in the presence of a few milligrams of $NaNO_2$, for reasons which will be explained later.

All etching was performed in a Teflon beaker immersed in a constant temperature bath regulated at 25°C. The heat transmission of the beaker was so poor, however, that the temperature of 25°C could not necessarily be maintained in the etch solution. Since the etching period was generally shorter than 1 min, and quite often of the order of only several seconds, it is extremely unlikely that thermal equilibrium was maintained, and the reaction may be considererd to have been run under essentially adiabatic conditions.

A triangular coordinate system was set up to represent the composition of the etchant. One vertex was arbitrarily chosen to represent the composition of the stock HNO_3 used to make up the solutions, and another vertex was similarly used to designate the stock HF. The third vertex, therefore, represents only the amount of added water, not the total amount of water present. This normalization of the axes results in a representation of the data valid only for one particular set of concentrations of reagents. However, the representation of the data in mole fraction units, which is free from this objection, led to identical conclusions.

In the preparation of the etching solutions, HF was weighed out to ±0.01 g. The weights of HNO_3 and water were converted to volumes and measured out in a buret to ±0.01 cc. Control of the composition of the etching solutions was established by analysis of the stock acids from which the solutions were to be made and adjustment of these stock acids to the proper concentration, which was arbitrarily taken as the analysis of the initial batch of reagents.

In order that the effect of crystal orientation and

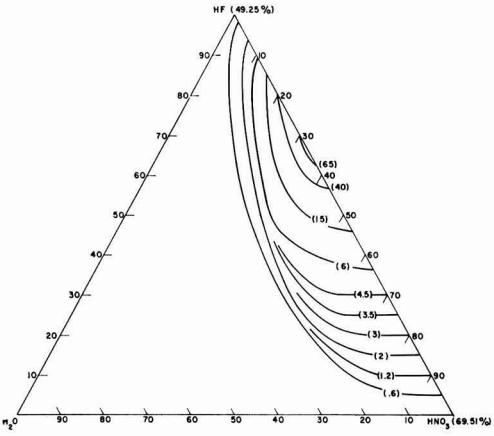

Fig. 1. Curves of constant rate of change of die thickness (mils per minute) as a function of etchant composition (weight per cent in the system 49.25% HF, 69.51% HNO_3, and water).

resistivity type on the etch rates might be checked, specimens of both p-type and n-type Si oriented along the 111, 110, and 100 planes, as well as small Si spheres, were etched in several compositions chosen at random.

Results and Discussion

Figure 1 is a plot of the etch rate (numbers in parentheses are the decrement in die thickness in mils per minute) as a function of the composition of the etchant. The reagents used in this study were the normally available concentrated acids, i.e., 49% HF and 70% HNO_3. It will be shown later that the range of compositions accessible through the use of these reagents was insufficient to clarify the mechanism in the HF-rich region, so that it was necessary to extend the range by employing more concentrated reagents, i.e., 60% HF and 90% HNO_3. Data corresponding to this system are plotted in Fig. 2.[1]

[1] Note that the 20%-added-water line of Fig. 2 corresponds approximately with the no-added-water line of Fig. 1.

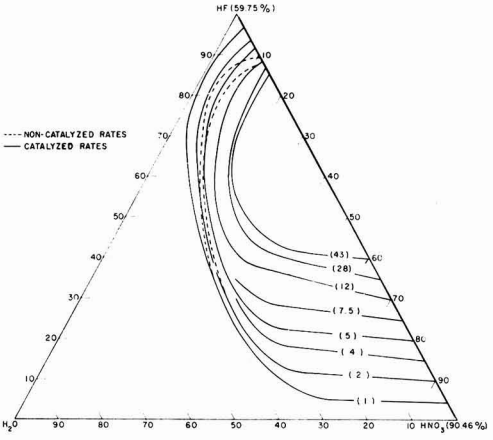

Fig. 2. Curves of constant rate of change of die thickness (mils per minute) as a function of etchant composition (weight per cent in the system 59.75% HF, 90.45% HNO_3, and water).

Rate-Limiting Reagents and Autocatalysis

The contours shown are lines of constant etching rate. In the high HNO_3 compositions the contours run parallel with lines of constant HF concentration, indicating a dependence of the rates only on the HF concentration. The slight inclination of the contours with respect to lines of constant weight per cent HF does not indicate a slight dependence of the rates on HNO_3, as a plot of the same data in mole fraction units results in an inclination of the contours in the other direction. In either case the inclination can be shown to be in the direction of constant molarity, which is kinetically a more significant unit, but which cannot be represented on a triaxial plot.

In the upper region of Fig. 2 there is a strong tendency for the contours to run parallel with lines of constant HNO_3 concentration, indicating that in this region only the HNO_3 concentration determines the rates. However, the behavior of the system is complicated by a second factor, autocatalysis. Rates shown by the dotted curves are second etch rates. They represent the action of fresh solution on a surface from which the work damage has been removed. The solid curves represent what shall be called catalyzed third-etch rates. These etches were performed in the presence of a trace of $NaNO_2$. Sodium nitrite decomposes in acid solution to yield oxides of nitrogen which are apparently catalysts for the reaction (1), as shown by the displacement of the solid contours in the direction of decreased HNO_3 concentration. At all compositions within the area bounded by the innermost dotted contour the added catalyst had no effect on the measured rates. The reaction is believed to require the presence of catalyst throughout the entire composition range. For the majority of compositions, however, the rates are sufficiently high that adequate catalyst is generated to assure its availability for the reaction, and other factors come into play to mask the effect of the catalyst concentration on the etch rates. It is only when the rates are very slow and HNO_3 dependent that the amount of generated catalyst is a prime factor in rendering the reaction self-sustaining.

Many etchant compositions have been found that attack a work-damaged surface readily but fail to re-etch the specimen after the work damage has been removed. This is another manifestation of the influence of the generated catalyst. Etch rates are initially more rapid on a work-damaged surface. The catalyst is either generated in adequate amounts or trapped in surface crevices, and the reaction rate can build up to the steady-state value. When the surface is free from work damage the initial reaction rate is very slow, and it is possible for the reaction products to be dispersed before they can become involved in the propagation of the reaction. The addition of oxides of nitrogen to the solution by any means, such as the addition of $NaNO_2$ or even a chip of work-damaged Si, will supply sufficient impetus to get the reaction started, and once it is started it will usually attain the same steady-state rate as a damaged specimen.

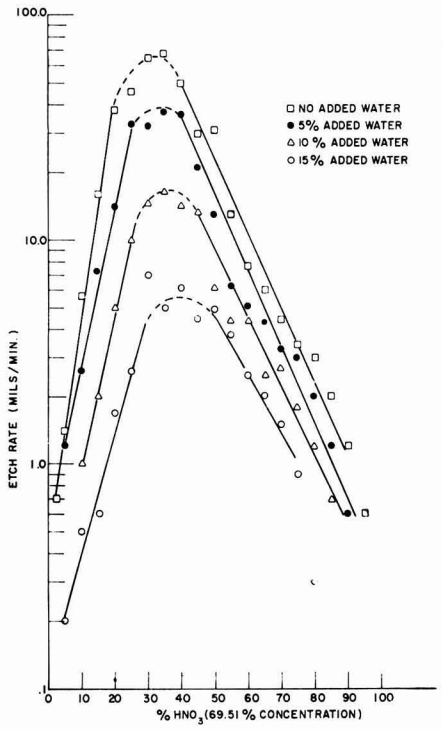

Fig. 3. Logarithm of the rate of change of die thickness as a function of the concentration of HNO_3.

In Fig. 2 the etch rates are initially insensitive to the addition of substantial amounts of water in both the high HF and the high HNO_3 regions, provided that the concentration of the rate-determining species in the region under consideration remains constant. However, at a fairly definite composition the system suddenly becomes critical with respect to the addition of water, and the etch rates rapidly vanish with a slight increase in the water concentration. It will be shown below that the etch rates are determined by the rate of diffusion of the kinetically important species to the Si surface in the regions where the system is insensitive to the addition of water. For this reason the etch rates do not respond to the concentration of added catalyst or to changes in the oxidizing potential of the HNO_3 resulting from the addition of the water. However, at the critical concentration of water, the oxidation potential of the solution has been reduced to the extent that the surface of the Si is no longer a nearly perfect sink for the HNO_3, and the etch rates decrease slightly. At this point the catalyst concentration begins to play a kinetic role. A slight decrease in the etch rates is amplified by the decreased production of the catalyst so that on further addition of water the etch rates rapidly vanish, even though the rate-determining reagent remains at the same concentration. It should be pointed out that the regular concentrated HF contains just the critical amount of water, so that the slope of the etch-rate contours in the very high HF region is just beginning to turn parallel with lines of constant HNO_3 concentration (see Fig. 1). It is for this reason that it was necessary to go to the more concentrated system, where the amount of water is less than critical.

Reaction Mechanisms

Figure 3 is a plot of the logarithm of the etch rate as a function of the concentration of HNO_3 for various levels of added water, i.e., in a direction parallel with the HF-HNO_3 axis of Fig. 1. A similar family of curves may be plotted for the more concentrated acid system. In the latter system the curves corresponding to compositions containing 0-20% added water and to the left of the maximum would coincide. To the right of the maximum the curves for both systems would coincide throughout if the data were plotted as a function of the HF concentration. In this region the displacement of the curves is the result of the varying amount of water in the etchant, which does not permit the simultaneous representation of the concentration axis in terms of both HF and HNO_3.

To the left of the maximum the etch rates are dependent on the HNO_3 concentration and on the amount of added water. Hydrofluoric acid is present in considerable excess, and decreasing amounts of that reagent are still sufficient to sustain increasing rates. The surface of the Si may be considered to be essentially stripped of oxidized Si until the composition corresponding to the maximum etch rate is approached. Then the rate of the reaction becomes sufficiently great, and the concentration of HF sufficiently reduced that a skin of oxidized Si begins to form. This skin renders the surface less accessible to HNO_3 so that the rate of the reaction decreases as the concentration of HNO_3 is increased still further. Beyond this point the rates are dependent only on the rate at which HF can attack the oxidized film.

The kinetics suggest a two-step process. In the first step the Si is oxidized by the HNO_3. This step is followed by a metathesis-type reaction in which the oxidized Si is attacked by the HF. In the composition region to the left of the maximum the oxidation step plays a rate-limiting role, and in the composition region to the right of the maximum the metathesis reaction plays a rate-limiting role.

The conformance of the data to a straight-line relationship indicates that the rates are possibly exponential functions of the concentration of the type $R = e^{ac+b}$. It is interesting to note that the logarithms of the maximum etch rates, when plotted against the concentration of water, also give a straight-line relationship. The constants a and b remain constant only as long as the etch rates are strictly diffusion limited. Thus the curves to the left of the maximum in the weaker acid system do not have the same slopes, although the exponential form of relationship is retained.

The exponential relationship between the etch rates and the concentration of the rate-limiting reagent suggests autocatalysis. As we have indicated above, the chemical catalyst cannot be expected to enhance the rate of a diffusion-governed process, and so we are obliged to postulate the existence of a physical factor which is capable of operating on the

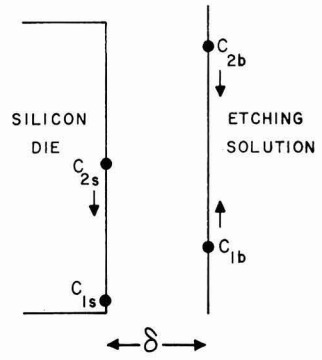

Fig. 4 Model used to explain the diffusion mechanism of the reaction.

diffusion mechanism. This factor is the heat of reaction, which sets up a thermal gradient in the vicinity of the specimen and therefore causes the diffusion coefficient to become a function of the distance from the reacting surface.

In favor of diffusion-governed kinetics is the evidence that differently oriented surfaces, as well as p- and n-type silicon of different resistivities, all appeared to etch at the same rate, whereas large differences in the etch rate of these surfaces are generally observed in other etching systems. Furthermore, the fact that the etch rates are insensitive to the concentration of added catalyst or to the variation of the oxidation potential of the solution, as explained above, supports the theory. The heterogeneous nature of the reaction also requires the consideration of transport phenomena as being kinetically important (2).

In Fig. 4 is shown schematically the surface of a Si specimen immersed in an etching solution under the condition of violent agitation. A thin layer of relatively immobile liquid of thickness δ adheres to the specimen as the solution moves past it. Since the amount of reaction is negligible relative to the total amount of reagents in solution, the bulk solution provides a constant source for reagents. The surface of the Si provides a nearly perfect sink for one of the reagents, the one that is rate limiting. The flow of the other reagent adjusts itself to the stoichiometric requirements of the reaction. Thus, if the stoichiometry of the reaction is assumed to be

$$3Si + 12HF + 4HNO_3 = SiF_4 + 4NO + 8H_2O$$

then the flow rate of HF will have to be three times that of the HNO_3.

In addition to the concentration gradients across δ there will exist a thermal gradient, because of the flow of the heat of reaction away from the surface. Our calculations show that the temperature profile across δ is linear, and the slope is proportional to the amount of heat dissipated, i.e., to the reaction rate. In the absence of the temperature gradient the concentration gradients across δ would also be linear, because of the assumption of the steady state. However, the temperature gradient causes a distortion of the concentration profile toward steeper gradients and thus enhanced reaction rates.

Let us now identify subscript 1 with HNO_3 and subscript 2 with HF, and let us consider the change in the reaction rate as the proportion of HF to HNO_3 is decreased at a given constant level of added water. As C_{1b} increases, the concentration gradient, and thus the reaction rate, also increases. C_{2b} falls because the sum of the two reagents $C_1 + C_2$ is constant. C_{2s} will also fall in a manner that takes into consideration both the fall of C_{2b} and the stoichiometry of the reaction, and will approach C_{1s}, which remains stationary. The finite surface concentration C_{2s} reflects the condition that the HF is present in excess, for the flow rate can be increased by a decrease in C_{2s}. As the maximum etch rate is approached, C_{2s} approaches C_{1s}, and the rate of the dissolution of the oxidized Si can no longer keep ahead of the rate of oxidation. The oxide coating thus impedes the HNO_3 reaction, and the decreased flow rate of HNO_3 is reflected in a rise in C_{1s}. The point where the two surface concentrations cross over marks the transition from a HNO_3 dependent rate to a HF dependent rate. Further increase in the proportion of HNO_3 causes a decrease in the reaction rate by virtue of the resultant decrease in C_{2b}, which is now rate determining.

It is interesting to speculate that if the diffusion coefficients of the two reagents are equal and if the stoichiometry indicated above is correct, then the composition of the fastest etching solution at a given level of added water would have to contain 3 molecules of HF per molecule of HNO_3. On the HF-HNO_3 axis, this composition corresponds to 56 wt % HF, which is not much removed from the observed 65%.

Acknowledgment

The authors wish to express their indebtedness to S. Pryor for her assistance in the experimental work and to F. Ludwig, S. Watelski, and P. Walker for most stimulating discussions and many helpful comments.

Manuscript received April 30, 1958. This paper was prepared for delivery before the New York Meeting, April 27-May 1, 1958.

Any discussion of this paper will appear in a Discussion Section to be published in the December 1959 JOURNAL.

REFERENCES

1. H. Remy, "Treatise on Inorganic Chemistry," Vol. 2, p. 712, Elsevier Publishing Co., New York (1956).
2. Ibid., p. 749.

Preparation of Crystals of InAs, InP, GaAs, and GaP by a Vapor Phase Reaction

G. R. Antell and D. Effer

Research Department, Metropolitan-Vickers Electrical Co. Ltd., Manchester, England

ABSTRACT

Small crystals of InAs, InP, GaAs, and GaP have been grown from a vapor composed of the monochloride or mono-iodide of the metal and phosphorus or arsenic. Crystal growth took place at from 100° to 300°C below the melting points of the compounds. Whiskers of InAs up to 2 cm long also have been grown.

Indium monochloride tends to disproportionate in some of its reactions forming the trichloride and a compound of indium. The reaction of indium monochloride and arsenic vapors to form InAs therefore seemed a practical possibility. $AsCl_3$ would not form as it is unstable at the temperatures of such a reaction.

The reaction was of practical interest especially as we had established that chlorine had little or no effect on the electrical properties of InAs. Crystals of InAs in fact were deposited by this reaction and the principle was extended to the preparation of crystals of GaAs, InP, and GaP, even though the solubility of chlorine or iodine in these latter compounds is not yet known.

Theory

From the free energies of formation of the indium halides at 298°C the free energy change of reactions [1] and [2] are small but negative.

$$3InCl \leftrightarrows InCl_3 + 2In \qquad [1]$$

$$2InCl \leftrightarrows InCl_2 + In \qquad [2]$$

As the temperature rises the free energy change becomes more positive and the reactions tend to go from right to left.

If arsenic vapor is added to reaction [1], the following becomes possible:

$$3InCl + \tfrac{1}{2}As_4 \leftrightarrows InCl_3 + 2InAs \qquad [3]$$

The decrease in free energy due to the formation of InAs should lead to a reasonable yield of InAs crystals.

Equation [3] is strictly applicable only if the pressure of arsenic equals the dissociation vapor pressure of InAs at the temperature of the reaction. For arbitrary pressures of arsenic vapor, the InAs formed might be expected to be associated with an indium or arsenic-rich liquid as shown in the phase diagram (1, 2). Hence, a more general description of the reaction in Eq. [3] is:

$$InCl + As_4 \text{ (arbitrary pressure) in equilibrium with } [InCl_3 + (InAs + \text{liquid})]$$

It should be noted that Eq. [1]-[3] have been used merely to illustrate the principle and that the actual reaction is not known.

Arguments similar to the above can be applied to the bromides and iodides of indium and to the chlorides, bromides, and iodides of gallium together with the cases where phosphorus replaces arsenic.

Crystal Growth

All the crystals were grown in evacuated silica reaction tubes approximately 20 cm long and having volumes of about 50 cm^3.

Method 1.—The reaction tube containing the reactants on the left hand side of Eq. [3] was heated uniformly. Initially the temperature was maintained high enough to prevent any crystals forming and was lowered gradually until nucleation occurred.

Method 2.—The reaction tube contained a small amount of chloride or iodide of gallium or indium or only iodine itself, together with a sample of the appropriate $A_{III}B_V$ compound. The tube was placed in a furnace which had a temperature gradient of between 40° and 70°C over the length of the tube, the sample of the compound being at the hotter end. As the temperature of the whole furnace was lowered slowly, crystals nucleated at the cool end. The furnace was held at this temperature, and it was possible to transport the whole of the sample of the compound from the hot to the cool end of the tube.

This result follows from the fact that Eq. [3] is a

Table I

Reaction number	Initial reactants	Temp. of growth, °C	Pressure of atmospheres: Halide	Pressure of atmospheres: As_4 or P_6
1	$InCl$, As_4	725	8	1.2
2	InI, As_4	690	8.2	1.65
3	$InCl_3$, As_4	No growth	3.1 (800°C)	1.8 (800°C)
4	InI_3, As_4	No growth	3.1 (800°C)	1.35 (800°C)
5	GaI, P_4	1050	5.0	2.6

Table II

Reaction number	Initial reactants	Temp. of sample, °C	Temp. of growth, °C	Press. atm of halide
6	InAs, $InCl_3$	890	840	1.6
7	InAs, InI_3	875	830	1.6
8	InP, InI_3	915	860	1.65
9	GaAs, I_2	1070	1030	2.15

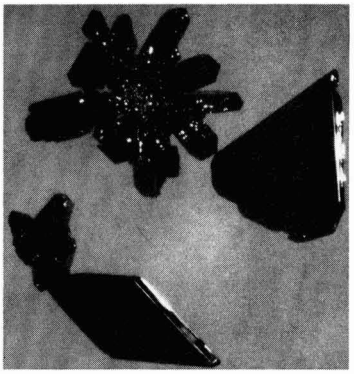

Fig. 1. InP crystals grown by reaction 8. Magnification 27X.

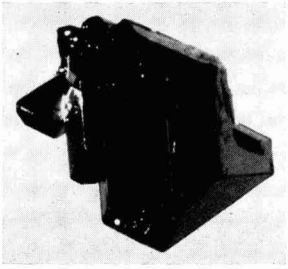

Fig. 2. GaAs crystals grown by reaction 9. Magnification 27X.

reversible reaction. At the hot end of the reaction tube the reaction tends to go from right to left and is reversed at the cool end.

Results

Table I gives a list of experiments that were performed according to method 1. The pressures that are listed are the partial pressures that the reagents would have at the temperature of growth but before they have reacted. Table II covers experiments that were performed by method 2. The pressure of the halide has been calculated as that which it would have been if the tube were at a uniform temperature equal to that of the cool end.

Crystals that have been grown by the reactions listed in Tables I and II are shown in Fig. 1-4.

Growth of InAs *Whiskers.*—Conditions under which whisker growth may be expected are not entirely clear, but it appears that there must be a low pressure of halide present in the tube and also a fairly rapidly falling temperature.

The whiskers always seemed to grow from what appeared originally to have been a molten globule.

The whisker shown in Fig. 4 was grown by reaction 6, Table II when the density of $InCl_3$ molecules was about $10^{16}/cm^3$. Whiskers up to 2 cm in length were grown by a combination of reactions 2 and 4 in Table I. The iodide vapor consisted of InI_3 at a pressure of about 3 atm at 800°C together with a trace of a lower iodide.

X-ray and electron diffraction data.—InAs crystallized mainly as flat plates which in many cases

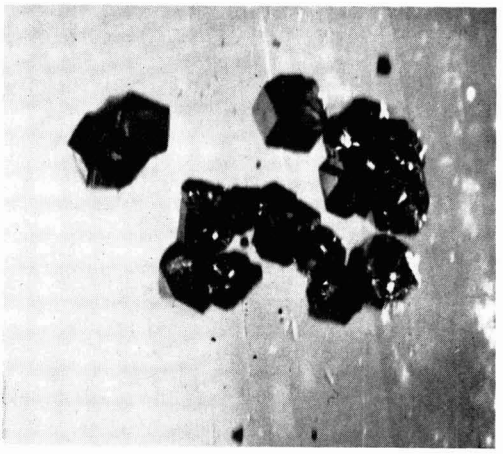

Fig. 3. GaP crystals grown by reaction 5. Magnification 40X.

Fig. 4. InAs whiskers grown by reaction 6. Magnification 40X before reduction for publication.

were up to 5 mm across. A sample was mounted in an electron diffraction camera and a "Kikuchi line" pattern was obtained by reflecting an electron beam at a glancing angle from the flat face of the crystal. From this it was deduced that the flat face was a (111) plane. This also was found to be the case with two other crystals.

The edge of the elementary cell was measured for each compound by the x-ray powder method using a copper anode and a nickel filter. The determinations are listed below together with other published results in brackets.

InAs	$a_o = 6.058_5$Å	[6.058$_4$Å] (1)
InP	$a_o = 5.868_8$Å	[5.869Å] (3)
GaAs	$a_o = 5.654_1$Å	[5.653$_1$] (4)
GaP	$a_o = 5.451_1$Å	[5.450$_5$] (4)

The close agreement between these determinations and previously published values shows that the various compounds have indeed been formed in all cases.

Acknowledgments

The authors are indebted to Mr. P. Worthington for his electron diffraction measurements, and to Miss K. Whitehead and Mr. L. Brownlee for the determination of unit cell sides.

We should also like to thank Dr. R. W. Sillars and Mr. R. P. Chasmar for their helpful criticisms of the manuscript and to Sir Willis Jackson, Director of Research and Education, and Dr. J. M. Dodds, Manager of Research Department, Metropolitan-Vickers Electrical Co. Ltd., for permission to publish this paper.

Manuscript received Nov. 3, 1958.

Any discussion of this paper will appear in a Discussion Section to be published in the December 1959 JOURNAL.

REFERENCES

1. T. S. Liu and E. A. Peretti, *Trans. Am. Soc. Metals*, **45**, 677 (1953).
2. J. von der Boomgaard and K. Schol, *Philips Research Repts.*, **12**, 127 (1953).
3. W. N. Reynolds, *et al.*, *Proc. Phys. Soc.*, **71**, 416 (1958).
4. G. Von Giesecke and M. Pfister, *Acta Cryst.*, **11**, 369 (1958).

Oxide Nucleation and the Substructure of Iron

E. A. Gulbransen and K. F. Andrew

Research Laboratories, Westinghouse Electric Corporation, Pittsburgh Pennsylvania

ABSTRACT

Electron optical studies were made of the initial stage of reaction of oxygen with pure iron. Oxidation occurred in a discontinuous manner with the oxide structure orienting to the metal grain. The sites for oxide nucleation depend on the initial pretreatment atmosphere. Thus, a vacuum annealing treatment showed a random arrangement of nucleation sites, while a hydrogen annealing treatment showed a highly ordered arrangement of nucleation sites.

Since iron was embrittled by annealing in dry and moist hydrogen and not by vacuum annealing, the nucleation sites probably show the substructure of iron responsible for embrittlement.

The theory of oxidation as developed by Wagner (1, 2), Mott (3), and others is based on the diffusion of metal or oxygen atoms and ions through interstitial sites or through cation and anion defects in the oxide film. The oxide film is assumed to be uniform while the metal underlying the oxide is assumed to be structureless over a particular grain. Recent developments in metal physics have shown that crystal orientation, dislocations, and other defects determine the mechanical properties of the metal. These factors also may determine the nature of chemical reactions on metal surfaces. The purpose of this paper is to show the effect of annealing environment on the oxide nucleation pattern for pure iron and to indicate a possible relation between the nucleation pattern and the mechanical properties of the metal.

The fact that iron reacts with oxygen in a nonuniform manner is well known. Early electron optical work was reviewed by Phelps, Gulbransen, and Hickam (4). These authors, in addition, studied the structure of oxide films formed on mechanically polished specimens of pure iron using electrochemical stripping methods for removal of the oxide film. Electron optical studies showed the oxide to consist of many small crystals several hundred to a thousand angstroms in size. The oxide crystals were nearly randomly oriented with respect to the metal grain.

Bardolle and Bénard (5) used carefully polished and annealed specimens of Armco iron to study oxide nucleation processes at temperatures between 650° and 850°C at low pressures of oxygen. At 850°C and a vacuum of 10^{-3} mm Hg, a few well oriented oxide nuclei of definite crystal habit were formed. Many nuclei were formed at pressures of 10^{-2}-10^{-1} mm Hg. Light micrographs of thick oxide films formed under these conditions showed the oxide film on a single metal crystal to consist of many similarly oriented crystals. In no case was a single crystal of oxide observed to form on a single crystal of iron.

Gulbransen, McMillan, and Andrew (6) extended the work of Bardolle and Bénard (5) by controlling conditions of oxidation and by use of electron optical methods. The latter method makes possible observation of finer details of the crystal habit.

Thermodynamic conditions for oxidation.—Since the formation of an oxide film, as well as its crystal habit, depends on the relative importance of one or more chemical reactions, it is necessary to consider the thermodynamic equilibria of these reactions. For iron at 650°-850°C, the more important reactions are the following: (*a*) direct oxidation of iron to FeO, (*b*) reaction of carbon in the metal with the surface oxide to form carbon monoxide and the metal, and (*c*) solution of oxygen in the metal.

Calculations show the dissociation pressure of oxygen over FeO and Fe to be $10^{-17.6}$ atm at 850°C (6). The extent of the oxygen reaction is limited only by the oxygen available and the time of reaction.

Under conditions of low pressure, carbon in the metal reacts with the surface oxide. To minimize this reaction, the concentration of carbon should be less than 0.005% by weight (6). The kinetics of this reaction has been shown by Gulbransen and Andrew (7) to be feasible above 610°C.

Several recent values exist for the solubility of oxygen in alpha-iron. Seybolt (8) found a value of 0.022 wt % at 850°C. Sifferlen (9) has shown that for iron recrystallized by a rigorous thermal treatment the solubility does not exceed 0.002 wt % at 850°C. Considering the low values for the solubility and that oxygen pressures of 10^{-2}-10^{-3} mm Hg were used, we feel that the amount of oxygen dissolving in the metal is small.

Good conditions for studying the initial nucleation process and the effect of pretreatments on iron are as follows: (*a*) carbon content of less than 0.005 wt %, (*b*) oxygen pressures of less than 0.01 mm Hg, (*c*) electropolished and annealed metal, and (*d*)

low concentration of other impurities such as Mn, S, P, Si, etc.

Structural factors in matter.—Four factors are important in discussing structural factors in the oxide nucleation process. These are as follows: (*a*) crystal structure or atomic geometry of the unit cell, (*b*) crystal size and shape, (*c*) particle size and shape, and (*d*) orientation of the oxide particles with respect to the underlying metal crystal.

The crystal structure is studied by electron diffraction while crystal size and shape and orientation factors are studied by the electron microscope.

Experimental

Samples.—"Puron" [1] iron was used for all of the experiments. The iron contains about 0.001% metallic impurities. Of nonmetallic impurities there exists about 0.04% oxygen, 0.005% C, and virtually no sulfur, phosphorus, or nitrogen.

The following steps were used in the preparation of specimens for this study: (*a*) mechanical polishing using polishing papers up to 4/0 under purified kerosene, (*b*) cleaning with soap and water, distilled water, petroleum ether, and absolute alcohol, (*c*) electrolytic polishing using Jacquet's solution, (*d*) washing in distilled water and absolute alcohol.

The following pretreatments were used: (*a*) annealing at 875°C for 24 hr in vacuum of 10^{-7} mm Hg plus 1-hr annealing in hydrogen passed through a palladium tube at 2.4 cm Hg pressure to remove any oxide formed in vacuum annealing, cooled in vacuum, (*b*) annealing at 850°C for 20 hr in 1 atm of hydrogen purified by passing over hot copper and dried with $CaCl_2$, cooled in hydrogen, (*c*) annealing at 850°C for 23 hr in tank hydrogen passed over a dry ice trap at −78.5°C at 59 cm Hg, cooled in vacuum, (*d*) annealing at 875°C for 21 hr in hydrogen passed through a palladium tube at 59 cm Hg pressure, cooled in vacuum, (*e*) same as (*d*) except with an additional annealing for 20 hr in vacuum of 10^{-7} mm Hg plus 1 hr in palladium purified hydrogen at 2.3 cm Hg pressure to remove any oxide formed, cooled in vacuum, and (*f*) annealing at 875°C for 23 hr with hydrogen passed through a palladium tube at 59 cm Hg plus 0.2 cm Hg of pure nitrogen, cooled in vacuum.

Reaction with oxygen.—Strips of 0.013 cm thick iron weighing about 0.1 g and having a surface area of 2.5 cm^2 were reacted in the microbalance system. Specimens were introduced singly and the system pumped overnight. A vacuum of better than 10^{-6} mm Hg was obtained. The furnace at the desired temperature was raised around the Mullite furnace tube. A given quantity of oxygen was introduced by means of a gas handling system. Weight changes were followed with the microbalance. Although the oxygen reacted very rapidly with the metal, the metal was kept in contact with the gas atmosphere for 25 min. Following reaction the residual gases in the system were evacuated, the furnace lowered, and the specimen allowed to cool in the vacuum.

The following facts were observed or calculated for each nucleation experiment: (*a*) weight of oxygen reacting, (*b*) average thickness of oxide film, (*c*) color of oxide, (*d*) crystal structure of oxide, (*e*) size and shape of oxide crystallites, and (*f*) crystal habit and orientation of oxide with respect to the metal grain.

Examination of crystal habit and structure.—The crystal structure of the oxide crystallites was studied by transmission electron diffraction while the crystal habit was studied by electron microscopy of the stripped oxide film. Electron diffraction patterns were taken with the electron diffraction adapter of the EMB-4 electron microscope. Polystyrene-silica replicas shadowed with chromium were prepared in the conventional manner. Stripped oxide films were prepared in an electrochemical stripping apparatus similar to one previously described (4). To support the oxide crystallites, the oxidized surface was covered with a Parlodion film.

Several modifications were made in the electron microscope to obtain large fields at low magnifications. A special internal screw mechanism was used for removing the projector-pole piece for carrying out studies in the range of 400X to 1600X. Most of electron micrographs were made at 1080X to 1600X and enlarged two to eight times.

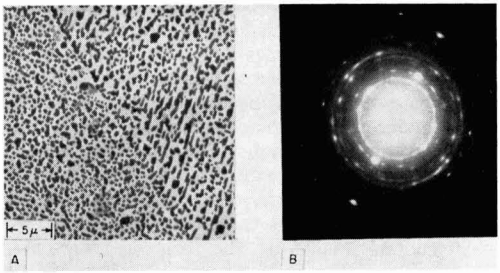

Fig. 1. Oxide film (453Å) stripped from vacuum pretreated Puron. Vacuum, 875°C, 20 hr.

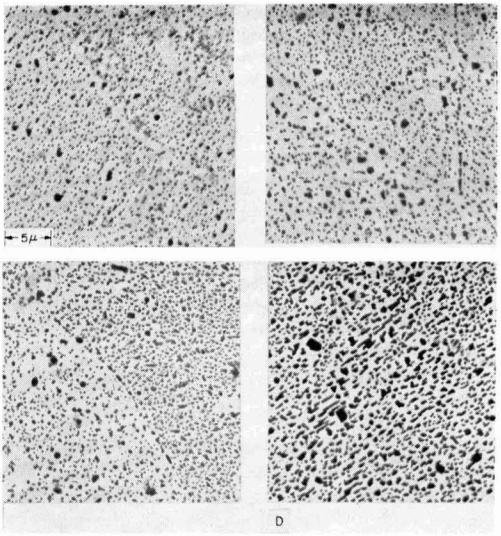

Fig. 2. Oxide films stripped from vacuum pretreated Puron. Vacuum, 875°C, 20 hr. A, upper left, 64Å; B, upper right, 106Å; C, lower left, 230Å; D, lower right, 453Å.

[1] "Puron" is a proprietary name for a grade of pure iron manufactured by Westinghouse Electric Corporation.

Table I. Summary of vacuum pretreatment experiments

Pretreatment	Nucleation conditions	Oxide thickness μg/cm²	Å	Color	Crystal size, μ	Remarks
For all experiments: 10^{-7} mm Hg, 875°C 24 hr, plus 1 hr H_2 at 2.4 cm Hg at 875°C, cooled in vacuum	O_2 at 5 x 10^{-4} mm Hg, 850°C, 25 min	0.92	64	Bright	<0.15 few larger	Random nucleation, oriented growth
	O_2 at 1 x 10^{-3} mm Hg, 850°C, 25 min	1.5	106	Nearly bright	<0.25 few larger	Same
	O_2 at 2 x 10^{-3} mm Hg, 850°C, 25 min	3.29	230	Blue-gray	<0.30 few larger	Same
	O_2 at 5 x 10^{-3} mm Hg, 850°C, 25 min	6.46	453	Blue-gray	<0.50 few larger	Same

Results and Discussion

Vacuum pretreatment.—Table I and Fig. 1 and 2 show the pretreatment and nucleation conditions and results. Figure 1A shows a typical electron micrograph of the stripped oxide film formed by low pressure oxidation at 850°C using oxygen at a pressure of 5 x 10^{-3} mm Hg. For this condition a blue-gray film was formed having an average film thickness of 453Å. The electron diffraction pattern shown in Fig. 1B shows a highly oriented oxide film of FeO and Fe_3O_4. The electron micrographs suggest that, although the oxide is highly oriented to the metal, the sites at which oxide nucleation takes place are nearly random.

Figure 2, A, B, C, and D, shows the effect of the amount of oxidation on the nucleation and growth processes. The average oxide film thickness varies from 64 to 453Å. The oxide crystal size increases with the amount of oxidation. In each experiment electron diffraction patterns showed oriented oxide crystals while the electron micrographs showed a random arrangement of the oxide nucleation sites.

Figures 1 and 2 show several interesting facts about the mechanism of oxidation when the specimen was annealed in high vacuum. (*A*) Single crystals of oxide do not form on a single crystal of metal. This confirms the results of a light micrograph study of Bardolle and Bénard (5) for a later stage of the reaction. The fact that many nucleating centers exist on a metal surface may be related to dislocations and defects in the structure of the metal. (*B*) The oxide structures were oriented to the metal structure. (*C*) Except for the grain boundaries, nearly random distribution of nucleation sites were observed. (*D*) The grain boundaries of the metal were not preferentially attacked.

Pretreatment with tank hydrogen passed over hot copper.—Table II shows details of pretreatment and oxide nucleation conditions together with information on the thickness and color of the oxide crystallites. Fig. 3, A and B, shows electron micrographs of the oxide film formed at 850°C by dosing with O_2 at 2 x 10^{-3} mm Hg and the oxide film formed at 750°C by dosing with O_2 at 1 x 10^{-3} mm Hg. Figure 4, A and B, shows similar results for the film formed at 650°C. A surface replica was included to check the film stripping technique.

Electron micrographs of specimens pretreated in partially purified hydrogen and cooled in hydrogen showed some similarities with and some differences from the results of vacuum annealing. For both pretreatments, a discontinuous oxide film was formed.

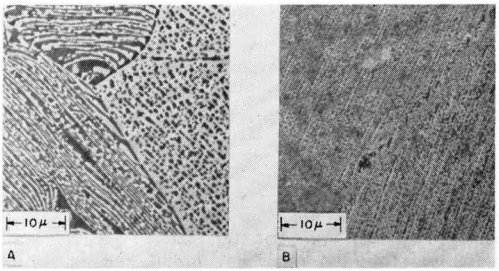

Fig. 3. Oxide film stripped from Puron annealed in hydrogen passed over hot copper. H_2, 850°C, 20 hr, cooled in H_2. A, 752Å thick oxide, 850°C; B, 322Å, thick oxide, 750°C.

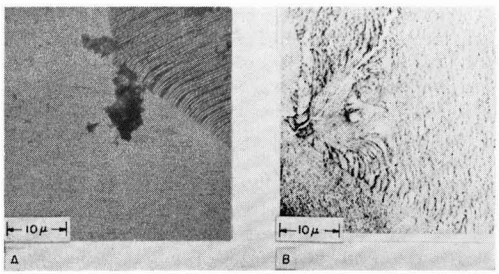

Fig. 4. Oxide film stripped from Puron annealed in hydrogen passed over hot copper and surface replica. H_2, 850°C, 20 hr, cooled in H_2. A, 252Å thick oxide, 650°C; B, surface replica.

Electron diffraction studies of the oxide films in both cases show orientation of the oxide structure to the metal. In addition, the particle size of the oxide crystals for the same degree of oxidation was nearly the same.

Several major differences were observed: (*a*) nucleation sites were not random but highly ordered in certain directions determined by the orientation of the metal grain; (*b*) spacings of these lines of nucleation sites were relatively constant over a given distance; (*c*) lines of nucleation were usually bent at the grain boundaries and join with lines of oxide growth of other metal grains, and (*d*) circular growth patterns were frequently seen. This is shown in Fig. 5. The circular growth patterns probably were related to inclusions or other local defects in the metal structure.

To test the influence of annealing in dry hydrogen, tank hydrogen was dried by passing through a dry ice trap at −78.5°C. Details of the experiment were

Table II. Summary of hydrogen pretreatments, tank hydrogen passed over hot copper

Pretreatment	Nucleation conditions	Oxide thickness $\mu g/cm^2$	Oxide thickness Å	Color	Crystal size, μ	Remarks
1 atm, 850°C, 20 hr, cooled in H_2	O_2 at 2 x 10^{-3} mm Hg, 850°C, 25 min	10.73	752	Light blue	1	Directed-nucleation pattern, oriented growth
1 atm, 850°C, 20 hr, cooled in H_2	O_2 at 1 x 10^{-3} mm Hg, 750°C, 25 min	4.59	322	Blue spots	0.5	Same
1 atm, 850°C, 20 hr, cooled in H_2	O_2 at 1 x 10^{-3} mm Hg, 650°C, 25 min	3.60	252	Blue spots	0.3	Same
56 cm, 850°C, 23 hr, cooled in vacuum dew point—78.5°C	O_2 at 5 x 10^{-3} mm Hg, 850°C, 25 min	6.35	451	Blue	1.0	Partially directed nucleation pattern, oriented growth

given in Table II. Figure 6, A, B, and C, shows three electron micrographs, while Fig. 6D shows an electron diffraction pattern of the oxide crystals. Although an ordered pattern of oxide nucleation was observed, the amount of order was smaller than that shown in Fig. 3, 4, and 5. The electron diffraction pattern showed oriented oxides of FeO and Fe_3O_4 were formed.

Pretreatment with hydrogen passed through palladium.—Table III and Fig. 7, 8, and 9 show details of pretreatment and nucleation conditions together with a summary of the results.

Figure 7, A and B, shows an electron micrograph and an electron diffraction pattern of a specimen pretreated in hydrogen passed through palladium and cooled in vacuum. The sample was oxidized at 850°C in O_2 at 5.0 x 10^{-3} mm Hg. The electron diffraction pattern shows a highly oriented structure while the electron micrograph shows a partially ordered oxide nuclei. Ordering of nucleation sites was not as well developed as for specimens annealed and cooled in less pure hydrogen.

Figure 8 shows an electron micrograph and an electron diffraction pattern of a specimen pretreated in palladium purified hydrogen and then held in a vacuum for 20 hr at 875°C before cooling. The electron micrograph shows a partial ordering of oxide nucleation sites.

Figure 9, A and B, shows electron micrographs of a specimen treated in palladium purified hydrogen plus a small amount of pure nitrogen. Nucleation sites show only a small amount of ordering. Nitrogen, as an impurity in the hydrogen, does not have an important influence on the ordering process.

We conclude from these experiments that water vapor in hydrogen is primarily responsible for ordering of nucleation sites for oxide formation.

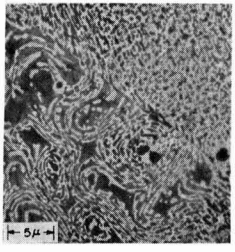

Fig. 5. Circular growth pattern in oxide film (752Å) formed on Puron annealed in hydrogen passed over hot copper. H_2, 850°C, 20 hr, cooled in H_2.

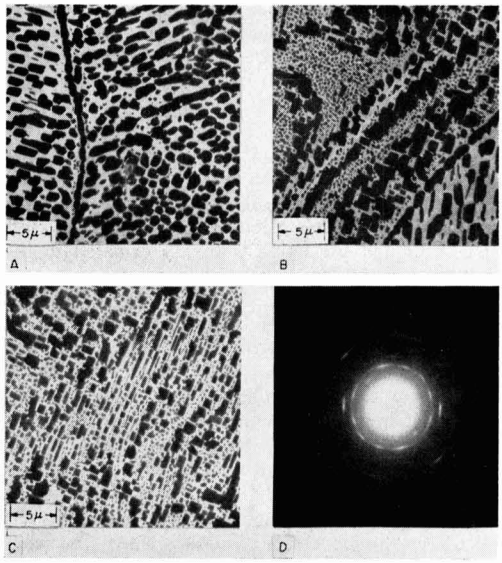

Fig. 6. Oxide film stripped from Puron annealed in hydrogen passed over hot copper and dried (—78.5°C). H_2, 850°C, 23 hr, cool in vacuum.

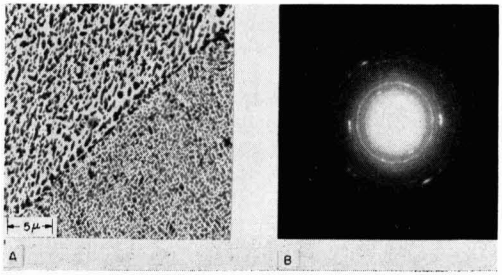

Fig. 7. Oxide film (417Å) stripped from Puron annealed in hydrogen passed through palladium. H_2, 875°C, 24 hr, vacuum cooled.

Discussion

It is of interest to note that the density of oxide crystallites in Fig. 1 is of the same order of magnitude as the density of dislocations in a well annealed metal crystal, i.e., of the order of $10^8/cm^2$. The growth of oxide nuclei may be related to the number and arrangement of dislocations in the metal crystal. Normally, these nucleation centers are random in arrangement. However, if iron is annealed

Table III. Summary of hydrogen pretreatments, palladium purified hydrogen

Pretreatment	Nucleation conditions	Oxide thickness μg/cm²	Oxide thickness Å	Color	Crystal size, μ	Remarks
59 cm Hg, 875°C, 21 hr, cooled in vacuum	O_2 at 5.0 x 10^{-3} mm Hg, 850°C, 25 min	5.96	423	Blue-black	0.3 few larger	Partially directed nucleation pattern, oriented growth
59 cm Hg, 875°C, 21 hr + 10^{-7} mm Hg, 20 hr + H_2 2.3 cm Hg, 1 hr, cooled in vacuum	O_2 at 5.0 x 10^{-3} mm Hg, 850°C, 25 min	6.36	452	Blue-black	0.3 few larger	Same
59 cm Hg + 0.2 cm Hg N_2, 850°C, 23 hr, cooled in vacuum	O_2 at 5.0 x 10^{-3} mm Hg, 850°C, 25 min	6.05	430	Purple	1.0	Same

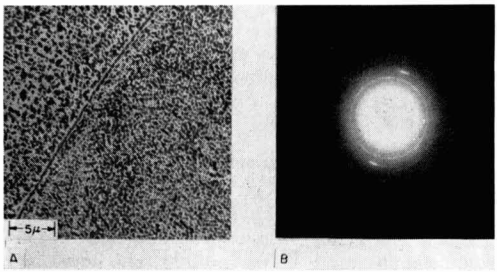

Fig. 8. Oxide film (445Å) stripped from Puron annealed in hydrogen passed through palladium. H_2, 875°C, 24 hr plus vacuum, 875°C, 20 hr.

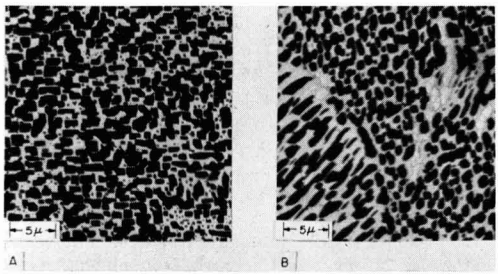

Fig. 9. Oxide film stripped from Puron annealed in palladium hydrogen plus nitrogen. H_2 + N_2, 850°C 23 hr, vacuum cooled.

in impure hydrogen, these nucleation centers become ordered along definite crystallographic directions. The mechanism of ordering is not clear. However, low pressure oxidation offers a new method for the study of the fine structure of iron not observable by light microscopic studies of low temperature etched surfaces.

These results may lead to an understanding of the effect of annealing treatments on the mechanical properties of Puron and other pure irons. Stanley (10) has made a thorough study of the embrittling of Puron when heated in high vacuum and in dry and moist hydrogen atmospheres at temperatures of 700°-1100°C. Puron is embrittled in dry hydrogen atmospheres at a dew point of −65°C in 10 hr for the temperature range of 700°-1150°C. In moist hydrogen, Puron was embrittled in about an hour. Vacuum annealing did not lead to embrittlement. Light micrographic studies showed only minor changes in metal structure.

Stanley's observations on the embrittlement of iron at 700°C and our studies on the effect of hydrogen and its impurities on the oxide nucleation pattern at 700°C appear to be related. Atmospheres which embrittle iron give ordered nucleation sites for oxide growth while atmospheres which do not embrittle iron give random nucleation patterns for oxide growth.

Manuscript received Dec. 2, 1958. This paper was prepared for delivery at the Philadelphia Meeting, May 3-7, 1959.

Any discussion of this paper will appear in a Discussion Section to be published in the December 1959 JOURNAL.

REFERENCES

1. C. Wagner, *Z. physik. Chem* (B), **21**, 25 (1953).
2. C. Wagner, Diffusion and High Temperature Oxidation of Metals in "Atom Movements," American Society for Metals, Cleveland (1951).
3. N. F. Mott, *Trans. Faraday Soc.*, **36**, 472 (1940).
4. R. T. Phelps, E. A. Gulbransen, and J. W. Hickman, *Ind. Eng. Chem., Anal. Ed.*, **18**, 391 (1946).
5. J. Bardolle and J. Bénard, *Rev. met.*, **49**, 613 (1952).
6. E. A. Gulbransen, W. R. McMillan, and K. F. Andrew, *Trans. Am. Inst. Mining Met. Engrs.*, **200**, 1027 (1954).
7. E. A. Gulbransen and K. F. Andrew, *J. Phys. & Colloid Chem.*, **53**, 690 (1948).
8. A. Seybolt, *J. Metals*, **6**, 641 (1954).
9. C. M. Sifferlen, [see discussion by R. Collongues of paper by W. R. McMillan and E. A. Gulbransen, *J. chim. phys.*, 643 (1956)].
10. J. K. Stanley, *Trans. Am. Soc. Metals*, **44**, 1097 (1952).

The Separation of Hydrogen and Deuterium by the Reaction of Iron with Water

Hilton A. Smith, Carl O. Thomas,[1] and John C. Posey[2]

Department of Chemistry, University of Tennessee, Knoxville, Tennessee

ABSTRACT

In the decomposition of water by reaction with iron, as in the electrolysis of water, the residual water is enriched in deuterium. Since the separation factor is an inverse function of the temperature, an attempt was made to increase the reaction rate at low temperatures. Introduction of cathodic surfaces by partial plating of cathodic impurities on steel increased the reaction rate by a factor of 2 to 4 at 98°-100°C. Separation factors from 4.8 to 6.1 were observed for the chemical reaction of these partially plated samples with water. In electrolysis experiments vigorous agitation of the electrolyte caused an increase in the separation factor.

An important part of the development of nuclear power is the procurement of heavy water which is used as a moderator in some types of nuclear reactors (1). Since the natural concentration of deuterium in water is approximately 1 part in 7000 and since separation factors are generally small for isotope separation processes, it is necessary in the initial concentration stages to process very large quantities of water (2). One of the largest separation factors is obtained in the electrolysis of water. However, the energy cost is high, and the method is practical economically only when a market exists for electrolytic hydrogen or when the method is used for the final concentration of water which has been enriched by a less expensive process (2).

Separation of the isotopes is obtained in the direct chemical reaction of a variety of metals with water or steam (3-5). Smith and Posey (6) reported separation factors of 3.2 to 1.4 for the reaction between iron and steam at 118°-340°C. The reaction rate in this temperature range is low for a practical production technique. Moreover, the commercial production of hydrogen by the reaction between iron and steam requires temperatures of 800°-1000°C (7).

Since the separation factor is an inverse function of the temperature (8), temperature requirements for a useful separation factor and a useful rate in the reaction of metals with water or steam appear to be mutually exclusive. The principle of sacrificial corrosion protection suggested the possibility that the reaction rate might be increased without increasing the temperature, so that the advantage of the larger separation factor at the lower temperatures could be retained. The present paper discusses reaction rates and separation factors in the direct chemical reaction of water with iron samples some of which had plated on a portion of their surfaces a variety of cathodic materials. The effect of vigorous stirring on the concentration gradient at the cathode also is discussed.

[1] Present address: Bell Telephone Laboratories, Murray Hill, N. J.
[2] Present address: Union Carbide Nuclear Company, Oak Ridge, Tenn.

Experimental

Reaction rates.—Reaction rate data were obtained by measuring the rate of hydrogen evolution at constant volume or at constant pressure. The constant volume apparatus is shown in Fig. 1. The liquid and gas-phase volumes were approximately 10 ml each. Since the apparatus is very simple and compact, as many as ten runs could be conducted simultaneously in a 5-gal thermostat. Constant-pressure apparatus is shown in Fig. 2. The volume of the reaction flask was approximately 500 ml. Before each run the receiving flask was evacuated. The check valve was set to operate at 85 cm Hg.

The electrolyte was ferrous chloride which was prepared by the reaction of hydrochloric acid with an excess of iron powder. In order to conserve heavy water, reaction rates were investigated using ordinary water only.

Iron samples were prepared from the following materials: Merck and Company iron powder (re-

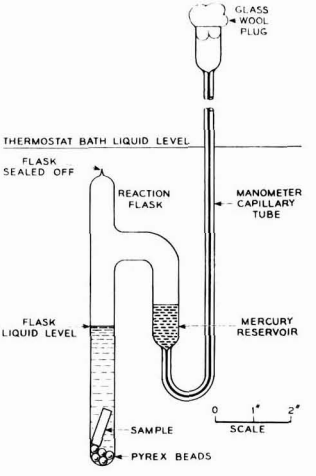

Fig. 1. Constant volume apparatus for measuring rate of hydrogen evolution.

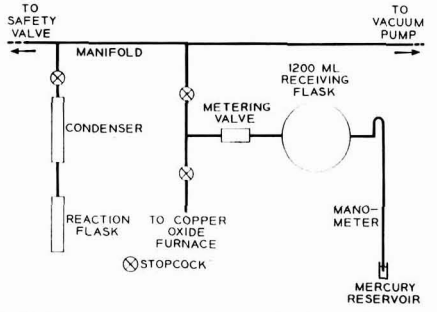

Fig. 2. Constant pressure apparatus for determining separation factors and rates of hydrogen evolution.

duced by hydrogen); J. T. Baker's and Baker and Adamson's reagent grade iron wire (size AWG-36); extremely pure bulk iron (9) provided by the Bell Telephone Laboratories and the Battelle Memorial Institute; and ordinary low-carbon steel plate, rod, and tubing. Iron powder was used as received. Wire samples approximately 1 meter in length were wound into spirals approximately 5 mm in diameter and 3 cm in length. Rectangular and cylindrical samples of the remaining materials were prepared by machining.

All of the samples except the iron powder were cleaned by washing with hot C.P. toluene and then by sulfuric acid pickling. Following cleaning, the absence of hydrophobic contaminants was verified by the wetting properties of the surface as exhibited by the contact angle of water droplets at the surface.

The surface area of the iron powder was measured by the BET-nitrogen-adsorption method and the krypton-adsorption method. The values found by these two methods were 3.5 $m^2\ g^{-1}$ and 3.4 $m^2\ g^{-1}$, respectively. In order to obtain a comparison between the reaction rates observed with powder and with bulk samples, the rate of hydrogen evolution was calculated in cm^3 atm of gas per cm^2 of substrate per minute, corrected to 30°C. For all of the samples, except the iron powder, the reaction rate was constant throughout the runs. Since the surface roughness of the bulk samples changed visibly during the runs, the rate per unit area for the bulk samples was calculated from their physical dimensions, arbitrarily assuming unit roughness factor.

For all of the samples, except iron powder, runs were made with a cathodic surface plated onto approximately 50% of the sample surface. Plating was accomplished by displacement, thermal decomposition, and electroplating.

Table I summarizes the reaction-rate data for a variety of conditions. It can be seen that the rate of hydrogen production may be increased by the application of cathodic metals to a portion of the surface of the iron samples. The data presented in Table I include rate values obtained with both types of apparatus. This suggests that the difference in the reaction rates at constant pressure and at constant volume is not significant.

Some measurements of the reaction rate, not included in Table I, were made with samples of wire, Bell Telephone iron, Battelle iron, and low-carbon steel which were partially plated by displacement with mossy deposits of platinum, palladium, and copper. In general, the initial rates were several times larger than those which were obtained with unplated samples. However, the hydrogen evolution rates dropped off rapidly and approached the values which were obtained with the unplated samples. The mossy deposits had a tendency to become detached from the iron, and they collected a layer of reddish-brown oxide very quickly. The oxide layer eventually turned black. The reproducibility of the rate measurements with this type of cathode surface was very poor.

Table I. Rate of hydrogen production in 1M ferrous chloride solutions at 98°-100°C

Substrate	Cathode	10^4 Reaction rate, (cm^3 atm) cm^{-2} min^{-1}
Iron powder	—	0.39 (0.01)‡
Iron powder	—	0.10 (0.01)
Iron wire (JTB)	—	1.54 (0.01)
Iron wire (B&A)	—	1.55 (0.05)
Pure iron (Battelle)	—	1.17 (0.07)
Pure iron (BTL)	—	1.04 (0.07)
Low carbon steel	—	1.07 (0.05)
Low carbon steel	Au*	4.3 (0.7)
Low carbon steel	Ag*	2.8 (0.4)
Low carbon steel	Cu*	3.1 (0.4)
Low carbon steel	Brass*	3.3 (0.4)
Low carbon steel	Ni*	3.9 (0.4)
Low carbon steel	Cd*	2.5 (0.4)
Low carbon steel	Pt†	4.1 (0.5)

* By electroplating 50% of surface.

† By thermal decomposition on 50% of surface.

‡ Average error in parentheses, defined as $\pm\Sigma d/n\ \sqrt{n}$, where d is the deviation of a single measurement from the arithmetical average, and n is the number of measurements.

Rates with iron powder were initially relatively rapid but decreased rapidly, presumably due to stifling by the reaction products. Prereduction of the powder, coating with copper, or use of other salts such as sodium chloride, ammonium chloride, sodium sulfate, ferrous sulfate, and zinc sulfate did not prevent the decrease in rate as the reaction proceeded.

Separation factors.—Ferrous chloride solutions of twice the desired strength were prepared as described above. A calculated amount of heavy water was added in order to produce a salt solution of the appropriate concentration which also contained approximately 45 mole % of heavy water. The heavy water[3] was reported to be 99.8% pure.

The reaction was carried out in the apparatus shown in Fig. 2. The hydrogen-deuterium mixture which was collected in the receiving flask was subsequently oxidized by copper oxide at 300°C in a Pyrex-tube furnace. The water which was produced by this reaction was collected in a cold trap. The method has been described in detail by Posey (6).

Approximately 130 ml of salt solution was used in each of the runs. The amount of water which was consumed in the reaction was small in comparison to the total amount of water present. However, the change in the composition of the residual water during a run was large enough to affect the calcu-

[3] Obtained from the Stuart Oxygen Company.

Table II. Separation factors in the reaction of cathodically coated steel samples with 1M ferrous chloride solutions at 98°-100°C

Cathode*	Separation factor
Uncoated steel	6.1 (0.5)†
Au	5.7 (0.4)†
Ag	5.6 (0.7)†
Cu	6.0 (1.0)†
Brass	6.0 (0.7)†
Ni	4.8 (0.9)†
Cd	5.3 (0.7)†
Fe powder	5.2 (0.1)†

* By electroplating on 50% of surface.
† Average error.

lation of the separation factor. Therefore, the arithmetical average of the compositions at the beginning and at the end of the run was used for the calculation of the separation factor. A small sample of the salt solution was taken before and after each run. The samples were vacuum distilled, and the water was collected in a cold trap. The isotopic compositions of the various water samples were determined by the falling-drop method of Combs, Googin, and Smith (10).

Steel tubing was used for these runs since it provided the most convenient form for plating, for obtaining a large surface area, and for physically supporting the samples in the reaction flask.

Table II lists the separation factors which were obtained in the reaction of 1*M* ferrous chloride solutions (45 mole % heavy water) at 98°-100°C with unplated and with partially plated samples of steel tubing. Separation factors were calculated by means of Eq. [1]

$$\alpha = (D/H)_e/(D/H)_g \qquad [1]$$

where D and H are the mole fractions of deuterium and of hydrogen, the subscript *e* refers to the electrolyte, and the subscript *g* to the gas produced by the reaction.

Separation factors also were determined in a series of electrolysis experiments with an external emf of 4 v and a current density of 0.06 to 4 amp cm^{-2}. All electrolysis experiments were conducted in 1*M* ferrous chloride solutions containing approximately 45 mole % heavy water. The only heating was that produced by the electrical-power dissipation in the cell, which established an operating temperature of 30°-45°C. The purpose of these runs was to determine the effect of vigorous stirring on the separation factor. Three levels of stirring were investigated: that provided by hydrogen evolution at the cathode, that provided by vigorous mechanical agitation, and that provided by ultrasonic agitation. The mechanical agitation was obtained in the apparatus shown in Fig. 3. The cathode, to which an off-balance weight was attached, was rotated at 1800 rpm, with consequent vigorous vibration. The ultrasonic generator[4] produced sufficient energy to create a Nujol-water emulsion in a test tube in approximately 1 min.

[4] Manufactured by the Crystal Research Laboratories, Hartford, Conn.

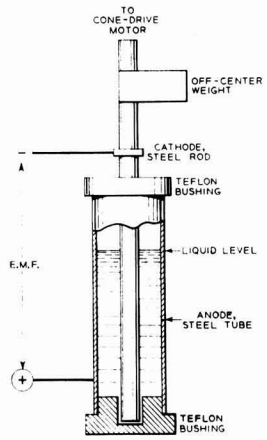

Fig. 3. Electrolysis cell with rotating off-balance cathode

A much larger fraction of the water was decomposed in the electrolysis runs than in the direct chemical reaction runs. Therefore it was not necessary to collect the hydrogen and deuterium. Instead, the separation factor was determined from the initial and the final concentrations of the reacting water by means of Eq. [2]

$$\alpha \ln (H_o/H) = \ln (D_o/D) \qquad [2]$$

where H_o and D_o are the initial concentrations, and H and D are the final concentrations of hydrogen and deuterium in the reacting material. The separation factors for the three types of electrolysis experiments are presented in Table III.

Discussion

The rate of hydrogen production per unit surface area of unplated sample was approximately the same for all of the materials, except iron powder. Therefore, for reasons of convenience, steel was chosen as the substrate material for the investigation of plated cathodic surfaces.

The increase in the reaction rate which was produced by the artificial introduction of galvanic couples was lower than expected. It is possible that cathodic polarization prevented the rates from being much larger. Since hydrogen was the desired product, it was not possible to take advantage of oxidative depolarization of the cathode in order to increase the rates. In fact, the preparation and handling of the salt solutions was done in such a manner as to minimize the amount of dissolved air, and the

Table III. Separation factors in the electrolysis with steel electrodes of stirred 1M ferrous chloride solutions at 30°-45°C

Method of stirring	Separation factor
Hydrogen evolution at cathode	7.23 (0.09)*
Rotating off-balance cathode	7.61 (0.08)*
Ultrasonic agitation	8.32 (0.07)*

* Average error.

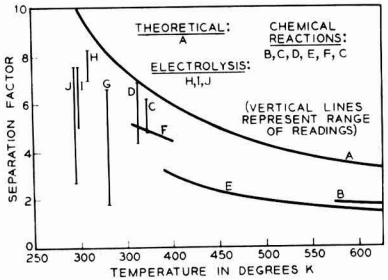

Fig. 4. Separation factors for reaction of metals with mixed protium oxide and deuterium oxide. A, Theoretical, Eyring and Cagle (8); B, Henderson and Bernstein (5); C, massive iron, present work; D, Hughes, Ingold, and Wilson (12); E, Smith and Posey (6); F, iron powder, present work; G, Johnston and Davis (13); H, electrolysis, present work; I, electrolysis, Topley and Eyring (11); J, electrolysis, Topley and Eyring (14).

ferrous chloride solutions were continually in contact with excess metal. The solutions were always blue-green in color.

Separation of hydrogen and deuterium by chemical or electrical decomposition of water depends on differences in the reaction rates of the two species. Therefore, the kinetic separation factor normally should be calculated by use of Eq. [2]. This was done in the electrolysis experiments where a relatively large fraction of water was decomposed. Since a very small fraction of the water was decomposed in the direct chemical reaction between iron and water, steady-state conditions were approximated, and it was possible to calculate the separation factor by use of Eq. [1].

The average values of the separation factors in the chemical reaction of iron with water vary from 4.8 for a brass cathode to 6.1 for uncoated steel. The values of the separation factors are not sufficiently precise to show conclusively any variation due to the nature of the cathode. From the data in Table II a composite separation factor of 5.7 may be calculated with an average error of ± 0.2.

No variation in the separation factor could be observed in the electrolysis experiments as a function of current density.

Topley and Eyring (11) discussed in detail the effect on the observed separation factor of a concentration gradient in the thin film of liquid at the cathode surface. They concluded that the effect should be small. The data in Table III show that efficient stirring can increase the separation factor.

The direct chemical reactions and the electrolysis experiments were performed at different temperatures and cannot be compared directly. In Fig. 4 the separation factors obtained in this investigation are compared with selected values from the literature. Figure 4 also includes the theoretical curve of separation factor vs. temperature which was calculated by Eyring and Cagle (8).

Acknowledgment

The authors are indebted to the U. S. Atomic Energy Commission for support of this work.

Manuscript received Oct. 1, 1958. This paper is taken from theses submitted by Carl O. Thomas and John C. Posey in partial fulfillment of the requirements for the Ph.D. degree in chemistry at the University of Tennessee, Knoxville.

Any discussion of this paper will appear in a Discussion Section to be published in the December 1959 JOURNAL.

REFERENCES

1. R. Stephenson, "Introduction to Nuclear Engineering," pp. 102-105, McGraw-Hill Book Co., Inc., New York (1954).
2. H. K. Rae, *Chemistry in Can.*, **7**, No. 10, 27 (1955).
3. W. Bleakney and A. J. Gould, *Phys. Rev.*, **44**, 265 (1933).
4. J. Horiuti and A. L. Szabo, *Nature*, **133**, 327 (1934).
5. W. G. Henderson and R. B. Bernstein, *J. Am. Chem. Soc.*, **76**, 5344 (1954).
6. H. A. Smith and J. C. Posey, *ibid.*, **79**, 1310 (1957).
7. W. L. Faith, D. B. Keys, and R. L. Clark, "Industrial Chemicals," John Wiley & Sons, Inc., New York (1950).
8. H. Eyring and F. W. Cagle, *J. Phys. Chem.*, **56**, 889 (1952).
9. G. A. Moore, *J. Metals*, **5**, 1443 (1953).
10. R. L. Combs, J. M. Googin, and H. A. Smith, *J. Phys. Chem.*, **58**, 100 (1954).
11. B. Topley and H. Eyring, *J. Am. Chem. Soc.*, **55**, 5058 (1933).
12. E. D. Hughes, C. K. Ingold, and C. L. Wilson, *J. Chem. Soc.*, **1934**, 493.
13. H. L. Johnston and C. O. Davis, *J. Am. Chem. Soc.*, **64**, 2613 (1942).
14. B. Topley and H. Eyring, *J. Chem. Phys.*, **2**, 217 (1934).

The Role of the Electrokinetic Potential in Some Surface Tension Phenomena

Lawrence Baylor Robinson

Space Technology Laboratories, Inc., Los Angeles, California

ABSTRACT

The Wagner-Onsager-Samaras theory (without adjustable constants) allows one to calculate the surface tension of an aqueous electrolyte solution as a function of concentration. It predicts that an electrolyte added to water would increase the surface tension. Precise measurements of the surface tension by the capillary rise method give an initial decrease and a minimum in the surface tension-concentration wave. Theory and experiment can be reconciled by taking the electrokinetic effects into account.

The available evidence indicates that a knowledge of the electrokinetic (commonly called zeta) potential is required for an interpretation of surface tension measurements of electrolyte solutions made with the capillary rise technique. The basic contributions to the theory of the surface tension of (Debye-Hueckel) electrolytes were made by Wagner (1) and by Onsager and Samaras (2). The quantitative discussions were limited to 1-1 electrolytes such as KCl. An extension of the theory to the case of asymmetrical electrolytes has been carried out by Thacher (3), and numerical results are given for 2-1 (e.g., $BaCl_2$) electrolytes and 3-1 (e.g., $LaCl_3$) electrolytes. More drastic approximations in the theory, used by Robinson (4), gave results for 2-1 and 3-1 electrolytes not too different from those obtained in Thacher's more refined treatment. The essential result in all of the cases is that the surface tension turns out to be an increasing monotone function of the concentration; the addition of any amount of a neutral salt to water will increase the surface tension according to theory.

Meanwhile, the theory of surface tension had received a serious challenge by the precise measurements of Jones and Ray (5) with a capillary rise apparatus which gave the ratio of the surface tension of an electrolyte solution to that of water. Their measurements indicated that the surface tension of water decreased sharply as a result of the addition of a small amount of a salt; the surface tension-concentration curve passed through a broad minimum at about 0.001 equivalents per liter for all electrolytes tested. Following this, the curve increased with concentration at a rate about that predicted by theory.

Jones and Ray initially interpreted the decrease in the surface tension as resulting from the interaction of the polarized water molecules (dipoles) with the ions of the electrolyte. They pointed out that these forces are neglected in the usual theoretical treatments, in which the principal effect is attributable to the presence of a boundary (so-called image forces). They postulated that the addition of ions to water would disturb the systematic arrangement of water dipoles. The electric forces among the water molecules, opposing this disturbance, would tend to thrust the disturbing ions into the surface. This initial positive adsorption was taken as the cause of the decrease in surface tension in the extremely dilute range.

Several other proposals were put forward by various theoreticians to account for the observed minimum in the surface tension-concentration curve. The interpretation given by Irving Langmuir (6) attracted more attention; it is subject to quantitative checks. Langmuir advanced the suggestion that the results obtained by Jones and Ray represented an instrumental effect rather than a pure surface tension property. He contended that the film of the liquid in the capillary above the meniscus was not of negligible thickness as was generally assumed, but could assume thicknesses which would be appreciable when compared with the radius of a tiny capillary. The thickness of the wetting film was postulated as being dependent on the nature and concentration of the electrolyte and especially on the potential existing at the interface between the capillary wall and the solution. This is essentially the so-called zeta-potential, the potential existing at the boundary between a flowing liquid and the layer of liquid attached to the wall. The film was supposed to be much thicker for water than for solutions of electrolytes of moderate concentrations, and the film evidently becomes negligible for concentrated solutions. Jones and Frizzell (7) developed the theory more rigorously so that the original surface tension data of Jones and Ray could be corrected in the manner proposed by Langmuir.

A significant result is that a connection is established between the surface tension and the electrokinetic potential. In principle, one can invert the problem and calculate the zeta potential from a static phenomenon. At the time of Langmuir's suggestions, reliable zeta potential measurements were very few. At present, reliable results have been made on a variety of electrolytes by Rutgers and De Smet (8) and by Jones, Wood, and Robinson (9). The results of these two groups of workers are in complete agreement.

The application of the correction, as suggested by

Langmuir, puts the results of Jones and Ray in substantial agreement with the theory.

Surface Tension by Capillary Rise

The method employed by Jones and Ray measured the ratio of surface tensions of solutions to that of water, by measuring relative rises in a capillary tube. The surface tension is given by

$$\sigma_c = h\ (d_c - \beta)\ gr_c/2 \qquad [1]$$

where d is the density of the solution , h is the height to which the liquid rises in the capillary, β is the density of air, g is the acceleration of gravity, and r_c is the radius of the capillary containing the liquid. The relative surface tension is

$$\sigma = \frac{\sigma_c}{\sigma_o} = \frac{h_c}{h_o}\,\frac{(d_c - \beta)}{(d_o - \beta)}\,\frac{r_c}{r_o} \qquad [2]$$

where the subscript zero refers to water. Jones and Ray assumed that $r_c = r_o$. Langmuir's suggestion that a wetting film (of significant dimensions) forms in the capillary requires that the original data of Jones and Ray be multiplied ("corrected") by a factor of $(r - \Delta r_c)/(r - \Delta r_o)$ where Δr is the thickness of the film.

The wetting film is established from the equilibrium of various forces at the meniscus. For films which are thick in comparison with the diameter of the water molecule, one may neglect short range forces. The other forces considered have their origin as follows:

1. The hydrostatic pressure exerted by the main body of the liquid in the capillary exerts a downward force (per unit area) on the film which tends to make this film thinner; this pressure has magnitude $-(d - \beta)\ hg$, where d is the density of the solution, β the density of air, h the capillary rise, and g the acceleration of gravity.

2. The surface tension in the inner surface of the annular wetting film tends to contract the entire inner surface, and hence make the film thicker; the pressure exerted has magnitude $p = \sigma/r = (d - \beta)\ hg/2$.

3. The difference between the osmotic pressure in the bulk solution and at the air-solution interface tends to make the film thicker in attempting to dilute the solution comprising the film; this pressure has magnitude

$$\Sigma_i\, n_i\, kT\left\{\exp\left(-\frac{Z_i \epsilon \Psi}{kT}\right) - 1\right\}$$

where n_i is the number of ions per cubic centimeter of the ith species in the main part of film (assumed to be the same as that in the bulk solution), Z_i is the number of electronic changes on the ion, and the other symbols have their usual significance. The above expression is a result of Vant Hoff's simple law that the osmotic pressure is $P = nkT$ (where n is the total number of ions per cubic centimeter), and from the assumption that the ions in the wetting film are in a Boltzmann distribution governed by the potential Ψ. At equilibrium, the sum of all of these pressures is zero, and therefore

$$\Sigma_i\, n_i\, kT\left\{\exp\left(-\frac{Z_i \epsilon \Psi}{kT}\right) - 1\right\} - (d - \beta)\ hg/2 = 0 \qquad [3]$$

where the potential Ψ is evaluated at the air-film interface. It is also assumed that at the air interface

$$\nabla\Psi = 0 \qquad [4]$$

The above two boundary conditions, plus the Poisson-Boltzmann equation

$$\nabla^2\Psi = \frac{d^2\Psi}{dr^2} + \frac{1}{r}\,\frac{d\Psi}{dr} = \Sigma_i\, n_i \epsilon Z_i \exp\left(-\frac{Z_i \epsilon \Psi}{kT}\right) \qquad [5]$$

constitute the problem to be solved. The problem is to find the Δr consistent with the boundary conditions and the specified potentials.

Equations [3] and [4] provide a means of determining both the function Ψ and its slope, respectively, at the air-solution boundary. Some refinements have been offered at various times to improve the theory, especially as far as Eq. [4] is concerned; the evidence suggests that the theory as proposed is substantially correct as long as the potential at the film-quartz interface (i.e., the zeta potential) is large in comparison with the potential at the air-film interface. This condition prevails in the cases of KCl and $BaCl_2$, but is not so for $LaCl_3$. In fact, in two of the $LaCl_3$ solutions studied, the air-film interfacial potential (as calculated) turned out to be larger than the zeta potential. Presumably, the wetting film thickness is zero in such cases; in any circumstance this film thickness would have to be calculated in some other way. Evidently the results for $LaCl_3$ are not as reliable as those for KCl and $BaCl_2$.

Electrokinetic Potentials

In order to carry out the corrections as suggested by the wetting film theory, one must have reliable values of the zeta potential. Recently significant gains have been made in regard to the experimental knowledge concerning this potential. Hitherto there has been no agreement among the various experimenters (10) in this field, and the reliability of much of the data is open to question. Many experimenters have not characterized their methods and instruments adequately and, therefore, a valid evaluation of their results is difficult. A hopeful indication that reliable information has been obtained concerning these potentials is furnished in the work of Rutgers and De Smet (8) at Ghent (Belgium) and Jones, Wood, and Robinson (9) at Harvard. This is perhaps the first time that systematic agreement has been obtained by different investigators, using different experimental techniques. Rutgers and De Smet, using both the method of electroendosmosis and of streaming potentials, studied the ζ-potential of solutions of a great variety of salts in contact with Jena 16 III glass, whereas the Harvard experimenters studied solutions of metallic chlorides in contact with quartz. The latter group used only the streaming potential method. It is remarkable that the results were practically identical.

An interesting regularity was observed in both sets of data. Instead of the curves passing through maxima, as shown in most textbooks (11), the potentials decreased in a more or less linear fashion

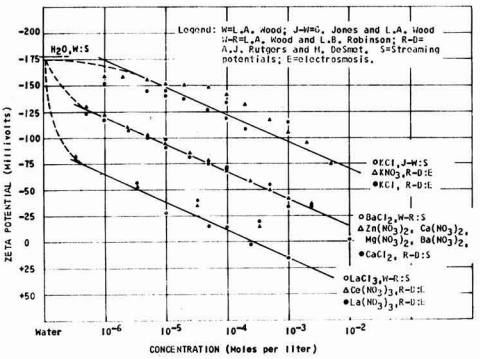

Fig. 1. Zeta potentials of neutral electrolyte solutions

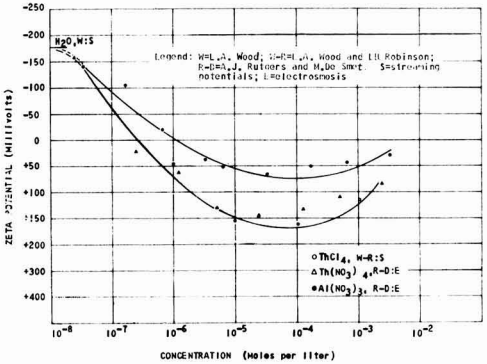

Fig. 2. Zeta potentials of hydrolyzable electrolyte solutions

with the logarithm of the concentration. Both groups of workers found out that thorium salts did not fit the general behavior pattern. This is also true of aluminum chloride. Hydrolysis and other effects with these salts gave their solutions properties not common to the other electrolytes.

Typical results for neutral electrolyte solutions are given in Fig. 1. One observes that all of the data of both groups of workers can be correlated very simply. Actually, only one slope and one intercept are needed to correlate all of the phenomena. The broken lines in the figure are used to give some indication of the expected behavior of the zeta potential in the very dilute range. The three solid lines represent the following equation:

$$\zeta(\text{mv}) = -336 + 55.0\, Z_+ + 26.3 \log c \qquad [6]$$

where Z_+ is the number of charges on the positive ion, and c is the concentration of the salt in moles per liter. The above formula describes the results accurately to about ±10 mv, which is the order of the experimental accuracy. Many times, reversing the direction of flow of the solutions gives an asymmetry potential of this order. In Eq. [6], the symbol c could represent the concentration of the anions (well within the experimental accuracy). There is perhaps some significance in that Eq. 6 can be rewritten as

$$2.27\,\zeta \text{ (volts)} = \zeta' = -0.760 + 0.1235\, Z_+ + 2.303 \frac{kT}{\epsilon} \log c \qquad [7]$$

where k, T, and ϵ have their usual significance.

The above equation makes ζ' immediately amenable to an electrochemical interpretation in which the ratio of the viscosity to the dielectric constant (η/D) in the double layer has been increased by a factor of 2.27 over this ratio in pure water. The zeta potential, as calculated both from streaming potential data and from electroendosmosis (electroosmosis) involves this (unknown) ratio as well as experimentally evaluated parameters. Remarks similar to this were made by Robinson (5) some time ago. It seems as though some independent determination of this ratio would be a very worthwhile contribution to the subject of electrokinetic phenomena.

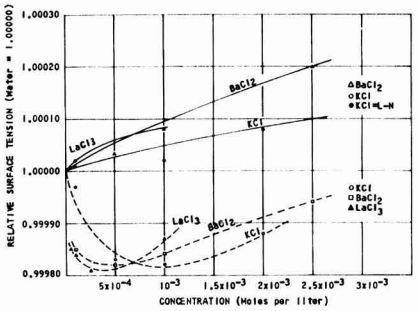

Fig. 3. Relative surface tension of some electrolyte solutions. Solid lines are calculations by H. C. Thacher, Jr.; broken lines connect experimental points of G. Jones and W. A. Ray. Points above 1.00000 (except the one solid circle) are the "corrected" experimental points. The one solid circle is an experimental point of F. A. Long and G. C. Nutting.

Figure 2 shows a different type of behavior for electrolytes which hydrolyze. An interesting problem here would be an attempt to determine the degree of hydrolysis of these salts from the data given

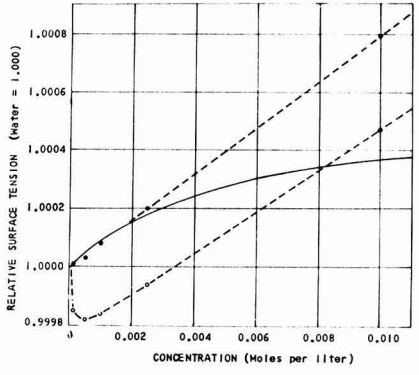

Fig. 4. Comparison of surface tension data of solutions of barium chloride with theories. Open circles are the measurements of Jones and Ray; solid circles are the "corrected" experimental points. The solid line is an approximation to the limiting law of Onsager and Samaras by L. B. Robinson. The upper broken line coincides with a linear extrapolation of the calculations of H. C. Thacher, Jr.

Table I. Wetting film thickness in the Jones-Ray capillary apparatus

Concentration $BaCl_2$	Δr (Å)	
	Reported previously	New
2.50×10^{-3}	87	88
1.00×10^{-3}	112	110
5.00×10^{-4}	152	135
1.00×10^{-4}	223	240
$LaCl_3$		
1.00×10^{-3}	56	277
1.00×10^{-4}	18	78

by Rutgers and De Smet for HCl and KOH and a formula similar to Eq. [6]. It is interesting to note that one single curve can represent the streaming potential data for $ThCl_4$ as well as the electroosmosis data for Th $(_7O_3)_4$. Such all around agreement as exhibited in Fig. 1 and 2 increases confidence in the reliability of both sets of measurements.

Results

Numerical results for the thickness of the wetting film as a function of the zeta potential have been reported by Jones and Frizzell and by Jones and Wood for 1-1 electrolytes, by Wood and Robinson for 2-1 electrolytes, and by Robinson for 3-1 electrolytes. In every case, the approximation was made that one could replace the Laplacian for a region of cylindrical symmetry by the one dimensional Laplacian operator. When this is done, the solution of the problem for the case of 1-1 and 2-1 electrolytes can be obtained in terms of elliptic function. For the case of 3-1 electrolytes, in addition to the approximation of the one-dimensional case, another approximation of a computational nature has to be made; the solution involves hyperelliptic integrals and these were approximated in terms of elliptic integrals. Since the publication of these results, a numerical analysis group at the Ramo-Wooldridge Corporation has assisted Robinson in obtaining numerical integrations of the differential equation involving the Laplacian in cylindrical coordinates. These new results show that the one-dimensional approximation is entirely justified for the 2-1 case; for the 3-1 case, the new wetting film thicknesses are larger by a factor of about four or five than those previously reported. The larger wetting films, however, made no significant difference in the qualitative behavior of the "corrected" surface tension-concentration curves. Table I shows the old and new results for $BaCl_2$ and $LaCl_3$ as well as the old results for KCl. No additional calculations have been made for KCl.

Figure 3 shows the original data of Jones and Ray, the theoretical curves as given by Thacher, and the "corrected" data of Jones and Ray for KCl and $BaCl_2$ solutions. The agreement between various aspects of theory and experiment is good for these two cases. One data point is given from the work of Long and Nutting; they did not have points at lower concentrations (12).

Figure 4 shows the results for $BaCl_2$ in more detail. In the very high dilution range, the calculations of Thacher and Robinson agree. Thacher's calculations were carried up to a concentration of 2.5×10^{-3} moles/l of $BaCl_2$. Figure 5 shows the corresponding results for $LaCl_3$. The only specific thing one can say in regard to the corrected data is that none of these corrected relative surface tensions is less than that of water.

The evidence suggests that the theory of the surface tension of electrolytes is satisfactory, and the minimum in the surface tension-concentration curve is an instrumental effect.

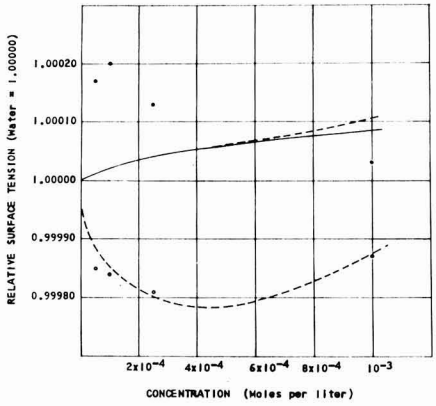

Fig. 5. Comparison of surface tension data of solutions of lanthanum chloride with theories. Open circles are the measurements of Jones and Ray; solid circles are the "corrected" measurements; solid line is the calculation given by H. C. Thacher, Jr. The calculation given by L. B. Robinson coincides with this below 6×10^{-4} moles/l; the broken line continues Robinson's results beyond this point.

Acknowledgment

The author is indebted to Dr. Henry C. Thacher, Jr. for allowing him to make use of the results of his thesis.

Manuscript received June 17, 1958. This paper was prepared for delivery before the New York Meeting, April 27-May 1, 1958.

Any discussion of this paper will appear in a Discussion Section to be published in the December 1959 JOURNAL.

REFERENCES

1. C. Wagner, *Physik Z.*, **25**, 474 (1924).
2. L. Onsager and N. N. T. Samaras, *J. Chem. Phys.*, **2**, 528 (1934).
3. H. C. Thacher, Jr., Ph.D. Thesis, Yale University, 1949 (unpublished).
4. L. B. Robinson, Ph.D. Thesis, Harvard University, 1946 (unpublished).
5. G. Jones and W. A. Ray, *J. Am. Chem. Soc.*, **59**, 187 (1937); **63**, 288 (1941); **63**, 3262 (1941); **64**, 2744 (1942).
6. I. Langmuir, *Science*, **88**, 430 (1938); *J. Chem. Phys.*, **6**, 894 (1938).
7. G. Jones and L. D. Frizzell, *J. Chem. Phys.*, **8**, 986 (1940).
8. A. J. Rutgers and M. De Smet, *Trans. Faraday Soc.*, **41**, 758 (1945); **47**, 102 (1947).
9. G. Jones and L. A. Wood, *J. Chem. Phys.*, **13**, 106 (1945); L. A. Wood and L. B. Robinson, **14**, 251 (1946); *J. Am. Chem. Soc.*, **69**, 1862 (1947).
10. H. Lach and J. Kronman, *Bull. Int. de L'Acad. Polonaise d. Sci. d. Let. (A), Sci. Math.*, 289 (1925); H. Freundlich and G. Ettish, *Z. physik. Chem.*, **116**, 401 (1925); H. R. Kruyt and van der

Willigen, *Kolloid Z.*, **45**, 307 (1928); Furutani, Kurokochi, and Asoda, *Jap. J. Gastroent.*, **2**, 148 (1930); H. Lachs and J. Biczyk, *Z. physik. Chem.*, **A148**, 441 (1930); R. duBois and A. H. Roberts, *J. Phys. Chem.*, **40**, 543 (1936); A. J. Rutgers, E. Verlende, and M. Moorkens, *Proc. K. Ned. Akad. Wetensch. Amsterdam*, **41**, 763 (1938); A. J. Rutgers, *Trans. Faraday Soc.*, **36**, 69 (1940).

11. H. A. Abramson, "Electrokinetic Phenomena," p. 203, Chemical Catalogue Co. (1934); S. Glasstone, "Text-Book of Physical Chemistry," p. 1201, D. Van Nostrand Co., New York (1940); S. Glasstone, "Introduction to Electrochemistry," p. 534, D. Van Nostrand Co., New York (1942).
12. F. A. Long and G. C. Nutting, *J. Am. Chem. Soc.*, **64**, 2476 (1942).

Technical Notes

Enhanced Surface Reactions

IV. The Adsorption of Hydrogen on $ZnO \cdot Cr_2O_3$

M. J. D. Low and H. A. Taylor

Nichols Laboratory, New York University, New York, New York

Recent experiments on gas-solid interactions (1-3) were explained in terms of a mechanism (4) intimately connected with the Elovich equation (4)

$$dq/dt = ae^{-\alpha q}$$

q being the amount of gas adsorbed at time t. It was thought of interest to study the change of the constants a and α with initial gas pressure, P_o, and temperature. The adsorption of hydrogen on $ZnO \cdot Cr_2O_3$ was measured using previously described techniques (3-6). The unreduced catalyst (33.4 g) (7) was reduced in flowing hydrogen at 1 atm at 450°C for 20 hr. Between runs the catalyst was degassed at 450° for 16 hr to $\leqq 10^{-6}$ mm Hg.

Most q-log t plots showed isothermal discontinuities (4) and were described precisely by the Elovich equation. At 147° and 200°C the change in slope corresponded to a decrease in α; at 257°, to an increase in α. Table I summarizes the data, numbered according to the order of their execution. The subscripts 1 and 2 refer to the a and α values calculated (8) before and after the break at time t_b and adsorption amount q_b.

Plots of $\alpha_1 - P_o$ show breaks, α_1 varying more rapidly with a change in P_o at low temperature, less rapidly at higher pressures. In contrast to previous studies, this break seems to be temperature dependent, changing from 16 cm at 147° to 20 cm at 257°C. Conversely, the breaks in q-log t plots occur approximately at $q = 8$ ml regardless of P_o or temperature. Further, the break occurs at $q = 8$ ml, whether the change in slope corresponds to an in-

Table I. H_2 adsorption on $ZnO \cdot Cr_2O_3$

Run	P_o cm Hg	α_1	$a_1 = n \cdot 10^x$		ln $a_1\alpha_1$	α_2	$a_2 = n \cdot 10^x$		ln $a_2\alpha_2$	t_B, min	q_B, ml
			n	x			n	x			
					147°C						
13	16.1	3.03	1.5	10	10.66						
14	10.6	3.59	5.0	9	10.26						
15	7.4	3.77	3.6	9	11.10						
16	23.6	2.91	3.0	9	9.90	2.30	1.5	7	7.55	20	8.85
17	30.7	2.80	3.0	9	9.89	2.13	8.0	6	7.25	13	9.00
					200°C						
9	5.0	2.84	3	5	5.90	1.34	89	0	2.08	21	5.8
10	19.1	2.25	1	6	6.45	0.69	18	0	1.10	17	7.8
11	35.2	2.20	8	5	6.19	0.71	41	0	1.46	15	8.5
12	16.5	2.32	8	6	7.72	1.04	370	0	2.58	16	8.4
18	14.3	2.42	4	6	6.93	0.82	53	0	1.64	13	7.6
19	10.7	2.07	3	5	5.82	0.67	14	0	0.98	21	7.9
					257°C						
2	41.5	0.77	5.2	2	2.60	2.88	2	12	12.25	8	10.5
3	24.0	0.77	3.2	2	2.40	2.56	5	9	10.11	8.7	10.0
4	11.1	0.97	2.0	2	2.29	2.71	5	7	8.12	8	7.7
5	37.7	0.80	3.3	2	2.42	2.58	3	8	8.92	3	8.4
6	6.3	1.07	2.1	2	2.35	8.52	2	26	27.22	17	7.7
7	18.3	0.82	3.1	2	2.41	3.15	2	11	11.84	8.5	9.3

Table II. H_2 on $ZnO \cdot Cr_2O_3$—Kubokawa and Toyama

°C	α	q_1	a
0	0.20	9.8	36.2
20	0.66	11.4	2.9×10^3
80	1.17	16.4	1.9×10^8
110	1.05	16.0	1.8×10^7
140	0.96	16.0	5.7×10^6
170	0.71	16.0	1.2×10^5
200	0.56	15.8	1.1×10^4

crease or decrease in α. Such behavior is similar to that found by Decrue and Susz (9) in part for the same system, but even more so for the system H_2-WS_2. A peculiar effect of initial pressure is discernible in the earlier work with hydrogen on zinc chromite by Taylor and Strother (10). At ¼ atm of hydrogen they calculated energies of activation which increase monotonously with the amount of hydrogen adsorbed over the range 80°-218°. At ½ and at 1 atm the change in the calculated energy of activation is different for the ranges 80°-110° and 110°-184°. The adsorption isobar showed a maximum around 184°. No energies of activation at temperatures higher than 184° at ½ or 1 atm are given. Kubokawa and Toyama (11) have called attention to this effect as different from their findings, remarking that "the reason for the difference is not yet clear." That they did not observe the effect is no doubt to be attributed to the low pressure, 6 cm, in their work. The low pressure would account also for the absence of breaks in the q-log t plots of their data, since none was found at the lowest pressures at 147° in the current study. Their data satisfy an Elovich treatment, Table II listing the calculated parameters. The value q_1 is the amount adsorbed after 1 min, obtained by extrapolation of the data given, and used to calculate the initial rate a from the integrated Elovich equation, $q = (2.3/\alpha) \log (1 + a\alpha t)$. From 0° to 80°C a increases steadily, but from 80° to 200°C a decreases. If the Arrhenius equation is applied to these values the energy of activation so calculated is 37 kcal in the first temperature interval, and −26 kcal in the second interval. If the a_1 values in Table I are similarly treated, an average energy of activation of −63 kcal is found. Similar negative activation energies have been pointed out by Decrue and Susz. The numerical discrepancy can undoubtedly be attributed to a difference in the catalytic activity of the adsorbent. At 140° Kubokawa and Toyama found 21 ml hydrogen adsorbed on 12.37 g catalyst at ≈6 cm pressure; the α value was ≈1.0. In the present study at 147° 33.4 g adsorb only 10 ml at that pressure, while α_1 is 2.1.

The a_2 values in Table I decrease in going from 147° to 200°C but increase from 200° to 257°C. It is obvious that the temperature dependence of the adsorption after the break is completely different from that before the break. Patently, at least two types of adsorption are involved, and much more kinetic data from other adsorbent-adsorbate systems are required to unravel the complexity. It may be noted, parenthetically, that the activation energies calculated from the times required to adsorb definite amounts of gas, in the ranges 3-4 or 7-13 ml found by Taylor and Strother and also by Kubokawa and Toyama, do not have the significance which these authors claim.

The Elovich equation shows adsorption to be a decelerating process, to an extent dependent on the value of α, which is itself temperature and initial-pressure dependent. To apply the Arrhenius equation to rates at constant amounts adsorbed disregards whatever is responsible for the parameter α. In view of the previously discussed mechanism the deceleration is the result of spontaneous site decay and hence, for the adsorption of a constant amount of gas, a different proportion of the surface sites has decayed at different temperatures, and thus the stages of reaction are not comparable.

Manuscript received May 13, 1958.

Any discussion of this paper will appear in a Discussion Section to be published in the December 1959 JOURNAL.

REFERENCES

1. M. J. D. Low and H. A. Taylor, *This Journal*, **104**, 439 (1957).
2. M. J. D. Low, *ibid.*, **105**, 103 (1958).
3. M. J. D. Low and H. A. Taylor, *ibid.*, **106**, 138 (1959).
4. H. A. Taylor and N. Thon, *J. Am. Chem. Soc.*, **74**, 4169 (1952).
5. M. J. D. Low and H. A. Taylor, *Canadian J. Chem.*, May 1959.
6. L. Leibowitz, M. J. D. Low, and H. A. Taylor, *J. Phys. Chem.*, **62**, 471 (1958).
7. H. S. Taylor and S. C. Liang, *J. Am. Chem. Soc.*, **69**, 2989 (1947).
8. J. N. Sarmousakis and M. J. D. Low, *J. Chem. Phys.*, **25**, 178 (1956).
9. J. Decrue and B. Susz, *Helv. Chim. Acta*, **39**, 619 (1956).
10. H. S. Taylor and C. O. Strother, *J. Am. Chem. Soc.*, **56**, 586 (1934).
11. S. Y. Kubokawa and O. Toyama, *J. Phys. Chem.*, **60**, 833 (1956).

Formation of Silicon Carbide Crystallites

Allen H. Smith

Research Division, Raytheon Manufacturing Company, Waltham, Massachusetts

A unique approach to the problem of growing silicon carbide crystals has produced free falling crystallites. This SiC "snow" is transparent and clear in typical hexagonal or triangular platelet form. The snow forms in a pressurized furnace containing an argon atmosphere.

Silicon carbide is known to sublime at elevated temperatures. Near 2700°C (1) decomposition takes place forming an atmosphere of silicon vapor and a solid residue of graphite. This experiment utilizes decomposition rather than sublimation. The Lely process (2,3) employs sublimation as the principal mechanism. The argon pressure of about 80 psi was established empirically. This pressure controls the diffusion rate of the silicon vapor rather than operation at some arbitrary point on a phase vs. pressure diagram.

Figure 1 shows the apparatus for this experiment in a schematic drawing. The essential parts include the pressure envelope of steel, with water cooling coils soldered on; graphite heater tube with graphite piston sliding fit; thermal insulation of lampblack; and a viewing port at the bottom through which the temperature is taken and events viewed. A neoprene "O" ring and a lavite washer electrically isolate the top electrode. The "O" ring also serves as the pressure seal around the water-cooled electrode. Argon circulates throughout the furnace for flushing and gives a supporting upward draft for the flakes at the point of entry. The furnace uses about 4 kw of power at 600 amp to maintain 2700°C. A saturable core reactor with a stepdown transformer supplies the power. Manual control regulates the power for temperature changes. The temperature remains at a constant value for a given power setting, as determined by a L&N optical pyrometer.

The operating zone, ¾ x 4 in., contains the graphite capsule with its supply of silicon carbide (see Fig. 2). A dense form of graphite[1] must be used for this capsule to prevent breakage when the silicon vapors react with it. The silicon vapor does not attack other parts of the system as much as the capsule. Spectroscopic grade[2] graphite works well for the piston, base, and heater sleeve. The capsule support with three thin legs minimizes heat loss by conduction to the base. A radiation shield above the capsule cuts radiation losses from the capsule top to the much cooler piston.

A simple concept of this experiment assumes the equilibrium reaction:

$$Si + C \rightleftarrows SiC$$

Silicon combines with carbon from 1600°C up to the decomposition temperature. As silicon carbide is very stable, the silicon remains localized until released at the decomposition temperature. As the silicon vapor builds up in the capsule, it streams out

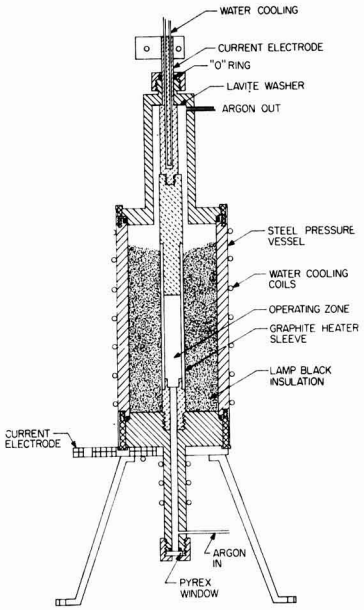

LONGITUDINAL SECTION OF THE GRAPHITE PRESSURE FURNACE FOR GROWING SiC CRYSTALS

Fig. 1. Longitudinal section of the graphite pressure furnace for growing SiC crystals; one inch equalled 40 mils before reduction for publication.

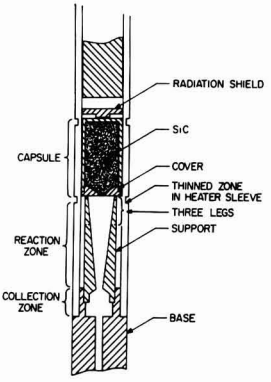

DETAIL OF PARTS USED IN OPERATING ZONE

Fig. 2. Detail of parts used in operating zone

[1] For example, "Graphitite," Graphite Specialties Co., Niagara Falls, N.Y.

[2] United Carbon Products, Bay City, Mich.

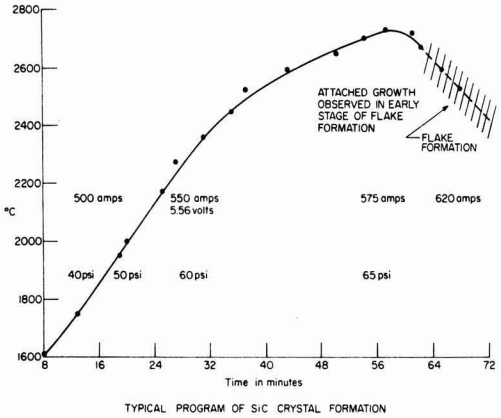

Fig. 3. Typical program of SiC crystal formation

a small hole in the cover. In the upper part of the reaction zone the silicon combines with carbon at a temperature just below decomposition. The inner wall of the support becomes coated with silicon carbide crystals. However, a thinned zone in the heater sleeve creates a "hot spot" from which carbon atoms evaporate readily. This carbon can react with silicon before it reaches the side walls of the reaction tube. When this happens free falling crystals occur.

The actual mechanism of the reaction has not been studied. Possibly intermediate carbides form before a silicon carbide crystal develops. A clear understanding of the reaction would help make a more efficient process. Three important observations lead to the mechanism suggested. The release of silicon from the silicon carbide has been abrupt enough to separate the cover from the capsule. The shape of the original sintered mass of silicon carbide remains in the soft, spongy, graphitic mass. The flutter of flakes visible in the pyrometer occurs abruptly about 2750°C at 80 psi. Those runs in which conspicuous erosion of the heater sleeve takes place, are most productive of silicon carbide crystals.

A run lasts for a little over an hour as shown in the typical program, Fig. 3. The drop in temperature at the end of the run comes from the masking effect of the silicon carbide snow, between the pyrometer and the reference surface. An upward flow of argon

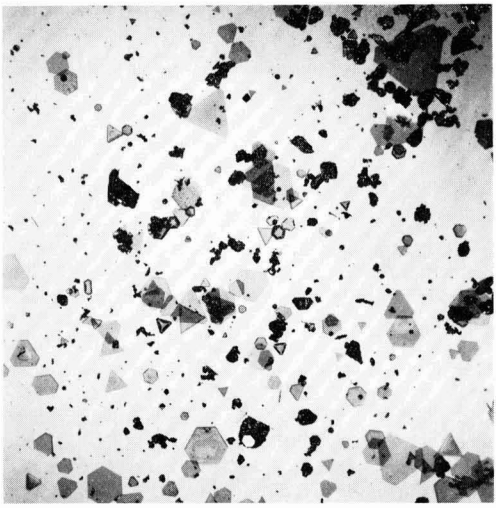

Fig. 4. Display of SiC crystallites as they fell in the furnace. Graphite dust and silicon spheres are also present. One inch equals 40 mils.

maintains the flakes in the reaction zone until they become large enough to fall under gravity. Typical shapes are shown in the display of Fig. 4. The largest dimensions observed are between 20 and 30 mils. Measurements on these crystals are very difficult because of their extreme thinness (~0.3 mil). The size of the crystals is limited largely by the small size of the reaction zone. Crystals which hit the side walls adhere and are no longer free falling. Further work on these free falling crystals is planned with a larger reaction zone so that larger crystals can form.

Manuscript received Nov. 18, 1958. This paper was prepared for delivery before the Ottawa Meeting, Sept. 28-Oct. 2, 1958.

Any discussion of this paper will appear in a Discussion Section to be published in the December 1959 JOURNAL.

REFERENCES

1. Hansen, "Constitution of Binary Alloys," p. 378, McGraw-Hill Book Co., New York (1958); possible phase diagrams of SiC from p. 378.
2. J. A. Lely, *Ber. deut. keram. Ges.*, **32**, 229 (1955).
3. D. R. Hamilton, *This Journal*, **105**, 735 (1958).

Corrections

In the paper by William T. Allen and C. H. Bachman, "Changes in Trapping Levels of Zinc Sulfide Phosphors Resulting from Positive Ion Bombardment," which appears in the March 1959 issue of the JOURNAL, in Figure 1, page 213, the curve labeled 350°K should read 280°K and the curve labeled 280°K should read 350°K.

In the Brief Communication by G. J. Schafer and P. K. Foster, "The Role of the Metal-Ion Concentration Cell in Crevice Corrosion," which appears on page 468 in the May 1959 JOURNAL, Reference 5 should read: R. V. Jelinek, *Chem. Eng.*, **65**, No. 17, 125 (1958).

The Diffusion Coefficient of Lead Ion in Fused Sodium Chloride-Potassium Chloride Eutectic

Richard B. Stein[1]

Ecole Nationale Supérieure d'Electrochimie et d'Electrométallurgie, Grenoble, France

Work in progress in this Laboratory (1) has indicated that the fused sodium chloride-potassium chloride eutectic displays an ideal behavior; the molten bath is completely ionized and solvation is absent. Electrode reactions taking place in this fused electrolyte are being investigated at present by the method of oscillographic polarography. The diffusion coefficient of the discharging metal ion can be measured directly by this method.

In the case of oscillographic polarography the discharge current is given by (2)

$$i = \pi^{1/2}\, n\, F\, A\, \beta^{1/2}\, D^{1/2}\, C^{o}\, \phi\, (\beta t)$$

where A is the surface of the electrode, D is the diffusion coefficient, C^{o} is the bulk concentration of the diffusing species, and $\phi(\beta t)$ is a complex function relating the discharge current, electrode potential, and rate constant. Once the electrode surface and bulk concentration are known, the diffusion coefficient can be obtained from the polarographic wave and the above equation.

Experimental

The polarographic reduction of Pb^{++} in the fused electrolyte was followed by means of a polarograph especially conceived for this system. The reduction cell consists of a cathode in the form of a microelectrode, made from a 0.5 mm platinum wire sealed into a quartz tube ($A = 1.89 \times 10^{-3}$ cm^2), and the Ag/AgCl electrode of Coriou, Dorian, and Hure (3).

The preparation and purification of the solvent bath have already been described (1). The lead chloride used to make up the electrolyte was purified by a flash distillation under vacuum. The dissolution of the lead chloride in the purified solvent was accomplished under a rigorously controlled inert atmosphere, and the resulting solution was electrolyzed immediately in such a manner that no impurities were introduced from the atmosphere. The polarographic cell was placed in a graphite resistor furnace where the temperature was regulated to $\pm\frac{1}{2}$ °C. Polarograms were taken at four different temperatures for a solution ($C^{o} = 2.187 \times 10^{-2}$ mmole Pb^{++}/g solvent) in order to determine the energy of activation of the diffusion process.

[1] Present address: 219 Grace Dr., South Pasadena, Calif.

Table I. Diffusion coefficient of Pb^{++} ion in fused NaCl-KCl eutectic

Temp, °C	Diffusion coefficient x 10^5, cm^2/sec
701	2.4±0.3
746	3.1±0.4
777	3.8±0.5
807	4.4±0.6

Discussion

If the solvent is considered as being a continuous medium in which the laws of classical hydrodynamics are applicable, then the diffusion coefficient can be calculated from the Stokes-Einstein equation. For the diffusion of the lead ion having a radius of 1.21Å, and using the viscosity data of Smithells (5), the diffusion coefficient is calculated at 780°C as $D = 4.6 \times 10^{-5}$ cm^2/sec. From Table I it is seen that the measured and calculated values for the diffusion coefficient are approximately equal, and it can be concluded that the solvent possesses the structure of a simple ionic fluid.

The energy of activation for the diffusion process as obtained from the experimental values is 12.5 kcal/mole. This value can be compared with the value of 13 kcal found by Nachtrieb and Steinberg (6) for the diffusion of Pb^{++} in a complex nitrate bath.

Manuscript received Dec. 29, 1958.

Any discussion of this paper will appear in a Discussion Section to be published in the December 1959 JOURNAL.

REFERENCES

1. R. B. Stein, *C. R. Acad. Sci.*, **246**, 2611 (1958).
2. P. Delahay, "New Instrumental Methods in Electrochemistry," Chap. 6, p. 126, Interscience Publishers, New York (1954).
3. H. Coriou, J. Dorian, and J. Hure, *J. chim. phys.*, **52**, 479 (1955).
4. L. Pauling, "The Nature of the Chemical Bond," 2nd ed., p. 345, Cornell University Press, Ithaca, N. Y. (1940).
5. C. J. Smithells, "Metals Reference Handbook," 2nd ed., Vol. 2, p. 635, Butterworths, London (1955).
6. N. H. Nachtrieb and M. Steinberg, *J. Am. Chem. Soc.*, **72**, 3558 (1950).

Brief Communications

Rectification by Zircaloy 2 in High-Temperature Water

J. N. Wanklyn and R. Aldred

Atomic Energy Research Establishment, Harwell, Berkshire, England

Recent corrosion tests of Zircaloy 2 under heat transfer in water at pH 10.5, 280°C, were vitiated by rectification effects. Strips of the material were heated by the passage of a large 50 cps alternating current, and this involved a voltage of about 12 v rms between the specimen and the wall of the apparatus. Corrosion was unexpectedly great, white oxide forming in less than 200 hr, and much hydrogen was taken up by the Zircaloy 2.

Polarization experiments with unheated Zircaloy 2 specimens in the same apparatus at 250°C, and in simpler apparatus at 20°C, showed that, as expected from work by Carmody (1), rectification occurred, producing a cathodic direct current. As shown in Fig. 1, there was a "barrier" voltage below which no significant d.c. flowed, and above this the curve rose to a final linear portion. At room temperature, curves for unalloyed zirconium lay to the right of those for Zircaloy 2, but had the same linear slope. Experiments in solutions of different concentrations showed the slope to be predominantly controlled by the electrolyte resistance. The "barrier" value was virtually unaffected by changing from a 1 g/l KOH solution to 50 g/l KOH and to a dilute Na_2SO_4 solution. The lower barrier for Zircaloy 2 (which contains iron among other additions) is interesting in view of Carmody's finding (1) that the addition of Fe^{++} to his electrolyte (H_2SO_4) lowered the barrier for unalloyed zirconium.

Similar curves were obtained at 250°C, but the currents were more variable, and the curves changed appreciably with time when sufficient polarization was applied to cause white oxide to form. Analysis after 100 hr at 12 v rms showed that the hydrogen entering the metal was about 15-25% of that equivalent to the charge passed cathodically. Micrographs showed precipitated hydride throughout the material and, generally, a "case" of massive hydride at the surface. The increased corrosion accompanying cathodic charging with hydrogen is presumably related to the similar effect of d-c polarization of zirconium alloys in high-temperature water (2).

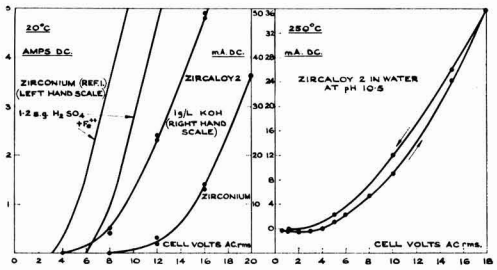

Fig. 1. Rectification curves of zirconium and Zircaloy 2

In contrast, virtually none (<1%) of the cathodic hydrogen entered zirconium and Zircaloy 2 polarized at 12 v rms at room temperature.

Provided the conductivity was at least several hundred μ mho/cm, variation of it, at 20°C, merely altered the linear slopes; but if it fell below roughly 100 μ mho/cm, little or no d.c. flowed even up to 50 v rms although, considering only the electrolyte resistance, there was sufficient voltage to produce a measurable current. Likewise, in neutral water at 250°C the currents were low, and the curves, although rather irreproducible, suggested that the barrier was raised to about 10-15 v rms and that the linear slopes were lower than corresponding merely to the reduced conductivity, compared with that at pH 10.5. No hydrogen was taken up in 100 hr at 12 v rms. In dilute solutions behavior appears to be determined by complex phenomena, probably in the oxide/solution interface.

Manuscript received Feb. 19, 1959.

Any discussion of this paper will appear in a Discussion Section to be published in the December 1959 JOURNAL.

REFERENCES

1. W. R. Carmody, *This Journal*, **91**, 309 (1947).
2. J. N. Wanklyn and B. E. Hopkinson, *J. Appl. Chem.*, **8**, 496 (1958).

Heater Cathode Breakdown

R. J. Jaccodine

Allentown Laboratory, Bell Telephone Laboratories, Inc., Allentown, Pennsylvania

This communication concerns a method of studying heater-cathode insulation breakdown (1). It further proposes a mechanism for this breakdown.

In some electron tubes, the heater is a helix of tungsten wire coated to several mils thickness by spraying with fine Al_2O_3. These heaters are then baked at high temperature prior to being inserted into the cathode sleeve. During use this insulating coating degrades allowing leakage, and in extreme cases a short develops between heater and cathode.

In order to study these phenomena under more controlled conditions, the following method is used. A regular sprayed heater is mounted vertically in a standard tube press. Coiled about this heater is another uncoated tungsten heater or a thin strip of metal (Fig. 1). This outside heater acts in the same manner as the cathode sleeve in an actual tube. This arrangement allows the environmental condition of a portion of the insulation to be controlled. If the effects of various metals or impurities are to be tested, they are applied on thin strips and wound in place of the uncoated heater. The current in each heater can be controlled separately and a d-c potential can be applied between the two heaters. This allows a wide range of temperature, potential and environmental conditions to be studied.

Using the above technique, breakdown was shown to occur only under the wound outside heater (Fig. 1); the appearance of the alumina varied from light gray to black. Under conditions where the heater voltage was 15% higher than normal rated voltage and the heater-cathode potential was 10% higher, breakdown was accelerated. Shorts occurred which caused a glassy, cratered appearance in the insulator probably due to large amounts of current passing through degraded spots raising the local temperature of these spots to the melting point.

In the course of studying factors influencing this breakdown, it was found that oxygen, in the form of metal oxides, caused the degradation process to occur in a fraction of the normal time. The alumina in tubes in which either of the tungsten heaters was oxidized broke down in a short time. In still other tubes, a source of oxygen was included in the form of a separate tungsten filament coated with cupric oxide. Heating this filament gently released oxygen. The alumina in these tubes, after the oxygen was released, broke down in the same order of time as the previous group. Heaters subjected to three and five times the normal processing time in dry hydrogen however have not degraded and are still on life.

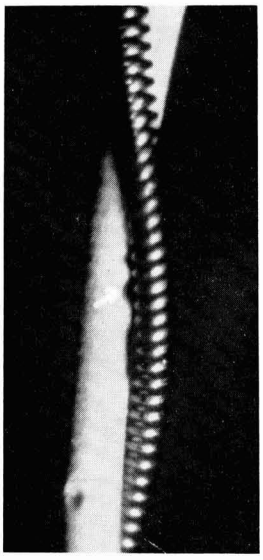

Fig. 1. Experimental arrangement showing "breakdown" region under outside tungsten heater.

It is proposed that in an actual tube, a metallic oxide is formed either of nickel or of tungsten depending in part on the polarity of heater-cathode potential. The oxide reacts with the Al_2O_3 to form a spinel (aluminum tungstate in the case of tungsten oxide).[1] It is this product that degrades the insulating quality of the alumina and allows leakage and eventually a short.

[1] In a paper by Rodinhuis, *et al.* (2), they mention that identification of the breakdown product has been made as aluminum tungstate.

Manuscript received Feb. 13, 1959.

Any discussion of this paper will appear in a Discussion Section to be published in the December 1959 JOURNAL.

REFERENCES

1. G. Metson, E. Rickard, and F. Hewlett, *Proc. Inst. Elec. Engrs., London*, **B102**, 678 (1955).
2. K. Rodinhuis, H. Santing, and H. J. M. Van Tol, *Philips Tech. Rev.*, **18**, 181 (1956).

Discussion Section

This Discussion Section includes discussion of papers appearing in the JOURNAL of The Electrochemical Society, **104**, No. 5 (May 1957), and **105**, No. 1, 5, 6, 7, and 11 (January, May, June, July, and November, 1958). Discussion not available for this issue will appear in the Discussion Section of the December 1959 JOURNAL.

Throwing Index; A New Graphical Method for Expressing Results of Throwing-Power Measurements

R. V. Jelinek and H. F. David (pp. 279-281, Vol. 104)

S. A. Watson[1]: One point which is not made clear in the experimental details given by the authors is that the distance between the anode and the nearer of the two cathodes must be kept constant if the metal distribution ratio at a given average current density is to be a linear function of the linear or primary ratio.

At a fixed average current density, the relationship between the metal distribution ratio, M, and the linear ratio, L, was found by the authors to be of the form $L = kM + C$ where k = Throwing Index and C is some constant. From this, it follows that throwing power expressed by Field's formula,

$$T^F = \frac{(k-1)+C}{(k+1)+C-2} = \text{a constant.}$$

But Gardam[2] showed that

$$T^F = \frac{1}{1+\frac{2dl_2}{N}}$$

where d is the average current density, l_2 is the distance from the anode to the nearer cathode, N is a constant related to solution resistivity and cathode polarization, and clearly T^F is constant at a fixed current density only if l_2 is constant. Therefore, Throwing Index is constant only if l_2 is constant.

The dependence of Throwing Index on the value of l_2 can be shown using data published by Wesley and Roehl[3] by taking advantage of the fact that $M = 1$ at $L = 1$. In Fig. 1 of this discussion, values of M determined at current densities of 0.01, 0.02, and 0.04 amp/cm^2 in a nickel chloride/boric acid solution are plotted against linear ratio and the lines for $l_2 = 10$ cm are extrapolated. Throwing Index is seen to be higher when $l_2 = 2.9$ cm than when $l_2 = 10$ cm at all three current densities. From similar data of Wesley and Roehl obtained with a hard nickel solution and a Watts solution (pH 2.0) at a current density 0.04 amp/cm^2, it can be shown that Throwing Index increases as l_2 decreases with these solutions, too, though the effect is smaller than in the chloride bath.

Although the influence of l_2 on the results obtained by Jelinek and David cannot be estimated from the data given in their paper, the data published by Pan[4] which they quote does show the effect of change in l_2. Pan's data for a cadmium cyanide solution at a current density 0.01625 amp/cm^2 are plotted in Fig. 2 of this discussion. Throwing index is seen to increase as l_2 is decreased. Throwing index can also be shown to vary with l_2 for the acid-zinc and nickel baths which Pan used.

The plots of Wesley and Roehl's data in Fig. 1 show that a threefold increase in l_2 may affect Throwing Index as much as a fourfold increase in current density, which emphasizes that l_2 must be kept constant during determinations of Throwing Index.

R. V. Jelinek: We certainly appreciate Mr. Watson's interest in our paper and his effort to offer constructive criticism. Unfortunately, his mathematical argument is rendered invalid by what appears to be an error in algebra. Using Mr. Watson's symbols, if we substitute the linear Throwing Index relationship

[4] L. C. Pan, *Trans. Electrochem. Soc.*, **58**, 423 (1930).

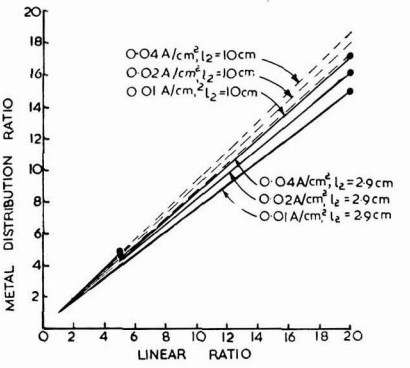

Fig. 1

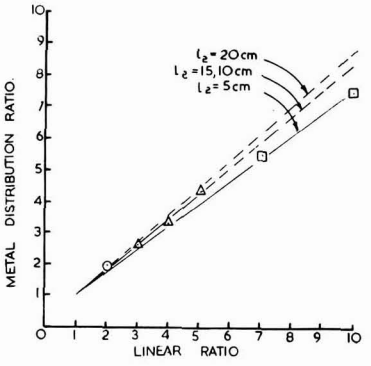

Fig. 2

[1] Electrodeposition Section, The Mond Nickel Co. Ltd., Birmingham, England.
[2] G. E. Gardam, *Trans. Faraday Soc.*, **34**, 698 (1938).
[3] W. A. Wesley and E. J. Roehl, *Trans. Electrochem. Soc.*, **86**, 79 (1944).

$$L = kM + C$$

into Field's formula [Eq. (III) of our paper], the correct result is

$$T_F = \frac{kM + C - M}{kM + C + M - 2} = \frac{M(k-1) + C}{M(k+1) + C - 2}$$

and not the equation stated by Mr. Watson. Since M remains in the equation T_F is clearly not a constant.

The data of Wesley and Roehl and of Pan, as interpreted by Mr. Watson, do appear to indicate some dependence of Throwing Index on electrode spacing. However, his rather ambitious extrapolation of some of the points is questionable at best. When we originally examined Pan's results, we noticed some drift in the cadmium cyanide data, but in preparing our Fig. 2 we thought it best to draw a single line through the points. We do not believe that the three separate lines in Mr. Watson's second figure are really justified. Also, we question seriously the 10-cm lines on his first figure.

Our own results were obtained by keeping the cathodes fixed at the ends of the throwing-power box and moving the anode. Thus, in successive runs, the spacing between the anode and both of the cathodes was varied; i.e., Mr. Watson's 1_2 was definitely not kept constant in our measurements.

Perhaps a careful evaluation of geometric factors and their influence on Throwing Index would be an interesting subject for study. However, we should remember that the rectangular throwing-power box is simply a convenient empirical device with many theoretical limitations. Throwing Index is offered principally as an interpretive tool, which we believe more convenient in practice than the various Throwing Power formulas in the literature, for the reasons stated in our paper.

The Anodic Oxidation of Cadmium, I. Mechanism of Film Formation

P. E. Lake and E. J. Casey (pp. 52-57, Vol. 105)

Indra Sanghi[5]: I was deeply interested in the paper by Lake and Casey as we also happen to be carrying on some investigations on the constant current polarization of Cd in our laboratory. Preliminary results were presented at the XLV Indian Science Congress Session.[6]

During our studies, we found that the behavior of Cd was more complicated than appears from the paper of Lake and Casey. The time-voltage curves obtained during anodic polarization with constant current show more than one arrest. The method adopted by us was similar to that already reported in connection with our studies on Zn[7] and generally resembled the procedure adopted by Lake and Casey. Cd rods or sheets (electrolytic 99.99% purity) were machined out and all the surface except the experimental portion was stopped off with suitable plastic coatings. The prepolarization preparation of the surface consisted of successive mechanical polishings with 0 to 6/0 grades of emery moistened with ethanol. Hg/HgO/KOH was used as the reference electrode and Philips GM 6010 type VTVM to read the potential variations. Both stirred and unstirred solutions were studied at room temperature (35°C) but no attempts were made to keep the solutions air free. Various current densities and concentrations of KOH solutions ($N/5$ to $5N$) were tried and some of the curves obtained are reproduced in Fig. 1 published here.

From these figures, it will be seen that sudden or single-step passivation, similar to that of Zn[7] and as reported by Lake and Casey, was not observed by us in the case of Cd. Also, if only one oxidation compound, CdO, is electrochemically formed and effective, then the reasons for the observed arrests in the neighborhood of −0.6 v with reference to the Hg/HgO/KOH electrode are not clear. Also, a uniform gradual variation of potential, as is observed with Al and other barrier layers, is not to be expected in the case of Cd. Moreover, the potential at which the polarization curve becomes horizontal appears to vary considerably from 0.2 to 1.2 v with different concentrations and current densities, more than can be accounted for on the basis of $(OH)^-$ concentration. All these points could be checked only if the authors had given actual detailed polarization curves obtained by them.

The authors do not give the order of variations in t_p experimentally observed by them. General experience has been that good reproducibility of t_p is obtained only when t_p is small and not greater than a few minutes.[8] There may be risks in taking average values for quantitative calculations, and we were not successful in getting satisfactory reproducibility in similar experiments, either with Zn or Cd. Accordingly, the discussed paper, based almost entirely on It_p measurements, appears to depend on rather uncertain grounds for deriving final conclusions. It would have been helpful if the authors had specifically mentioned the actual method of measuring t_p in cases of prolonged polarization wherein the curves would not steeply rise, clarifying particularly whether the determining criterion was a low slope or atttainment of a particular potential (say 1.1 v). Also in Table I of the discussed paper, measured It_p value for KOH is shown to be 0.52; but the concentration of the electrolyte and the current density are not clearly mentioned. If a low slope determines t_p, then, in our experiments, It_p varies from 0.004 to 0.20 in KOH depending on current density and concentration.

Quantitative calculations and electrometrics depend on the assumption that all oxide films are reduced before hydrogen evolution starts. But it has been suggested, and some evidence adduced, that in some cases hydrogen is actually liberated even on thin oxide films,[9] and hence it is necessary to check this point in the particular case of Cd. It is possible that metals like Zn and Cd are never completely free of oxide films in aqueous solutions, as suggested also by Huber.

The authors have presented only the derived

[5] Central Electro-Chemical Research Institute, Karaikudi, India.
[6] I. Sanghi and R. Rao, *Proc. Indian Sci. Congr.*, 45th Congr., 1958, Part II, p. 202, Abs. No. 423.
[7] I. Sanghi and W. F. K. Wynne-Jones, *Proc. Indian Acad. Sci.*, **46A**, 309 (1957); *ibid.*, **47A**, 49 (1958).
[8] Bicri, Ph.D. Thesis, Berne University, Switzerland (1949); P. Delahay, *Anal. Chem.*, 27, 478 (1955).
[9] I. Sanghi, *et al.*, Paper presented at C.I.T.C.E. 10th Reunion (1958), In press.

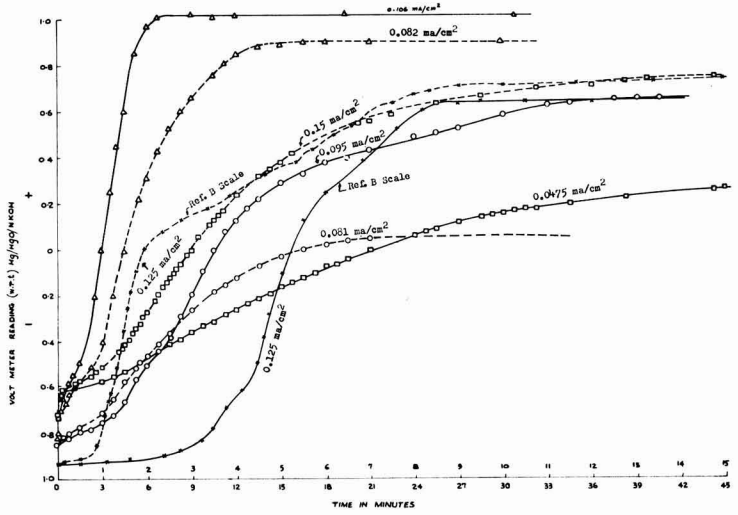

Fig. 1. Some current densities and concentrations of KOH solutions: - - - - -, stirred; ————, unstirred; X, 5N KOH; triangle with dot, 2N KOH; O, 1N KOH; □, 0.2N KOH.

graphs and have not reported the direct measurements. This has resulted in some loss of clarity. For example, in Fig. 1 of the discussed paper, the dotted gas evolution curve appears to indicate that oxygen is discharged in the negative region of potential itself and that as much as 40% of current goes toward oxygen evolution at as low a potential as 0 v with respect to Hg/HgO/KOH. This is not possible in view of the high oxygen overvoltage on Cd and in view of the definite minimum potential required for the reaction $2O\overline{H} \rightarrow H_2O + O$. Also, on page 54 of this paper, the full significance of Fig. 5a and b in connection with the depassivating reaction is not quite clear. Some average rate of depassivation R_2 has been discussed, and probably what the authors imply is that $R_2 = \frac{I\,t'_p}{t_s\,t'_p}$. Similarly, on page 56 (bottom of column 1), it is stated that "if $R'_2 >> R_1$ initially, the CdO film may build up even before supersaturation is reached." This does not appear to be correct, and perhaps there is a typographical error and it should read "$R'_2 << R_1$."

Ionic conduction through very thin oxide films is governed by the high field theory[10] and would be expected to assist the oxide film growth. However, correct ideas about this can be had only by measuring current growth and decay transients or by applying square wave polarization.

Stirring appears to have very interesting effects in the present case. Generally, stirring is expected to delay the passivation considerably, but we find that stirring decreases t_p for 0.2N and N-KOH but increases it for 2N and 5N-KOH. This aspect has perhaps not been considered by Lake and Casey. Also, there appear to be certain difficulties and limitations in evaluating the kinetics of electrode processes and in measuring the rate of film thickening or growth by constant current polarization alone. It has been suggested that potentiostatic measurements are more fruitful[11, 9] and are, therefore, being carried out in these laboratories.

P. E. Lake and E. J. Casey: *Potential arrests.*— Preliminary work showed that extra prolonged potential arrests exist if the current density distribution through the electrode is not uniform and/or constant. In all of the electrometric work reported, a cylindrical cell of which the electrodes formed the ends was used and, within the limits of sensitivity of the multipoint recorder used (±0.005 v, 4 points per min), the extra steps were no longer present. Dr. Sanghi's instrumentation may have detected a real "fine structure." However, if this fine structure is not reproducible, one must consider that the current distribution may be changing from run to run.

Reproducibility of the value of It_p was not as good as could be desired, as was reported in the paper. Best reproducibility was obtained by us if the surface was first cleaned with nitric acid and then prereduced. The possibility that all oxide was not removed was suggested in the paper but accepted as a possible small constant error. When parallel-plate geometry was used, the determination of the value of It_p was usually reproducible to ±10% in experiments done within the fiftyfold range of current densities reported. If successive experiments disagreed by a larger amount, some extraneous factor, such as peeling of the stop-off lacquer, could usually be found to be the reason. However, at Dr. Sanghi's room temperature of 35°C (if this is indeed not a misprint!), the conversion reaction would be expected to be more rapid than at the temperatures (≦25°C) used in the study reported by us, and would probably lead to irreproducible passivation. This comment is strengthened by the further facts that the solubility of $Cd(OH)_2$ in KOH is much higher[12] than is usually supposed, even at 25°C, and

[10] N. F. Mott and N. Cabrera, *Repts. Progr. in Physics*, 12, 163 (1948); D. A. Vermilyea, *This Journal*, 104, 426 (1957).

[11] M. Fleischmann and H. R. Thirsk, *Trans. Faraday Soc.*, 51, 71 (1955); M. Fleischmann and H. R. Thirsk, Paper presented at C.I.T.C.E. 10th Reunion (1958), In press.

[12] P. E. Lake and J. M. Goodings, *Can. J. Chem.*, 36, 1089 (1958).

that the electrolyte can supersaturate during the oxidation. The effect of the supersolubility on potential is simply not known because there are no activity data available.

For the above reasons, the use of It_p as a quantitative measure of the depth to which Cd is oxidized before passivation is certainly justified on the basis of reproducibility. Its variation, as OH^- is replaced by $CO^=_3$ at constant $[K^+]$, is real and can be described in terms of the mechanism proposed in the paper. An interesting further fact, the one which suggested the reported study, is that the changes in It_p with experimental conditions are amplified, sometimes up to tenfold, in the sintered negative plate of the Ni-Cd battery. We are driven to the conclusion that the amplification is due to an important factor not usually considered, *viz.*, the effective volume of the reaction product. It is considered that the product could, in favorable circumstances, seal off at the neck the pores which contain still-unoxidized Cd.

Passivation.—The criterion for choosing t_p was low value of $d\,E/dt$ following the onset of oxygen evolution. To choose a definite potential over so wide a range of experimental conditions would have been meaningless, as Dr. Sanghi's graph testifies. However, it is necessary to restate that sharp passivation depicted in Fig. 1 of the original paper is typical of the behavior of pure Cd at 25° and below.

Dr. Sanghi has simply misinterpreted Fig. 1 in his discussion of gas evolution rate. It is the time base which is common to both the potential and the O_2 evolution rate. What the graph shows, for example, is that a small fraction of the current goes into O_2 evolution while the average potential of the electrode is still below 0 v w.r.t. Hg/HgO (this is not surprising because the potential distribution on the actively corroding metal is probably not completely uniform), and that gas evolution accounts for 40% of the current by the time the rapidly rising potential has reached 1.1 v. What is interesting is the fact that, in the experiment reported in Fig. 1, for some hours *after* passivation a small fraction of the current continued to split off to oxidize Cd and to keep in repair the CdO film which is continually etched away by the conversion reaction.

New work.—A study of the decay of overpotential before, during, and after passivation has recently been completed and will be submitted shortly. At any time after passivation, the decay is of the form usually found for gas electrodes and referred to as activation overpotential decay. However, at times before passivation, after an *IR* drop has been separated the first part of the decay is *exponential* in time. The exponential part is not described by activation theory and is tentatively interpreted as the decay of an inner double layer of $O^=/OH^-$, of fixed dimensions, in the CdO layer at the CdO-electrolyte interface. Passivation occurs when the field strength across this inner double layer increases to the value at which OH^- discharge to OH occurs more easily than the ionization reaction $OH^- \rightarrow O^= + H^+$.

The role of adsorption of OH^- on the CdO surface thus becomes quite important, and is manifested through unexpected variations of overpotential with activity of KOH. In general, the new work supports and extends the mechanism of passivation already proposed:

$$\mathrm{Cd} \xrightarrow{R_1} \mathrm{CdO} \xrightarrow{R'_2}$$

$$\text{Soluble Complex} \xrightarrow{R''_2} \begin{matrix}\mathrm{Cd(OH)_2}\\ \text{or}\\ \mathrm{CdCO_3}\end{matrix}$$

where R_1 refers to the oxidation process, and R_2 to the conversion.

In fact, the proposed mechanism, which incidentally has been strengthened by recent work of Huber,[13] has proven to be quite versatile. For instance, poor reproducibility at high temperatures and low currents is predictable when considered in terms of the role of the conversion reaction and the new information on solubility. At high temperatures, the conversion reaction is fast; a thick and probably loose layer of product is built up on the surface before passivation occurs. The first evolution of oxygen may simply undermine the protecting film of product, and force the process to start over again. At very low currents, the solubility is high enough that the product can actually be transported to and plated out on the negative electrode, and the passivation time will be longer than expected, probably will be irreproducible, and indeed the electrode may never passivate. Stirring will obviously have its greatest effect at low current densities, by aiding dissolution of the CdO layer and aiding transport of complex to the negative where it can be plated out.

The supposed role of adsorption of OH^- on the CdO layer predicts longer passivation times for increasing a_{KOH}, because the decrease in *p*H in the pores of the conversion product will be less the higher the a_{KOH}. Stirring should shorten t_p in low concentrations by raising the *p*H in the pores. On the other hand, increased a_{KOH} increases the rate of the conversion reaction and, once the CdO surface is saturated with OH^-, stirring should lengthen t_p as the a_{KOH} is further increased. It is encouraging that Dr. Sanghi has observed that t_p is shortened in low concentrations of KOH and lengthened in high concentrations.

General.—The conditions under which the values in Table I were obtained could have been approximated from Fig. 4a; they were 0.07 ma/cm^2 and 7.2*N* electrolytes.

As Dr. Sanghi has kindly pointed out, on page 56, line 15, the misprint should read $R_2' << R_1$.

We agree with Dr. Sanghi's comment that the reaction is a complicated one on which further work is necessary.

Uncommon Valency Ions and the Difference Effect

M. E. Straumanis (pp. 284-286, Vol. 105)

Ph. Brouillet, I. Epelboin, and M. Froment[14]: In his article, Dr. Straumanis expresses surprise that the Δ-effect has not been considered to explain the deviations from faradaic yield in the anodic dissolution of certain metals. However, examination of experiments carried out in recent years shows that the Δ-effect cannot explain the anomalous yields obtained in certain electropolishing procedures.

[13] K. Huber, *Z. Elektrochem.*, **62**, 675 (1958).

[14] Laboratoire de Physique, Faculté des Sciences de Paris, Paris, France.

The Δ-effect supposes that in the absence of current there is a protective film on the metal, and that this film is disrupted in certain spots on passing anodic current.

We have observed the surface of metals undergoing anodic dissolution with a noninverting metallographic microscopic whose objective was immersed in the electrolyte. Examination was made in two ways: (*a*) with an interferometric arrangement using two polarized waves (Nomarski system), and (*b*) with ordinary polarized light. The first method gives a resolution of a few dozen angströms; the second makes evident the existence of crystalline layers as they are formed at the anode surface. The results have been observed visually, and recorded by means of microphotography and microcinematography.[15-17]

We have established that during electropolishing the surface becomes more and more uniform and can become perfectly smooth within a few dozen angströms. If polishing is continued on such a surface, its appearance does not change. The homogeneity of the dissolution seems to contradict the Δ-effect, heterogeneous by definition.

The polishing sometimes can be accomplished without the appearance of a layer on the anodic surface. But, if it appears (and it is clearly visible in polarized light), it is quite homogeneous, and an important fact is that it disappears on interrupting the current. Optical examination, as well as chemical analysis,[16] shows that this film has nothing in common with the oxide film which is formed when the anode is just below the polishing potential; this oxide film disappears when the polishing range is attained.

From a chemical point of view, the reactions involved in the mechanism of the Δ-effect raise additional difficulties.

In the experiments to which we refer, for example the anodic dissolution of pure Al in solutions containing ClO_4^- ions,[18-22] the electrode does not undergo any "spontaneous" dissolution when there is no applied current. In electropolishing, no gas evolution is apparent. If, according to the argument of Straumanis, a "spontaneous dissolution" occurs on parts of the metal made bare by anodic dissolution, one must indeed consider the possibility of unusual chemical reactions, for example the reduction of perchlorate to chloride on the metal surface. According to authors who have studied this question,[23] the reduction is difficult, even if the surface has been "made bare" by amalgamation.

We have explained the appearance of reduction products in the electrolyte by the return to their stable valence of ions formed at the anode in a lower and unstable valence state. Quantitative analysis has confirmed this hypothesis, [19,21,22,24] and the work of others with quite different solutions[25] has shown that the reduction products can be formed at some distance from the electrode.

In addition, we have described[22,26] the precise measurement of the electrode potential with respect to a reference electrode. The anodic overpotential is considerable, and it is difficult to postulate a reasonable mechanism of reduction at the electrode surface. Even if this chemical reaction exists, we do not see how it could explain the constancy of the yield when such parameters as time of electrolysis and current density are varied. We have observed a yield constant to about 1% as both parameters were varied over a range of 1 to 20.[22,24]

On the other hand, the importance of the "spontaneous dissolution" ought to vary if the potential of the electrode is changed, with a consequent change in the yield. Now, experiment has shown that the anomalous yield is not modified by change in the polishing potential.[16,24,27] Even on changing the potential by incorporating the metal studied in an alloy, for example Al-Ni,[16,24,27] the Al retains the same abnormal valence. In this case, the electrochemical potential is changed as much as 500 mv, without any external polarization. Again, we do not see how the Δ-effect can explain these results.

Finally, we wish to point out, in response to a question of the author, that we have measured the yield of anodic dissolution during electropolishing of most of the common metals.[16,22,24] With certain metals, the valence calculated from these measurements has been the lowest customary value: Mo^{3+}, Bi^{3+}, V^{2+}, Mn^{2+}, Zr^{2+}, Fe^{2+}, Cd^{2+}, Co^{2+}, Ni^{2+}, Sn^{2+}, Pb^{2+}, Ga^{+}, In^{+}, Hg^{+}, Ag^{+}, Cu^{+}, Li^{+}. With others, we have found a valence lower than the lowest accepted values: La^{+}, Ce^{+}, Ti^{+}, Zn^{+}, U^{+}, Mg^{+}, Al^{+}, Be^{+}. The values found are in no case greater than a known valence, and they are never less than unity.

M. E. Straumanis: The negative difference effect is found when the rate of *self-dissolution* of a metal electrode increases while under an anodic current, and the positive Δ-effect—when under the same conditions this rate decreases. From the loss of weight of the electrode and from the time and strength of the current passing the anode, the valency of the metallic ions pushed into solution can be calculated. If, now, the difference effect (that is, the increase or decrease of self-dissolution rate during the flow of current) is disregarded, one will calculate in the first case a decrease in the valency of ions going anodically into solution (because the weight of the metal which dissolved outside the faradaic current was not taken into consideration), and, vice versa, an increase in the ionic charge in the second case.

Both effects were studied by the author[28] and they also were observed by others, e.g., the negative effect by Heumann and associates during the anodic

[15] I. Epelboin, M. Froment, and G. Nomarski, *Rev. Métall.*, **55**, 260 (1958).
[16] M. Froment, Thesis 1958, *Corrosion et anti-corrosion*, **6** (Nov. 1958).
[17] "Etude Microscopique du Polissage Electrolytique," Film prepared by I. Epelboin and M. Froment (with the assistance of G. Nomarski).
[18] I. Epelboin and M. Froment, *Comp. rend.*, **238**, 2416 (1954).
[19] Ph. Brouillet, I. Epelboin, and M. Froment, *Compt. rend.*, **239**, 1795 (1954).
[20] M. Froment, Dissertation, Paris (1954).
[21] Ph. Brouillet, Thesis 1955, *Métaux (Corrosion-Indus.)*, **30**, No. 356—April, No. 357—May, No. 358—June (1955).
[22] I. Epelboin, *Z. Elektrochem.*, **59**, 691 (1955).
[23] W. R. King and C. S. Garner, *J. Phys. Chem.*, **58**, 29 (1954).
[24] I. Epelboin and M. Froment, 73rd Colloque International du C.N.R.S., Paris, 1956, *Métaux (Corrosion-Indus.)*, **32**, 55 (1957).
[25] M. D. Rausch, W. E. McEwen, and J. Kleinberg, *J. Am. Chem. Soc.*, **77**, 203 (1955).
[26] Ph. Brouillet and F. Monnot, *Bull. soc. franc. électriciens*, **8**, 493 (1958).
[27] M. Froment, *Bull soc. franc. électriciens*, **8**, 505 (1958).
[28] M. E. Straumanis, *This Journal*, **105**, 284, 286 (1958).

passivation of Cr[29] and on stainless steel by Tomaschow.[30] Both effects are proportional to the current density, meaning that the ratio of the rate of self-dissolution and of enforced rate (through current) is constant, and independent of the pH of the solutions.

In the case of Al corroding in KCl, the increase in rate of self-dissolution while the anodic current was on could be directly observed. Besides, it could be seen that the protective (oxide) layer on Al broke down under the impact of anodic current. Thus, the increase in self-dissolution could be attributed to the scale breakdown. It is not said that the latter should in all cases be an oxide scale; it can be a salt layer as well. Even a metal without any scale at all could produce a Δ-effect if the metal in the surface becomes activated by the anodic current. The same effect could be produced by a decreasing thickness of the scale while under anodic current. If in the experiment with Al in KCl the increase in self-dissolution is disregarded, a valency lower than 3 can be calculated for Al ions from the experimental data. This, in the opinion of the author, happened in the work of Drs. Brouillet, Epelboin, and Froment.

Although the discussors state that in an electrolyte containing ClO_4^- there was no gas evolution (at the anode) during electropolishing, and that the reduction of ClO_4^- is difficult by the metal, they nevertheless write in the next paragraph that there are reduction products present but produced by the Al ions of lower valency. Is it not simpler to write: $Al + 3H^+ \rightarrow Al^{3+} + 3H$ (self-dissolution while under anodic current, Δ-effect) and then $ClO_4^- + 8H \rightarrow Cl^- + 4H_2O$?[31]

The (active) hydrogen has a certain solubility in water and may act at some distance from the electrode; no lower valency Al-ions are necessary for the reduction. In addition, no such ions were obtained by the discussors when electropolishing was made in solutions containing phosphoric acid, chlorides, or fluorides.[32] It is clear that there was no negative Δ-effect, but probably a positive one during the passage of current, as it is well known that the effect may change its sign if a metal is anodically dissolved in different electrolytes.[33]

Furthermore, in the last paragraph of the discussion, two series of metal ions are given. Is it not surprising that the metals which supposedly produce ions of lower valency during electropolishing all are *the most active metals* (Zr^{2+} should be transferred into the second series because its most common valency is 4)? These metals react with the electrolyte (self-dissolution) as soon as the protective layer is removed or changed (e.g., by the anodic current, Δ-effect). Even ions with a valency lower than 1 can be found by calculation in such cases.[34] More noble metals exhibit only very slight Δ-effects[30] and, therefore, no ions of unusual valency (1st series) were found by the discussors with such electrodes.

Finally, the assumption of the discussors, that during anodic polarization ions of lower valency are going into solution, is contrary to experience gained in passivation experiments. For instance, Fe or Cr,[29] as it, e.g., follows from the recent work of Pourbaix,[35] at small current densities go into solution with low but normal valencies and with the valency increasing at higher current densities (or potentials), which is in accordance with our theoretical considerations.

Of course, if the discussors can show that there is absolutely no change in the rate of self-dissolution of an anode made of an active metal during polarization (no Δ-effect), then their conclusions should be regarded as correct (or *see* last sentence in the discussed paper).

Studies of Natural Convection at Vertical Electrodes

N. Ibl and R. H. Müller (pp. 346-353, Vol. 105)

G. Wranglén[36]: This paper is of great interest since it shows that the velocity profiles obtained in the rigorous numerical solutions of the boundary layer equations by Ostrach and by Sparrow and Gregg can be realized also in electrolysis experiments under ideal flow conditions just as they already have been realized in experiments on thermal boundary layers. In addition, a new contribution is the application in the approximate analytical treatment, according to von Kármán, of velocity profiles that are in agreement with theoretical expectations and experimental findings. The method adopted by the authors is to vary certain parameters in the velocity and concentration functions so that the calculated values of u_m and τ fit the experimental data. However, this method will not admit a comparison between a purely theoretical solution and experimental results. This comparison can be made if the functions introduced are adapted instead to the profiles obtained by a rigorous numerical treatment. It should further be emphasized that any functions will give results that are correct dimensionally. Only the numerical coefficients in the expressions for maximum flow velocity, limiting current density, diffusion layer thickness, concentration difference, etc., will differ. However, exact values of these coefficients can easily be obtained by comparison with the rigorous numerical solutions for the appropriate Schmidt (or Prandtl) number.

According to these principles, the discussor has performed calculations, the main results of which were recently published in a short communication.[37] While the concentration profiles used were the conventional ones, corresponding to Eq. (V) of the paper discussed, the following approximation was used for the velocity profile, *viz.*,

$$u = 3.375\, u_m \frac{y}{\delta}\left(1 - \frac{y}{2\delta}\right)^2 \qquad [1]$$

for

$$0 \leqq y \leqq 2/3\ \delta$$

[29] Th. Heumann and W. Rösener, Z. *Elektrochem.*, **59**, 722, 730 (1955); Th. Heumann and F. W. Diekötter, *ibid*,. **62**, 745, 748 (1958), however, the authors do not mention the words "difference effect," but that there was such an effect follows from the description.
[30] N. D. Tomaschow, Z. *Elektrochem.*, **62**, 717, 725 (1958).
[31] I. Epelboin, Z. *Elektrochem.*, **59**, 689, 690 (1955).
[32] I. Epelboin, Z. *Elektrochem.*, **62**, 813, 815 (1958).
[33] M. E. Straumanis and Y. N. Wang, *This Journal*, **102**, 304 (1956).
[34] M. D. Rausch, W. E. McEwen, and J. Kleinberg, *J. Am. Chem. Soc.*, **77**, 2093 (1954).
[35] M. Pourbaix, Z. *Elektrochem.*, **62**, 670 (1958).
[36] Div. of Applied Electrochemistry, Royal Institute of Technology, Stockholm 70, Sweden.
[37] G. Wranglén, *Acta Chem. Scand.*, **12**, No. 4 (1958).

Table I

Quantity	Constant liquid density A.A.	Constant liquid density R.N.	Constant current density A.A.	Constant current density R.N.
u_m	1.18	0.98	1.33	1.1
$\delta_{0.99}$	3.48	3.54	3.00	3.09
τ	2.32	2.69	2.00	(2.1)
i_{lim}	0.575	0.499	—	—
$/c_o - c_e/$	—	—	1.50	1.59

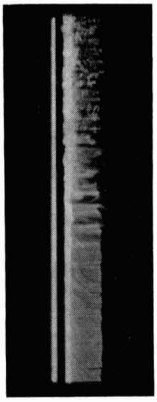

Fig. 1. Transition from laminar to turbulent flow in the electrode film in electrodeposition of Cu under free convection conditions.

and

$$u = 0.070\, u_m\, Sc^{-1/3}\left(1.5\, Sc^{1/3} - \frac{y}{\delta}\right) \qquad [2]$$

for $2/3\ \delta \leqq y \leqq 1.5\ Sc^{1/3}\ \delta$. In these expressions, $\delta = \delta_{0.99}$ is defined as the value of y for which $/c - c_e/ = 0.99/c_o - c_e/$. This definition also allows an exact meaning to be assigned to δ. Eq. [1] implies that u_m is reached at $2/3\ \delta$, which is approximately true for high Schmidt numbers. Eq. [2] takes into account the fact that the thickness (1) of the hydrodynamic boundary layer is a function of the Schmidt number. Generally, $1 \simeq \delta \cdot Sc^{1/3}$.

For the numerical constants of interest here, the results listed in Table I were obtained. They refer to $Sc = 1000$, which is a good mean value for aqueous electrolytes, particularly if higher temperatures are also considered.

A.A. means approximate analytical solution and R.N. rigorous numerical solution. The table shows that the approximate profiles introduced, although comparatively simple, are a satisfactory substitution for those obtained in the rigorous numerical treatments. This can also be shown by plotting the respective profiles in the same diagram. In a comparison with experimental results, the constants derived from the numerical solutions should be used. Experimental values for the coefficients are: 1.04 for u_m, 1.63 for τ (at constant c.d.), and 0.505 for the limiting c.d.[38]

The fact that the flow becomes turbulent at relatively low values of the Grashof number is illustrated by Fig. 1 published here which was obtained by a schlieren technique without lenses.[39] A cathode in a 1M $CuSO_4$-solution was placed in a beam of parallel light and the shadow was photographed. The electrode, filling the whole cross section of the electrolyte, was 180 mm high and the photograph was taken between $x = 80$ and $x = 140$ mm. The current density was 1.5 amp/dm^2 and the temperature 20°C. While laminar flow on the lower part of the cathode is evident from the constant deviation of light and a regular vertical motion in the bright band, the conditions on the upper part of the cathode are clearly turbulent. The transition from laminar to turbulent flow under the conditions mentioned occurs at $x \simeq 100$ mm both at the cathode and the anode. The same result was obtained with electrodes, 1000 mm in height. These results seem to agree with those reported in the paper under discussion. They obviously imply that in full-scale electrolysis (e.g., copper refining) the free convective flow is turbulent over the main part of the electrodes. Calculations, based on an assumption of laminar flow, are then of qualitative value only. This situation stresses the need for at least empirical relations for mass transfer under turbulent free convection conditions.

N. Ibl: The interesting results reported by Wranglén on the onset of turbulence in natural convection are in agreement with the findings of R. Müller. In our optical experiments, the flow became turbulent[40] for instance at a height of 8 cm with a current density of 20 ma/cm^2 and at a height of 14 cm with a current density of 4 ma/cm^2. This corresponds to a Rayleigh number, Ra (Ra = Sc x Gr) of roughly 4×10^{11} (compared to a Ra of 2×10^9 reported by Saunders[41] for the transition to turbulence in heat transfer). As Wranglén points out, the question arises as to how far the relations hitherto derived are still valid with tall electrodes, of the kind used in technical cells. M. G. Fouad has studied experimentally in our laboratory the mass transfer by natural convection at Rayleigh numbers above 10^{11}. His unpublished experiments show that the limiting current has a tendency to become almost independent of the height with tall electrodes. The slope of the line log Nu vs. log Ra is somewhat larger than ¼. In this investigation, the cathodic limiting current was measured in the usual way with electrode heights up to 100 cm and $CuSO_4$-solutions acidulated with H_2SO_4, the concentration of the $CuSO_4$ ranging from 0.01 to 0.73M.

Concerning the question of the profiles as discussed by Wranglén, there is no doubt that the results obtained by von Kármán's method should become better with increasing accuracy of the profiles employed. However, it is interesting to note that the profiles hitherto commonly used in the application of von Kármán's method to natural convection [Eq. (V) and (VII) of the discussed paper], although they are far from true, yield limiting currents which differ by only 2%[42] from those derived from the rigorous treatment given by Ostrach. In the case of the maximum flow velocities, the agreement is less good but

[38] C. R. Wilke, M. Eisenberg, and C. W. Tobias, *This Journal*, **100**, 513 (1953).
[39] E. Schmidt, *Forsch. Gebiete Ingenieurw.*, **3**, 181 (1932).
[40] R. H. Müller, Dissertation No. 2668, Swiss Federal Institute of Technology, Zurich (1956).
[41] R. Saunders, *Proc. Roy. Soc. (London)*, **A157**, 278 (1936).
[42] C. R. Wilke, C. W. Tobias, M. Eisenberg, *Chem. Eng. Progr.*, **49**, 663 (1953); S. Ostrach, *Nat. Advisory Comm. Aeronaut., Technote 2635* (1952).

the difference is still not very large, the numerical coefficient in the equation for the flow velocities being 0.98 for the rigorous method[43] and 0.77 in the case of von Kármán's approximation using the above profiles (Table I of the discussed paper). It was thus felt worth while to study in some more detail the influence of the assumed profiles on the results obtained with von Kármán's method. This was achieved by varying the parameters of Eq. (VIII) to (X) of the discussed paper. It was found that the results depend greatly on the assumption made on the relative location of the velocity maximum and the shape of the velocity profile up to the maximum, but, within a wide range, they are almost not affected by a variation of the slope of the velocity profile beyond the maximum. This might help to understand how it is possible that Eq. (V) and (VII) give good results in spite of the fact that they are quite wrong in the outer parts of the boundary layer. It might be noted that, with velocity profiles of the type used by Wranglén, the results are also practically independent of the slope beyond the maximum. This slope is in this case inversely proportional to $Sc^{1/3}$, which is roughly 10 in aqueous solutions. However, if a value of 5 or 20 is used instead of 10, the calculated maximum of the flow velocity at constant liquid density, for instance, is changed by less than 2%.

In the discussed paper, the measured velocities were not compared with the values obtained by the rigorous method, since the extrapolation to high Schmidt numbers of the velocity distributions shown graphically by Sparrow and Cregg[44] for a few Prandtl numbers between 0.1 and 100 appeared inaccurate. It is encouraging that the figure of 1.1 given in Wranglén's discussion for the numerical coefficient of the equation for the flow velocity (which was extrapolated to Sc = 1000 from more accurate values of the rigorous solution communicated by Sparrow and Cregg) is in very good agreement[45] with the experimental value of 1.04.

A Contribution to the Theory of Stress Corrosion in Al-4% Cu Alloys

W. H. Colner and H. T. Francis (pp. 377-384, Vol. 105)

G. J. Schafer and T. Marshall[46]**:** The comments regarding H_2O_2 concentration variability during tests are of great interest. Partly for this reason, we have much greater confidence in the acid chloride gas evolution test for intercrystalline corrosion susceptibility than in the salt-peroxide test. It has been shown[47] that important composition variables remain constant during the former test.

We do not entirely agree with the interpretation of some of the results presented by the authors. The polarization curves in Fig. 7 and 8 of the discussed paper indicate mixed rather than cathodic control. Cathodic control implies a large difference in polarization curve slopes with the cathode polarization curve being relatively much steeper. Again, in Fig. 6, current is only influenced by cathode area at large cathode: anode ratios, which indicates mixed control.

The area effect demonstrated in Fig. 2 of the paper does not necessarily support the contention that the grain boundary-grain center corroding cell is under cathodic control. In the case of the specimens not connected to auxiliary electrodes, the ratio of grain-center to grain-boundary areas is constant. Therefore, the failure time vs. exposed area curve must be explained purely on the basis that, when a larger specimen area is exposed, more grain-boundary trenches are formed in the stressed metal surface, and the time required for a given deflection is therefore shorter.

The disappearance of the area effect when auxiliary electrodes were used is not very relevant. It is shown in Fig. 8 that stressed 2024 is anodic to unstressed 2024 (this effect of stress has been observed on other materials),[48] so, when a stressed specimen is electrically coupled to an unstressed specimen, the system under consideration is equivalent to a bimetallic couple and has no simple relation to a stressed specimen by itself. Auxiliary electrodes of any more noble metal having appropriate polarization characteristics would have a similar effect on times to failure of the stressed specimens.

We would appreciate the authors' comments on our interpretation of their data.

H. T. Francis and W. H. Colner: It is conceded that Fig. 7 and 8 could be interpreted as indicating mixed control rather than cathodic control. In the couples of Fig. 6, however, the current was determined by the total cathode area when the anode area was held constant (C curves). Conversely, the current was unaffected by changes in anode area when the cathode area was held constant (A curves). This we interpret as cathodic control.

With regard to the area effect demonstrated in Fig. 2, we agree that the ratio of grain-center area to grain-boundary area is constant in any given specimen. For small specimens, however, we contend that the cathodic area is insufficient to produce enough total anodic attack to promote cracking. With larger specimens, the total cathodic area promotes rapid enough attack on *some* of the anodic zones to permit cracking. Reference is made to the work of Mears, Brown, and Dix on this point.[49]

We agree that coupling to other suitable cathode material would cause small-area specimens to crack. The question then remains: Why do small-area specimens not fail by themselves? We know they possess anodic grain-boundary zones, since they crack readily when coupled to auxiliary cathodes. The conclusion then must be that they cannot in themselves provide sufficient cathodic action to cause cracking.

[43] The K value of 0.98 indicated on the third line of Table I of the discussed paper is equal to the rounded numerical coefficient in Wranglén's equation for the flow velocity at constant liquid density along the interface [*Acta Chem. Scand.*, 12, 1143 (1958)]. The figure of 0.98 was directly obtained from the value of F' (η) given by Ostrach for a Prandtl number of 1000, the method used in the derivation being probably very similar to that employed independently by Wranglén (G. Wranglén, *Trans. Roy. Inst. Technol., Stockholm*, In press).

[44] E. M. Sparrow and J. L. Cregg, *Trans. Am. Soc. Mech. Engrs.*, 78, 435 (1956).

[45] The numerical factor of 2 in the right-hand side of Eq. (XXIII) of the discussed paper is a misprint and should be omitted.

[46] Dept. of Scientific and Industrial Research, Dominion Lab., P. O. Box 8023, Wellington, New Zealand.

[47] T. Marshall and G. J. Schafer, *J. Appl. Chem. (London)*, 8, 303 (1958).

[48] U. R. Evans, "Metal Corrosion Passivity and Protection," p. 471, Edward Arnold & Co., London (1937).

[49] R. B. Mears, R. H. Brown, and E. H. Dix, Jr., "Symposium on Stress-Corrosion Cracking of Metals," ASTM-AIME, 323-337 (1944).

Fundamentals of the Theory of Electrodes and Galvanic Cells

E. Lange and P. Van Rysselberghe (pp. 420-428, Vol. 105)

Patrizio Gallone[50]: I would like to take the liberty to submit some very modest considerations about some particular points of this paper, which deserves the most careful study by all electrochemists wishing to keep abreast with the fundamentals of their subject.

[2.3] About the last statement made by the authors in this paragraph of their paper one may object that "if chemical forces were alone effective" the "corresponding reaction" could only be spontaneous, so that in this hypothetical case A would only be positive.

[2.7] The electrochemical affinity is defined as the sum of the chemical affinity and of a term derived from the galvanic tension. This term, which also has by consequence the dimension of an affinity, is, among all the physical quantities considered by the authors, the only one that has not been given its own name. From the concepts underlying the definition of the Galvani tension, one may deduce that such nameless quantity should be called *Galvani affinity*, or *inner electric affinity*, or *electrostatic affinity*.

[2.9] With regard to the sign of the reversible Galvani tension of a given electrode, one may note that the way in which this quantity has been defined under [2.5] is clearly based on the spontaneous reaction, *viz.*, either α or β, as the case may be, irrespective of considering the electrode x or its reverse y. This is the reason for the change in sign when considering the reverse electrode. Consequently, the statement that the Galvani tension "is the same whether the electrode reaction is regarded as being α or β," instead of adding any further clarification, may seem to be at variance with the definition of the Galvani tension itself, which is based on the consideration of the spontaneous reaction only.

These same considerations essentially apply also to the sign of the corresponding chemical tension.

[4.11] As to the mutual interdependence of the cell tension U and the electromotive force E, may it be emphasized that we "always" have $U = -E$ provided that the equilibrium conditions of the reversible process are satisfied. For a better understanding of the reciprocal behavior of U and E, as well as of their different nature, it can be noted that these two tensions are in the same relationship as an acting and a reacting force in a mechanical system. The chemical tension, or electromotive force, E of the Galvanic cell can be compared to a static pressure exerted by a fluid against the wall of its container, and the electrostatic tension U is comparable to the reaction force opposed by the vessel. Whenever the reaction force is decreased, e.g., by establishing a metallic connection between the two cell electrodes, or by opening an aperture through the wall of a fluid-containing vessel, a new equilibrium of a dynamic sort comes about, with a flow of electric charges or of fluid and the consequent appearance of forces having a dissipative nature.

A mechanical comparison such as the above may sound somewhat trivial at the higher stages of theoretical standing, but it is extremely helpful at the lower ones in giving more concreteness to the fundamental concepts expounded by the authors.

E. Lange and P. Van Rysselberghe: The authors appreciate Dr. Gallone's interest in their paper.

The statement made about paragraph [2.3] is erroneous. The chemical affinity of an electrode reaction will be positive or negative according to the direction in which the reaction is written.

In connection with paragraph [2.7], we agree that an expression such as *electric affinity* could well be used. This has, in fact, been suggested in the 1958 version of the report on Electrochemical Nomenclature and Definitions of the International Committee of Electrochemical Thermodynamics and Kinetics (C.I.T.C.E.).

The statement made about paragraph [2.9] is erroneous. Paragraph [2.5] defines the chemical tension, not the electric or Galvani tension. Moreover, the direction in which these tensions, chemical and electric, are taken corresponds to the manner in which the phases are counted and not to the direction in which the electrode reaction may be spontaneous.

We agree that the analogy developed by Dr. Gallone in connection with paragraph [4.11] may be of some help in an elementary discussion of electrochemical equilibrium and of the departure from this equilibrium.

The Mechanism of Passivating-Type Inhibitors

M. Stern (pp. 638-647, Vol. 105)

H. H. Uhlig[51]: The electrochemical mechanism for passivation of metals by oxidizing passivators, as outlined by Dr. Stern, is a reasonable proposal and, in my opinion, fits the facts as we now know them. In a paper by Dr. King and myself, presented at this same meeting (ECS, Ottawa, September 1958), we have arrived at essentially the same mechanism. Dr. Stern appears to lean toward a definition of passivity which excludes nonoxidizing passivators. I concur in the advantages of such a definition, especially if the metal admitted to be passive exhibits a Flade potential. But many investigators have traditionally defined passivity on the basis of a low corrosion rate (Definition II, "Corrosion Handbook") which includes as passivators nonoxidizing substances like pickling inhibitors, Na_3PO_4, Na_2SiO_3, and carbon monoxide. Perhaps we are now at the point where a clearer definition of passivity can be formulated, and, in this regard, Dr. Carl Wagner has already moved in this direction.[52]

Of course, oxidizing property is not the only factor that enters passivation even in the presence of a

[50] Oronzio de Nora, Impianti Elettrochimici, Milan, Italy.

[51] Corrosion Lab., Massachusetts Institute of Technology, Cambridge 39, Mass.

[52] C. Wagner, International Symposium on Passivity, Jugenheim, West Germany, September 1957.
A metal is called passive if: (a) on increasing the electrode potential toward more noble values, the rate of anodic dissolution in a given environment as a function of electrode potential under steady-state conditions is found to be less than the rate at a lower, less noble potential; or (b) if, on increasing the concentration of an oxidizing agent in an adjacent solution or gas phase, the rate of oxidation without flow of external electrical current under steady-state conditions is found to be less than the rate at a lower concentration of the oxidizing agent.

strong oxidizer. In an experiment we did some years ago, 18-8 stainless steel in 10% ferric chloride was found to corrode by pitting at a very high rate, but, on addition of 3% sodium nitrate, the corrosion rate fell to less than one millionth its original value. It is not possible that the nitrate ion contributed to the cathodic depolarizing action of the ferric ion; instead, the nitrate ion probably adsorbed on anodic areas displacing chloride ion and thereby reduced the critical current density required for passivity of 18-8. This mechanism fits in with the general picture outlined by Dr. Stern. Incidentally, it is difficult in this instance to conceive of any mechanism involving build-up of thick oxide films as cause of the tremendous decrease in corrosion rate.

With regard to Fig. 2, it is unfortunate that point E is described in the text as the Flade potential. This potential is not the same as the critical potential observed on decay of passivity first described by F. Flade, and after whom the Flade potential is named. Point E includes an unknown increment of potential caused by concentration polarization and *IR* drop through temporary thick films of anodic corrosion products. Such films are not present and do not cause error in measurement of the true Flade potential when passivity decays.

Whether a critical concentration of passivator exists with accompanying sudden shift of potential to the passive value, or instead the shift in potential is more gradual on increasing the passivator concentration, depends on the rapidity with which the passivator can be cathodically reduced. If reduction is slow, as is apparently the case with chromates, chromate can adsorb increasingly on the metal surface (thereby producing more cathodic area) in accord with the Langmuir adsorption isotherm. If reduction is rapid, a critical concentration should be found above which, but not below, passivity is observed. For the latter case, a Langmuir adsorption behavior of potential vs. passivator concentration may then be found only on a surface already passive. This situation probably obtained in the course of Geary's measurements showing a Langmuir relationship for 18-8 and titanium in sulfuric acid in presence of Cu^{++} and Fe^{+++}. It is my conclusion that the passive film in presence of ferric or cupric sulfate is essentially an adsorbed film of oxygen in accord with the ideas described in the paper by Dr. King and myself, on top of which Cu^{++} or Fe^{+++} is adsorbed in amount dependent on concentration.

It is not entirely clear what experimental conditions of Okamoto led to a constant corrosion potential of iron short of 10^{-3} moles chromate/liter and a passive potential thereafter. Careful work of Heyn and Bauer[53] shows a gradual change of potential on increase of chromate concentration more nearly in accord with data of Geary.[54,55] The lower purity iron used by Okamoto is not the cause,[56] and it is not certain whether Okamoto's use of beeswax-rosin to shield a portion of his electrode surface reduced some chromate at the wax-metal interface and produced a passive-active cell which disturbed the potential.

It is true that Fig. 4 indicates that the corrosion rate in a passivator solution should be the same as that which occurs when the metal is passivated by anodic polarization to the same potential, but with one important provision. This provision is that the anode to cathode ratio should be the same in the passivator solution as during anodic polarization. This situation may or may not prevail in practice, depending on the metal and the passivator.

From data of Fig. 8, it is probable that chemical equivalents of passive film substance on Ti are less than 0.02 coulomb/cm^2 in view of the fact that Ti corrodes rapidly in boiling sulfuric acid before passivity is achieved. The calculated coulombs under these conditions partly include those measured in forming an insulating reaction product film preceding build-up of the true passive film. The situation is analogous to Fe where the measured coulombs in sulfuric acid are found to be 1.6/cm^2 [57] which includes build-up of ferrous sulfate or similar film before passivity is achieved. But as Weil[58] observed, the true passive film accounts for only about 0.008 coulombs/cm^2 of the 1.6 coulombs/cm^2. It well may be, therefore, that the chemical equivalents of passive film substance on Ti are also consistent with the value of about 0.01 coulomb/cm^2 for Fe, which is the value found for the passive film on Cr-Fe and 18-8 stainless steels.[57,59]

With respect to Fig. 6, Dr. Stern states that, when the redox system is essentially at equilibrium on the passive surface, there is no net reduction of inhibitor. Thermodynamically, of course, the total system still tends to react and hence some corrosion undoubtedly occurs. The actual situation is probably one in which the net reduction of the redox system is finite, but nevertheless so small that the conditions of equilibrium are not appreciably upset.

The effect of oxygen on passivity of Fe in presence of molybdates and tungstates (and also on the rate of passivation in presence of chromates), in addition to factors mentioned by Dr. Stern, is a probable increase in the cathode to anode ratio favoring anodic passivation of the smaller anodic areas. This factor is mentioned in our paper.

Finally, I should like to mention that Dr. Stern's paper helps clarify our understanding of passivity and passivation, and is a welcome contribution. It comes at a time when serious effort is being made, as was evident at the International Symposium on Passivity held at Jugenheim, West Germany, in September 1957, to arrive at a more satisfactory knowledge of the structure and composition of passive films in general in metals and alloys.

E. E. Nelson[60]: This paper is another example of Dr. Stern's excellent discussions of previous publications and of his original work on electrode processes. The explanations of the roles of the reversible poten-

[53] E. Heyn and O. Bauer, *Mitt. Materialprüfungsamt. Berlin-Dahlem*, 26, 95 (1908).
[54] Although relative values of potential are reported correctly in the paper by Uhlig and Geary, absolute values are apparently too active by about 0.1 v.
[55] H. H. Uhlig and A. Geary, *This Journal*, 101, 215 (1954).
[56] G. Okamoto, Private communication.
[57] R. Olivier, "Proceedings 6th Meeting, International Committee for Electrochemical Thermodynamics and Kinetics," p. 314, Butterworths, London (1954).
[58] K. Weil, *Z. Elektrochem.*, 59, 11 (1955).
[59] H. Uhlig and P. King, Unpublished data.
[60] Socony Mobil Oil Co., Inc., 412 Greenpoint Ave., Brooklyn 22, N. Y.

tials, the exchange currents, and concentrations of oxidizing agents will aid greatly in the eventual complete understanding of passivity.

In this discussion, the relationship of Stern's arguments to particular anode-cathode reactions will be considered. It is believed that this supports Stern's conclusions and develops some additional information. The particular reactions were discussed by Pryor and Evans[61] and were named "autoreduction" by them. Later, they have been studied by Oswin and Cohen,[62] Buob, Beck, and Cohen,[63] and Nelson.[64]

"Autoreduction" is the combination of reactions (I) and (II) given below.

$$Fe_2O_3 + 6H^+ + 2e \leftrightarrows 2Fe^{++} + 3H_2O \qquad (I)$$

$$Fe \leftrightarrows Fe^{++} + 2e \qquad (II)$$

Pourbaix[65] shows that in the pH range of about 2 to 8, the equilibrium potential of reaction (II) is negative to the equilibrium potential of reaction (I). Therefore, when ferric oxide is in metallic contact with Fe in solution, reaction (II) will be mostly in the anodic direction and reaction (I) will be mostly in the cathodic. Footnotes 61, 62, and 63 give proof that this actually does occur. Many writers have felt that passivation is due to a covering of ferric oxide over the metallic Fe. The theory of "autoreduction" indicates that an extensive film of ferric oxide can not start forming until the Fe anode is polarized to the equilibrium potential for reaction (I).

Some authorities feel that passivity is due to absorbed oxygen rather than to an oxide. The arguments here could apply also to absorbed oxygen, but the work on autoreduction seems to favor the oxide theory.

Referring to Fig. 2 of Dr. Stern's paper, the corrosion rate of Fe increases along the curve from A to B. The reduction of ferric oxide would predominate over its formation at point A. These two rates would approach each other and become equal at point B. As the potential becomes more positive, the formation of the oxide increases and its reduction decreases. In the region from B to E, the coverage of the oxide increases. This decreases the anode area and also the total corrosion rate. The corrosion rate per unit of active anode is probably increasing in this area. This would account for the tendency for steel to pit in an inhibitor solution of a concentration below a safe minimum. At point E, the film development is completed and maximum protection is achieved.

In many of the figures of Dr. Stern's paper, current is plotted rather than current density. This has the advantage of showing the decrease in anodic current (and the total amount of corrosion) as passivity is developing. However, it fails to show that the current density on the active anode is probably increasing up to the establishment of a complete film. If current density is considered, the curve would look more like Fig. 1 of the original paper. This would avoid the multiple intersections between the polarization curves for the oxidizing agent and for the Fe anode. It seems probable that only one of these intersections represents an electrochemical state. The other is due merely to the method of plotting the data. The current density of the Fe anode, of course, cannot be plotted since we do not know the true anode area. This does not alter the above reasoning, however, At least if this concept is kept in mind, the curves in the original paper are no longer ambiguous.

The Discussion indicates that, for passivity to start, the cathodic curve for the oxidizing agent must intersect the anodic curve for Fe at a potential more positive than the oxidation-reduction potential of Fe_2O_3. For complete passivity, the intersection must be more positive that the abrupt break in potential (E in Stern's Fig. 2). This agrees with Dr. Stern's conclusions.

The combination of Dr. Stern's position with autoreduction" correlates well with certain known facts about inhibitors. For instance, at room temperature, sodium hydroxide requires dissolved oxygen in order to reduce corrosion. According to Pourbaix,[65] the difference between the equilibrium potential of reactions (I) and (II) decreases with increasing pH. Adding sodium hydroxide increases the stability of any ferric oxide that forms, but it does not produce any ferric oxide. For Fe_2O_3 to result, there must be some oxidizing agent, such as dissolved oxygen, present. At higher temperatures, water alone can probably oxidize iron to Fe_2O_3.

Sodium nitrite acts as an oxidizing agent to produce the higher Fe oxide. Also, the reduction of sodium nitrite provides a cathodic reaction so that a high anodic current is possible on the Fe anodes. This polarizes the Fe anodes to a more positive potential than the equilibrium potential of Fe_2O_3. At this more noble potential, a protective film of ferric oxide can develop.

Chromate ions probably have an additional action. They produce an oxide film and also permit a high anodic current to flow and polarize the Fe anode. Additionally, the reduction product of chromate has an oxidation-reduction potential more negative than that of bare Fe.[65] Therefore, chromate can form a stable film even though the Fe anode is not greatly polarized. This stable film reduces the anode area and aids in producing a condition where ferric oxide becomes stable.

D. M. Brasher[66]: We have read with much pleasure Dr. Stern's illuminating exposition of the electrochemical principles underlying the passivity of metal surfaces brought about by oxidizing inhibitors.

In his reference to the amount of inhibitor associated with the passivated surface, the author states that the amounts reported have "varied considerably from system to system." With regard to surfaces passivated in chromate, it is probable that this variation in the amount of Cr^{51} found (by radiometric means) is due to the fact that some workers have determined Cr^{51} on the surface without reference to the variation of this quantity both with time of immersion of the specimen, and also with "age" of the

[61] M. J. Pryor and U. R. Evans, *J. Chem. Soc.*, **1950**, 1259.
[62] H. G. Oswin and M. Cohen, *This Journal*, **104**, 9 (1957).
[63] K. H. Buob, A. F. Beck, and M. Cohen, *This Journal*, **105**, 74 (1958).
[64] E. E. Nelson, Paper submitted to *Corrosion* for publication.
[65] M. Pourbaix, *Corrosion*, **5**, 121 (1949).
[66] Dept. of Scientific and Industrial Research, National Chemical Lab., Teddington, Middlesex, England.

surface oxide film before immersion. In this laboratory, in work on steel, we have shown that adsorption of the inhibitor (presumably as $CrO_4^=$ ions) is followed by "logarithmic" growth of a film containing Cr_2O_3.[67] The work has also demonstrated the logarithmic growth of an oxide film on steel, both in air[68] and also in other inhibitive solutions such as sodium nitrite, aerated fenzoate, phosphate, etc.,[69] at rates comparable to that occurring in chromate solution.

The logarithmic nature and similarity in rates of film growth in all these environments has led us[70] to suggest a common mechanism, based on theories of Mott, and Hauffe and Ilschner,[71] whereby electron transfer through the film is the rate-controlling step in the growth of the film. It would be of much interest to know whether this logarithmic growth can be alternatively accounted for on the electrochemical principles set forth in Dr. Stern's paper.

Milton Stern: Before commenting on the above discussion, it should be mentioned that the description of passivity in the subject paper was devised in order to obtain a *useful* description of passivity. The mechanism proposed is kinetic in character and relies on simple, measurable parameters which determine the corrosion rate and electrode potential of the system. Descriptions of passivity which embrace films of one type or another are still embryonic in character and do not promise utility for some time.

I heartily agree with Professor Uhlig's suggestion that a clearer definition of passivity is in order. Dr. Wagner's definition appears quite reasonable and is consistent with the mechanism of passivity in the subject paper. I further agree that it is unfortunate that point E in Fig. 2 is described as the Flade potential—not necessarily for the reasons given by Professor Uhlig, since the figure is schematic, but rather because of the special nature of Flade's experiments. I would prefer to let the term "Flade potential" decay to nonexistence and believe point E would best be called the critical potential for passivity. This point, then, divides the potential scale into active and passive regions.

Since "oxidizing" is a relative term, it should be clear that a passivating-type inhibitor must exhibit a redox potential more noble than the critical potential for passivity of the metal. This is why a metal like Fe, which exhibits particularly noble critical potentials for passivity, requires rather strong oxidizing agents, whereas a metal like Ti, which exhibits relatively active critical potentials for passivity, is passivated by only mildly oxidizing solutions. As described in the text, many factors other than the oxidizing nature of the inhibitor are also pertinent to determining whether passivity is achieved.

The subject description of the mechanism of passivating inhibitors requires that a critical concentration of passivator exist which is accomplished by a sudden shift of potential from active to passive values. The data of Geary are not consistent with this since they show a gradual change of potential with inhibitor concentration. However, since the data do not appear to traverse the critical potential for passivity, they cannot be considered a test of the theory since the electrochemical picture also shows a gradual change of potential with inhibitor concentration in either the active or the passive potential region.

Miss Brasher's interesting work with Cr^{51} deserves considerable attention and careful study. The electrochemical description of passivating inhibitors is consistent with her observation that Cr associated with the surface is in the reduced form. It is also consistent with the observation that the amount of Cr found on the surface is not dependent on the concentration of the chromate solution provided the mixed potential is between points E and F of Fig. 2. The mechanism further predicts that in the presence of oxygen the amount of Cr associated with the surface should be less than that found in the absence of oxygen.

There is some evidence that current in the potential region between E and F (Fig. 2) is time dependent and actually decreases in magnitude in a manner which is logarithmic with time.[72] This has been observed for stainless steel. If it is also true for Fe, then Miss Brasher's observations and this electrochemical description (modified to consider time effects) may be considered completely compatible.

Mr. Nelson's suggestion that current density be substituted for current is not clear, since it is necessary to plot polarization diagrams on a current basis in order to have the intersection of anodic and cathodic curves represent the mixed potential. I believe it is not only correct to show multiple intersections between polarization curves, since this is a characteristic of passive systems, but also that this is highly desirable and represents one of the characteristic features of this description. Note, for example, that the diagram in Fig. 10 shows an abrupt change in potential would occur when the limiting diffusion current for reduction of inhibitor exceeds the critical current for passivity. Fig. 9 illustrates this behavior experimentally.

The introduction of area effects into the electrochemical description of passive systems could probably be accomplished in the manner described for systems controlled solely by activation polarization.[73] However, this additional complexity was not introduced (along with possible time effects) because it was believed it would mask the more elementary and equally important features of the description and because these effects could not (at the time) be handled in a quantitative manner.

[67] D. M. Brasher, A. H. Kingsbury, and A. D. Mercer, also D. M. Brasher and C. P. De, *Nature*, **108**, 27 (1957); D. M. Brasher and A. H. Kingsbury, *Trans., Faraday Soc.*, 54, 1214 (1958).

[68] D. M. Brasher, A. H. Kingsbury, and A. D. Mercer, *Nature*, **108**, 27 (1957).

[69] "Chemistry Research 1957," p. 12, Her Majesty's Stationery Office, London (1958).

[70] O. Kubaschewski and D. M. Brasher, In press.

[71] N. F. Mott, *J. Inst. Metals*, 65, 333 (1939); *Trans. Faraday Soc.*, 35, 1179 (1939). K. Hauffe and B. Ilschner, *Z. Elektrochem.*, 58, 382 (1954).

[72] M. Stern, *This Journal*, **106**, 376 (1959).

[73] M. Stern, *Corrosion*, 14, 329t (1958).

News from the Bureau of Standards

Mechanism of Stress-Corrosion Cracking

The mechanism of stress-corrosion cracking in AZ31B magnesium alloy was investigated in an aqueous solution of 3.5% sodium chloride plus 2.0% potassium chromate. Specimens immersed in the corrodent and extending at an average rate of 500 ± 100 μin./in./min 1 min after the stress was applied generally failed within 5 min. For slower rates, the specimens did not fail in 1000 min. Stress-corrosion cracking could be stopped by the application of a cathodic current of 0.5 ma/cm² of exposed area. The experiments indicated that stress-corrosion cracking of AZ31B magnesium alloy is primarily an electrochemical process and is dependent on strain rate.

References

1. H. L. Logan, "Mechanism of Stress-Corrosion Cracking in the AZ31B Magnesium Alloy," *J. Research Nat. Bur. Standards*, **60**, 503 (1958), RP2919.
2. H. L. Logan and H. Hessing, "Stress Corrosion of Wrought Magnesium Alloys," *ibid.*, **44**, 233 (1950), RP2074.
3. H. L. Logan, "Film-Rupture Mechanism of Stress Corrosion," *ibid.*, **48**, 99 (1952), RP2291.

New Nickel Oxide Standard for Spectrographic and Chemical Analysis

A new standard sample of nickel oxide powder is available from the National Bureau of Standards. Analyzed and certified for nine minor and trace elements, the standard is intended for checking and calibrating spectrochemical and chemical methods employed in the analysis of high-purity nickel, particularly electronic-grade and electrolytic nickel.

Nickel is available in many forms and, because of its hardness and resistance to corrosion and heat, has many electronic and electrical applications. For instance, nickel is used in support wires and rods, wire mesh for grids, wire for spark plugs, and plates (anodes). The thermionic properties of nickel are also of special interest to the electronics industry. Since these and other properties depend on chemical composition, the new standard should be of value in developing high-purity nickel materials.

The new standard NBS 673 supplements the nickel oxide standard samples NBS 671 and 672, issued in 1957. All three samples have been prepared by a cooperative program between the Bureau and a task group of Committee F-1 of the American Society for Testing Materials. Similar to the other two, the new standard is designed primarily for application in the spectrographic analysis of nickel and nickel alloys by Tentative Method E 129-57T, "Methods for Emission Spectrochemical Analysis," American Society for Testing Materials, 1916 Race St., Philadelphia, Pa., 1957. The three standards are also equally suited for chemical analysis.

The nickel oxide standard is packaged in bottles containing 25 grams and is available from the Standard Sample Clerk, National Bureau of Standards, Washington 25, D. C. The fee is $8.00 per sample. A provisional certificate of analyses accompanying the standard sample lists the analytical results of the cooperating laboratories.

Determination of Dielectric Constants of Pure Liquids

As part of a National Bureau of Standards program to obtain more precise information on the dielectric properties of scientifically and industrially important pure liquids, the dielectric constant of deuterium oxide [heavy water (1)] has been determined with a high degree of accuracy. Although the a-c bridge method used in this determination is not basically new, it incorporates several techniques and procedures, developed by C. G. Malmberg and A. A. Maryott, which extend the range and accuracy of the method, particularly when dealing with semiconducting liquids.

Evaluation of the results obtained with deuterium oxide and other liquids indicates that with suitable cells this method is generally useful for accurate measurements of the dielectric constant of liquids whose conductivity may range as high as 5 micromho/cm. For liquids of low conductivity (10^{-3} micromho/cm or less), an accuracy in dielectric constant approaching 0.01% may be possible. The method is simultaneously useful for adequate determinations of conductivity down to 10^{-5} micromho/cm.

Determinations of the dielectric constant of deuterium oxide were conducted at 5-degree intervals between 4° and 100°C. These and corresponding values for ordinary water (2) were made at conductivities up to nearly 2 micromho/cm. Samples of heavy water containing 99.4 mole % deuterium oxide were used to obtain precise data from which static values of the dielectric constant (ϵ) of deuterium oxide were derived. The data were reproducible to better than ±0.01 unit and the values are believed to be accurate to ±0.05 unit or better. The temperature coefficient [fractional change of dielectric constant with temperature, $(1/\epsilon)$ $(d\epsilon/dt]$ varies by less than 1.5% between 4° and 100°C while the uncertainty in the measured values of this coefficient is believed to be less than 1 part in 100.

A general survey of the literature on pure liquids (3) has shown that the dielectric constants of only a few liquids are known to better than ±0.2%. In the usual case, the uncertainty is of the order of 1 or 2%. The temperature dependence is, in general, correspondingly less well known, if at all. Considering the sources of error involved, the discrepancies observed in the literature are probably the result of some combination of imperfections in the procedures employed and of impurity of the sample.

References

1. For further information, *see* C. G. Malmberg, "Dielectric Constant of Deuterium Oxide," *J. Research, Nat. Bur. Standards*, **60**, 609 (1958), RP2874.
2. C. G. Malmberg and A. A. Maryott, "Dielectric Constant of Water from 0° to 100°C," *ibid.*, **56**, 1 (1956), RP2641.
3. A. A. Maryott and E. R. Smith,

"Table of Dielectric Constants of Pure Liquids," NBS Circular 514 (1951).

Separation and Determination of Certain Metallic Elements in High-Temperature Alloys

To check the composition of high-temperature alloys which incorporate a large variety of metals, suitable methods of analysis must be developed. Until recently, it had not been possible to analyze completely alloys containing combinations of titanium, zirconium, tungsten, molybdenum, niobium, and tantalum—because all these metals belong to the same group of the periodic table and thus behave similarly. However, the National Bureau of Standards has developed a procedure based on the formation of soluble metal complexes which can be separated on an anion-exchange column and retained for analysis.

References

1. J. L. Hague, E. D. Brown, and H. A. Bright, "Separation of Tungsten, Molybdenum, and Niobium by Anion Exchange," *J. Research Nat. Bur. Standards*, **53**, 261 (1954), RP2542.
2. J. L. Hague and L. A. Machlan, "Determination of Titanium, Zirconium, Niobium, and Tantalum in Steels by Anion Exchange Separation," *ibid.*, **62**, 11 (1959), RP2923.
3. J. L. Hague and L. A. Machlan, "Determination of Niobium and Tantalum in Titanium-Base Alloys," *ibid.*, **62**, 53 (1959), RP2929.
4. The National Bureau of Standards distributes over 600 different standard materials of chemicals, ores, ceramics, metals, and other substances. Information is contained in "Standard Materials," NBS Circular 552 (third edition), which can be obtained by writing to the Superintendent of Documents, U. S. Government Printing Office, Washington 25, D. C. (25 cents).

Low-Temperature Distillation of Hydrogen Isotopes

Experimental work at the National Bureau of Standards' Cryogenic Engineering Lab., Boulder, Colo., has advanced a practical solution to the problem of separating hydrogen isotopes. A pilot plant capable of distilling liquid hydrogen by fractionation has yielded specific amounts of pure liquid deuterium and deuterium-free hydrogen.

The unit, the only one of its kind in the country, was designed by Cryogenic Engineering Lab. (CEL) staff members T. M. Flynn, K. D. Timmerhaus, and D. H. Weitzel. The designers feel that it is feasible for industry to produce large quantities of deuterium by this cryogenic distillation method; it is, in fact, particularly well-suited for industrial areas where extensive supplies of hydrogen gas are available—near ammonia plants.

Of the three isotopes of hydrogen—protium, deuterium, and tritium—protium, the lightest, is the most abundant; over 99% of available hydrogen is in the form of protium. Tritium, extremely rare in nature, is radioactive and has a half-life of about 12½ yr. Deuterium, twice as heavy as "ordinary" hydrogen, occurs naturally in an abundance ratio of 1:7000.

The demand for deuterium is growing. Recent declassification of thermonuclear fusion research programs has shown deuterium to be one of the most promising "fuels of the future." Furthermore, "heavy water," or deuterium oxide, has been one of the most desirable nuclear reactor moderators ever since the early days of the Manhattan Project. At that time, unavailability and economies restricted its use. At present, synthesis of heavy water is carried out on a commercial scale.

Deuterium-free hydrogen, although currently confined to research-quantity needs, is required in amounts sizeable enough to necessitate pilot plant manufacture. For instance, bubble chambers, including those containing liquid hydrogen, are supplementing the Wilson Cloud Chamber and similar detection equipment used in elementary particle investigations. For this research, some scientists demand deuterium-free liquid hydrogen; others use liquid hydrogen containing all isotopic modifications.

References

1. K. D. Timmerhaus, D. H. Weitzel, and T. M. Flynn, "Low-Temperature Distillation of Hydrogen Isotopes," *Chem. Eng. Progr.*, **54**, 35 (1958).
2. A thorough discussion of low-temperature insulation problems is given in *"Cryogenic Engineering,"* by R. B. Scott, D. Van Nostrand Co., New York (1959).

Section News

India Section

Aluminum Industry in India.—The Tariff Commission has estimated that the country's current requirements are 35,000 tons per year, and this is expected to go up to 40,000 tons at the end of the Second Five Year Plan. The present installed capacity is 7700 tons per year, the producing units being the Aluminium Corp. of India and the Indian Aluminium Co. They are equipped not only for making virgin metal but also for fabricating the metal into various types of semi's. The government has approved the Aluminium Corp.'s scheme to treble their output capacity, and to fabricate the metal into finished products. The Indian Aluminium Co. also has in hand an ambitious project, the first phase of which is the setting up of a 10,000-ton smelter at Hirakud. From the country's point of view, the aluminum industry is vital, next in importance only to steel.

Symposium on Electrolytic Cells.—The Central Electrochemical Research Institute held a Symposium on Electrolytic Cells at Karaikudi from December 30, 1958 to January

December 1959 Discussion Section

A Discussion Section, covering papers published in the January-June 1959 JOURNALS, is scheduled for publication in the December 1959 issue. Any discussion which did not reach the Editor in time for inclusion in the June 1959 Discussion Section will be included in the December 1959 issue.

Those who plan to contribute remarks for this Discussion Section should submit their comments or questions in triplicate to the Managing Editor of the JOURNAL, 1860 Broadway, New York 23, N. Y. *not later than September 1, 1959.* All discussions will be forwarded to the author(s) for reply before being printed in the JOURNAL.

1, 1959. The 39 papers presented covered the following topics: General, Inorganic Electrochemical Products, Electro-Organic Preparations, Electro-Metallurgical Processes and Electrodeposition, Miscellaneous. The Institute has planned to publish the proceedings in a Special Number.

Coordination Compounds Symposium.—A Symposium on the Chemistry of Coordination Compounds was held at Agra in February 1959, under the auspices of the National Academy of Sciences, India. A large number of papers were presented by scientists in India and foreign countries under the following sections: General Survey; Valence Bond Considerations, Stereochemistry and Structure; Techniques and Methods of Investigation; Reactions, Stability, and Thermodynamic Considerations; Stabilization of Valence States; Miscellaneous. Topics of particular interest to electrochemists are: Physicochemical Studies, including Electrometric; Application to Electrodeposition.

Golden Jubilee of the Indian Institute of Science.— The Indian Institute of Science, Bangalore, the oldest research and teaching institution of its kind in India, celebrated its semicentennial in February 1959. Distinguished scientists and engineers from different parts of the world attended the function. There were several lectures and symposia, and an exhibition during the Jubilee week. The following are some of the topics chosen for the symposia spread out during 1959: Power System Planning, Polarography, Crystal Physics, Beneficiation of Minerals, Structural Changes in Metals and Alloys, and Industrial Automatic Controls.

Electroplating Journal for India.— Grauer and Weil (India) Ltd., Bombay, has finalized plans for the starting of a monthly periodical *Electroplating.* This journal will be the first of its kind in India.

T. L. Rama Char,
India Correspondent

Personals

Herbert Miller has accepted a position as development engineer (chemist) with the Silicon Engineering Group, Chatham Electronics Div., Tung-Sol Electric Inc., Livingston, N. J.

Sidney M. Selis has left the Catalyst Research Corp., Baltimore, Md., to join the Research Labs., General Motors Technical Center, Warren, Mich., as senior research physical chemist.

James Emlen, formerly with the Quaker Chemical Co., Conshohocken, Pa., is now associated with the Fluid Energy Processing & Equipment Co., Philadelphia.

Meier Sadowsky has resigned as manager of chemical engineering for the Lansdale Tube Plant of Philco to assume the position of executive vice-president of the Industrial and Government Div. of Continental Electronics Corp. of California, Los Angeles.

Bernard Porter has resigned from the Reduction Research Section of Kaiser Aluminum & Chemical Corp. to accept a position as supervisory chemist (physical) in the Federal Bureau of Mines, Rare and Precious Metals Experiment Station, Reno, Nev.

Edgar C. Pitzer, of the General Electric Co., has transferred from Louisville, Ky., to Schenectady, N. Y., returning to more fundamental work in electrochemistry, principally batteries. He also is doing some work in corrosion.

James E. Wells, III, is on leave of absence from the Metals Research Labs., Union Carbide Metals Co., Niagara Falls, N.Y., to continue his education. He is employed by the University of Michigan Research Institute in Ann Arbor.

Bruce Walker, formerly product engineering manager of Canadian Carborundum Co., Ltd., Niagara Falls, Ont., has been promoted to manager of the newly established Technical Branch of the company's Electro Minerals Div. in Niagara Falls, N. Y.

M. S. Thacker has been appointed a member of the Board of Directors of the Hindustan Aircraft (P) Ltd., Bangalore. He also has been nominated a member of the Central Advisory Board of Education.

T. L. Rama Char has been appointed a member of the Editorial Committee of *Electroplating,* a new monthly journal.

J. Vaid and **S. Satyanarayana** have been appointed as Lecturers in Electrochemical Technology, Indian Institute of Technology, Bombay. J. Vaid has been awarded the Ph.D. degree of the Panjab University for his thesis "Electrodeposition of Metals and Alloys from the Pyrophosphate Bath."

S. K. Panikkar has been designated as chief chemist at Grauer and Weil (India) Ltd., Bombay.

Notice to Members and Subscribers
(Re Changes of Address)

To insure receipt of each issue of the JOURNAL, please be sure to give us your old address, as well as your new one, when you move. Our records are filed by states and cities, not by individual names. The Post Office does not forward magazines.

News Items

Capacity of Floating Zone Refiners Increased by New Method

A striking improvement in the floating zone refining technique, substantially increasing the volume of material which can be purified, was described recently to the American Physical Society by W. G. Pfann, K. E. Benson, and D. W. Hagelbarger of Bell Telephone Laboratories. Paradoxically, the new technique also makes it possible to treat much thinner cross sections than have been feasible before.

The floating zone technique has proven highly valuable in producing extreme purity in reactive metals and semiconductors, because the molten material is never in contact with a container. However, it has been limited until now to use with small amounts of material.

In conventional floating zone refining, a rod of the material to be purified is held in a vertical position, while a zone is melted by a heat source. The molten zone is held in place within the rod by its own surface tension. This zone is then made to move along the rod, and the impurities which collect in the molten material move to one end.

The primary limitation on the conventional method is the fact that for any given material there is a maximum height of molten zone which can be supported by the surface tension.

The new method gets around this difficulty by using specially shaped cross sections, such as flat plates and tubes. These shapes provide a cross section small in thickness to permit melting through without ex-

ceeding the maximum height, and large in width to increase the total cross-sectional area treated. The inventors have shown that molten zones in such shapes are surprisingly stable.

For example, it is almost impossible to produce a stable molten zone in a 1-in. diameter iron rod, because the maximum height of the zone is generally exceeded during the heating required to melt through the rod. However, it is relatively easy to melt the entire cross section of a 2-in. diameter, ⅛-in. wall tube of the same material, without exceeding this maximum height. The areas in both forms are the same.

Stable, wide molten zones have been maintained experimentally in one or both cross-sectional shapes, in materials such as silicon, iron, tin, gold, lead, bismuth, and water.

The new method works well at very small plate thicknesses in contrast to the rod floating zone method, in which the maximum stable zone height decreases to zero as the rod diameter decreases. Such a decrease in maximum zone height can be avoided in the new method. Hence, treatment of sheets in the order of mils or less in thickness becomes feasible.

Both the original zone refining technique and the floating zone extension of the method were discovered at Bell Labs., by W. G. Pfann and H. C. Theuerer, respectively.

Graphite Cloth

National Carbon Co., a Div. of Union Carbide Corp., has announced the production of graphite in flexible fiber and fabric form. Any fabric, yarn, braid, felt, etc., of suitable low ash content, may serve as starting material; it is carbonized, and the carbon converted to crystalline graphite by electrical heating. In addition to being flexible and impervious to thermal shock, the

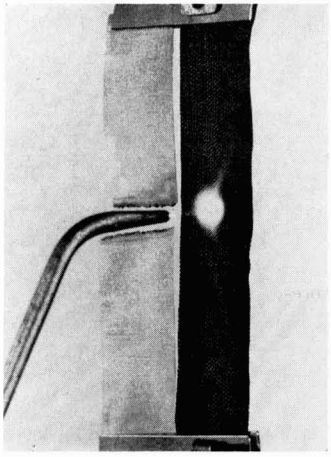

The nonoxidizing part of an oxyacetylene flame is passed over a strip of stainless steel mesh (left) and onto a strip of graphite cloth, which becomes incandescent but does not melt or vaporize at this temperature. The heat is rapidly conducted away.

material then shows the other usual properties of graphite: thermal and electrical conductivity, chemical inertness, lack of oxidation in air below 400°C, does not melt (sublimes at very high temperatures). The ash content can be made very low for special purposes, normally is about 0.08%. Tensile strength depends on type of material, is about 10-15 lb/in. width for a 28 x 28 square weave cloth weighing 0.04 lb/ft^2. Such cloth can be flexed on the bias for a long time.

Various materials are being made in experimental quantities. Cloth such as that mentioned is available in 40-in. width up to 7 ft long. Suggested uses are: to reinforce plastics and high-temperature refractories; to impart thermal and electrical conductance to plastics, ceramics, and other textiles; for hot gas filters, for flame retarding; for high-temperature heating elements in nonoxidizing atmospheres, for low-temperature panel heating; infrared emitters; self-lubricating high-temperature packing and gasket materials.

Inquiries should be sent on company letterhead to Mr. C. E. Ford, Industrial New Products Marketing Manager, National Carbon Co., 30 E. 42 St., New York 17, N. Y.

Corrosion Test Sites Needed

The High Alloys Committee of the Welding Research Council is currently conducting extensive field corrosion tests to determine what industrial process media cause intergranular attack of austenitic stainless steels. To accomplish this, several hundred corrosion test racks containing welded and unwelded specimens with a variety of heat treatments have been prepared. Two series of test racks, measuring 4 by 4 by 12 in., are being used. One contains molybdenum-bearing alloys (Types 316, 317, etc.), the other, molybdenum-free alloys (Types 304, 310, etc.).

The results of this program should permit a more accurate description of the types of media which cause intergranular corrosion. Also, they will be used to check the boiling 65% nitric acid test as a method for predicting intergranular corrosion susceptibility.

A search for industrial exposure sites is in progress. Specifically, media which have produced intergranular failure of stainless steel components are most desirable. Those interested in participating in this program are invited to submit a description of the exposure site to the address below. Specific process details are unnecessary, but a description of solution composition and the local exposure conditions will be required. Upon completion of the exposure, each cooperating group will receive a detailed evaluation of the corrosion test results.

Manuscripts and Abstracts for Spring 1960 Meeting

Papers are now being solicited for the Spring Meeting of the Society, to be held at the Lasalle Hotel in Chicago, Ill., May 1, 2, 3, 4, and 5, 1960. Technical sessions probably will be scheduled on Electric Insulation, Electronics (including Luminescence and Semiconductors), Electrothermics and Metallurgy, Industrial Electrolytics, and Theoretical Electrochemistry.

To be considered for this meeting, triplicate copies of abstracts (*not exceeding 75 words in length*) must be received at Society Headquarters, 1860 Broadway, New York 23, N. Y., *not later than January 1, 1960. Please indicate on abstract for which Division's symposium the paper is to be scheduled, and underline the name of the author who will present the paper.* Complete manuscripts should be sent in triplicate to the Managing Editor of the JOURNAL at the same address.

* * *

The Fall 1960 Meeting will be held in Houston, Texas, October 9, 10, 11, 12, and 13, 1960, at the Shamrock Hotel. Sessions will be announced in a later issue.

Interested parties should write to: R. M. Fuller, International Nickel Co., Inc., 67 Wall St., New York 5, N. Y.

C.I.T.C.E. Meeting

The 11th meeting of the International Committee of Electrochemical Thermodynamics and Kinetics (C.I.T.C.E.) will be held in Vienna, Austria, September 29-October 2, 1959. Sessions of the following commissions are scheduled: 1—Tension-pH Diagrams; 2—Electrochemical Definitions and Nomenclature; 3—Experimental Methods in Electrochemistry; 4—Batteries; 5—Corrosion; 6—Kinetics; 7—Semiconductors. The general theme of the meeting will be Electrocrystallization.

Communications regarding attendance at the meeting can be addressed to N. Ibl, Lab. of Physical Chemistry, Swiss Federal Institute of Technology, Universitätstr. 6, Zurich, Switzerland.

First Unit of Nation's Largest Silicon Power Rectifier System Starts Operation

The nation's first three units of what will be the largest silicon power rectifier installation have been energized by the Hooker Chemical Corp. at its Niagara Falls, N. Y., plant.

Engineered and built by the General Electric Co., the equipment is being used to convert 60-cycle current to direct current for the operation of Hooker electrolytic cells to produce chlorine, caustic soda, and hydrogen. The fourth and last unit was to be installed by May of this year.

Each of the four 96-tray silicon rectifier units provides 12,000 amp, at 360 v d.c.

With closed-cycle cooling, the unit is rated for a continuous electrolytic load and operates from an input voltage of 13.8 kv, 60 cycles.

When the installation is completed, the four silicon rectifiers will have replaced twelve rotary converters, and will deliver 17,280 kw of d-c power.

AMF Battery Laboratory Sold to Electric Storage Battery Co

The Electric Storage Battery Co., of Philadelphia, has purchased from American Machine & Foundry Co., New York, the assets and business of its Battery Laboratory at Raleigh, N. C. The cash transaction was revealed in a joint announcement by C. F. Norberg, president of ESB, and Morehead Patterson, chairman of the board of AMF. The purchase price was not disclosed.

Mr. Patterson said AMF had sold the battery business because it does not fit into those areas of government work in which the company is currently interested.

The Battery Lab. is engaged in the development, manufacture, and sale of silver-zinc batteries for missiles and other special applications, an area in which the Electric Storage Battery Co. has been active for some years. ESB plans call for continuing operations at the Raleigh location.

Operation of the new acquisition will be under the direction of M. G. Smith, vice-president of ESB and general manager of its Industrial Division.

Two New Volumes Available in ECS Series

The Electrochemical Society is pleased to announce the availability of the following two new volumes in The Electrochemical Society Series:

Semiconductor Abstracts, 1956 Issue, Volume IV, Abstracts of Literature on Semiconducting and Luminescent Materials and Their Applications, edited by E. Paskell. Price: $12.00. (A review of the 1956 Issue appears on page 131C of the May JOURNAL.)

Also available is **The Structure of Electrolytic Solutions,** edited by Walter J. Hamer; based on a symposium held in Washington, D. C., in May 1957, sponsored by The Electrochemical Society, New York, and The National Science Foundation, Washington, D. C. Price: $18.50. The subjects covered include a wide range of topics relating to the properties of electrolytic solutions, and represent the significant items under investigation in the present age.

Both volumes are available from the publisher, John Wiley & Sons, Inc., 440 Fourth Ave., New York 16, N. Y. *A 33 1/3% discount is offered to Electrochemical Society members only and can be obtained by ordering through Society Headquarters, 1860 Broadway, New York 23, N. Y.*

Book Reviews

International Committee of Electrochemical Thermodynamics and Kinetics (C.I.T.C.E.). Proceedings of the Eighth Meeting (Madrid, 1956). Published by Butterworth & Co. (Canada) Ltd., Toronto, 1958. ix + 497 pages; $19.00.

The Comité International de Thermodynamique et de Cinétique Electrochimique is a small but vigorous group which meets each year to receive the reports of its committees and study groups, to hear a number of invited papers, and to discuss topics of current interest in electrochemistry. This volume, like its predecessors, reports full details of the meeting, so that it almost incidentally includes the 37 theoretical and research papers, which range in length from mere abstracts to comprehensive studies. The publishers have done an excellent job of printing and binding the book, and typographical errors are negligible. There is so much of interest in the volume to research workers in the field that it should be freely available to them for examination and reference. It is unfortunate, first, that publication has taken a full two years and, second, that the price must be so high.

This volume contains a 15-page report, printed in full in both English and French, of the C.I.T.C.E. Commission on Electrochemical Nomenclature and Definitions, which is also the 1956 report of the I.U.P.A.C. Subcommission of the same name. This report was the basis for the article "Fundamentals of the Theory of Electrodes and Galvanic Cells" by E. Lange and P. Van Rysselberghe [*This Journal,* **105,** 420 (1958)]. A 7-page report by the commission on experimental methods in electrochemistry is also printed in the two languages. There are briefer reports by the commissions on potential-pH diagrams, and on batteries and accumulators. Of the research papers and abstracts, 17 are in English, 15 in French, 5 in German. The original oral discussion is included. Nearly all the papers are presented in the following groups.

1. Experimental Methods (139 pages): papers on polarization of iron (Okamoto and others); electrodes in fused salts (G. J. Hills); mercury jet electrode (Rius, Llopis); electrodeposition study with tracers (Llopis); water electrolysis at high pressure (Ibarz, Diez); alternating-current methods (T. P. Hoar); impedance at electrodes, hydrogen evolution

(Bockris, Conway, and others); mass transfer with natural convection (Ibl); silver-silver chloride electrode in molten salts (Bonnemay, Pineaux).

2. Potential-pH Diagrams (76 pages): detailed information and diagrams for the systems Mg (with water, CO_2, H_3PO_4) and Mo, W, U with water (Pourbaix and co-workers); and two other papers. It is to be hoped (and it is expected) that the numerous studies of potential-pH relations with metals, now scattered in the literature, will soon be collected in one volume, with the best available data and the most careful interpretation.

3. Corrosion and Protection against Corrosion (104 pages): some of the papers are on corrosion and cracking of stainless steels, electropolishing of steel, passivation of iron by chromates, molybdates, tungstates, vanadates. There is a detailed study (J. van Muylder, M. Pourbaix) of the behavior of Mg and Zn as sacrificial anodes.

4. Batteries and Accumulators (27 pages): papers by Winkler (Zwickau) and Brenet (Strasbourg).

5. Electrochemical Kinetics (60 pages): among others, papers on impedance at a Pt anode, electroreduction of persulfate, mechanism of oxygen evolution in alkaline solution, Fe/Fe^{++} electrode kinetics, electrolysis with traces of metals.

C. V. King

Effect of Surface on the Behaviour of Metals. Lectures delivered at the Institution of Metallurgists Refresher Course, 1957. Edited by G. L. J. Bailey. Published by Philosophical Library, New York City, 1958. 100 pages, 10 plates; $10.00.

These four lectures were intended to bring some recent scientific and technical developments dealing with surfaces to the attention of metallurgists not specializing in this area and to the attention of many members of the engineering and scientific community with whom metallurgists have interests in common. The brief and introductory nature of the presentations has the advantage of attracting many who would be discouraged by the more formidable treatment usually directed toward the specialist. On the other hand, this makes the lecturer's task more difficult in that he has little space in which to provide the theoretical and technological background needed to establish the significance of recent

developments. On this score, F. T. Barwell's contribution on friction and wear suffers least; his summary of a number of studies indicates that we are close to an understanding of friction and wear, at least in principle, in terms of welding, plastic deformation, films, adsorption, surface heating, chemical reactions, and electro-erosion. G. L. J. Bailey has partly solved the space difficulty by restricting his discussion on preparation and examination of surfaces to a few topics: surface energy and thermal etching, field-emission microscopy, deformation produced by abrasion and polishing, and electron-probe microanalysis. Likewise, T. P. Hoar presents a well-organized discussion of the influence of surface treatments on chemical behavior, limiting himself mainly to anodic and chemical film formation and to mechanical working. In contrast, R. W. B. Stephens runs through the effect of surface on optical, electrical, thermal, and magnetic properties without providing the background most of his readers will require in this area. Both Bailey's and Hoar's contributions, especially the latter, would have benefited from additional references; there are several serious omissions.

The value of a book such as this is that it presents in concise form information in a certain field drawn from scattered sources, and provides an easy first step for the transfer of information across the barrier between the researcher and the practicing engineer and across the boundary of the field of specialization. It can be recommended for rapid reading to those who are not specialists in surface phenomena. In view of its transient value and its stiff price, an individual purchase of the book is not warranted.

Marvin Metzger

Progress in Semiconductors, III. Edited by A. F. Gibson, R. E. Burgess, and P. Aigrain. Published by John Wiley & Sons, Inc., New York City, 1958. 210 pages; $8.50.

The successive volumes in this series continue to improve in quality and timeliness. As with the earlier volumes, the spectrum of interest to which the editors cater is quite wide; the emphasis continues to be directed toward germanium and silicon, but there is something for the physicist, something for the chemist, and something for the device engineer.

M. Glicksman has contributed an article on "The Magnetoresistivity of Germanium and Silicon" in which is

included a discussion of cyclotron resonance; the article is good, if a little overcompressed, and one may perhaps hope for a second installment later to cover the more recent work on magneto-optic effects. Turning to macroscopic physics, we find articles on lifetime of excess carriers, by A. Many and R. Bray, and on carrier mobility, by M. S. Sodha. J. M. Wilson gives a thorough account of "The Chemical Purification of Germanium and Silicon." The article by D. E. Mason and D. F. Taylor on "Silicon Junction Diodes" will be of particular interest to American readers in the indication it gives of the extent to which semiconductor technology in England has caught up with the American art. Finally, there are two articles outside the realm of germanium and silicon: "Electronic Conductivity of Silver Halide Crystals," by J. W. Mitchell, the acknowledged master of that subject, and "Electronic Processes in Cadmium Sulphide," by J. Lambe and C. C. Klick, who give a clear account of work in what may turn out, once the chemical difficulties have been mastered, to be a material as interesting scientifically and as important technologically as germanium and silicon themselves.

C. G. B. Garrett

Analysis of Electroplating and Related Solutions, 2nd Edition, by Kenneth E. Langford. Published by Robert Draper, Ltd., Teddington, Middlesex, England, 1958. 423 pages; $9.00 plus postage.

This book has been written specifically for the practitioner in the electroplating and electroforming industries. It is a complete series of detailed procedures for the analysis of all commonly used electroplating, anodizing, cleaning, pickling, and other metal-finishing baths. The presentation is clear and well organized. All procedures are given with no attempt to introduce analytical theory. The analytical methods described are quite up to date. The book will be found useful in the analytical laboratories of all metal-finishing organizations.

Henry S. Myers

Announcement from Publisher

"Physics Express." Published by International Physical Index, Inc., 1909 Park Ave., New York City, 1958. $57.50 per year.

"Physics Express" is a new digest of current Russian literature dealing with physics. Vol. 1, No. 1, June 1958, contains 9 complete translated articles, 29 translated digests, and 65 excerpts, the digesting and excerpting being done by technical personnel.

Members of The Electrochemical Society probably will be most interested in the sections on Dielectrics and Ferroelectricity, Luminescence, Electrical Discharge, Solid State and Semiconductors, and Cryogenics and Superconductivity. Typical digests are entitled "Mechanism of Electron Emission from Thin Dielectric Layers due to a Strong Electric Field," "Narrow Luminescent Bands of NaBr-CuBr Phosphor," "On Determining the Individual Components in the Magnetic Susceptibility of a Semi-Conductor," and "Non-radiative Recombination of Electrons at Impurity Centers in N-Type Germanium."

Considering the extensive translations, the price seems reasonable.

Employment Situation

Position Available

For Engineer desiring broad scope of responsibility, and not requiring maximum security. Small company located in attractive resort community now commencing production of special Epoxy glass laminate bases for printed circuitry industry. Speculative undertaking, but outlook unusually good. Ideal qualifications: Age 30-35; depth of background in printed circuitry and electrical grade laminates. Sandymac Corporation, Traverse City, Michigan.

Advertiser's Index

The Electrochemical Society

Patron Members

Aluminum Co. of Canada, Ltd.,
Montreal, Que., Canada
International Nickel Co., Inc.,
New York, N. Y.
Olin Mathieson Chemical Corp.,
Niagara Falls, N. Y.
Industrial Chemicals Div., Research
and Development Dept.
Union Carbide Corp.
Divisions:
Union Carbide Metals,
New York, N. Y.
National Carbon Co., New York, N. Y.
Westinghouse Electric Corp., Pittsburgh, Pa.

Sustaining Members

Air Reduction Co., Inc.,
New York, N. Y.
Ajax Electro Metallurgical Corp.,
Philadelphia, Pa.
Allen-Bradley Co., Milwaukee, Wis.
Allied Chemical & Dye Corp.
General Chemical Div., Morristown, N. J.
Solvay Process Div., Syracuse, N. Y.
(3 memberships)
Allied Research Products, Inc.,
Detroit, Mich.
Alloy Steel Products Co., Inc., Linden, N. J.
Aluminum Co. of America,
New Kensington, Pa.
American Machine & Foundry Co.,
Raleigh, N. C.
American Metal Co., Ltd.,
New York, N. Y.
American Potash & Chemical Corp.,
Los Angeles, Calif. (2 memberships)
American Zinc Co. of Illinois,
East St. Louis, Ill.
American Zinc, Lead & Smelting Co.,
St. Louis, Mo.
American Zinc Oxide Co., Columbus, Ohio
M. Ames Chemical Works, Inc.,
Glens Falls, N. Y.
Auto City Plating Company Foundation,
Detroit, Mich.
Basic Inc., Maple Grove, Ohio
Bell Telephone Laboratories, Inc.,
New York, N. Y. (2 memberships)
Bethlehem Steel Co., Bethlehem, Pa.
(2 memberships)
Boeing Airplane Co., Seattle, Wash.
Burgess Battery Co., Freeport, Ill.
(4 memberships)
C & D Batteries, Inc., Conshohocken, Pa.
Canadian Industries Ltd., Montreal, Que.,
Canada
Carborundum Co., Niagara Falls, N. Y.
Catalyst Research Corp., Baltimore, Md.
Chrysler Corp., Detroit, Mich.
Ciba Pharmaceutical Products, Inc., Summit,
N. J.
Columbian Carbon Co., New York, N. Y.
Columbia-Southern Chemical Corp.,
Pittsburgh, Pa.
Consolidated Mining & Smelting Co. of
Canada, Ltd., Trail, B. C., Canada
(2 memberships)
Continental Can Co., Inc., Chicago, Ill.
Cooper Metallurgical Associates, Cleveland,
Ohio
Corning Glass Works, Corning, N. Y.
Crane Co., Chicago, Ill.
Diamond Alkali Co., Painesville, Ohio
(2 memberships)
Dow Chemical Co., Midland, Mich.
Wilbur B. Driver Co., Newark, N. J.
(2 memberships)
E. I. du Pont de Nemours & Co., Inc.,
Wilmington, Del.
Eagle-Picher Co., Chemical Div., Joplin, Mo.
Eastman Kodak Co., Rochester, N. Y.
Electric Auto-Lite Co., Toledo, Ohio
Electric Storage Battery Co.,
Philadelphia, Pa.
Englehard Industries, Inc., Newark, N. J.
(2 memberships)
The Eppley Laboratory, Inc., Newport, R. I.
(2 memberships)
Erie Resistor Corp., Erie, Pa.
Fairchild Semiconductor Corp., Palo Alto,
Calif.
Federal Telecommunication Laboratories,
Nutley, N. J.
Food Machinery & Chemical Corp.
Becco Chemical Div., Buffalo, N. Y.
Westvaco Chlor-Alkali Div., South
Charleston, W. Va.
Ford Motor Co., Dearborn, Mich.
General Electric Co., Schenectady, N. Y.
Chemistry & Chemical Engineering
Component, General Engineering
Laboratory
Chemistry Research Dept.

(Sustaining Members cont'd)

General Electric Co. (cont'd)
General Physics Research Dept.
Metallurgy & Ceramics Research Dept.
General Motors Corp.
Brown-Lipe-Chapin Div., Syracuse, N. Y. (2 memberships)
Guide Lamp Div., Anderson, Ind.
Research Laboratories Div., Detroit, Mich.
General Transistor Corp., Jamaica, N. Y.
Gillette Safety Razor Co., Boston, Mass.
Gould-National Batteries, Inc., Depew, N. Y.
Grace Electronic Chemicals, Inc., Baltimore, Md.
Great Lakes Carbon Corp., New York, N. Y.
Hanson-Van Winkle-Munning Co., Matawan, N. J. (3 memberships)
Harshaw Chemical Co., Cleveland, Ohio (2 memberships)
Hercules Powder Co., Wilmington, Del.
Hill Cross Co., Inc., New York, N. Y.
Hoffman Electronics Corp., Evanston, Ill.
Hooker Chemical Corp., Niagara Falls, N. Y. (3 memberships)
Houdaille Industries, Inc., Detroit, Mich.
Hughes Aircraft Co., Culver City, Calif.
International Business Machines Corp., Poughkeepsie, N. Y.
International Minerals & Chemical Corp., Chicago, Ill.
Jones & Laughlin Steel Corp., Pittsburgh, Pa.
K. W. Battery Co., Skokie, Ill.
Kaiser Aluminum & Chemical Corp.
Chemical Research Dept., Permanente, Calif.
Div. of Metallurgical Research, Spokane, Wash.
Kennecott Copper Corp., New York, N. Y.
Keokuk Electro-Metals Co., Keokuk, Iowa
Libbey-Owens-Ford Glass Co., Toledo, Ohio
P. R. Mallory & Co., Indianapolis, Ind.
McGean Chemical Co., Cleveland, Ohio
Merck & Co., Inc., Rahway, N. J.
Metal & Thermit Corp., Detroit, Mich.
Metals and Controls Corp., Attleboro, Mass.
Minnesota Mining & Manufacturing Co., St. Paul, Minn.
Monsanto Chemical Co., St. Louis, Mo.
Motorola, Inc., Chicago, Ill.
National Cash Register Co., Dayton, Ohio
National Lead Co., New York, N. Y.
National Research Corp., Cambridge, Mass.
National Steel Corp., Weirton, W. Va.
New York Air Brake Co., Vacuum Equipment Div., Camden, N. J.
Northern Electric Co., Montreal, Que., Canada
Norton Co., Worcester, Mass.
Olin Mathieson Chemical Corp., Niagara Falls, N. Y.
High Energy Fuels Organization (2 memberships)
Pennsalt Chemicals Corp., Philadelphia, Pa.
Phelps Dodge Refining Corp., Maspeth, N. Y.
Philco Corp., Philadelphia, Pa.
Philips Laboratories, Inc., Irvington-on-Hudson, N. Y.
Pittsburgh Metallurgical Co., Inc., Niagara Falls, N. Y.
Poor & Co., Promat Div., Waukegan, Ill.
Potash Co. of America, Carlsbad, N. Mex.
Radio Corp. of America, Harrison, N. J.
Ray-O-Vac Co., Madison, Wis.
Raytheon Manufacturing Co., Waltham, Mass.
Reynolds Metals Co., Richmond, Va. (2 memberships)
Schering Corporation, Bloomfield, N. J.
Shawinigan Chemicals Ltd., Montreal, Que., Canada
Speer Carbon Co.
International Graphite & Electrode Div., St. Marys, Pa. (2 memberships)
Sprague Electric Co., North Adams, Mass.
Stackpole Carbon Co., St. Marys, Pa.
Stauffer Chemical Co., New York, N. Y.
Sumner Chemical Co., Div. of Miles Laboratories, Inc., Elkhart, Ind.
Sylvania Electric Products Inc., Bayside, N. Y. (2 memberships)
Tennessee Products & Chemical Corp., Nashville, Tenn.
Texas Instruments, Inc., Dallas, Texas
Titanium Metals Corp. of America, Henderson, Nev.
Udylite Corp., Detroit, Mich. (4 memberships)
Universal-Cyclops Steel Corp., Bridgeville, Pa.
Upjohn Co., Kalamazoo, Mich.
Victor Chemical Works, Chicago, Ill.
Western Electric Co., Inc., Chicago, Ill.
Wyandotte Chemicals Corp., Wyandotte, Mich.
Yardney Electric Corp., New York, N. Y.

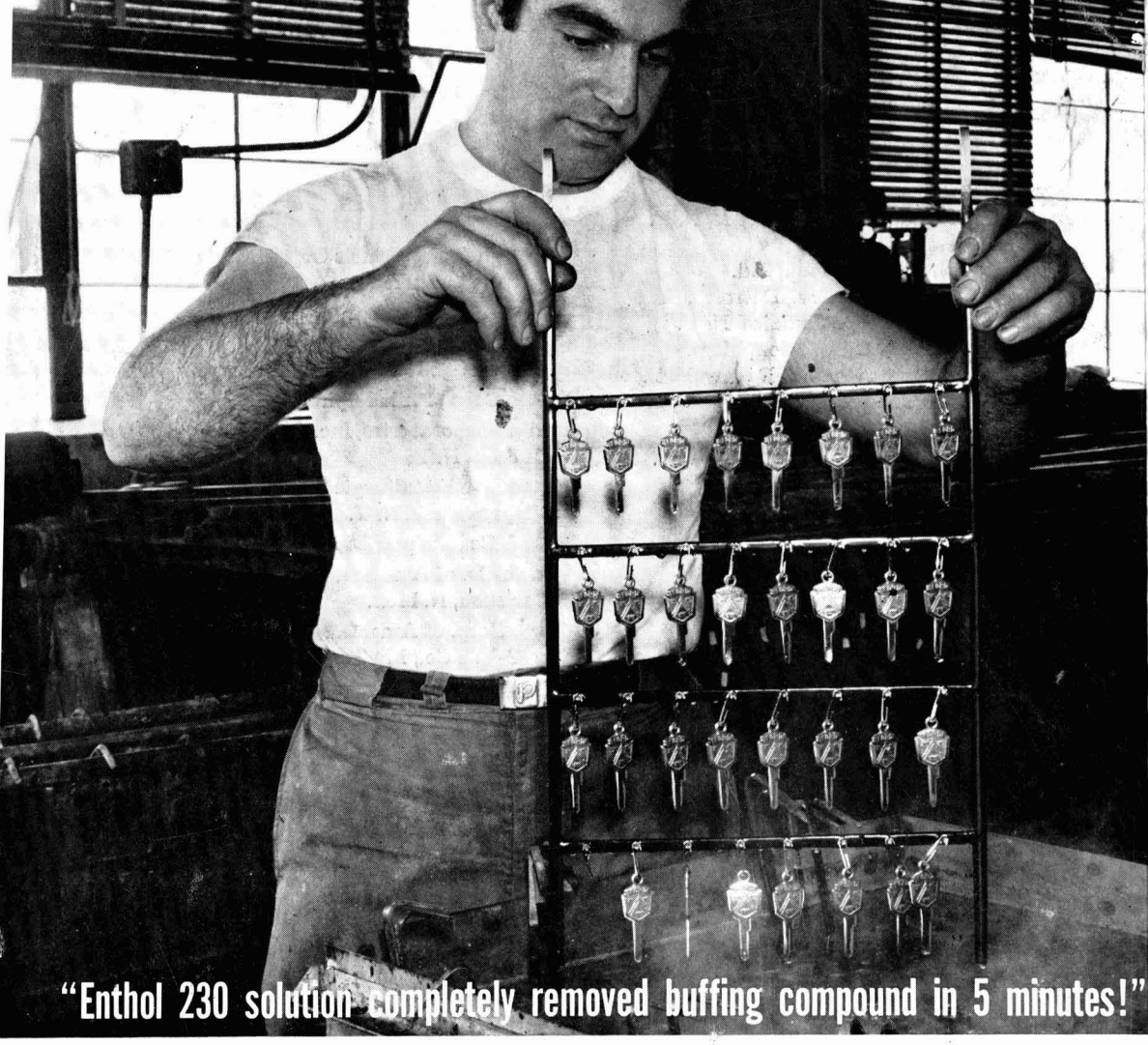

At Regal Plating Company, Providence, R. I., these brass keys have just been soaked for 5 minutes in a 3.5% by volume solution of Enthol 230 at 180° F. Buffing compound packed in design work and crevices has been effectively dissolved away.

Regal joins a growing list of platers who have discovered the efficiency of new Enthol 230 in cleaning out the deep crevices, engravings, and filigree work in ornate costume jewelry. As for economy, Regal reports that an 85-gallon tank of cleaning solution required only 3 gallons of Enthol 230 for make-up and 1 gallon for replenishment over a 6 week period! The "ammonia wash" used previously, could not compete with this low operating cost.

Whatever your buffing compound removal problem, this new, mildly alkaline, liquid detergent should solve it. Enthol 230 solutions penetrate and dissolve even hardened buffing compounds, and, in many instances, have eliminated hand brushing of parts. The solutions have extremely long life and high tolerance to contamination by dissolved soils. Enthol 230 solutions can clean steel, zinc die castings, aluminum, copper, brass, white metal, lead, nickel plate, gold, and silver. They are excellent for use in ultrasonic cleaning. Write today for complete information, to Enthone, Inc., 442 Elm Street, New Haven, Conn.

ASARCO

ANOTHER PRODUCT OF Enthonics RESEARCH

ENTHONE

A Subsidiary of American Smelting and Refining Company